

**UNIVERSITY OF SOUTHERN QUEENSLAND**

**Rainfall Variability in the Austral-Indonesian Region  
and the Role of Indo-Pacific Climate Drivers**

**A Dissertation submitted by**

**Akhmad Faqih**

**For the award of**

**Doctor of Philosophy**

**2010**

## **Abstract**

The tropical Austral-Indonesian region (95°E-155°E, 25°S-10°N) is a strategically important region in the climate system and is sensitive to extreme events caused by climate variability and change. Its unique position induces significant consequences in global and regional climate distributions and is challenging for climate model studies. Rainfall is one of the economically most significant climate variables in the region and is sensitive to regional and large-scale climate events on various timescales. The present study delivers a comprehensive assessment and analysis of rainfall variability and its link with Indo-Pacific climate drivers such as the El Niño-Southern Oscillation (ENSO), the Indian Ocean Dipole (IOD) and the low-frequency modulation of the Interdecadal Pacific Oscillation (IPO). It involves some analyses of observational datasets as well as analyses of global climate model (GCM) outputs. Firstly, the study presents an assessment of historical and future rainfall simulated by twenty-one climate models that contributed to the Intergovernmental Panel on Climate Change Fourth Assessment Report. It then evaluates the basic features of seasonal rainfall climatology as well as their variability and trends. The results determine the three best-performing models for rainfall simulations in the region. Secondly, leaning on the observed data, the study investigates seasonal patterns of regional sea surface temperature and rainfall and their associations with Indo-Pacific climate drivers on interannual and interdecadal timescales. The results show the significant role of regional sea surface temperature in regulating the effect of Indo-Pacific climate drivers on rainfall variability in the region as well as in moderating the ENSO-IOD dependency. Thirdly, more specific analysis aims to identify the physical processes of the leading rainfall patterns relied on climate model output in pre-industrial control run simulations. The analysis finds that the independency of IOD from ENSO is more regulated by the regional SST condition in the Austral-Indonesian region.

## **CERTIFICATION OF DISSERTATION**

I certify that the ideas, experimental work, results, analyses, software and conclusions reported in this dissertation are entirely my own effort, except where otherwise acknowledged. I also certify that the work is original and has not been previously submitted for any other award, except where otherwise acknowledged.

---

Signature of Candidate

---

Date 10/02/2010

## **ENDORSEMENT**

---

Signature of Supervisor/s

---

Date

## **Acknowledgements**

I would like to express profound gratitude to my principal supervisor, Associate Professor Joachim Ribbe, for his invaluable support, encouragement, supervision and useful suggestions throughout this research work. His moral support and continuous guidance and understanding enabled me to complete my work successfully. I am indebted to my co-supervisor, Professor Holger Meinke, whose support, encouragement, and guidance from the initial to the final level enabled me to accomplish my study. I heartily thank the Australian Government and the University of Southern Queensland for the IPRS scholarship.

I gratefully acknowledge Dr. Wenju Cai from CSIRO for providing me many GCMs data from the CMIP3 database and the output of CSIRO-Mk3.5 climate model. I would also like to express the deepest appreciation to Professor Rizaldi Boer for his exceptional support. I owe my gratitude to Dr Cassandra Star, who helps me with the editing of this dissertation.

I am as ever, especially indebted to my parents for their love and support throughout my life. The thesis would not have been possible without love, support and affection from my lovely wife, Widiya Hastuti. I am fascinated with her perseverance and patience in looking after our beloved daughter, Safa Aisha Faqih, in very difficult moments.

The hardest times during the period of my study when we also have to help the struggle of our daughter lives who suffer from VATER Association would not have been easier without the help and hard works from the team of doctors, surgeons and nurses at the Base Hospital, Toowoomba and at the Mater Children Hospital (MCH), Brisbane. Therefore, I wish to express my special gratitude and admiration to them. I would also like to thank the experts from the Complex Care Services, at MCH, and the Cerebral Palsy League, Toowoomba that have done wonderful jobs in helping families like us. Many thanks go in particular to Mr. Ahmad Suriadi and family as well as to the Indonesian Community in Toowoomba and Brisbane; I am indebted for their assistances and friendships. Lastly, I offer my regards and blessings to all of those who supported me in any respect during the completion of this study.

## Table of Contents

List of Figures .....	vii
List of Tables.....	xi
Chapter 1 Introduction .....	1
1.1 Overview .....	1
1.2 Rainfall in the Austral-Indonesian region .....	2
1.2.1 Rainfall in Indonesia .....	2
1.2.2 Rainfall in northern Australia .....	4
1.3 Indo-Pacific climate drivers and rainfall variability .....	5
1.3.1 The effect of El Niño-Southern Oscillation (ENSO).....	5
1.3.2 The effect of the Indian Ocean Dipole (IOD).....	6
1.3.3 The effect of the Interdecadal Pacific Oscillation (IPO) .....	7
1.4 Aims of the study .....	7
1.5 Rationale and structure of the thesis .....	8
1.5.1 Simulated Rainfall Assessment for Austral-Indonesia .....	8
1.5.1.1 Current knowledge.....	8
1.5.1.2 Scope of study.....	9
1.5.2 The Impact of Regional SST on Rainfall Variability .....	9
1.5.2.1 Current knowledge.....	9
1.5.2.2 Scope of study.....	9
Chapter 2 Data and Methodologies.....	11
2.1 Data .....	11
2.1.1 Observations .....	11
2.1.2 The WCRP CMIP3 multi-model dataset .....	13
2.1.3 CSIRO-Mk3.5 pre-industrial control run data .....	14
2.2 Methodologies.....	15
2.2.1 Cumulative Distribution Functions (CDF) and KS test.....	15
2.2.2 Correlation and Root Mean Square Error (RMSE) .....	15
2.2.3 Empirical Orthogonal Functions (EOF) analysis.....	16
Chapter 3 Simulated Rainfall Assessment for Austral-Indonesia.....	19
3.1 Background .....	19
3.2 Simulated rainfall climatology .....	21
3.3 Seasonal rainfall assessment .....	23
3.3.1 Land and ocean rainfall.....	30
3.3.1.1 Differences of seasonal rainfall climatology .....	30
3.3.1.2 Ranking the models: Cumulative Absolute Differences (CAD) ...	31
3.3.2 Land only (terrestrial) rainfall.....	32
3.3.2.1 Differences in seasonal rainfall climatology .....	32
3.3.2.2 Ranking the models: Cumulative Distribution Function (CDF)....	33
3.4 Assessment of rainfall variability and trends .....	39
3.4.1 Interannual rainfall variability .....	39
3.4.2 Rainfall trends.....	42
3.5 Future rainfall projections .....	42
3.6 Summary .....	46
Chapter 4 The Impact of Regional SST on Rainfall Variability.....	48
4.1 Background .....	48

4.2	Data .....	49
4.3	The structure and connectivity of seasonal rainfall and SST .....	50
4.3.1	Rainfall patterns and connectivity with climate drivers .....	50
4.3.1.1	Seasonal rainfall patterns, 1901-2002.....	50
4.3.1.2	Relationships of rainfall patterns with Indo-Pacific SST and SLP anomalies .....	52
4.3.2	Regional SST patterns and their link with rainfall anomalies .....	57
4.3.2.1	Regional SST patterns, 1901-2002 .....	57
4.3.2.2	Relationship of regional SST patterns with rainfall and Indo-Pacific SLP anomalies .....	59
4.3.3	Results of power spectral analysis .....	62
4.3.3.1	Variability of the seasonal rainfall patterns .....	63
4.3.3.2	Variability of regional SST patterns .....	65
4.4	Low-frequency components of regional SST and rainfall .....	68
4.4.1	Interdecadal structures .....	68
4.4.2	Rainfall climatology and low-frequency modulation of local SSTs.....	69
4.4.3	Impacts of climate epochs on regional rainfall and SST patterns.....	73
4.5	Summary .....	76
Chapter 5	Rainfall Variability and ENSO-IOD Dependency in Pre-Industrial Climate .....	78
5.1	Background .....	78
5.2	Simulated rainfall climatology and time series .....	79
5.2.1	Rainfall climatology.....	79
5.2.2	Terrestrial rainfall: interannual and decadal time series .....	79
5.3	The simulated rainfall patterns .....	81
5.3.1	Terrestrial rainfall patterns based on EOF analysis .....	81
5.3.2	Links with Indo-Pacific climate variables .....	83
5.3.2.1	Relationship during DJF .....	83
5.3.2.2	Relationship during MAM.....	86
5.3.2.3	Relationship during JJA.....	87
5.3.2.4	Relationship during SON .....	89
5.4	SST-based Indo-Pacific climate indices, and rainfall composites .....	90
5.4.1	Variability of ENSO indices .....	90
5.4.1.1	Warm and cold ENSO episodes.....	92
5.4.1.2	ENSO composites .....	93
5.4.2	Variability of IOD index (DMI).....	94
5.4.2.1	Positive and negative IOD events .....	95
5.4.2.2	IOD composites .....	97
5.4.3	Dependency of IOD and ENSO in pre-Industrial climate .....	97
5.5	Summary .....	98
Chapter 6	Conclusions .....	99
6.1	Simulated Rainfall Assessment for Austral-Indonesia.....	99
6.2	The Impact of Regional SST on Rainfall Variability.....	100
6.3	Rainfall Variability and ENSO-IOD Dependency in Pre-Industrial Climate .....	101
6.4	Future Directions.....	102
References	.....	103
Glossary and Acronyms	.....	118

## List of Figures

Figure 1.1: The Austral-Indonesian region investigated in this study: Rainfall region (inside dash (--) box) and regional SST region (whole box).....	2
Figure 1.2: Observed rainfall ‘climatology’ and their leading time-space patterns from 3541 stations in Indonesia gridded onto 0.5° grid resolutions (unit in mm/day). The length of data among stations differs from only 1 to 103 year records a) Spatially averaged monthly rainfall, b) seasonal rainfall maps, c) the first two PC time series, representing three dominant types of rainfall, and d) EOF eigenvectors, showing three different region as similarly shown in Aldrian & Susanto (2003) (Source of raw ‘climatology’ data: Laboratory of Climatology, Bogor Agricultural University, Indonesia).....	3
Figure 1.3: Major seasonal rainfall zones of Australia. ....	4
Figure 2.1: Seasonal climatology (1979-1999 periods) from two observed data: CMAP (top) and CRU TS2.1 (below).....	11
Figure 2.2: Seasonal climatology maps of: a) SST from HadISST 1.1 dataset, and b) SLP from HadSLP2 dataset (1901-2002 periods). ....	12
Figure 2.3: Land-sea masks of twenty-one CMIP3 GCMs defined by using land fraction data (IPCC terminology for this parameter is ‘SFTLF’). Except for MRI-CGCM2.3.2a, the land-sea mask is based on the grid used in soil moisture content (‘MRSO’ data). ....	13
Figure 3.1: a) Monthly rainfall climatology of twenty-one CMIP3 GCMs (1979-1999 periods) spatially averaged over the studied region, and b) their RMSE (units in mm/day) and $r$ (unitless) diagram. ....	20
Figure 3.2: Meridional movement of monthly rainfall climatology calculated from zonally averaged data for a region of interest (90°E - 155°E) of twenty-one CMIP3 GCMs (1979-1999 periods). The models are compared to observed CMAP data. ....	22
Figure 3.3: Seasonal rainfall climatology of twenty-one CMIP3 GCMs (1979-1999 periods).....	24
Figure 3.4: Seasonal rainfall anomalies for the period 1979-1999 (in percent (%)).....	27
Figure 3.5: Cumulative Absolute Differences (CAD) from seasonal (CAD <sub>S</sub> ) (below) and annual (CAD <sub>T</sub> ) (top) time series (1979-1999 periods) from twenty-one CMIP3 GCMs (1979-1999 periods). See Table 2.1 to match model numbers with model names. ....	31
Figure 3.6: Seasonal differences in rainfall climatology over land area only from twenty-one CMIP3 GCMs (1979-1999 periods). ....	34
Figure 3.7: Cumulative Distribution Functions (CDF) of seasonal rainfall series (1979-1999 periods) from twenty-one CMIP3 models and CRU TS2.1 gridded observational data for a) the Austral-Indonesian region, b) Indonesia, and c) northern Australia. ....	37
Figure 3.8: Vertical distance ( $KSDist$ ) between rainfall cumulative distributions (CDF) derived from simulated and CRU TS2.1 datasets for a) Austral-Indonesia (90°E-155°E, 20°S-10°N), b) Indonesia maritime continent (90°E-	

155°E, 10°S-10°N), and c) northern Australia (90°E-155°E, 20°S-10°S). Horizontal lines correspond to threshold with $KSDist=0.10$ . $KSDist \leq 0.10$ is used as a threshold of ‘no difference’ between CDF to indicate ‘good’ model performance. ....	39
Figure 3.9: Interannual variability and trend of annual terrestrial rainfall over the Austral-Indonesian region.....	40
Figure 3.10: Interannual variability of seasonal rainfall of twenty-one CMIP3 GCMs and observed CMAP data: a) temporal variation of spatially averaged data (raw data; in mm), and b) $r$ and RMSE diagram calculated from standardised data. Red dash-line is confidence bound at 5% significance level.....	41
Figure 3.11: Percentage of differences between projected future rainfall and historical baseline from three selected models with three different SRES scenarios: a) ECHO-G (15) SRES A1B, A2 and B1, b) MRI-CGCM2.3.2 (17) SRES A1B, A2 and B1, and c) UKMO-HADGEM1 (21) SRES A1B and A2. ....	44
Figure 3.12: CDF of projected future rainfall of HADGEM1 (21) model on two SRES scenarios: A1B and A2 compared with its 20c3m simulation and observation: a) Austral-Indonesia, b) Indonesia, and c) northern Australia. ....	45
Figure 4.1: The first three EOF eigenvectors calculated to identify the leading time-space seasonal CRU TS2.1 rainfall patterns for the period 1901-2002; EOF eigenvectors (top) and principal component (PC, below). Red bars correspond to positive PC time series, while blue bars point to negative. ....	51
Figure 4.2: Spatial correlations between the first three EOFs of seasonal rainfall with Indo-Pacific SST anomalies (1901-2002 periods). The correlation area is significant at 5% significance level. ....	54
Figure 4.3: Same as Figure 4.2, but with Indo-Pacific SLP anomalies.....	55
Figure 4.4: As Figure 4.1, but using SST data within the 1901-2002 period for the Austral Indonesian region; EOF eigenvectors (top) and EOF scores (below). ....	58
Figure 4.5: Spatial correlations between the first three EOFs of regional SST with seasonal rainfall anomalies in the Austral-Indonesian region (1901-2002 periods). ....	60
Figure 4.6: Spatial correlations between the first three EOFs of regional SST in Austral-Indonesia with seasonal Indo-Pacific SLP anomalies (1901-2002 periods). ....	61
Figure 4.7: FFT Spectral analyses from IPO, ENSO (Nino 3.4 SST anomalies) and IOD (Dipole Mode Index, DMI) (1901-2002 periods). Horizontal (x) axis is transformed into logarithmic scale. ....	62
Figure 4.8: FFT Spectral analyses from the first three leading EOF of CRU TS2.1 seasonal rainfall dataset. Horizontal (x) axis is transformed into logarithmic scale. ....	63
Figure 4.9: Comparison of the first three leading EOFs of rainfall with the standardised (a-c) Niño 3.4 index, (d-f) IOD index, and (g-i) IPO index. The data used is between 1901 to 2002 periods.....	65

Figure 4.10: FFT Spectral analyses from the first three leading EOF of regional SST (1901-2002). Horizontal (x) axis is transformed into logarithmic scale. ....	66
Figure 4.11: As Figure 4.9, but for three leadings EOFs of region SST.....	67
Figure 4.12: Interdecadal variability of regional SST data, a) EOF eigenvector of 14 year filtered regional SST data, b) EOF scores from the same EOF analysis, and c) correlation of EOF scores with 14 year filtered rainfall. ....	70
Figure 4.13: The time series of local SST filtered using 14 years moving average. The results are compared with the IPO and PDO indices performed using the same filter. ....	71
Figure 4.14: The anomalies of seasonal rainfall climatology during different phases of interdecadal variability; a) 1925-1946, b) 1947-1976, and c) 1977-2002 (units in mm/month) .....	72
Figure 4.15(a-b): The first EOF mode of rainfall index calculated from different phases of climate regimes (1925-1946, 1947-1976 and 1977-2002) and their correlations with Indo-Pacific SST and SLP anomalies; a) DJF, and b) MAM (continue). Correlation results between the rainfall index with SST anomalies are presented by filled contour and overlaid with the correlation result of the index with SLP anomalies performed by solid (+) and dash (-) contours. The correlation patterns are significant at 5% significance level. ....	73
Figure 4.16: EOF2 of regional SST eigenvector distributions for three periods: a) 1925-1946, b) 1947-1976, and c) 1977-2002 (unitless). ....	76
Figure 5.1: Seasonal rainfall climatology from (a) observations (100 year periods, 1901-2000), and CSIRO-Mk3.5 data: b) 1901-2000, c) 2001-2100, d) 2101-2200, and e) 2201-2300 periods (units in mm/day).....	80
Figure 5.2: Terrestrial rainfall anomalies (mm/day) in the Austral-Indonesia region, a-d) CSIRO-Mk3.5 pre-industrial control monthly rainfall anomalies and 5-year and 13-year low-pass filtered, e-f) observed CRU TS2.1 monthly rainfall anomalies with 5-year and 13-year filtered. ....	81
Figure 5.3: The first three modes of EOF from the standardised terrestrial rainfall anomalies (500 year periods, 1801-2300): a) DJF and b) MAM (continue)...	82
Figure 5.4: Correlations between the first three leading modes of terrestrial rainfall PC time series with several climate variables during DJF (1801-2300 periods). The coloured contour refers to significant correlations at 1% significance level. ....	84
Figure 5.5: Correlations between the first three leading modes of terrestrial rainfall PC time series with several climate variables during MAM (1801-2300 periods). The coloured contour refers to significant correlations at 1% significance level. ....	86
Figure 5.6: Correlations between the first three leading modes of terrestrial rainfall PC time series with several climate variables during JJA (1801-2300 periods). The coloured contour refers to significant correlations at 1% significance level. ....	88
Figure 5.7: Correlations between the first three leading modes of terrestrial rainfall PC time series with several climate variables during SON (1801-2300 periods).	

The coloured contour refers to significant correlations at 1% significance level.  
..... 90

Figure 5.8: Monthly SST ENSO indices and their 5-year and 13-year filtered data from different ENSO regions: a) Nino1.2, b) Nino3, c) Nino4, and d) Nino3.4 region. .... 91

Figure 5.9: ENSO episodes defined by the 5-year filtered of standardised monthly SST anomalies in Niño 4 region. The standard deviation of the monthly-mean ENSO index averages about 0.5°C. Hence, warm and cold ENSO are considered when the value is above 0.5 and below -0.5, respectively. .... 92

Figure 5.10: Composites of each warm and cold ENSO episodes during 1801-2300 periods simulated by CSIRO-Mk3.5 model as defined in Figure 5.9: a) monthly-mean rainfall, b) rainfall standard deviation, and c) rainfall anomalies (units in mm/day). .... 93

Figure 5.11: Monthly Indian Ocean SST indices and their 5-year and 13-year filtered data: a) western IO, b) south-eastern IO, and c) IOD index. .... 95

Figure 5.12: IOD events defined by the 5-year filtered of standardised monthly SST differences between the western and south-eastern Indian Ocean as defined by Saji et al. (1999). The standard deviation of the monthly-mean DMI is about 0.35°C. Hence, positive and negative IOD are considered when the values are larger than 0.35° and lower than -0.35°, respectively. .... 96

Figure 5.13: Composites of each positive and negative IOD events during 1801-2300 periods simulated by CSIRO-Mk3.5 model as defined in Figure 5.12: a) monthly-mean rainfall, b) rainfall standard deviation, and c) rainfall anomalies (units in mm/day). .... 96

Figure 5.14: Combined ENSO-IOD occurrences as defined in Figure 5.9 and 5.12. .... 97

## List of Tables

Table 2.1: GCMs from IPCC AR4 databases used in the study (note: the model numbers in column 1 will be consistently used in this study to refer the model names).....	13
Table 2.2: CSIRO-Mk3.5 pre-industrial control data (monthly-mean 2-d atmosphere or land surface data) used in the study (Source: IPCC (2005)) .....	14
Table 3.1: P-values ( $p$ ) resulted from KS-test of twenty-one CMIP3 models. ....	38
Table 3.2: Trends ( $m$ ) of seasonal rainfall data from climate models and observation during late 20th century (1979-1999) .....	42
Table 3.3: the number of ensemble members for the 21 <sup>st</sup> century for each model ....	43
Table 4.1: Explained variance from each EOF mode (%) .....	50
Table 4.2: Explained variance from each EOF mode (%) .....	57
Table 4.3: Correlations between PC time series of regional SST and rainfall. Bold values show significant correlations at 5% significance level.....	59
Table 4.4: Correlations between Indo-Pacific climate drivers SST indices with PC time series of rainfall in the Austral-Indonesian region based on 10% (*), 5% (**), and 1% (***) significance levels. ....	64
Table 4.5: Correlations between Indo-Pacific climate drivers SST indices with PC time series of regional SST in the Austral-Indonesian region (1870-2006 periods) based on 10% (*), 5% (**), and 1% (***) significance levels.....	66
Table 4.6: Identified local SST zones with strong eigenvectors obtained from interdecadal regional SST analysis.....	71
Table 5.1: Correlations ( $r$ ) between 5-year and 13-year filtered standardised SST anomalies in various ENSO regions with terrestrial rainfall .....	91
Table 5.2: Correlations ( $r$ ) between 5-year and 13-year filtered standardised SST anomalies in a single IOD domain (western or eastern Indian Ocean) and IOD index with rainfall terrestrial rainfall in the Austral-Indonesian region. ....	94
Table 5.3: Correlations ( $r$ ) between 5-year and 13-year filtered standardised ENSO indices and DMI .....	98



# Chapter 1 Introduction

## 1.1 Overview

The tropical Austral-Indonesian region is a strategically important region due to its specific geographical position, natural resources, economic prosperities and demographic features. It is covered mostly by Indonesia and northern Australia (Figure 1.1). In this region, many sectors such as agriculture, forestry, fisheries, transportation, etc. are climate sensitive, and must therefore strive to enhance their adaptive capacity and improve their resilience to extreme climate events.

The economically most important climate variable in the region is rainfall. It not only determines agricultural productivity, but it also affects other domains such as water resources management, food security, environment, energy, and disaster mitigation programs (Boer & Subbiah 2005; Meinke et al. 2006; Naylor et al. 2007). A better understanding of the physical processes governing the irregularity and complexity of rainfall can advance our capacity to deliver improved predictions and future climate change projections for the region.

The use of state-of-the-art Global Circulation Models (GCMs) to research the physical mechanisms driving rainfall is essential. Nevertheless, the difficulties in modelling the biophysical complexity of the region remain a major problem in GCM simulations (AchutaRao & Sperber 2006; Covey et al. 2003; Ferranti et al. 1997; Gadgil & Sajani 1998; Lau et al. 1996; Meehl et al. 2005; Moise et al. 2005; Zhang et al. 1997). The recent Fourth Assessment Report by the Intergovernmental Panel on Climate Change (IPCC AR4) relied heavily on outputs from more than twenty different GCMs developed by different institutions across the globe (IPCC 2007). Comprehensive studies to assess and validate the performance of these models based on different evaluation metrics are essential to inspire confidence in their projected rainfall scenarios. This is especially necessary because they are heavily relied upon by policy makers for important, climate-related policy decisions (e.g. Benestad 2005; Dai 2006; Maxino et al. 2007; Perkins et al. 2007; Sun et al. 2007; Vera et al. 2006). Although individual model evaluations for Australia have been performed in several studies (e.g. Suppiah et al. 2007), a detailed, regional evaluation of model performance for the Austral-Indonesian region has so far not been conducted. Such work is essential to further advance our ability to understand and simulate the complex dynamics of this region (e.g. Naylor et al. 2007).

The variability of rainfall in the region is strongly influenced by large-scales climate phenomena such as the El Niño-Southern Oscillation (ENSO), the Indian Ocean Dipole (IOD) and the Interdecadal Pacific Oscillation (IPO). The definitions/explanations of these phenomena are described in Section 1.3. Prominent impacts of these events are frequently felt throughout this region and manifest themselves in floods, droughts and forest or bushfires. A good example of this is the ENSO event in 1997/98 that resulted in considerable damage due to drought in many of Indonesia's climate-sensitive sectors (Boer & Subbiah 2005; UNDP 1998). Although the underlying theories of each of these phenomena have been significantly improved in the last few decades, there are still considerable research gaps requiring further investigation. The dynamic interactions between these phenomena are not yet fully understood. In particular, the impact of local and regional sea surface

temperature (SST) and their impact on larger-scale teleconnection on interannual to multidecadal timescales are still poorly understood.

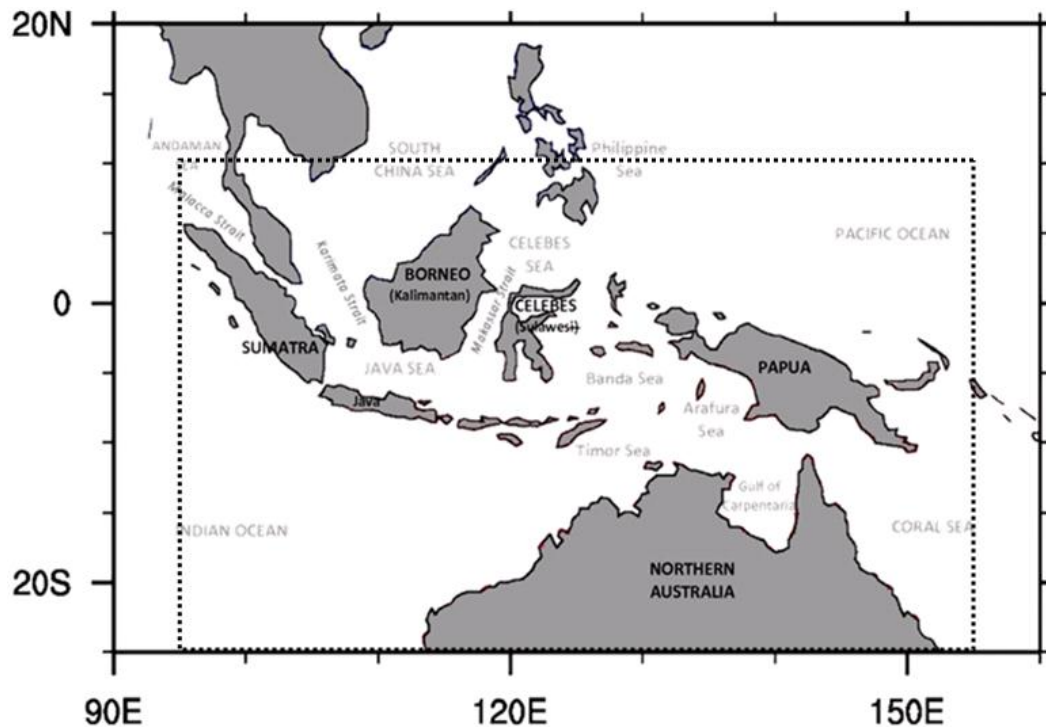


Figure 1.1: The Austral-Indonesian region investigated in this study: Rainfall region (inside dash (--) box) and regional SST region (whole box).

## 1.2 Rainfall in the Austral-Indonesian region

In order to understand rainfall in the Austral-Indonesian region, this section discusses the basic features of rainfall within the two main areas shaping the region, i.e., Indonesia and northern Australia.

### 1.2.1 Rainfall in Indonesia

Figure 1.2a shows observed monthly mean rainfall from a spatially averaged climatological data set within geographical boundaries of Indonesia ( $11^{\circ}08'S-6^{\circ}N$ ,  $95^{\circ}E-141^{\circ}45'E$ ). The peak of rainfall appears during the Austral summer monsoon season (December-January-February) with a minimum during the Asian Summer Monsoon activity (June-July-August). The two monsoons dominate the rainfall patterns in the region resulting in different rainfall distributions (Oldeman & Frere 1982; see Figure 1.2b) from bi-modal to uni-modal annual distributions. Bimodal patterns can be identified in the regions that have two peaks of rainy seasons in a year, while the regions with uni-modal pattern will only accept one peak of rainfall annually.

Due to its location around the Equator and its intricate topography, Indonesia is characterised as having three distinct, dominant rainfall types (see McBride & Winarso 2002). These include (1) a uni-modal monsoonal pattern with a rainfall peak during the Austral summer monsoon, (2) a bi-modal, equatorial pattern marked by two peaks of rainfall during the transition periods in March-April-May and September-October-November, respectively, and, (3) local pattern, which often

opposite the uni-modal monsoonal pattern due to very specific orographic features (see Figure 1.2c). A similar classification was used based on a method that separated dominant rainfall regions into the south monsoonal, the northwest semi-monsoonal and the Molluca anti monsoonal region (Aldrian & Susanto 2003) (as similarly shown in Figure 1.2d). In another study, Aldrian et al (2003) found that these three rainfall regions correspond with the interannual variability of Pacific climate drivers, i.e. ENSO.

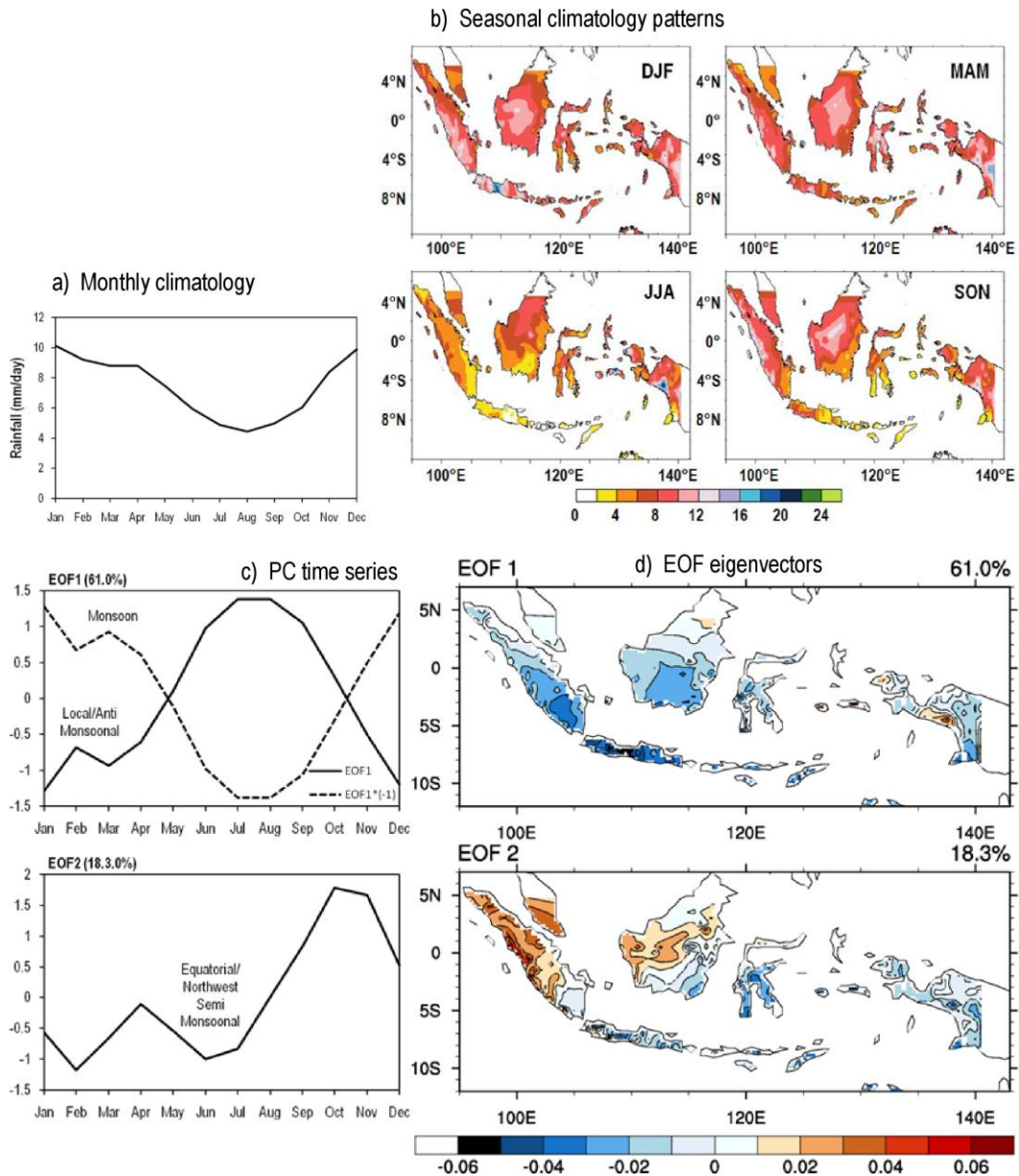


Figure 1.2: Observed rainfall 'climatology' and their leading time-space patterns from 3541 stations in Indonesia gridded onto  $0.5^\circ$  grid resolutions (unit in mm/day). The length of data among stations differs from only 1 to 103 year records a) Spatially averaged monthly rainfall, b) seasonal rainfall maps, c) the first two PC time series, representing three dominant types of rainfall, and d) EOF eigenvectors, showing three different region as similarly shown in Aldrian & Susanto (2003) (Source of raw 'climatology' data: Laboratory of Climatology, Bogor Agricultural University, Indonesia).

ENSO and IOD are the main climate drivers affecting the interannual variability of rainfall in Indonesia (e.g. Boer & Faqih 2004; Faqih 2004; Haylock & McBride 2001; Hendon 2003; Kirono et al. 1999; Saji et al. 1999). A previous study also found decadal variation on the Indonesian rainfall relationship with ENSO (Chang et al. 2004) indicating a strong coupling with the large-scale climate system (D'Arrigo et al. 2006).

## 1.2.2 Rainfall in northern Australia

Northern Australia, part of the flattest, driest continent in the Southern Hemisphere, is a tropical region characterised by a wet summers and dry winters (Figure 1.3). The effects of the Austral summer monsoons are dominant resulting in a similar monsoonal rainfall pattern to Indonesia (Figure 1.2c). The duration of the wet season in the region decreases with the increasing latitude (Cook & Heerdegen 2001). The region often experiences tropical cyclones (Dare & Davidson 2004; Grant & Walsh 2001; Hall et al. 2001; Nott 2006; Pezza & Ambrizzi 2003) causing torrential rainfall and floods.

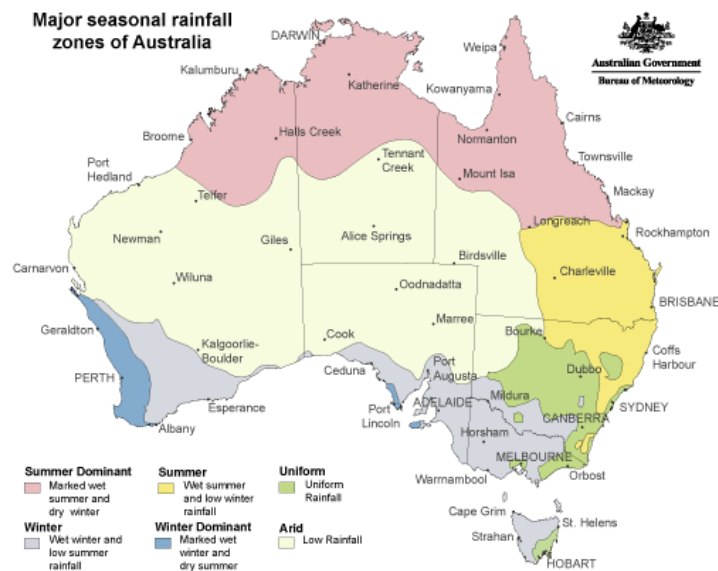


Figure 1.3: Major seasonal rainfall zones of Australia.

(Source: <http://www.bom.gov.au/lam/climate/levelthree/ausclim/zones.htm> 2006)

One of the major factors determining the primary characteristics of the Australian climate is the fact that the continent is surrounded by vast oceans (Hobbs 1998), i.e. Pacific and Indian Oceans. This results in a great interaction with the coupled ocean-atmospheric processes within the climate system in the region. The three main climate drivers of the Australian climate creating extreme climate events and rainfall variability are ENSO in the Pacific Ocean, IOD in Indian Ocean, and the Southern Annular Mode (SAM) of the Southern Hemisphere in the Southern Ocean (Shi 2008). SAM is defined as the standardised difference in the zonal mean sea-level pressure between 40°S and 65°S (Goosse et al. 2009). It is the dominant mode of atmospheric circulation variability in the Southern Hemisphere (SH) (Thompson & Wallace, 2000). The relationships of SAM with seasonal rainfall over Australia differ across regions (Belinda et al. 2007; Cai et al. 2003), where in particular positive relationship was identified between SAM and rainfall in northern Australia (Belinda

et al. 2007). Due to the limitation of this thesis that only focuses on the Indo-Pacific climate drivers, SAM will not be discussed any further. At decadal scales, rainfall variability in Australia was found to be associated with phenomena such as the IPO (Power et al. 1999a) that could be a low frequency component of ENSO (Meinke et al. 2005).

### **1.3 Indo-Pacific climate drivers and rainfall variability**

The climate drivers impacting the rainfall variability in the region range from high-to low-frequency variability on seasonal to multidecadal time scales. Monsoon is the main climate driver controlling rainfall on a seasonal time scale (e.g. Ananthakrishnan 1977; Bhaskaran & Mitchell 1998; D'Arrigo et al. 2006; Hackert & Hastenrath 1986; 1987). The monsoon system, which is strongly related to seasonal rainfall distributions over the Austral-Indonesian region, is known as the Asian-Australian monsoon. This monsoon system is associated with seasonal shifts of wind directions that bring excessive rainfall over most of the region. One of the energetic components of this system is the Australian monsoon that influences atmospheric general circulation (Kajikawa et al. 2009) and a major source of rainfall occurrences over northern Australia and most parts of Indonesia.

On the intraseasonal time scale, the variability of rainfall is affected by the 40-50 days oscillation known as the Madden-Julian Oscillation (MJO) (Donald et al. 2006; Madden & Julian 1994; Potemra et al. 2002; Shinoda et al. 1998; Waliser et al. 2003; Wheeler et al. 2009). The interannual variability of rainfall is mostly determined by ENSO (e.g. Chang et al. 2004; Haylock & McBride 2001; Hendon 2003; Kirono et al. 1999). Recent studies identified another climate driver known as IOD (Saji et al. 1999; Saji & Yamagata 2003; Webster et al. 1999) affecting the rainfall particularly in the western Austral-Indonesian region. On other timescales, the low-frequency variability in the Pacific identified as IPO has also been connected with the rainfall variability in the region (Folland et al. 1999, 2002; Meinke et al. 2005; Power et al. 1999a).

In this thesis, the focus is on the three large scale climate drivers that significantly impact the region and have been the main focus of climate research in the last few years. Those climate drivers are the ENSO, the IOD and the IPO.

#### **1.3.1 The effect of El Niño-Southern Oscillation (ENSO)**

El Niño-Southern Oscillation (ENSO) is a coupled ocean-atmospheric process in the Pacific Ocean related to extreme climate events over a major part of the globe. The terms El Niño and La Niña are used to describe the extremes of the oceanic phenomena interacting with the atmospheric response known as the Southern Oscillation (Philander 1983, 1990), whereby the term 'El Niño' refers to the warm SST phase of ENSO, while La Niña refers to the cold SST phase. This warm (cold) phase of ENSO occurs when the SST anomalies in the eastern and central Pacific Ocean are positive (negative). The SST anomaly is defined here as departure from its long term mean. The changing of zonal and vertical circulation, namely Walker circulation, during an El Niño event can reduce the rainfall due to formation of subsidence zone over the Austral-Indonesian region.

ENSO impacts on rainfall variability in Indonesia are diverse in time and space (e.g. Chang et al. 2004; Haylock & McBride 2001; Hendon 2003; Kirono et al. 1999). The dominant effect of the warm phase of ENSO on rainfall starts in June or July to November and begins to decline in December (Aldrian et al. 2003) delaying the onset of the Monsoon (Lo et al. 2007; Moron et al. 2009) and therefore prolonging the dry season (Kirono et al. 1999; Ropelewski & Halpert 1987). Previous studies have shown that wet season rainfall in Indonesia has a very weak association with ENSO (Haylock & McBride 2001; Nicholls 1981). During 1997/1998 El Niño event, many meteorological stations in Indonesia recorded their lowest rainfall (Kirono et al. 1999). However, it is interesting to note that this event did not impact on rainfall in Australia at all. Several studies have shown that the eastern part of the Indonesian region is more sensitive to ENSO compared to other regions in the middle and western part of Indonesia (e.g. Aldrian et al. 2003; Chang et al. 2004).

The effect of ENSO contributes to the variability of rainfall in Australia (e.g. McBride & Nicholls 1983; Suppiah 2004), mainly by influencing the number and intensity of rain events (Nicholls & Kariko 1993). McBride & Nicholls (1983) identified that the strongest ENSO-rainfall relationship occurs in the Austral spring (SON) with some areas significantly correlated with the Southern Oscillation Index (SOI) six months earlier. Particularly in the northern Australian region, ENSO influences on rainfall are evident with some fluctuations in their relationship (Cai et al. 2001). Murphy & Ribbe (2004) suggest that the rainfall variability in southeastern Queensland is weakly correlated with SOI, but has a relatively strong relationship with the Niño 4 index.

The El Niño event in 1997 has been recorded as one of the strongest in terms of global impact, causing large economic losses in different countries. Other events, including 2002, had strong regional impacts (Potgieter et al. 2005). However, the debate continues amongst climatologists whether or not 2002 event met the technocratic definition of El Niño (McPhaden 2004). The impact of the 1997 event on the Indonesian economy, for example, was estimated at 275 million US dollars in the forestry sector, 90 million US dollars in the agricultural sector, and approximately 10 million US dollars in the sector of transportation (UNDP 1998).

### **1.3.2 The effect of the Indian Ocean Dipole (IOD)**

Another climate driver affecting rainfall variability in Indonesia is the Indian Ocean Dipole (IOD). This dipole mode event in the Indian Ocean was first introduced by Saji et al. (1999) and Webster (1999). Its structure is characterised by differences in SST anomalies between the west and southeast Indian Ocean. During the positive episode of IOD, SST in the west part of the Indian Ocean is warmer than usual, while the east/southeast Indian Ocean becomes cooler. This condition leads to intensive convections in the west that increase the rainfall over tropical eastern Africa and the western Indian Ocean. Conversely, the rainfall tends to decrease over Sumatra and some parts of the Indonesian region. The IOD events are also associated with the rainfall variability in Australia (Ashok et al. 2003; Cai et al. 2005a; England et al. 2006), where negative (positive) IOD is associated with an increase (decrease) of rainfall over parts of Australia.

Further, the IOD events are sometimes phase-locking with ENSO (Annamalai et al. 2003; Gualdi et al. 2003; Yu & Rienecker 2000). This is evidently shown by a

statistically strong seasonal relationship between ENSO and IOD, particularly during SON (Allan et al. 2001). The strong link between those two events during this season is related to the mature phase of IOD (Saji et al. 1999) that occurs simultaneously with ENSO event. Despite this relationship, debate still continues on how independent IOD events are of ENSO events (Allan & Coauthors 2001; Dommengeset & Latif 2002; Dommengeset et al. 2006; Fischer et al. 2005; Saji et al. 1999; Saji & Yamagata 2003).

### **1.3.3 The effect of the Interdecadal Pacific Oscillation (IPO)**

ENSO variability is modulated by low-frequency (LF) variations (e.g. Barnett et al. 1999; White & Cayan 2000) that are linked with interdecadal variability of rainfall in Indonesia (Chang et al. 2004) and, in fact, many other parts of the globe (Meinke et al. 2005). A similar link between ENSO modulations and rainfall variability has been documented for Australia (Power et al. 1999a) and the large-scale climate process driving this variability is referred to as the Interdecadal Pacific Oscillation (IPO) (Folland et al. 1999). The IPO index is described from the third principal component of 13 year low-pass filtered SST (Folland et al. 1999) and has been associated with changes in the intensity of cold and warm ENSO events, rainfall, surface temperature, stream flows and wheat crop yields (Power et al. 1999a), although its predictability is still being questioned (Meinke et al. 2005).

## **1.4 Aims of the study**

The term ‘Maritime Continent’ (Ramage 1968) is normally used to describe a specifically defined area in Southeast Asia with unique features such as islands of variable size featuring significant mountain ranges of volcanic origin and surrounded by vast waters. This area mostly covers the Indonesian region and the surrounding Southeast Asian countries. This thesis focuses on two main regions, i.e. (1) Indonesia, the dominant part of the ‘Maritime Continent’ and (2) northern Australia. Therefore, it adopts the term of ‘Austral-Indonesia’ in order to represent both regions.

Based on an extensive literature review, this study aims to understand rainfall variability in the tropical Austral-Indonesian region and identifies the key climate phenomena driving rainfall variability. Specifically, this study focuses on:

1. *A simulated rainfall assessment for Austral-Indonesia.* The aim of this study is to evaluate the performance of state-of-the-art General Circulation Models (GCMs) in simulating basic features of rainfall by comparing different metrics to assess the models.
2. *The impact of regional SST on rainfall variability.* This study aims to investigate the contribution of regional seas in the Austral-Indonesian region in terms of ocean/atmosphere teleconnections. Their interactions with large-scale climate drivers such as ENSO, IOD and IPO, including the associated consequences in terms of rainfall variability are also assessed. This will reveal the regional patterns of seasonal SST and rainfall associated with those climate drivers.

3. *Rainfall variability and ENSO-IOD dependency in the pre-industrial climate.* Extending from the research focus in point 2, this study aims to analyse rainfall variability and ENSO-IOD dependency in the simulated pre-industrial climate. This study relies on the output of the CSIRO-Mk3.5 pre-industrial control run to analyse rainfall variability and its link with climate drivers in the absence of climate change impact. The issue of ENSO-IOD dependency in the pre-industrial climate will also be investigated.

## **1.5 Rationale and structure of the thesis**

This thesis represents a study of rainfall variability and the role of Indo-Pacific climate drivers in controlling the regional processes involving the SST-rainfall relationship in the Austral-Indonesian region over various timescales. The thesis is structured into three main sections as described in Section 1.4. Below the current knowledge is summarised and the scope for each of these sections is outlined.

### **1.5.1 Simulated Rainfall Assessment for Austral-Indonesia**

#### ***1.5.1.1 Current knowledge***

The uniqueness of the vast waters in the Indonesian Archipelago, combined with the complex topographical features of the region, as well as a relatively flat Australian mainland that is impacted by the coupled ocean-atmospheric mechanisms, results in the complexity of the rainfall process in the region. These regional and local factors are difficult to model in many Global Circulation Models (GCMs). These issues are largely responsible for the failure to adequately simulate rainfall. Some problems can be traced back to, for example, an incorrect positioning of the Inter Tropical Convergence Zone (ITCZ) (Barsugli et al. 2004; Dai 2006; Hack et al. 2006; Lau et al. 1996), difficulties in representing the land-sea distributions in coarse resolution models (Lau et al. 1996), as well as in simulating the Monsoon circulations (Gadgil & Sajani 1998; Zhang et al. 1997). These problems have been identified in the previous generations of GCMs through several joint studies/groups for the model intercomparison projects, such as the Atmospheric Model Intercomparison Project (AMIP) (e.g. Ferranti et al. 1997; Gadgil & Sajani 1998; Lau et al. 1996; Zhang et al. 1997) and the Coupled Model Intercomparison Project (CMIP) (e.g. AchutaRao & Sperber 2006; Covey et al. 2003; Meehl et al. 2005; Moise et al. 2005).

The recent IPCC AR4 used more than twenty models to support their future assessment on climate change (IPCC 2007). Many studies have evaluated those models for their capability to simulate rainfall in different regions (e.g. Benestad 2005; Dai 2006; Sun et al. 2007; Vera et al. 2006) including in Australia (e.g. Maxino et al. 2007; Moise et al. 2005). Some of these studies also used different metrics for assessing the models accuracy (e.g. Perkins et al. 2007). Nevertheless, further attention is needed to assessing the rainfall over the Austral-Indonesian region. Meanwhile, the requirement to use the model for future projections as a tool to support policy decisions in the region is increasing (e.g. Naylor et al. 2007). Therefore, evaluating the ability of GCMs to simulated rainfall for this particular region is important as a first step towards improving GCM performance. This requires the use of a range of different metrics and various timescales.

### ***1.5.1.2 Scope of study***

Assessing simulated historical rainfall patterns from various GCMs provide essential basic information needed for model developments in the future. The evaluation results can provide useful information for climate science community in using the data for climate analysis specific for the region. It also can be used by model developer to improve the model capability in simulating more realistic rainfall features. This study will assess the GCMs' ability to simulate the basic features of rainfall in the Austral-Indonesian region. It will focus on assessing the climatological consistency, interannual variability and trends during 20<sup>th</sup> century as well as on assessing future rainfall projections by selecting the best performing model based on the results of several ranking methods.

## **1.5.2 The Impact of Regional SST on Rainfall Variability**

### ***1.5.2.1 Current knowledge***

The relationships between remote SST in the Pacific and Indian Ocean regions with rainfall variability in the Austral-Indonesian region have been addressed in many studies (Aldrian & Susanto 2003; Arblaster et al. 2002; Chang et al. 2004; Hendon 2003; Saji et al. 1999; Saji & Yamagata 2003). These remote SST regions are usually connected with the ENSO and IOD. Other studies have identified the role of regional SSTs of the Austral-Indonesian region in responding to ENSO and IOD events (Annamalai et al. 2003; England et al. 2006). The processes involve the oceanic mass and heat transports (Cai et al. 2005b) via the Indonesian Throughflow (ITF) (Annamalai et al. 2005; England & Huang 2005; Gordon 1986; Gordon et al. 2003), resulting in some changes to the SST patterns in the region. The ITF is an ocean current that transports water mass and heat between the Pacific and Indian Oceans through the Indonesian waters.

In addition, changes to the large-scale Indo-Pacific climate system on interdecadal timescales known as IPO (Folland et al. 1999, 2002; Meinke et al. 2005) moderates the impact of ENSO events by increasing La Niña (El Niño) occurrences during its cold (warm) phases (Saji & Yamagata 2003; Salinger et al. 2001; Wang et al. 2008). This moderation contributes to the change of regional SST and influence the rainfall patterns. A previous study has found a link between decadal SST variability in the central Pacific Ocean and Australian rainfall (Power et al. 1999b). This indicates that the interdecadal signal from the Pacific Ocean might also influence the variability of regional SST and rainfall in the Austral-Indonesian region. Therefore, the changes in the regional SST pattern and its response to large-scale climate events on different timescales need to be investigated further.

### ***1.5.2.2 Scope of study***

Although the impact of large-scale changes in ocean-climate interactions such as ENSO, IOD and IPO on rainfall are well documented, little is known about the exact physical causes, thus prompting a need for further investigation. Of particular concern is the exact role of local processes, including changes in regional SSTs (Aldrian & Susanto 2003; Hendon 2003; McBride et al. 2003; Nicholls 1995). In this part, the study will investigate this issue using two different approaches, each presented in individual chapters.

Firstly, the study will focus on analysing the structures of regional SST and rainfall patterns and their relationships with large-scale climate drivers on interannual and interdecadal timescales. The analysis presented in Chapter 4 takes into account the impact of climate regime shifts associated with interdecadal Pacific variability, known as IPO. Several aspects will be discussed regarding the role of regional SST in moderating the effect of ENSO, IOD and IPO on rainfall and the inter-dependencies between them.

Secondly, the study will investigate the issue in more detail by deploying the output data the of CSIRO-Mk3.5 pre-industrial control run. Here more variables will be analysed in order to research their relationship with the rainfall patterns and this is discussed in Chapter 5. An analysis of the ENSO-IOD dependency under the pre-industrial climate is also presented.

## Chapter 2 Data and Methodologies

The study uses multiple data sets sourced from observations and global climate model outputs. The data are analysed based on different analytical and statistical techniques (simple and multivariate) involving elaborate computations especially for handling huge datasets and analyses. In this Chapter, specific data deployments and methodologies are described.

### 2.1 Data

#### 2.1.1 Observations

For the analysis, a number of observational datasets including rainfall data, sea surface temperature (SST) and sea level pressure (SLP) are used. The observed rainfall data are taken from two different sources, (i) from the Climate Prediction Center Merge Analysis of Precipitation (CMAP), and (ii) from the Climatic Research Unit (CRU) TS2.1 dataset. The CMAP data is used for analysis in Chapter 3, while the CRU data are utilised for analyses in Chapters 3, 4, 5 and 6.

The CMAP data used here is a monthly dataset of global precipitation analysed by merging the data from rain gauges with estimated rainfall obtained from satellite data. The data set has a monthly temporal resolution starting in 1979 and a spatial grid resolution of  $2.5^{\circ} \times 2.5^{\circ}$ . A full description of the dataset is provided by Xie, P. & Arkin (1996, 1997). This dataset has been widely used in many studies (e.g. Chen et al. 2004; K.-M. Lau 2007; Kumar & Sreejith 2005; Mitra et al. 2003; Takahashi & Yasunari 2006; Zhou & Lau 2001; Zveryaev & Allan 2005) including a recently published paper that focuses upon the seasonal predictability of monsoon onsets in Indonesia by using CMAP pentad analysis product (Moron et al. 2009).

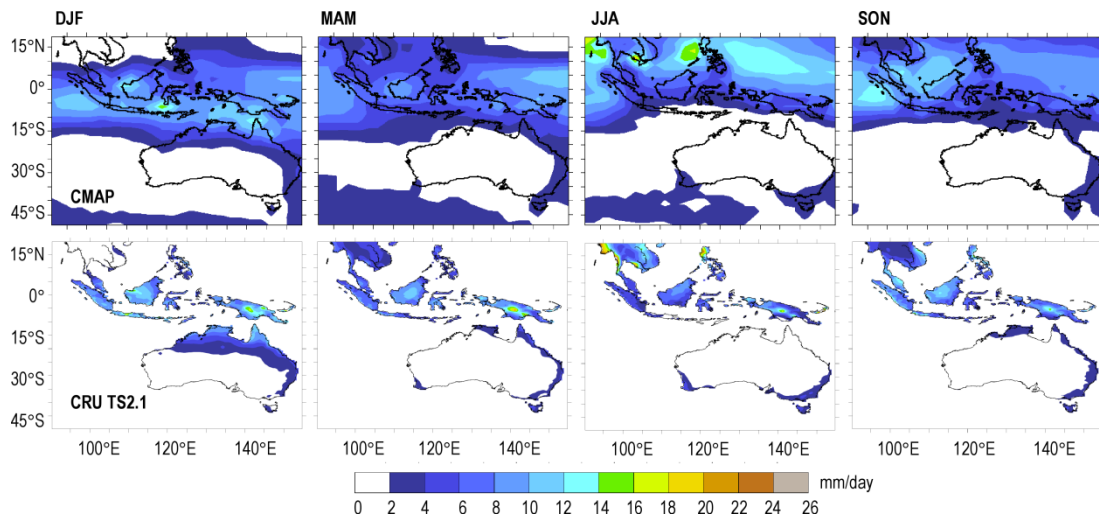


*Figure 2.1: Seasonal climatology (1979-1999 periods) from two observed data: CMAP (top) and CRU TS2.1 (below).*

The CRU TS2.1 data is a reconstructed monthly climate observations obtained from meteorological stations. It comprises of up to nine climate variables, including rainfall data (Mitchell & Jones 2005) that is used in this thesis. This global land surface dataset is reconstructed for the period of 1901-2002 with a horizontal grid resolution of  $0.5^{\circ} \times 0.5^{\circ}$ . The station records used to reconstruct the data were

obtained from seven sources for the whole variables as described by Mitchell & Jones (2005). Of all those seven sources, four sources contribute to precipitation data, including *Hulme* and Global Historical Climatology Network (GHCN) v2 datasets. Since the data was also sourced from GHCN, the distribution map of rain gauge stations over the Austral-Indonesian region can be seen in Aldrian and Susanto (2003). Further details of CRU TS2.1 data and its sources can be found in Mitchell & Jones (2005).

A comparison between the CMAP and CRU seasonal rainfall climatology data over the Austral-Indonesian region is shown in Figure 2.1. The figure demonstrates reasonable agreement and consistent seasonal rainfall patterns, particularly over land areas. Given that the datasets are derived from very different sources and differ in spatial and temporal resolution, their similarity adds credibility to both datasets and gives more confidence to their use in this study.

For the observed SST and SLP, the study uses HadISST 1.1 (Rayner et al. 2003) and HadSLP2 (Allan & Ansell 2006) datasets, respectively. The HadISST 1.1 data is a recent product that substitutes for the global sea ice and sea surface temperature (GISST) dataset. It covers global SST and sea ice concentration with a  $1^\circ \times 1^\circ$  horizontal grid resolution available from 1871 to the present. The HadISST data has a better representation of regional SST than the GISST data and compares well with other scientific datasets (Rayner et al. 2003). The newly published HadSLP2 is a combination of quality controlled terrestrial and marine pressure series. It was set in a  $5^\circ \times 5^\circ$  horizontal grid resolution from 1850 to 2004. The dataset has been able to retain many of the important climate features and indices such as the North Atlantic Oscillation, the Arctic Oscillation, the North Pacific index, the Southern Oscillation index, the Trans-Polar index, the Antarctic Oscillation, the Antarctic Circumpolar Wave, the East Asian summer monsoon index, and the Siberian High index (Allan & Ansell 2006). Both SST and SLP datasets are used in this study, analyses of which are presented in Chapter 4. The seasonal climatology maps of both SST and SLP are presented in Figure 2.2.

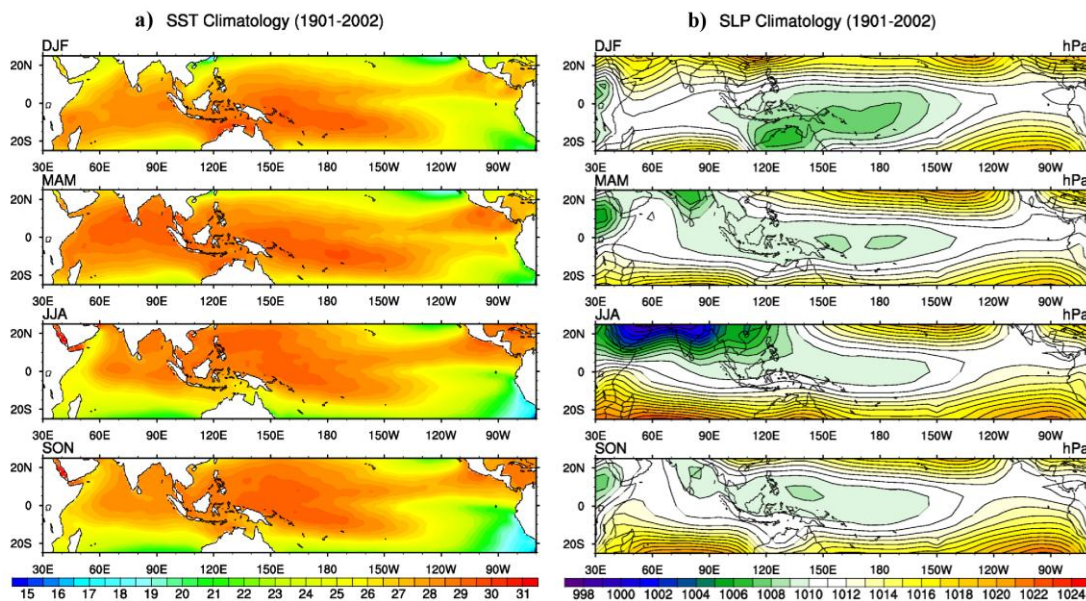


Figure 2.2: Seasonal climatology maps of: a) SST from HadISST 1.1 dataset, and b) SLP from HadSLP2 dataset (1901-2002 periods).

Table 2.1: GCMs from IPCC AR4 databases used in the study (note: the model numbers in column 1 will be consistently used in this study to refer the model names)

No	Model Name	Ensemble Member	Institution	Atmosphere Resolutions	Ocean Resolutions	References
1	CGCM3.1(T47)	5	CCCMA (Canada)	T47 L31	1.85°x1.85° L29	Kim et al. (2002)
2	CGCM3.1(T63)	1	CCCMA (Canada)	T63	-	-
3	CNRM-CM3	1	Meteo-France/CNRM (France)	T63 L45	2°x0.5° L31	Salas-Méla (2002)
4	CSIRO-Mk3.0	3	CSIRO (Australia)	T63 L18	1.875°x0.84° L31	Gordon et al. (2002)
5	GFDL-CM2.0	3	GFDL (USA)	2.5°x2.0° L24	1°x1/3° L50	Delworth et al. (2006)
6	GFDL-CM2.1	3	GFDL (USA)	2.5°x2.0° L24	1°x1/3° L50	Delworth et al. (2006)
7	GISS-AOM	2	NASA/GISS (USA)	4.0°x3.0° L12	4°x3° L16	Lucarini & Russell (2002)
8	GISS-EH	5	NASA/GISS (USA)	5.0°x4.0° L20	2°x2° L16	Schmidt et al. (2005)
9	GISS-ER	8	NASA/GISS (USA)	5.0°x4.0° L20	5°x4° L13	Schmidt et al. (2005)
10	GOALS-g1.0	3	LASG/IAP (China)	2.8°x2.8° L26	1°x1° L33	Yu et al. (2004)
11	INM-CM3.0	1	INM (Russia)	5.0°x4.0° L21	2.5°x2° L33	Volodin & Diansky (2004)
12	IPSL-CM4	1	IPSL (France)	3.75°x2.5° L19	2°x1° L31	Marti et al. (2005)
13	MIROC3.2(hires)	1	CCSR/NIES/FRCGC (Japan)	T106 L56	0.28°x0.1875° L47	K-1 model developers (2004)
14	MIROC3.2(medres)	3	CCSR/NIES/FRCGC (Japan)	T42 L20	1.4°x0.5° L43	K-1 model developers (2004)
15	ECHO-G	5	MIUB (Germany), IKMA (Korea)	T30 L19	0.5° L20	Legutke & Voss (1999)
16	ECHAM5/MPI-OM	2	MPI-M (Germany)	T63 L31	1.5°x1.5° L40	Jungclaus et al. (2005)
17	MRI-CGCM2.3.2	4	MRI (Japan)	T42 L30	2.5°x0.5° L23	Yukimoto & Noda (2002)
18	CCSM3	8	NCAR (USA)	T85 L26	1.125°x0.27° L40	Collins et al. (2006)
19	PCM	3	NCAR (USA)	T42 L26	2/3°x1/2° L32	Washington et al. (2000)
20	UKMO-HADCM3	2	Hadley Centre (UK)	3.75°x2.5° L19	1.25° L20	Gordon et al. (2000)
21	UKMO-HADGEM1	2	Hadley Centre (UK)	1.875°x1.25° L38	1°x1/3° L40	Johns (2004)

### 2.1.2 The WCRP CMIP3 multi-model dataset

In Chapter 3 the rainfall output from twenty-one climate models of the World Climate Research Programme, phase 3 of the Coupled Model Intercomparison Project (formally known as WCRP CMIP3 Multi-Model Dataset) are assessed. The models, which have been used in the latest IPCC Fourth Assessment Report (IPCC 2007), are provided online by the PCMDI (<http://www.pcmdi.llnl.gov/>) through the ESG data portal (<https://esg.llnl.gov:8443/index.jsp>), ftp link, or the OPeNDAP server. The model names and numbers are listed in Table 2.1 along with their ensemble member, institutions, atmosphere and ocean resolution, as well as their corresponding references.

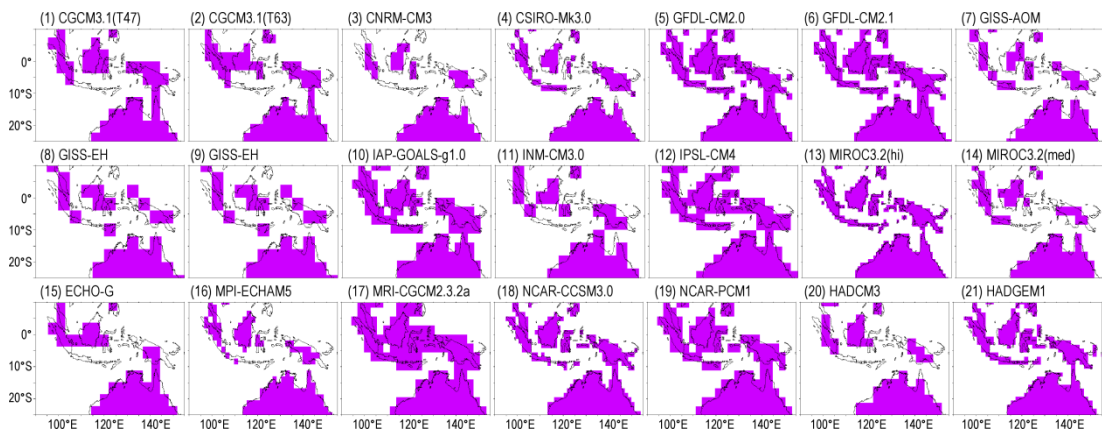


Figure 2.3: Land-sea masks of twenty-one CMIP3 GCMs defined by using land fraction data (IPCC terminology for this parameter is ‘SFTLF’). Except for MRI-CGCM2.3.2a, the land-sea mask is based on the grid used in soil moisture content (‘MRSO’ data).

Table 2.1 shows that the atmosphere and ocean grid resolutions differ between models. Horizontal grid resolutions of the atmospheric variables vary from the coarsest (5°x4°) to the finest (1.1°x1.1°, T106). Especially for the Austral-Indonesian region, where the geographical positions and the land-sea distribution are unique, the representation of the land-sea mask in the climate models is crucial as this affects not only to the representation of local/regional processes, but also influences large-scale simulations in general. In Figure 2.3, the land distribution represented by each model is shown. It is important in model evaluation studies to consider the various grid resolutions given that each model delivers a different result.

### 2.1.3 CSIRO-Mk3.5 pre-industrial control run data

Development of the CSIRO-Mk3 climate model (Gordon et al. 2002) has continued over the past few years. Version Mk3.0 was used in AR4 (Collier et al. 2008; IPCC 2007), while Mk3.5 is included in the CMIP3 PCMDI database and is being prepared for the next IPCC assessment report (Collier et al. 2007). Version Mk3.5 contains many improvements and its control climate experiment has a relatively small drift for a long period of simulation (Collier et al. 2007; Mpelasoka et al. 2007).

*Table 2.2: CSIRO-Mk3.5 pre-industrial control data (monthly-mean 2-d atmosphere or land surface data) used in the study (Source: IPCC (2005))*

CF standard name	Output variable name	Units	Notes
precipitation flux	pr	Kg m <sup>-2</sup> s <sup>-1</sup>	includes both liquid and solid phases
surface temperature	ts	K	"skin" temperature (i.e. SST for open ocean)
air pressure at sea level	psl	Pa	
atmosphere water vapor content	prw	Kg m <sup>-2</sup>	vertically integrated through the atmospheric column
surface downward eastward stress	tauu	Pa	
surface downward northward stress	tauv	Pa	
surface upward latent heat flux	hfls	W m <sup>-2</sup>	
surface upward sensible heat flux	hfss	W m <sup>-2</sup>	

The improvement of the CSIRO-Mk3.5 in representing a scheme to control the strength of the ocean eddy-induced transport and vertical ocean mixing as a consequence of wind generated turbulent kinetic energy (Collier et al. 2007) is very important to improve simulation of the ocean-climate dynamics, particularly for the Austral-Indonesian region. In addition, the model also includes a better scheme to compute wind surface stresses by using the surface wind velocity that is relative to the moving ocean surface layer. This is different to its predecessor that used the absolute wind velocity (*see* model's documentation on the PCMDI website: [http://www-pcmdi.llnl.gov/ipcc/model\\_documentation/CSIRO-Mk3.5.pdf](http://www-pcmdi.llnl.gov/ipcc/model_documentation/CSIRO-Mk3.5.pdf)). Given that most of the IPCC AR4 models are having difficulties in simulating realistic rainfall due to a too strong coupling between local SST and tropical convection (Dai 2006; Lin 2007; Lin et al. 2006), a better representation of the ocean component in the Mk3.5 may improve rainfall simulations.

The study investigates several ocean-atmosphere variables from the CSIRO-Mk3.5 pre-industrial control simulations (Table 2.2). In addition to the listed variables, the

study also uses SST data derived from the ocean component (namely TOS). All of the data are analysed for a 500-year simulation between 1801-2300 periods.

## 2.2 Methodologies

In this section the statistical methods used in this study are described.

### 2.2.1 Cumulative Distribution Functions (CDF) and KS test

The study uses the Kolmogorov-Smirnov Distance (*KSDist*) as a measure to compare the absolute differences between CDFs from the modelled and the observed data. *KSDist* is a parameter used by the two-sample Kolmogorov-Smirnov test that quantifies the maximal vertical distance between CDFs (KS-test; Hollander & Wolfe 1999; Maia et al. 2007). The quality of *KSDist* is measured using nominal significance levels (p-value;  $p$ ) based on a KS-test. The null hypothesis of this test is that the paired data arise from the same continuous distribution. It is supposed that the data from the model will have the same continuous distribution as the observation if the resulting  $p$  is larger than the significant level ( $p > \alpha$ ).

For each model, region and season under evaluation, the study calculates the corresponding *KSDist* and ranks the models accordingly:

$$KSDist = \text{Max}_i |CDF_1(x_i) - CDF_2(x_i)| \quad (2.1)$$

where  $x_i$  is any observed or modelled rainfall value (mm/day) and  $CDF_1$  and  $CDF_2$  are the cumulative distribution arising from the modelled and CRU data, respectively. This metric is specifically used to compare the modelled terrestrial rainfall distribution and observations in Chapter 3.

### 2.2.2 Correlation and Root Mean Square Error (RMSE)

The product of correlation analysis, known as the Pearson product-moment correlation coefficient ( $r$ ) is used in this study to measure the degree of linear association between two datasets. The derivation process used for the correlation coefficient ( $r$ ) is as follows. Given that  $x = (x_1, x_2, \dots, x_n)$  and  $y = (y_1, y_2, \dots, y_n)$  are two time series of length  $n$ , the correlation coefficient (Walpole et al. 2002) between the two time series is defined as:

$$r = \frac{S_{xy}}{\sqrt{S_{xx} S_{yy}}} \quad (2.2)$$

$$\text{where: } S_{xx} = \sum_{i=1}^n (x_i - \bar{x})^2, \quad S_{yy} = \sum_{i=1}^n (y_i - \bar{y})^2, \quad S_{xy} = \sum_{i=1}^n (x_i - \bar{x})(y_i - \bar{y}), \quad (2.3)$$

$$\bar{x} = \frac{\sum_{i=1}^n x_i}{n}, \quad \bar{y} = \frac{\sum_{i=1}^n y_i}{n} \quad (2.4)$$

The significance of the result for  $r$  can be tested based on a Student's t-test (Walpole et al. 2002). The  $t$ -value is given by

$$t = \frac{r \sqrt{n-2}}{\sqrt{1-r^2}} \quad (2.5)$$

where  $r$  is the correlation coefficient between the two measured time series of length  $n$ , with  $n - 2$  degrees of freedom. The null hypothesis for the test is that  $H_0: r = 0$  and  $H_1: r \neq 0$ . This means that the  $H_0$  will be rejected whenever the  $p$ -value is lower than the selected significance level  $\alpha$  and the correlation between the two datasets is significant.

In Chapter 3, the  $r$  result is used simultaneously with the Root Mean Square Error (RMSE) in order to evaluate the likeness of the modelled data compared to the observations. The RMSE is based on the Mean Square Error (MSE) derivation, defined as:

$$MSE = s^2 = \sum_{i=1}^n \frac{(y_i - \hat{y}_i)^2}{(n-2)} \quad (2.6)$$

Therefore, the RMSE is derived as:

$$RMSE = \sqrt{MSE} = s = \sqrt{\sum \frac{(y_i - \hat{y}_i)^2}{(n-2)}} \quad (2.7)$$

In Chapter 4 and 5 the spatial correlation analysis is deployed to investigate the relationship of the time series coefficient derived from the Empirical Orthogonal Function (EOF) analysis with the spatial anomalies of the Indo-Pacific climate variables.

### 2.2.3 Empirical Orthogonal Functions (EOF) analysis

The EOF analysis is a prominent statistical method commonly used to identify patterns of simultaneous variation (von Storch & Zwiers 1999). It has been widely used for analysing complex meteorological and climate data since Lorenz (1956) due to its simplicity and analytic derivation (Hannachi 2004). This method has been described in more detail by, for example, von Storch & Zwiers (1999), Jolliffe (2002) and Wall, Rechtsteiner & Rocha (2003). Technical explanation of the method is presented in Halldor & Venegas (1997) and a summarised description of this concept applied to climate data is described in Hannachi (2004). The deployment of the method in this study can be found in Chapter 4 and 5.

Considering that most of the climate data used in this study is in grided format and is non-uniformly distributed across the globe, several steps to prepare the dataset prior to performing the EOF analysis are needed (Hannachi 2004). Those steps are (i) anomaly calculation, and (ii) area weighting calculation. The area weighting is important for correcting the spatial grid data as a result of the map projection methods. This will help to diminish the impact of incorrect grid representation on the results from the EOF analysis.

It is supposed that gridded climate data ( $Y$ ) at time  $t$  and spatial grid position  $f$ , e.g. SST, is in the form of a  $p \times q$  matrix, where  $p$  represents monthly time series with a discrete time element  $t_i$  ( $i = 1, \dots, p$ ); and  $q$  is of a spatial element formed by latitude ( $\theta$ ) and longitude ( $\varphi$ ) defining a discrete spatial grid point  $f_j$  ( $j = 1, \dots, q$ ). Therefore the data  $Y(t, f)$  can be illustrated in the following matrix:

$$Y = \begin{pmatrix} y_{11} & y_{12} & \cdots & y_{1q} \\ y_{21} & y_{22} & \cdots & y_{2q} \\ \vdots & \vdots & & \vdots \\ y_{p1} & y_{p2} & \cdots & y_{pq} \end{pmatrix} \quad (2.8)$$

Given that the EOF is calculated from the anomaly data, the climatology of the horizontal grid data can then be expressed as:

$$\bar{Y} = (\bar{y}_{\cdot 1}, \dots, \bar{y}_{\cdot q}) \quad (2.9)$$

and therefore the anomaly is designated by the departure of the spatial time series data from its climatology:

$$y'_{if} = y_{if} - \bar{y}_{\cdot f} \quad (2.10)$$

In order to avoid any effect of the gridded data on the EOF calculation, an area weighting method is carried out. This is done by weighting the data point with the cosine of its latitude ( $\theta$ ). Thus, the diagonal matrix is represented as follows:

$$Z_\theta = \text{Diag} [\cos\theta_1, \dots, \cos\theta_p] \quad (2.11)$$

It contributes to the correction of the  $Y$  dataset in the form of a weighted anomaly matrix:

$$Y\omega = Y'Z_\theta \quad (2.12)$$

After performing these two steps of dataset preparation, the EOF calculation is derived by initially calculating the covariance matrix of the weighted anomaly:

$$C = \frac{1}{n-1} Y'^T Y' \quad (2.13)$$

This covariance matrix is then used to find a linear combination of all the grid points that have a maximum variance, where  $\mathbf{v}$  represents the orthonormal vector from optimum real data, so the  $Y' \mathbf{v}$  reaches maximum variability:

$$\text{var}(Y' \mathbf{v}) = \frac{1}{n-1} \|Y' \mathbf{v}\|^2 = \frac{1}{n-1} (Y' \mathbf{v})^T (Y' \mathbf{v}) = \mathbf{v}^T C \mathbf{v} \quad (2.14)$$

In this case, the  $\max_{\mathbf{v}} (\mathbf{v}^T C \mathbf{v})$  leaves a variational problem that can be simply solved by a symmetrical relationship between the covariance with eigenvalue  $\lambda_k$ . Hence the eigenvalue  $\lambda_k$  is linked with the eigenvector ( $\mathbf{v}_k$ ) of the covariance matrix.

$$C \mathbf{v}_k = \lambda_k \mathbf{v}_k. \quad (2.15)$$

The eigenvalue  $\lambda_k$  corresponds to the explained variance of each corresponding order of the EOF that is usually written as a percentage:

$$\frac{\lambda_j}{\sum_{j=1}^p \lambda_j} 100\% \quad (2.16)$$

The projection of the spatial anomaly of  $Y'$  into the eigenvector  $v_k$  results in the Principal Component (PC) that represents a newly reproduced time series of each EOF modes.

$$c_k(t) = \sum_{f=1}^q y'(t, f)v_k(f) \quad (2.17)$$

Although the EOF analysis is purely based on the mathematical approach, its first few leading modes are sometimes associated with the physical processes (von Storch & Zwiers 1999) that represent the maximum variability of the data. The method is also sensitive to domain selections (Aldrian & Susanto 2003) and often loses some details of local or regional variation when it is used to analyse global data. Therefore, in Chapter 4 and 5, this study presents a more detailed EOF-based analysis on local/regional domain in order to delineate the time-space pattern on a regional scale.

## **Chapter 3 Simulated Rainfall Assessment for Austral-Indonesia**

In this Chapter, the study addresses an assessment of the simulated rainfall from twenty-one WCRP CMIP3 Global Circulation Models (GCMs) for the Austral-Indonesian region. The focus of the evaluation is on the model's capability in performing climatological (i.e. long term mean) consistency, interannual variability and trends during the late 20<sup>th</sup> century, and projected future rainfall scenarios. So far, a detailed regional evaluation of model performance for the Austral-Indonesian region has not been conducted and no systematic study has been done for the Indonesian region. Nevertheless, such work is essential to further advance our abilities to understand and simulate the complex dynamics of this region.

Here the study identifies the rainfall mismatch reproduced by most of the models of the region and highlights the importance of improving model resolution and ocean physics. The three best-performing models (i.e. ECHO-G, MRI-CGCM2.3.2, and UKMO-HADGEM1) are selected in this study based on one of two ranking methods, either by cumulative absolute difference (CAD) or cumulative distribution function (CDF). Their projected rainfall assessment demonstrate future rainfall changes during monsoonal transitions in MAM and SON that may lead to prolonged wet and dry seasons in the Austral-Indonesian region.

### **3.1 Background**

The credibility of climate projections from Global Circulation Models (GCMs) depends on their ability to simulate observed climate data accurately (e.g. IPCC 2007; Reichler & Kim 2008). Simulated climatic changes should result solely from variations in climate forcing such as rising greenhouse gas concentrations and any model bias due to the model architecture (e.g. grid resolution and parameterisations) should be minimised. Yet, these requirements are seldom met. Model evaluations are essential in order to identify the models that perform best for a particular purpose and geographical region. Assessments of simulated data and climate scenarios against historical observations not only provide information needed to improve model performance, but also underpin the accuracy and credibility of future climate change projections.

A particular issue is the need to assess simulated rainfall from the current generation of GCMs, which still have problems in simulating precipitation patterns in the tropical region realistically (e.g. Dai 2006; Lin 2007; Lin et al. 2006). Unrealistic rainfall simulations appear to be a consequence of misrepresented convective activity in the tropical atmosphere (Dai 2006; Lin 2007). It was found in previous study that up to 95% of total precipitation simulated by the models is related to convective rainfall due to an unrealistically strong coupling between local SST and the tropical atmosphere driving local convection (Dai 2006). On the interannual time scale, this leads also to an incorrect representation of ENSO dynamics (Dai 2006), where excessive tropical rainfall is related to intrinsic model errors that lead to the formation of a double Intertropical Convergence Zone (ITCZ) causing low simulated precipitation in the equatorial Pacific (Lin 2007).

Since AR4 (IPCC 2007), several studies have been conducted in order to evaluate the regional rainfall pattern (e.g. Benestad 2005; Maxino et al. 2007; Perkins et al. 2007; Vera et al. 2006). These results are important in identifying regional problems and, if rectified, are likely to improve the models' capability in projecting future rainfall. Some studies have also introduced new approaches to evaluate models, including for example, the use of probability density functions (PDFs) by Perkins et al. (2007) and Watterson (2008) in their assessment of Australian rainfall scenarios. A similarly detailed study using the recent generation of climate models for the Austral-Indonesian region, in particular for the Indonesian region, has not yet been conducted.

Due to the study region's location in the tropics, rainfall simulations are likely to suffer from the same problems identified in previous studies. This includes the formation of the double-ITCZ (Lin 2007), the intricacy of the monsoon circulations (Gadgil & Sajani 1998; Zhang et al. 1997), the weak variances and propagations of the Madden-Julian Oscillation (MJO) (Lin et al. 2006), the unrealistic rainfall distribution and intensity (Moise et al. 2005; Srinivasan et al. 1995) and the inadequate representation of the both land-sea distribution and the topographic features of Indonesia (Lau et al. 1996). Many of these problems were identified prior the IPCC AR4 and a detailed analysis of IPCC AR4 rainfall scenarios for the region of interest is still outstanding. A particular characteristic feature of this region is the land to ocean ratio and local SST characteristics are likely to contribute to the rainfall driving mechanisms. In addition, as the GCMs' capability to correctly simulate major climate drivers improves, the wide range of results between the models, for example in precipitation, remains problematic (AchutaRao & Sperber 2006; Guilyardi 2006; Szoek & Xie 2007) and contributes to various rainfall biases (Dai 2006). Therefore, an assessment of the models is required for identifying their performances in simulating rainfall over the region.

In this Chapter, a model assessment study for the Austral-Indonesian region is presented. The focus is upon the evaluation of precipitation against historical observations as well as an assessment of future rainfall scenarios. This approach leads to the identification of the models that perform best in the region of interest and are likely to yield the most reliable information about future climatic trends.

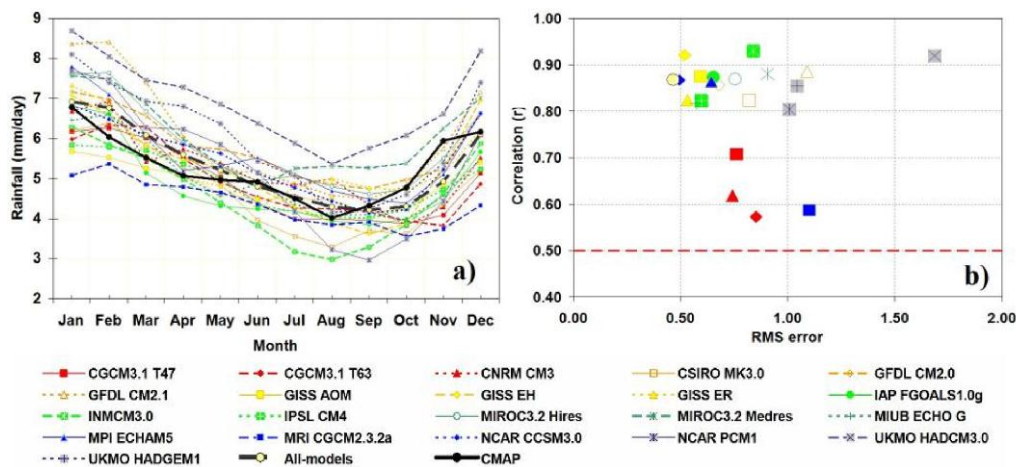


Figure 3.1: a) Monthly rainfall climatology of twenty-one CMIP3 GCMs (1979-1999 periods) spatially averaged over the studied region, and b) their RMSE (units in mm/day) and  $r$  (unitless) diagram.

## 3.2 Simulated rainfall climatology

Figure 3.1a shows simulated monthly rainfall climatology of twenty-one CMIP3 (IPCC AR4) GCMs compared to the observed CMAP data (*see* Chapter 2 for descriptions of data and methodology). Most models show a uni-modal monsoonal pattern despite their inadequacy to correctly estimate the rainfall amount. A uni-modal monsoonal pattern is shown by a rainfall-peak (wet) during the Austral summer monsoon season around December-January-February (DJF) and a rainfall-trough (dry) during the Austral winter season in June-July-August (JJA) (*see* Chapter 1 for more details).

A diagram based on the combination of correlation coefficient ( $r$ ) and root mean square error (RMSE) is used to measure proximity of the modelled climatology to the observed data (Figure 3.1b). Both metrics are computed using the monthly climatology data presented in Figure 3.1.a. The diagram identifies a good model as having a high  $r$  and low RMSE value. The analysis finds that different versions of the GISS model (GISS-AOM (7), GISS-EH (8) and GISS-ER (9)) are among the best. Other models that can be considered to reproduce the climatological rainfall quite well are GFDL-CM2.0 (5), FGOALS1.0g (10), IPSL-CM4 (12), ECHAM/MPI-OM (16), and CCSM3 (18). In addition, the climatology of the multi-model ensemble mean fits the observations well. All of these models have  $r$  and RMSE values of  $> 0.8$  and  $< 0.75$  respectively.

Measuring the climatology from the spatially averaged rainfall data is insufficient for assessing the models as it provides only basic information from the models and can be misleading. As previous studies have shown the models' problem in simulating the double-ITCZ (Dai 2006; Lin 2007), the zonally averaged monthly rainfall climatology over the region of interest ( $90^{\circ}\text{E}$ - $155^{\circ}\text{E}$ ) is analysed to assess meridional propagation of rainfall simulated by the models (Figure 3.2). CMAP data shows regions of high rainfall propagation mostly south of the Equator between  $0^{\circ}$  to  $15^{\circ}\text{S}$  in January and February with mean rainfall  $> 10$  mm/day in the centre of the propagated region. This propagation gradually decreases northward to  $10^{\circ}\text{N}$  and southward to  $20^{\circ}\text{S}$ . During the March-April-May (MAM) transition period, rainfall zones shift northward and reach the Equator during April. These propagate further north during June-July-August (JJA) in the area between  $8^{\circ}\text{N}$  to  $20^{\circ}\text{N}$  and back again to the Equator in October-November. During JJA, rainfall reaches its maximum amount which is 12-13 mm/day on average.

The twenty-one models differ significantly in their ability to simulate the meridional movement of zonally averaged rainfall variation (Figure 3.2). Models such as CGCM3.1 (T47 (1) and T63 (2)) are able to simulate the movement similar to the observed. The problem that these models have is in reproducing the high rainfall north of the equator during JJA, which is a bit underestimated and less far to the north particularly in CGCM3.1 T63 (2). These CGCM3.1 models also underestimate the rainfall during SON. The ECHO-G (15) and MRI-CGCM2.3.2 (17) models are positioning high rainfall during the DJF and JJA seasons correctly, although they tend to prolong the wet season over southern Indonesia into the MAM transition period.

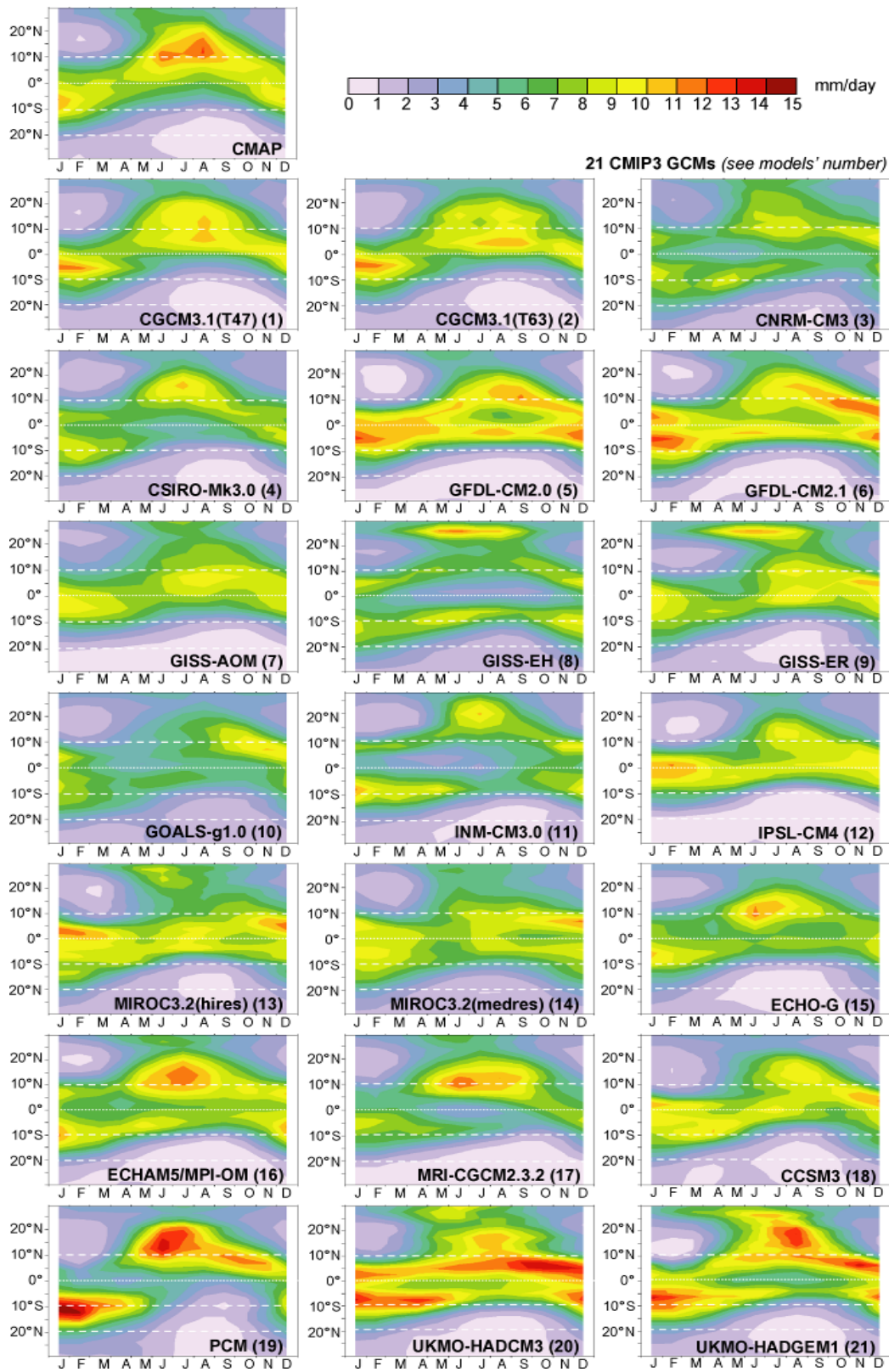


Figure 3.2: Meridional movement of monthly rainfall climatology calculated from zonally averaged data for a region of interest ( $90^{\circ}\text{E} - 155^{\circ}\text{E}$ ) of twenty-one CMIP3 GCMs (1979-1999 periods). The models are compared to observed CMAP data.

More than half of the models suffer from simulating a double-ITCZ, but with different characteristics. Most of them, including CNRM-CM3 (3), GFDL-CM2.1 (6), GISS-EH (8), INM-CM3.0 (11), MIROC (hires (13) and medres (14)), ECHAM5/MPI-OM (16) and UKMO (HadCM3 (20) and HADGEM1 (21)), experience the mismatch during all seasons, while several others simulate a false ITCZ only during a particular season (*see* Figure 3.2 for detail). These conditions are confirmed in Figure 3.3. Double-ITCZ can be identified in Figure 3.2 from the rainfall that is concurrently distributed in the north and south of the Equator.

Due to this double-ITCZ problem, excessive rainfall is simulated north of the Equator during DJF and also over south of the Equator during JJA. A problem also appears during the transition period (MAM) with additional false rainfall over the south of the Equator. The propagation area of this faulty ITCZ in the region is usually not far from 10°N in DJF and 10°S in JJA. It means that the simulated rainfall problem affects the Indonesian region (10°S - 10°N) more than northern Australia (25°S - 10°S). Details of the seasonal rainfall distributions are shown in Figure 3.3 and will be discussed further in the next section.

Figure 3.3 shows the models' ability to simulate seasonal rainfall climatology. Most of the models have difficulty reproducing the spatial evolution of seasonal rainfall distribution. The reasons for this vary but are consistent with previous findings that showed the model problems in simulating monsoon circulations (Gadgil & Sajani 1998; Zhang et al. 1997). The consequences of the double-ITCZ artefact are often incorrect location of maximum rainfall, seasonal average positions of the ITCZ, or the meridional narrowing (widening) of the convective belt causing reduced (enhanced) regional rainfall not found in the observed data. Similar problems related to the ITCZ and the Monsoon simulations were found in the older versions of GCMs as reported in several studies (e.g. Dai 2006; Gadgil & Sajani 1998; Lau et al. 1996; Zhang et al. 1997). Another inconsistency found in several models is the configuration of dry area over the equatorial western Pacific Ocean. This problem was also documented in most of the earlier model generation where it was caused by a failure to simulate large-scale convection (Gadgil & Sajani 1998; Zhang et al. 1997). Additionally, while some models were able to simulate wet conditions along the eastern Australia quite well, several others failed.

### **3.3 Seasonal rainfall assessment**

In the following sections simulated rainfall over land and ocean, as well as over land only, is compared to climatology using CMAP (land and ocean) and CRU TS2.1 (land only) data. The two-tier analyses use different approaches to (i) evaluate the rainfall for the whole area over land and ocean, and (ii) assess the terrestrial rainfall in the region. The latter is unique and requires higher resolution observational data for reference (refer to the Methodology in Chapter 2).

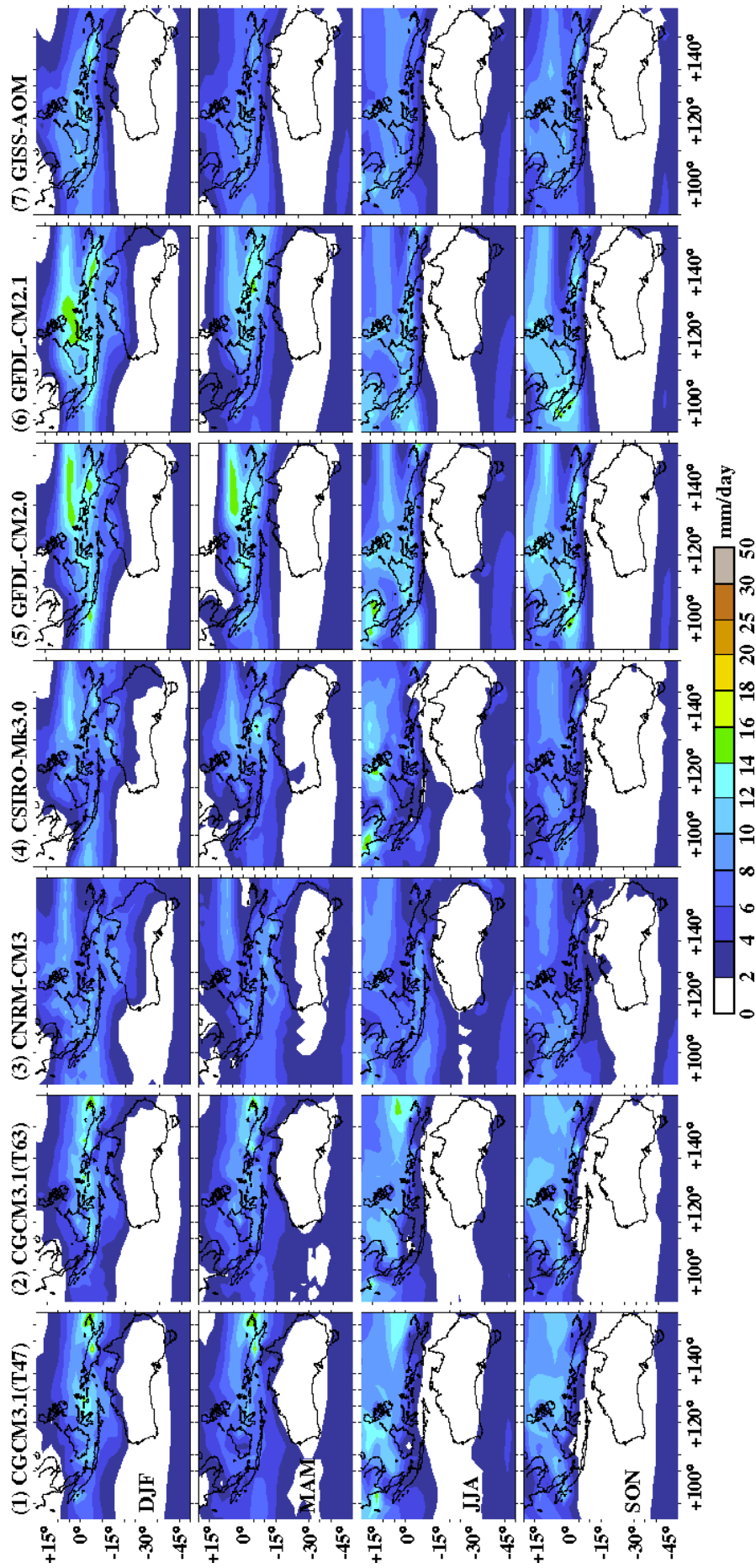


Figure 3.3: Seasonal rainfall climatology of twenty-one CMIP3 GCMs (1979-1999 periods).

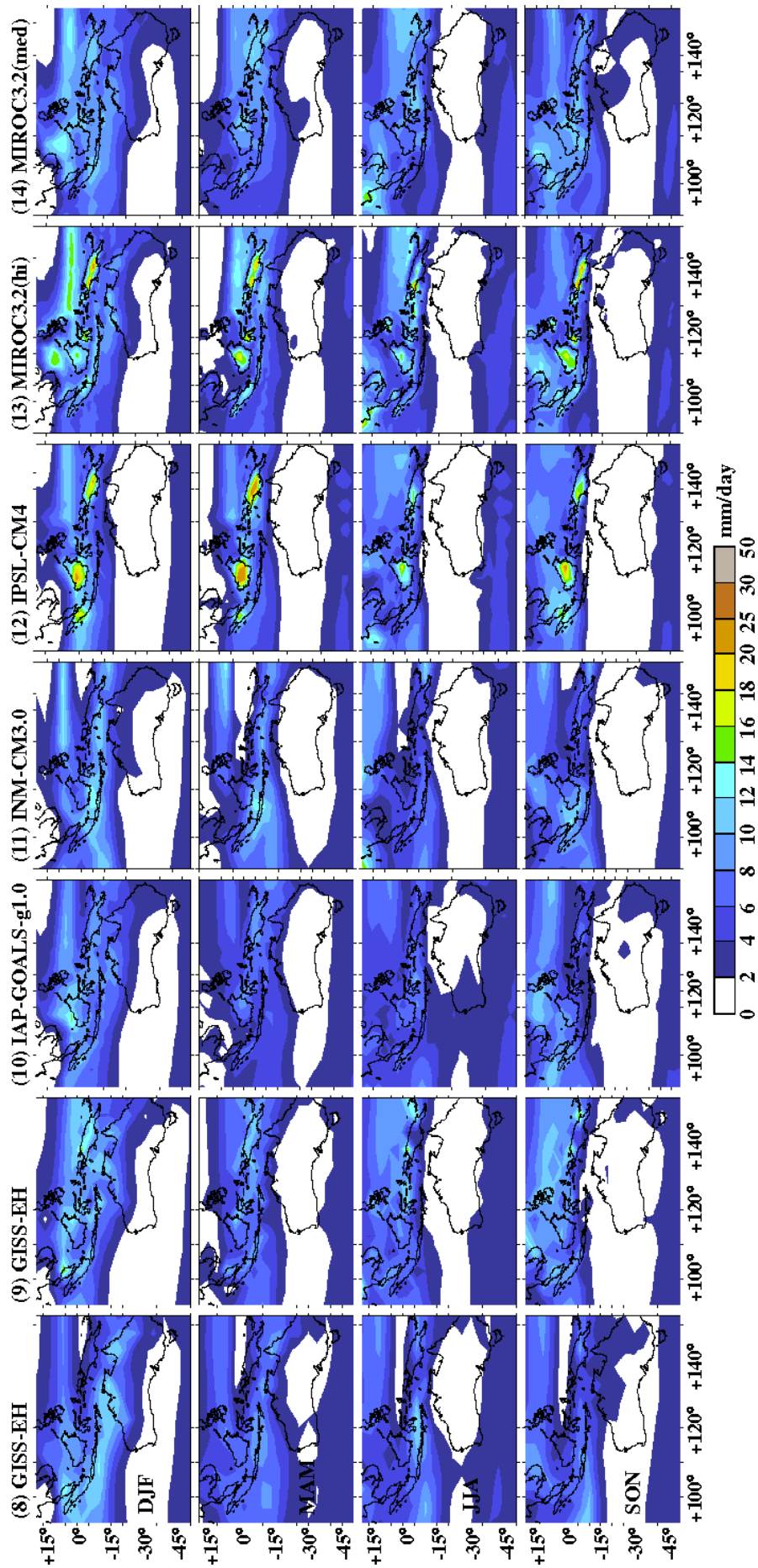


Figure 3.3: Seasonal rainfall climatology of twenty-one CIMP3 GCMs (1979-1999 periods) (continued from previous page).

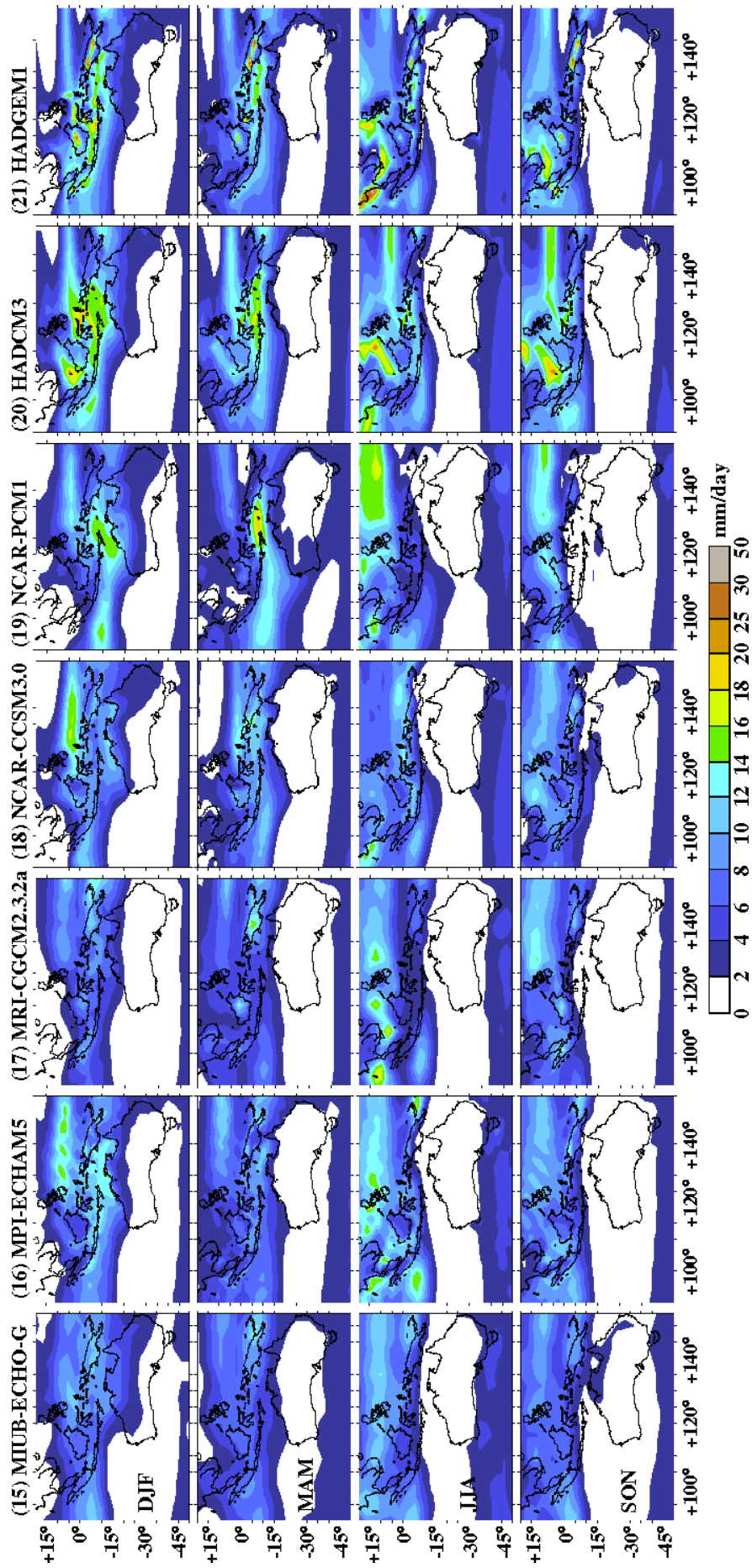


Figure 3.3: Seasonal rainfall climatology of twenty-one CMIP3 GCMs (1979-1999 periods) (continued from previous page).

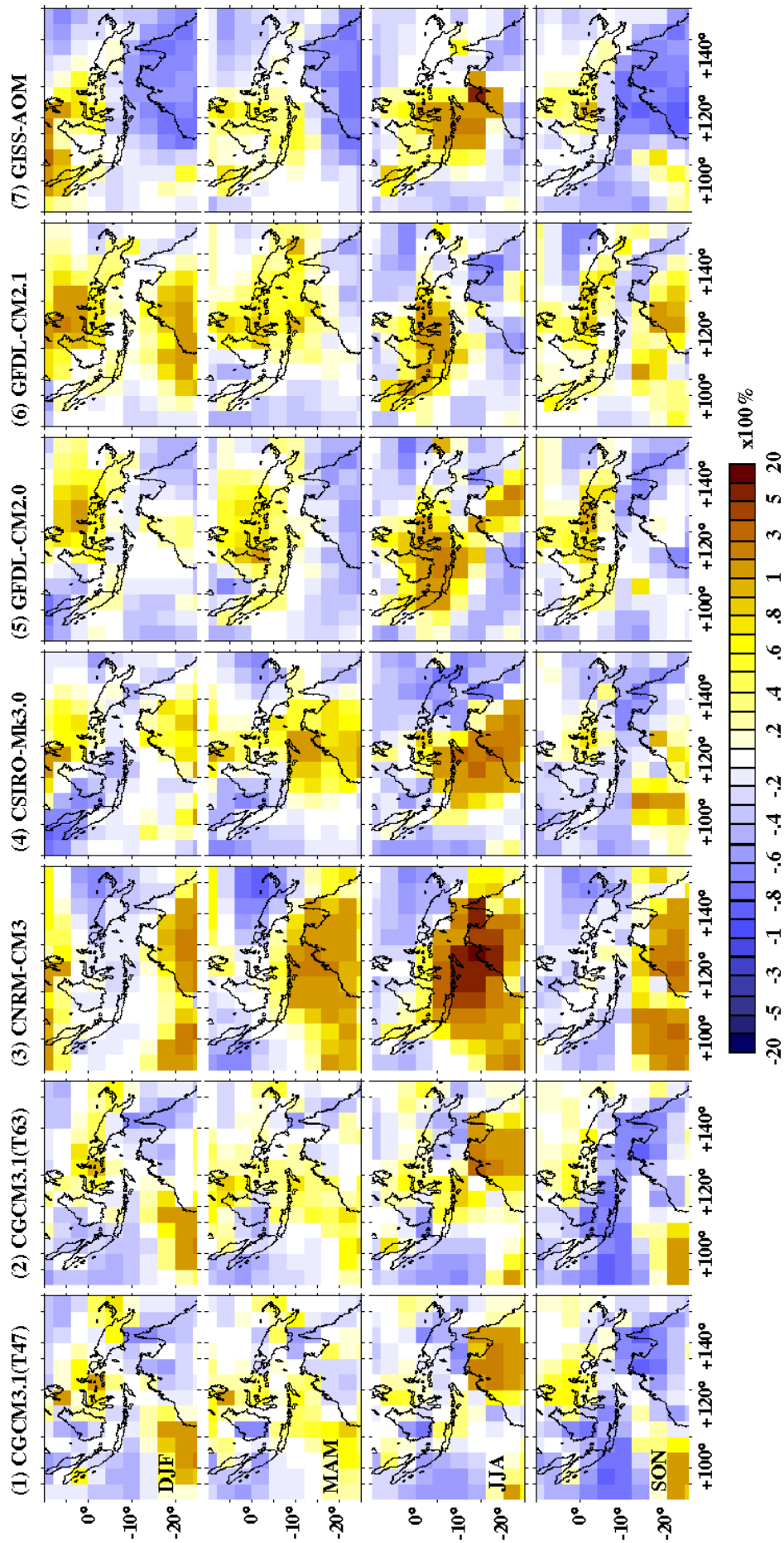


Figure 3.4: Seasonal rainfall anomalies for the period 1979-1999 (in percent (%)).

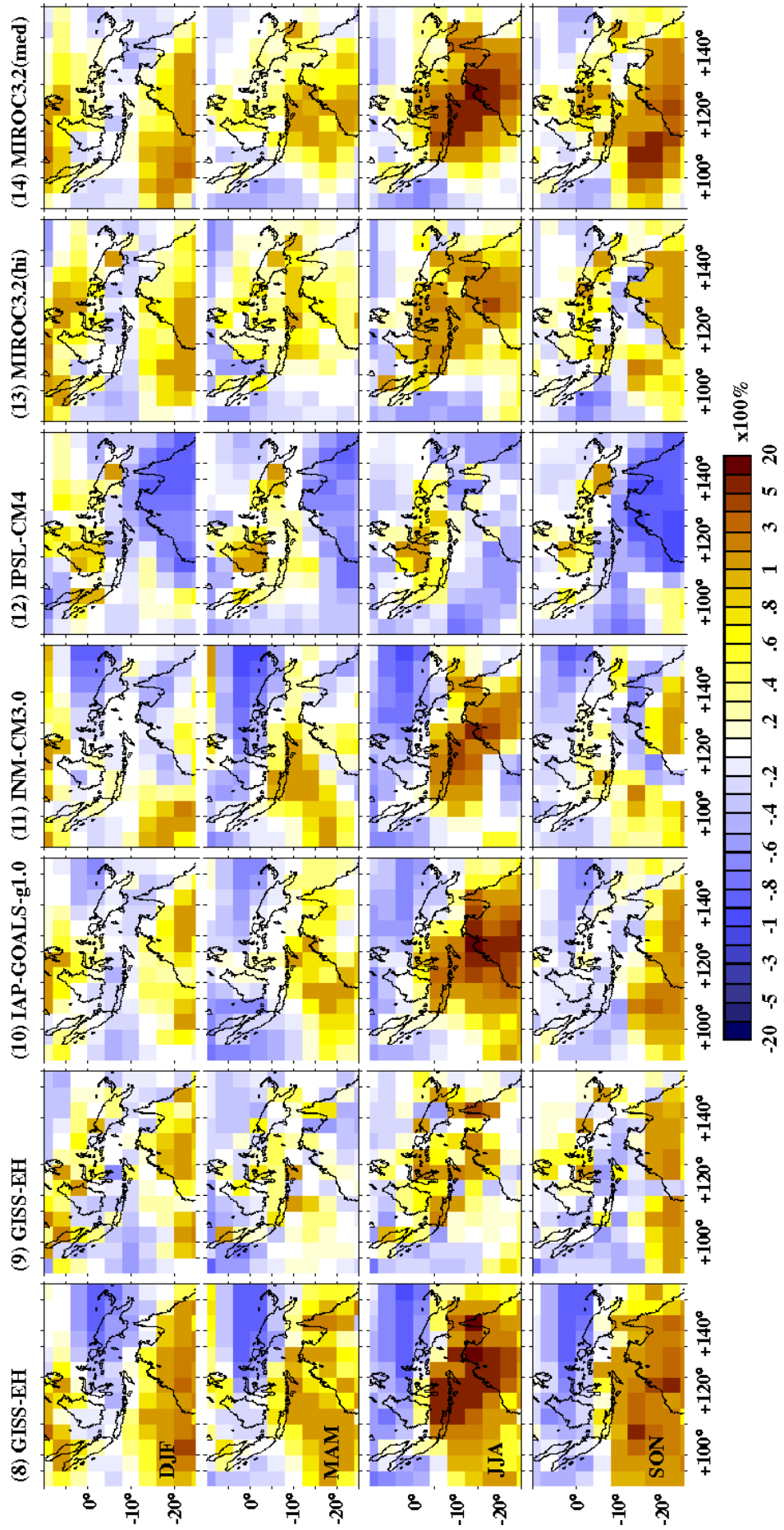


Figure 3.4: Seasonal rainfall anomalies for the period 1979-1999 (in percent (%)) (continued from previous page).

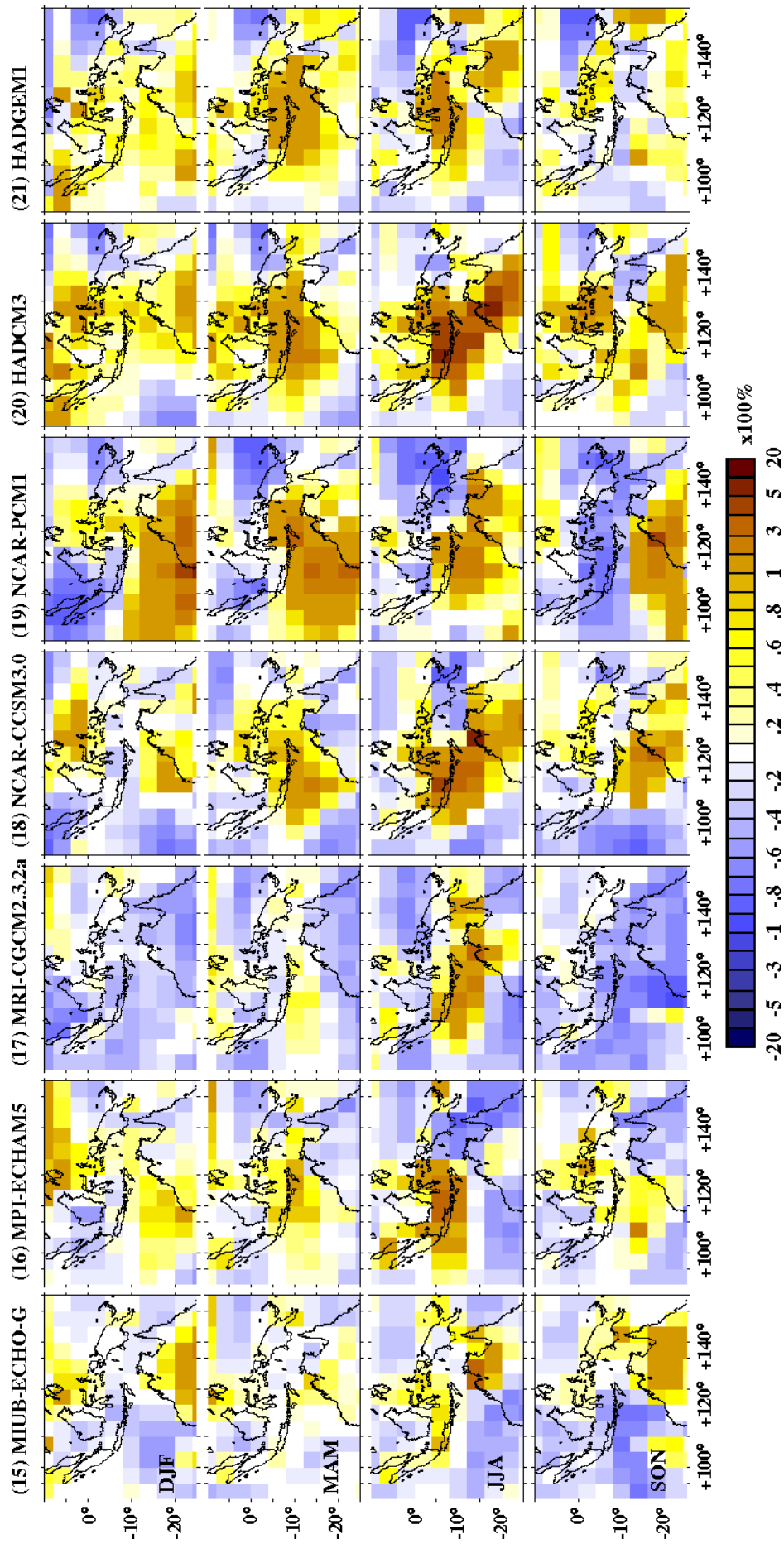


Figure 3.4: Seasonal rainfall anomalies for the period 1979-1999 (in percent (%)) (continued from previous page).

### 3.3.1 Land and ocean rainfall

#### 3.3.1.1 Differences of seasonal rainfall climatology

Figure 3.4 shows the relative differences of seasonal rainfall climatology between the modelled and the observed data (in percent; %). It provides quantitative measurement of rainfall bias that is useful to identify unrealistic rainfall distribution in the region. For consistency, the study follows the approach used by Vera et al. (2006) by converting the grid into the coarsest resolution ( $5^{\circ} \times 4^{\circ}$  grid resolution) of any of the datasets compared. Re-gridding the data onto coarse resolution is chosen in this study to avoid the potency of more unwanted biases as a result of interpolation if the grid is changed onto higher resolution.

The main problem of simulating tropical rainfall such as in Indonesia and northern Australia is related to intrinsic atmospheric model error (Lin 2007). The double-ITCZ effect propagates unrealistic rainfall to the north of the Equator during DJF and south of the Equator during JJA. This can be identified from Figure 3.4 when overestimated rainfall distribution is found in the opposite part of the Equator where the monsoon propagation occurs. Alternatively, it can also be identified when the region simultaneously experiences overestimated rainfall proportions over north and south of the Equator. Several models such as CNRM-CM3 (3), CSIRO-Mk3.5 (4), GFDL-CM2.1 (6), GISS\_EH (8), INM-CM3.0 (11), MIROC3.2 (13, 14), NCAR-CCSM3.0 (18), HADCM3 (20) and HADGEM1 (21) also experience excessive rainfall over southern Indonesia and northern Australia in MAM and/or SON.

In particular for the DJF season, more than half of the assessed models demonstrate excessive rainfall (up to twice of the observed data), particularly north of the equator (Figure 3.4). These problems cause considerable under- or overestimation for the northern Australian rainfall, depending on the model. These are related to unrealistic spatial propagation of the ITCZ during the season, such as (i) average positions too far north (GISS-AOM (7) and IPSL-CM4 (12)), (ii) narrowing (MRI-CGCM2.3.2 (17)), or (iii) the widening (most models) of the meridional ITCZ that leads to increased rainfall over northern Australia, particularly in the west part of the region.

It is commonly found that the timing and the magnitude of monsoonal transitions are poorly captured by the models that suffer from the double-ITCZ problem. Consequently, prolonged rainfall during MAM and an early monsoon onset in SON are sometimes reproduced by those models. Another common problem is consistent underestimation of seasonal rainfall over the Western Pacific, which is found in CNRM-CM3 (3), GISS-EH (8), INMCM3.0 (11) and NCAR-PCM1 (19). Nevertheless, several models including CGCM3.1 (1, 2), GFDL (5, 6), ECHO-G (15) and MRI-CGCM2.3.2 (17) perform reasonably well in simulating realistic rainfall differences of less than 100%.

Unrealistic rainfall simulated south of the equator during JJA leads to rainfall overestimations across southern Indonesia and northern Australia, particularly around Java, Bali and Nusa Tenggara, and some parts of the Northern Territory. This problem is described in more than half of the assessed models and is notably found in CNRM-CM3 (3), GISS-EH (8), GOALS-g1.0 (10), MIROC3.2 (13, 14), and UKMO-HADCM3 (20). It should be carefully noted that a large percentage of rainfall anomalies are likely due to seasonally dry condition found in the observed

data, creating large differences when the model reproduces excessive rainfall in the region.

### 3.3.1.2 Ranking the models: Cumulative Absolute Differences (CAD)

Selecting the models is important for future rainfall assessment. In this section the models are ranked based on summary statistics calculated from the accumulated differences in seasonal time series data over the period of 1979 to 1999 between simulated and observed seasonal rainfall (cumulative absolute difference, *CAD*). The *CAD* values are calculated for seasonal ( $CAD_S$ , Equation 3.1) as well as for annual rainfall ( $CAD_T$ , Equation 3.2) for the entire land and ocean area across the region of interest from the following relationship:

$$CAD_{S_k} = \sum_i^m \sum_j^n AD_{ij} \quad (3.1)$$

and

$$CAD_T = \sum_{k=1}^s CAD_{S_k} \quad (3.2)$$

where  $CAD_S$  = seasonal absolute cumulative difference between simulated and observed seasonal rainfall time series (*AD*) from year *i* at land and ocean grid point *j*, and  $CAD_T$  = total  $CAD_S$  at all season *k*; *i* = 1979, 1980, ..., *m*=1999; *j* = 1, 2, ..., *n*=104; and *k* = 1(DJF), 2(MAM), 3(JJA), *s*=4(SON).

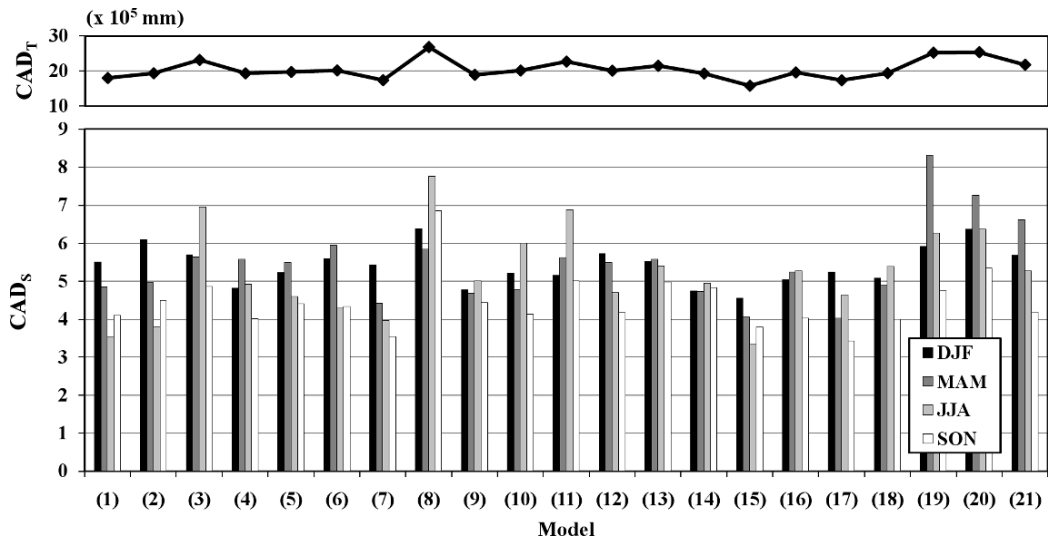


Figure 3.5: Cumulative Absolute Differences (*CAD*) from seasonal ( $CAD_S$ ) (below) and annual ( $CAD_T$ ) (top) time series (1979-1999 periods) from twenty-one CMIP3 GCMs (1979-1999 periods). See Table 2.1 to match model numbers with model names.

The summary statistics of *CAD* provides a simple and robust method to rank the models in terms of their ability to simulate absolute rainfall amounts. The smaller the *CAD* value, the smaller the difference between modelled and observed data indicating a more realistic performance (Figure 3.5). The *CAD* value formulated in this study depends on the length of data (*m*) and the number of grid points (*n*) used in the calculation. This means that a longer period of data with a higher grid resolution

used in the calculation will result in a higher  $CAD$  value. Therefore, the accumulated absolute rainfall difference ( $CAD$ ; unit in millimetres (mm)) does not represent the real rainfall discrepancy, but can be used as a parameter to determine which model shows the least deviation from measured data.

Figure 3.5 shows seasonal  $CAD$  values ( $CAD_S$ ; below) and total annual  $CAD$  values ( $CAD_T$ ; top). The ECHO-G (15) model is the best model with the smallest  $CAD_S$  in DJF and JJA seasons with a total value of  $4.55 \times 10^5$  mm and  $3.35 \times 10^5$  mm, respectively. In the transition seasons (MAM and SON), the best model is MRI-CGCM2.3.2 (17) with respective values of  $4.02 \times 10^5$  mm and  $3.42 \times 10^5$  mm. In the overall assessment based on  $CAD_T$ , both models are consistently ranked better than other models. The ECHO-G is positioned in the first place with the lowest  $CAD_T$  while the MRI-CGCM2.3.2 model is next. The accumulated discrepancies in seasonal time series data ( $CAD_S$ ) is consistent with the climatology presented in the previous subsection. The two models are also capable of simulating the meridional rainfall propagation in the region and positioning high rainfall during DJF and JJA seasons (*see* Figure 3.2).

The model ranked consistently last is GISS-EH (8) with the largest  $CAD_S$  in most of the seasons, except for MAM season.  $CAD_T$  also places this model last with a total highest value of  $26.84 \times 10^5$  mm. In contrast, another variant of the GISS model (GISS-ER (9)) coupled with a different ocean component (Russell et al. 1995; Russell et al. 2000) performs much better with  $CAD_S < 5 \times 10^5$  mm in all seasons (note that GISS-EH (8) with HYCOM ocean component (Bleck 2002) has  $CAD_S > 5 \times 10^5$  mm in all seasons). The GISS-ER (9) simulates better spatial rainfall patterns in the region (*see* Figure 3.3 and 3.4 for both models). The cause of the mismatch following a change of the ocean component is probably due to the difference in the simulated SST patterns. These patterns determine the atmospheric circulation and precipitation (IPCC 2007) as well as the strength of coupling between local SST and tropical convection (Dai 2006) forcing the double-ITCZ formations (Lin 2007).

### 3.3.2 Land only (terrestrial) rainfall

#### 3.3.2.1 Differences in seasonal rainfall climatology

Evaluating the simulated terrestrial rainfall for Austral-Indonesia is challenging due to the uniqueness of its land-sea distribution being represented differently by climate models. The horizontal resolutions among the latest generation of GCMs vary from  $5.0^\circ \times 4.0^\circ$  to  $1.125^\circ \times 1.125^\circ$  (T106), resulting in different land-sea mask representation for the region (*see* Table 2.1 and Figure 2.3). For this terrestrial rainfall comparison, an evaluation approach that considers the models' resolution and land-sea mask representation from each model needs to be adopted.

This study purposely up-scales the observed data from the CRU TS2.1 dataset that has  $0.5^\circ \times 0.5^\circ$  grid resolution in order to match the resolution of each model. This method differs from the approach used previously where all the observed and modelled data were converted into the coarsest model resolution. The reason for this is to keep the actual representation of the land-sea mask distribution defined by the land area fraction data intact for each model (IPCC terminology for this parameter is SFTLF) (*see* Figure 2.3). Here "land area" is defined as any grid point that contains at least 10% of land area.

Figure 3.6 shows seasonal rainfall climatology differences calculated by retaining the actual models' resolution (in percent; %). In general, the results are similar to Figure 3.4, particularly for northern Australia. However, for the Indonesian region, where most of the islands are too small to feature properly in climate models, such assessments are critically important. It will assist in understanding the models' capability in providing rainfall simulations for land area in the region that can be used for advanced studies.

Results show that all models under- or overestimate terrestrial rainfall over most of the region, with different percentages between western and eastern regions. The problem is presumably related to zonally asymmetric rainfall propagation as a result of excess double-ITCZ rainfall in only some parts of the region and/or an extension of dry area due to the failure of modelling of large scale convection in the western Pacific warm pool. The related problems seem to be specific for every model. In many models, the western area of northern Australia exhibits more rainfall than its eastern part. This is also similar in the west of southern Indonesia. This study also reveals that most of the rainfall overestimations occurred during the JJA period (in more than 70% of the models) with excessively high rainfall evident in CNRM-CM3 (3), IAP-FGOALS (10), MIROC3.2 (13, 14), and HadCM3 (20).

Classic problems associated with coarse horizontal grid resolution result in most models' failure to adequately simulate terrestrial rainfall in this region. Coarse resolution models have difficulties simulating the temporal-meridional movement of monsoonal convection. Therefore, more attention should be paid to models with better resolution, such as MIROC3.2 (hires) (13) and UKMO-HADGEM1 (21), which are able to represent the land distribution fairly over the region. The extreme rainfall is mostly in tolerable discrepancies, except for the rainfall discrepancies over the southern hemisphere (southern Indonesia and northern Australia) during JJA season, where problems are caused by a false meridional rainfall propagation.

This study suggests that creating a finer model resolution to simulate the climate over the region is essential. In addition to the improvement of model resolution, enhanced representation of meridional tropical SST (Chung & Ramanathan 2007) is also important to advance terrestrial rainfall simulation. This will reproduce better coupling between local SST and tropical convection (Dai 2006) and can reduce the double-ITCZ problem (Lin 2007).

### **3.3.2.2 *Ranking the models: Cumulative Distribution Function (CDF)***

Different approaches have been used to assess the seasonal climatology differences in terrestrial rainfall. Contrasting model resolutions maintained in the previous analysis also require different methods for assessing their qualities based on the seasonal time series data. Considering the previous simple CAD method that requires the same number of grids in its calculations for each model, the method is inapplicable for assessing terrestrial rainfall. Given that this study is particularly interested in knowing how well the models simulate regional rainfall distributions, empirical cumulative distribution function (CDF) of simulated seasonal rainfall with the observed CRU TS2.1 data are compared (Figure 3.7).

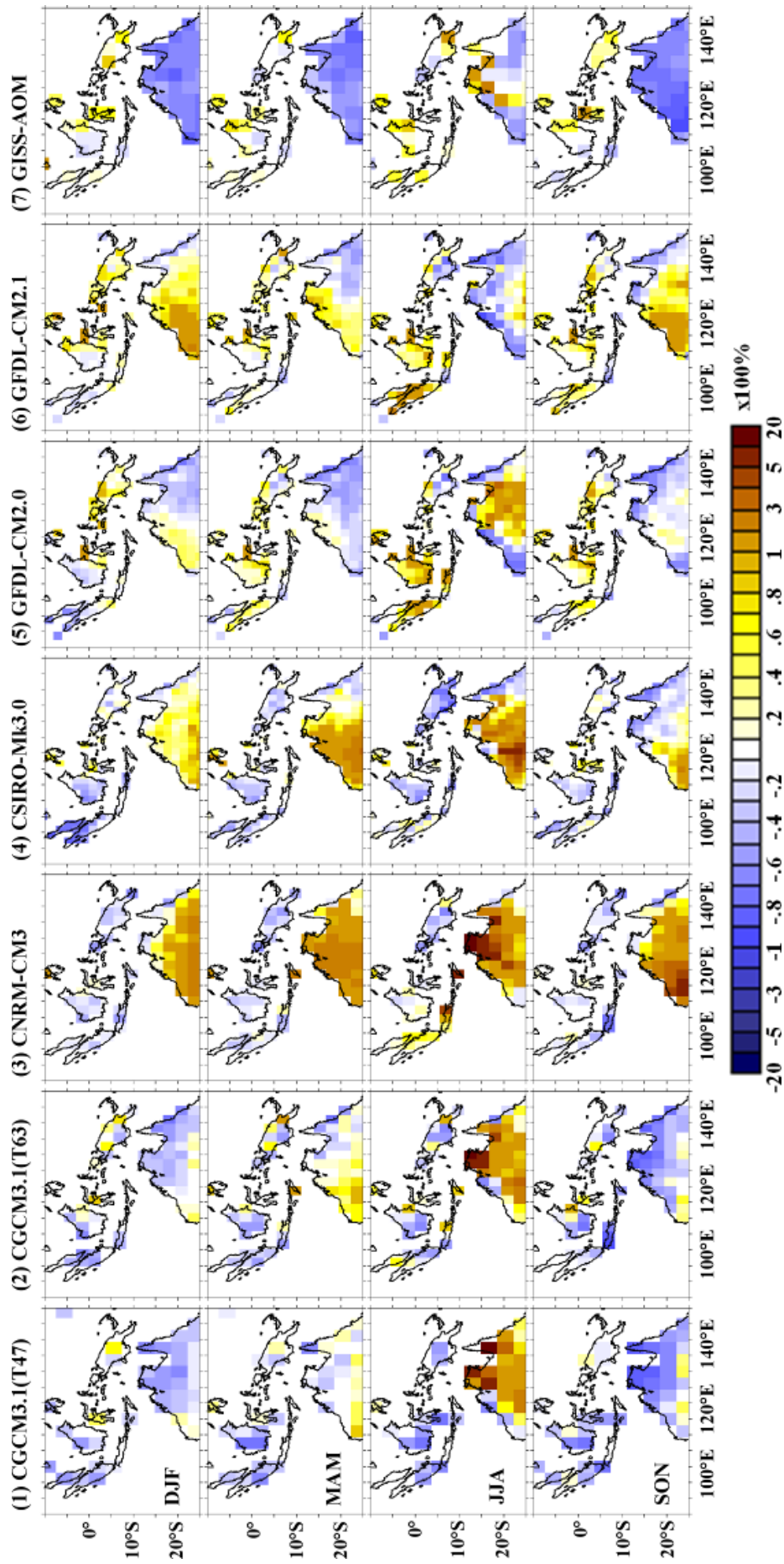


Figure 3.6: Seasonal differences in rainfall climatology over land area only from twenty-one CMIP3 GCMs (1979-1999 periods).

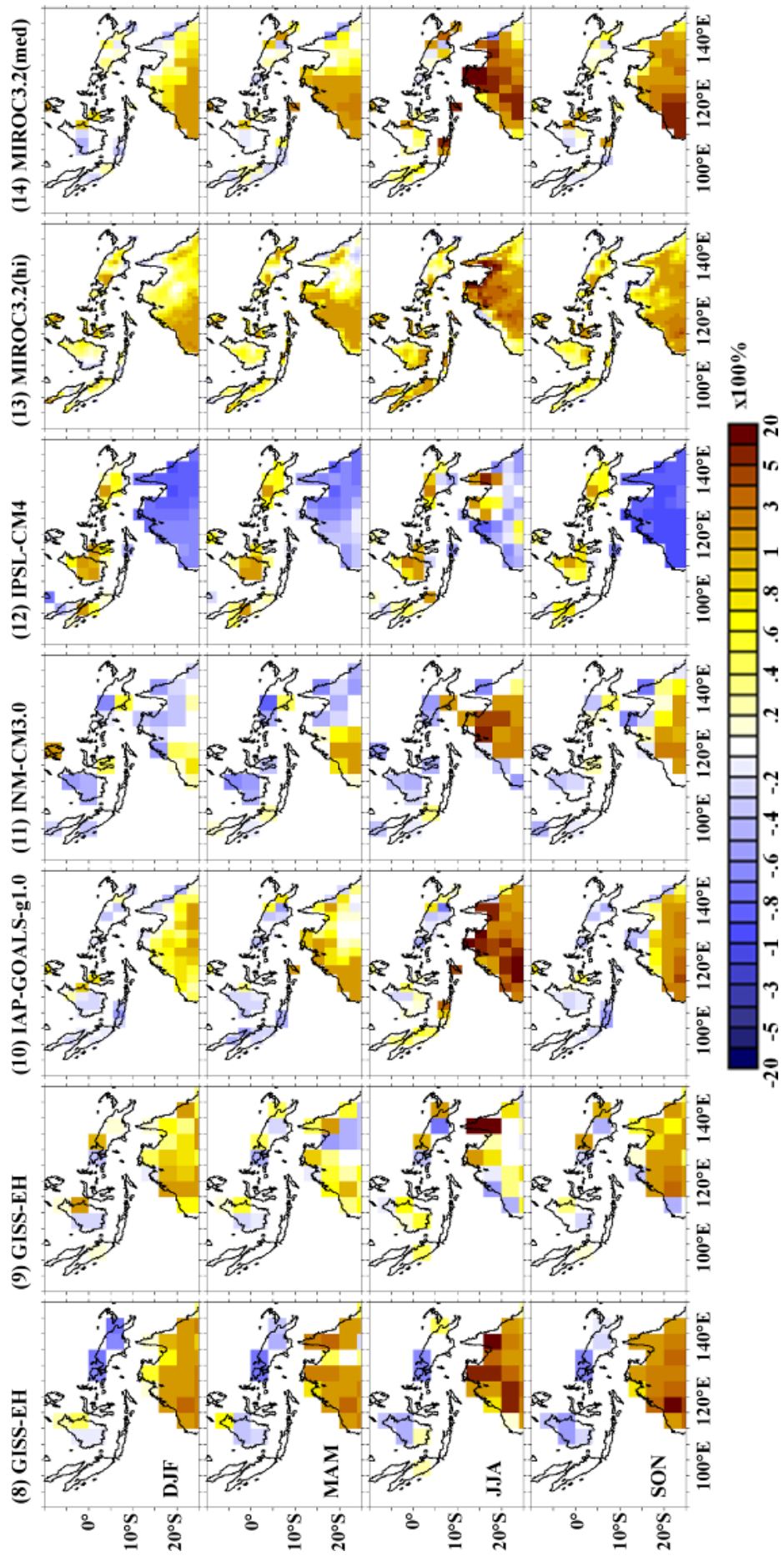


Figure 3.6: Seasonal differences in rainfall over land area only from twenty-one CMIP3 GCMs (1979-1999 periods) (continued) from previous page).

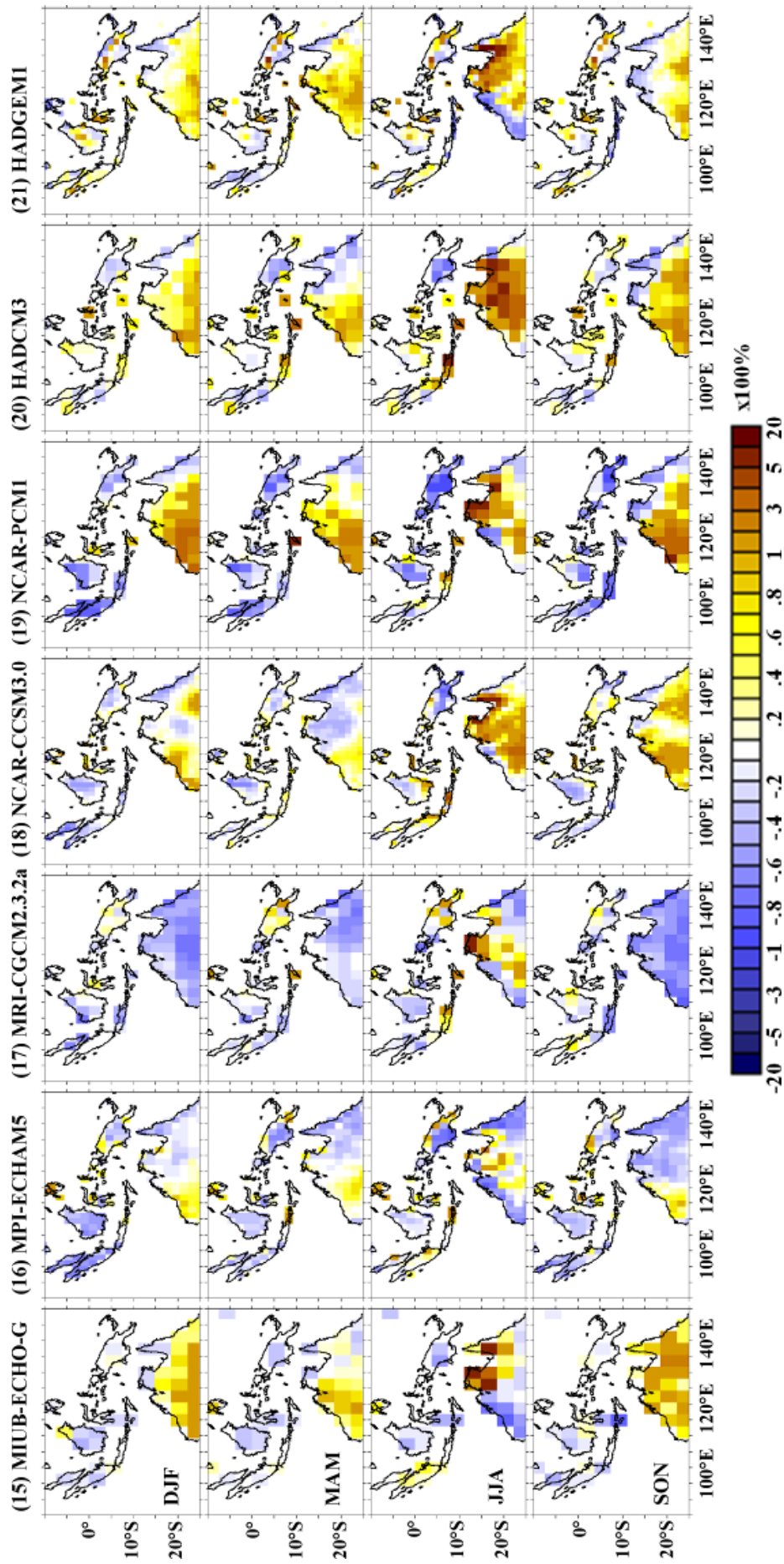


Figure 3.6: Seasonal differences in rainfall climatology over land area only from twenty-one CIMP3 GCMs (1979-1999 periods) (continued) from previous page).

Assessments using CDFs are provided for each season, as well as for the overall studied region, and separately for Indonesia and northern Australia. The seasonal time series data reference set (observations) cover the period from 1979 to 1999. Following the method to define the terrestrial rainfall grids from each model, the actual representation of land-sea mask distribution is also defined by the land area fraction data individually obtained from each model (*see* Figure 2.3). In this assessment, the grid resolution of the CRU TS2.1 dataset is retained. The study uses Kolmogorov-Smirnov Distance ( $KSDist$ ) as a measure to compare the absolute differences between CDFs from the modelled and the observed data (*see* Chapter 2 on methodology).

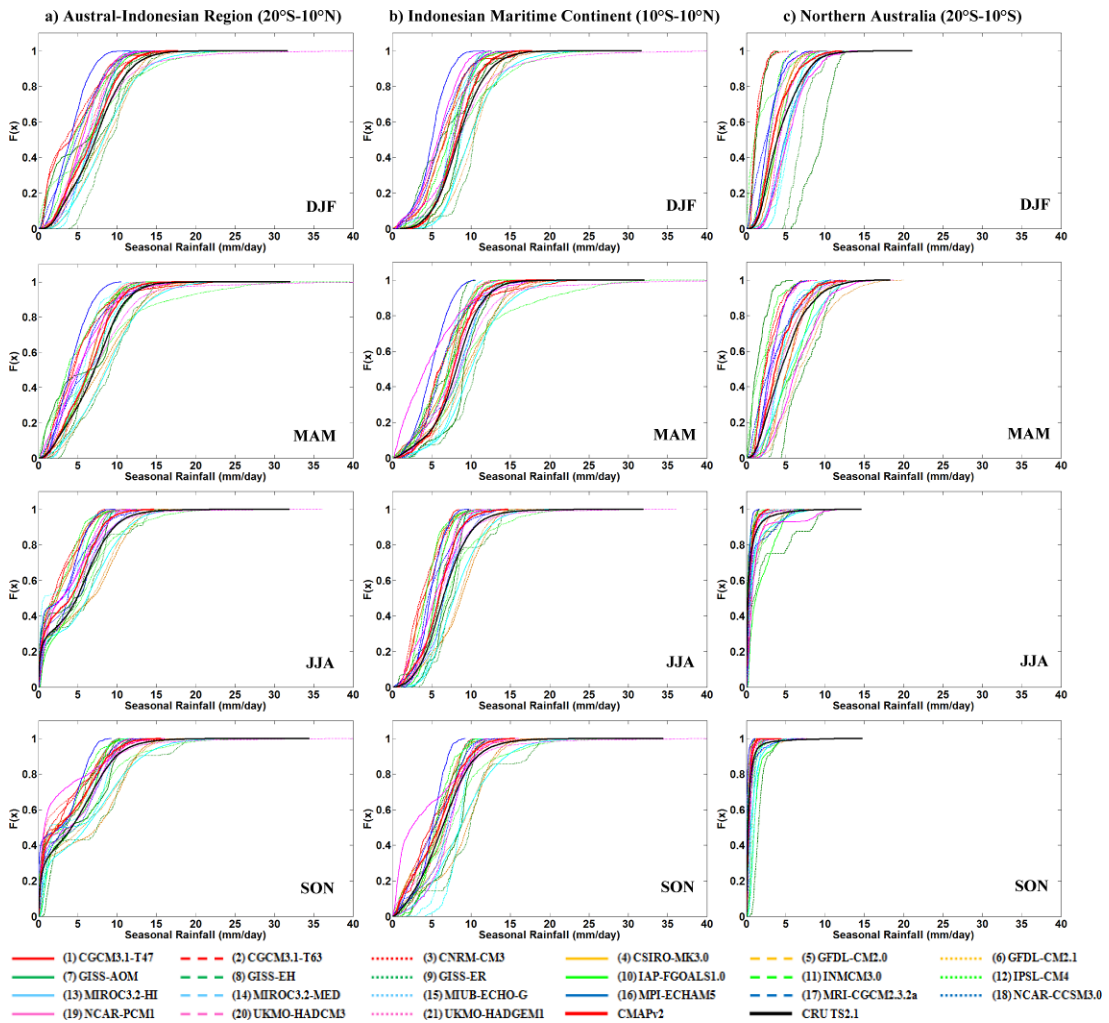


Figure 3.7: Cumulative Distribution Functions (CDF) of seasonal rainfall series (1979-1999 periods) from twenty-one CMIP3 models and CRU TS2.1 gridded observational data for a) the Austral-Indonesian region, b) Indonesia, and c) northern Australia.

The results of the KS-test presented in Table 3.1 show that only two pairs of tested models had  $p > 0.01$ . Those models are CNRM-CM3 (3) for Indonesia during SON and HADCM3 (20) for northern Australia during JJA, with respective  $p$  of 0.037 and 0.015. Therefore, most of the simulated rainfall distributions differ significantly ( $p < 0.05$ ) with very strong evidence of bias. These can be clearly seen in Figure 3.7 from the CDFs of most of the models that deviate considerably from the observed CDFs.

Table 3.1: *P*-values (*p*) resulted from KS-test of twenty-one CMIP3 models.

No.	Model	Austral-Indonesia (20°S-10°N)				Indonesian (10°S-10°N)				Northern Australia (20°S-10°S)			
		DJF	MAM	JJA	SON	DJF	MAM	JJA	SON	DJF	MAM	JJA	SON
1	CGCM3.1(T47)	< 0.01	< 0.01	< 0.01	< 0.01	< 0.01	< 0.01	< 0.01	< 0.01	< 0.01	< 0.01	< 0.01	< 0.01
2	CGCM3.1(T63)	< 0.01	< 0.01	< 0.01	< 0.01	< 0.01	< 0.01	< 0.01	< 0.01	< 0.01	< 0.01	< 0.01	< 0.01
3	CNRM-CM3	< 0.01	< 0.01	< 0.01	< 0.01	< 0.01	< 0.01	< 0.01	<b>0.037</b>	< 0.01	< 0.01	< 0.01	< 0.01
4	CSIRO-Mk3.0	< 0.01	< 0.01	< 0.01	< 0.01	< 0.01	< 0.01	< 0.01	< 0.01	< 0.01	< 0.01	< 0.01	< 0.01
5	GFDL-CM2.0	< 0.01	< 0.01	< 0.01	< 0.01	< 0.01	< 0.01	< 0.01	< 0.01	< 0.01	< 0.01	< 0.01	< 0.01
6	GFDL-CM2.1	< 0.01	< 0.01	< 0.01	< 0.01	< 0.01	< 0.01	< 0.01	< 0.01	< 0.01	< 0.01	< 0.01	< 0.01
7	GISS-AOM	< 0.01	< 0.01	< 0.01	< 0.01	< 0.01	< 0.01	< 0.01	< 0.01	< 0.01	< 0.01	< 0.01	< 0.01
8	GISS-EH	< 0.01	< 0.01	< 0.01	< 0.01	< 0.01	< 0.01	< 0.01	< 0.01	< 0.01	< 0.01	< 0.01	< 0.01
9	GISS-ER	< 0.01	< 0.01	< 0.01	< 0.01	< 0.01	< 0.01	< 0.01	< 0.01	< 0.01	< 0.01	< 0.01	< 0.01
10	GOALS-g1.0	< 0.01	< 0.01	< 0.01	< 0.01	< 0.01	< 0.01	< 0.01	< 0.01	< 0.01	< 0.01	< 0.01	< 0.01
11	INM-CM3.0	< 0.01	< 0.01	< 0.01	< 0.01	< 0.01	< 0.01	< 0.01	< 0.01	< 0.01	< 0.01	< 0.01	< 0.01
12	IPSL-CM4	< 0.01	< 0.01	< 0.01	< 0.01	< 0.01	< 0.01	< 0.01	< 0.01	< 0.01	< 0.01	< 0.01	< 0.01
13	MIROC3.2(hires)	< 0.01	< 0.01	< 0.01	< 0.01	< 0.01	< 0.01	< 0.01	< 0.01	< 0.01	< 0.01	< 0.01	< 0.01
14	MIROC3.2(medres)	< 0.01	< 0.01	< 0.01	< 0.01	< 0.01	< 0.01	< 0.01	< 0.01	< 0.01	< 0.01	< 0.01	< 0.01
15	ECHO-G	< 0.01	< 0.01	< 0.01	< 0.01	< 0.01	< 0.01	< 0.01	< 0.01	< 0.01	< 0.01	< 0.01	< 0.01
16	ECHAM5/MPI-OM	< 0.01	< 0.01	< 0.01	< 0.01	< 0.01	< 0.01	< 0.01	< 0.01	< 0.01	< 0.01	< 0.01	< 0.01
17	MRI-CGCM2.3.2	< 0.01	< 0.01	< 0.01	< 0.01	< 0.01	< 0.01	< 0.01	< 0.01	< 0.01	< 0.01	< 0.01	< 0.01
18	CCSM3	< 0.01	< 0.01	< 0.01	< 0.01	< 0.01	< 0.01	< 0.01	< 0.01	< 0.01	< 0.01	< 0.01	< 0.01
19	PCM	< 0.01	< 0.01	< 0.01	< 0.01	< 0.01	< 0.01	< 0.01	< 0.01	< 0.01	< 0.01	< 0.01	< 0.01
20	UKMO-HADCM3	< 0.01	< 0.01	< 0.01	< 0.01	< 0.01	< 0.01	< 0.01	< 0.01	< 0.01	< 0.01	<b>0.015</b>	< 0.01
21	UKMO-HADGEM1	< 0.01	< 0.01	< 0.01	< 0.01	< 0.01	< 0.01	< 0.01	< 0.01	< 0.01	< 0.01	< 0.01	< 0.01

The UKMO-HADGEM1 (21) model has the best performance in simulating terrestrial rainfall distribution based on the *KSDist* criteria ( $\leq 0.1$ ). The model consistently performs better than any other model for the whole region for all seasons and for particular seasons on a region specific analysis. In addition, the model is also able to reproduce the probability of extreme rainfall. These consistent achievements indicate an improvement of the model (Johns et al. 2004) compared to its predecessor the HadCM3 (20) model (Gordon et al. 2000; Pope et al. 2000).

Given that the conventional *p*-value threshold ( $\alpha$  level) of 0.05 or 0.01 used by the KS-test appears to be too stringent to be useful for this study,  $KSDist \leq 0.1$  is defined to constitute ‘adequate’ model performance (Figure 3.8). This is appropriate, given that statistics need to serve the purpose of the investigation (Nicholls 2001). It should be noted that the relationship between *KSDist* and *p* is non-linear, although there seems to be a strong opposite relationship between them. In order to represent a ‘good’ model, one would expect a lower *KSDist*, so the similarity of continuous rainfall distribution will be higher. Based on this metric, assessment for the entire region shows that only the UKMO-HADGEM1 (21) had consistently low *KSDist* values for all seasons ( $KSDist \leq 10\%$ ), while other models only performed adequately in particular seasons. Those models are MIROC3.2-med (14) in MAM, IPSL-CM4 (12) in JJA and MRI-CGCM2.3.2a (17) in SON.

Separate analysis based on the *KSDist* value for the Indonesian region shows that the UKMO-HADGEM1 (21) performs best with  $KSDist \leq 0.1$  in all seasons, except in MAM. Other models that perform relatively well for this particular region are CCSM3.0 (18) in MAM and JJA, UKMO-HADCM3 (20) only in MAM, and IPSL-CM4 (12) only in JJA. Meanwhile, separate analysis for northern Australia shows that only UKMO-HADGEM1 (21) simulates better terrestrial rainfall distribution during MAM and SON with  $KSDist \leq 0.1$ .

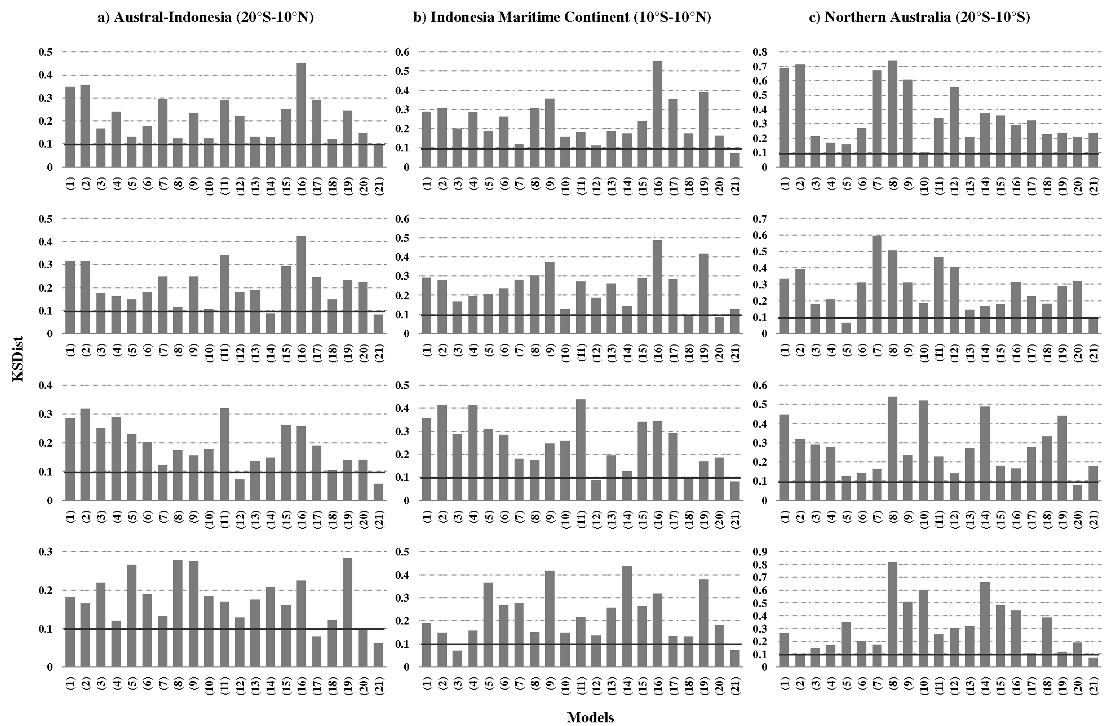


Figure 3.8: Vertical distance (*KSDist*) between rainfall cumulative distributions (*CDF*) derived from simulated and *CRU TS2.1* datasets for a) Austral-Indonesia ( $90^{\circ}\text{E}$ - $155^{\circ}\text{E}$ ,  $20^{\circ}\text{S}$ - $10^{\circ}\text{N}$ ), b) Indonesia maritime continent ( $90^{\circ}\text{E}$ - $155^{\circ}\text{E}$ ,  $10^{\circ}\text{S}$ - $10^{\circ}\text{N}$ ), and c) northern Australia ( $90^{\circ}\text{E}$ - $155^{\circ}\text{E}$ ,  $20^{\circ}\text{S}$ - $10^{\circ}\text{S}$ ). Horizontal lines correspond to threshold with  $KSDist=0.10$ .  $KSDist \leq 0.10$  is used as a threshold of 'no difference' between *CDF* to indicate 'good' model performance.

### 3.4 Assessment of rainfall variability and trends

#### 3.4.1 Interannual rainfall variability

In the previous section the simulated monthly and seasonal rainfall were assessed. Several problems and recommendations were identified for the region. Another issue found in the modelled tropical rainfall is inaccurate association with ENSO. Recent studies suggest that the problem is likely due to the strong coupling of local SST with tropical convections (Dai 2006) and insufficient equatorial Pacific rainfall (Lin 2007). Given that the ENSO has a leading role in impacting interannual rainfall variability, investigating the simulated Austral-Indonesian rainfall sensitivity to this climate driver is important. Hence, interannual variability of simulated rainfall based on their response to ENSO events is compared to the observed data. Despite the fact that the impact of ENSO on rainfall variability varies between areas across the region (Aldrian et al. 2003; Chang et al. 2004), the average response to the impact of ENSO is significant.

Figure 3.9 provides a brief demonstration associated with the significant range of interannual rainfall variability resulted from the models in contrast to observations. For more details, each model is individually analysed in order to identify the best performing model in reproducing interannual rainfall variability on seasonal data. Here, the spatially averaged seasonal land and ocean rainfall from the models are assessed against the observed CMAP data for the period of 1979-1999. During this

period, six warm ENSO events occurred in every season, while five cold ENSO events occurred in DJF, three in MAM and JJA, and six in SON season (*see* Figure 3.10). The study uses the definition of ENSO episodes adopted by the Climate Prediction Center (CPC-NOAA) based on a 3-month running mean of sea surface temperature (SST) anomalies in the Niño 3.4 region above or below 0.5 (the data was downloaded from [http://www.cpc.noaa.gov/products/analysis\\_monitoring/ensostuff/ensoyears.shtml](http://www.cpc.noaa.gov/products/analysis_monitoring/ensostuff/ensoyears.shtml)).

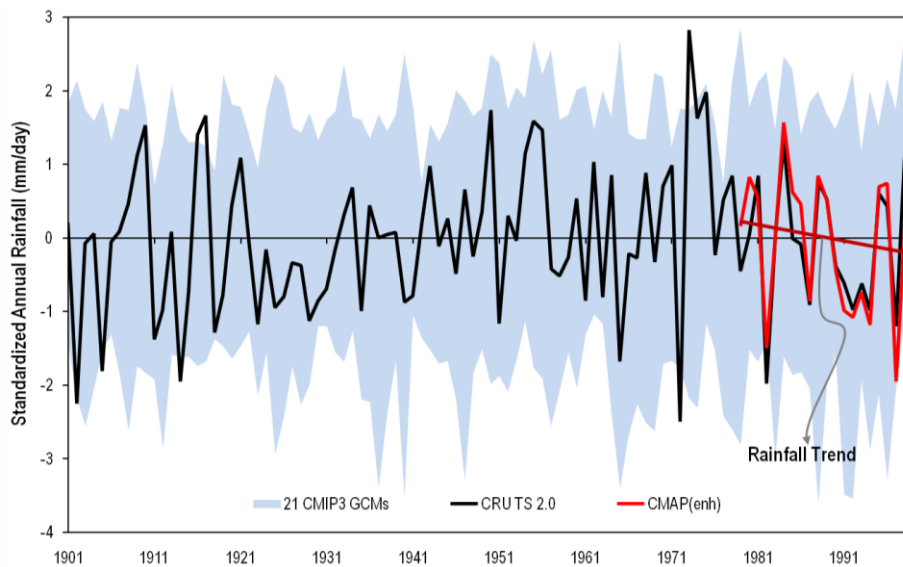


Figure 3.9: Interannual variability and trend of annual terrestrial rainfall over the Austral-Indonesian region.

To evaluate the interannual variability of simulated rainfall compared to the observed data, the study uses the correlation coefficient ( $r$ ) and RMSE diagram calculated from the standardised rainfall anomalies (*see* Chapter 2). The method is similarly used in Section 3.2, except that for the present calculations it uses standardised anomaly data for  $r$  and RMSE estimates. Calculating RMSE from the standardised anomalies is most likely to create an inverse linear relationship with  $r$ , where the highest correlation corresponds to the lowest RMSE and can be considered as ‘the best’ model. Therefore, the diagram created by these metrics solely considers the degree of similarity between variability from the modelled and observed data constituted by the  $r$ -value. Nevertheless, the diagram simplifies the visualisation that is useful for assessing the models’ capability in simulating the interannual rainfall variability.

Figure 3.10a shows that most models do not simulate interannual rainfall variability well. The models tend to represent below (above) normal rainfall during warm ENSO (cold ENSO) episodes that deviate considerably from observation. In Figure 3.10b, it is found that two models (i.e. GISS-ER (9) and UKMO-HADCM3 (20)) in DJF, one model (INM-CM3.0 (11)) in MAM and another model (ECHAM5/MPI-OM (16)) in SON that are significantly correlated at 5% significance level. These results show that most models are unable to adequately simulate interannual rainfall variability in the region. In Figure 3.10b, about half of the models correlate negatively with observed rainfall, resulting in an incorrect correlation with ENSO as indicated by (Dai 2006). Despite of this dispute, it is likely that the unrealistic interannual rainfall variability caused by the teleconnection process driven by

unrealistic Indo-Pacific climate drivers such as ENSO and IOD as simulated by most models (Cai et al. 2009).

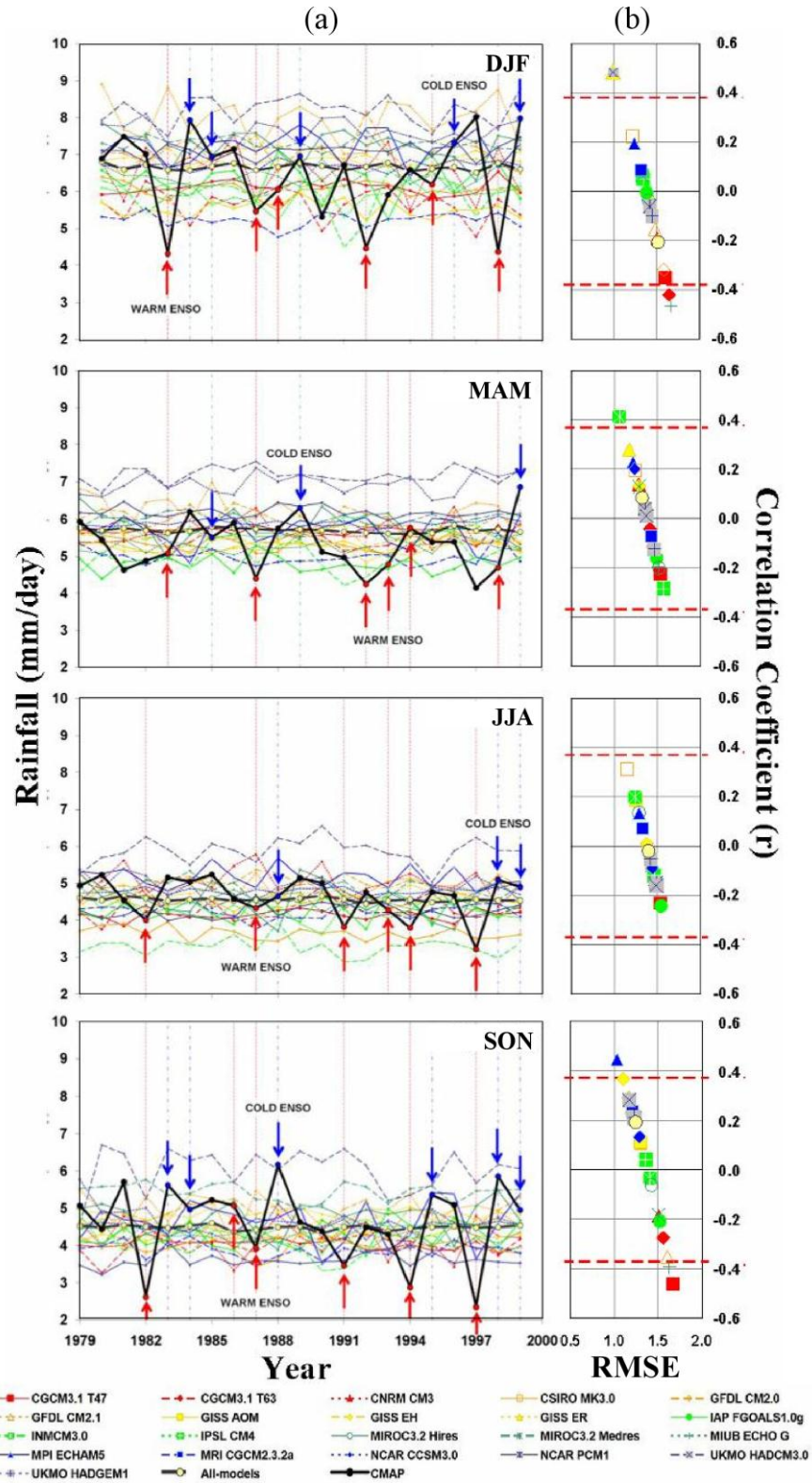


Figure 3.10: Interannual variability of seasonal rainfall of twenty-one CMIP3 GCMs and observed CMAP data: a) temporal variation of spatially averaged data (raw data; in mm), and b)  $r$  and RMSE diagram calculated from standardised data. Red dash-line is confidence bound at 5% significance level.

### 3.4.2 Rainfall trends

Table 3.2: Trends ( $m$ ) of seasonal rainfall data from climate models and observation during late 20th century (1979-1999)

No	Data (Model)	DJF	MAM	JJA	SON
<b>A</b>	<b>CMAP (obs)</b>	<b>-0.011</b>	<b>-0.007</b>	<b>-0.026</b>	<b>-0.024</b>
<b>B</b>	<b>All-models</b>	<b>-0.003</b>	<b>-0.003</b>	<b>-0.003</b>	<b>-0.002</b>
1	CGCM3.1(T47)	0.001	0.001	0.004	-0.008
2	CGCM3.1(T63)	-0.013	-0.018	0.006	0.008
3	CNRM-CM3	-0.019	0.008	-0.009	-0.009
<b>4</b>	<b>CSIRO-Mk3.0</b>	<b>-0.005</b>	<b>-0.007</b>	<b>-0.011</b>	<b>-0.004</b>
5	GFDL-CM2.0	-0.006	-0.017	-0.005	0.000
<b>6</b>	<b>GFDL-CM2.1</b>	<b>-0.010</b>	<b>-0.033</b>	<b>-0.003</b>	<b>-0.006</b>
7	GISS-AOM	-0.005	0.006	0.002	0.005
8	GISS-EH	0.001	-0.003	-0.002	-0.010
9	GISS-ER	-0.001	0.006	0.003	-0.001
10	IAP-GOALS-g1.0	0.000	-0.002	0.007	0.012
11	INM-CM3.0	0.001	0.017	-0.005	-0.017
12	IPSL-CM4	0.003	-0.003	-0.011	0.007
13	MIROC3.2(hires)	-0.017	-0.018	-0.014	0.010
14	MIROC3.2(medres)	-0.008	0.001	-0.013	-0.011
15	MIUB-ECHO-G	0.001	0.004	-0.013	0.003
16	MPI-ECHAM5	0.001	-0.010	-0.009	-0.009
17	MRI-CGCM2.3.2	0.001	-0.003	-0.001	-0.003
<b>18</b>	<b>NCAR-CCSM3.0</b>	<b>0.005</b>	<b>0.004</b>	<b>0.001</b>	<b>0.002</b>
19	NCAR-PCM1	0.011	-0.004	0.007	0.008
20	UKMO-HADCM3	0.003	0.003	0.006	-0.002
21	UKMO-HADGEM1	0.000	0.011	-0.010	-0.020

Table 3.2 displays the trends ( $m$ ) of rainfall of all the modelled data and observation during the late 20<sup>th</sup> century. The observed data confirms relatively small downward trends in all seasons. These trends are consistently simulated by only two models (CSIRO Mk3.0 (4) and GFDL-CM2.1 (6)). Conversely, one model (CCSM3.0 (18)) has opposite upward trends in all seasons. Other models are inconsistent in reproducing the rainfall trends, either by rising or declining against the trend in particular seasons. The mean values of the multi-model ensemble indicate consistently downward trends similar to the observation, although it is not as steep as the observed.

### 3.5 Future rainfall projections

Assessments of the future rainfall projections of the IPCC AR4 data have been performed in many studies for many different domains. In general, the models seem to reproduce more extreme and intense precipitation during the twenty-first century with more rainfall amount over the wet tropical regions (Sun et al. 2007). The IPCC suggests that less than 66% of the models used for the assessment agree on the sign of rainfall changes (A1B scenario) over Indonesia and northern Australia (IPCC 2007). In addition, a recent climate change report for Australia indicated that the rainfall might decrease by 10% under the high emission scenario (CSIRO & BOM 2007).

Given that a good simulation of historical rainfall will raise confidence in the projected rainfall and can increase a model's credibility (Whetton et al. 2007), the selection of good models for future rainfall projections is essential. In this section the

study assesses the future rainfall projection based on the three best-performing models as identified in the previous sections (*CAD*; 3.3.1.2 and CDF comparisons; 3.3.2.2). The selected models are ECHO-G (15), MRI-CGCM2.3.2 (17) and UKMO-HADGEM1 (21). The ECHO-G (15) is best in simulating the rainfall amount for the whole land and ocean area during DJF and JJA, while MRI-CGCM2.3.2 (17) is best during MAM and SON. Both models have been chosen based on the *CAD* criteria. UKMO-HADGEM1 (21) is selected as the best-performing model based on its best performance in consistently simulating terrestrial rainfall distributions (CDF, *KSDist* criteria). The number of ensemble members of each model is shown in Table 3.3.

Table 3.3: the number of ensemble members for the 21<sup>st</sup> century for each model

Model	SRES		
	A1B	A2	B1
ECHO-G	3 runs	3 runs	3 runs
MRI-CGCM2.3.2	5 runs	5 runs	5 runs
UKMO-HADGEM1	1 run	1 run	-

Future rainfall projections are evaluated for the selected models under three different scenarios of Special Report on Emissions Scenarios (SRES), i.e. A1B, A2 and B1, except for UKMO-HADGEM1 (21) that only has A1B and A2 scenarios. SRES A1B is part of A1 storyline and scenario family. It is differentiated by technological emphasis that balances the uses of all energy sources (fossil and non-fossil) in the future by not relying only on one particular source of energy. SRES A2 scenario family highlights a very heterogeneous world with continuously growing populations, regionally oriented economic development and technological change that are more fragmented and slower than in other scenarios. The storyline of SRES B1 has similar global population as in the A1 scenario but with more emphasises on global solutions with reductions in material intensity and the introduction of clean and resource efficient technologies. It also emphasises social and environmental sustainability, including improved equity, but without additional climate initiatives.

Projected rainfall from each model is evaluated based on the percentage of seasonal climatology differences by calculating the departure of future rainfall projection (2079-2099 periods) from its simulated historical baseline (1979-1999 periods) and dividing the result by that baseline value. Separately, the projected rainfall from the UKMO-HADGEM1 (21) model is also assessed based on its empirical CDF (tested by using *KSDist* metric).

Figure 3.11 shows some changes in the projected future rainfall. The ECHO-G (15) model shows increases in future rainfall projections in most land areas in the region during DJF and MAM. Considerable increases are found mainly over northern Australia in MAM with the highest on SRES A1B scenario. During the JJA season, there is almost no sign of rainfall changes over Indonesia, especially in the SRES B1 scenario. However, some parts of southern Indonesia and northern Australia might experience rainfall decreases during winter (dry season) up to 40%, a big number in relative terms, but probably with little absolute impact, given the seasonally dry conditions at that time of the year. However, this trend continues into spring (SON) affecting a wider area over the southern Indonesian region that might lead to prolonged dry seasons and to delay in monsoon onsets (*see* Figure 3.11a). This has potentially far greater consequences than the projected decline in winter rain.

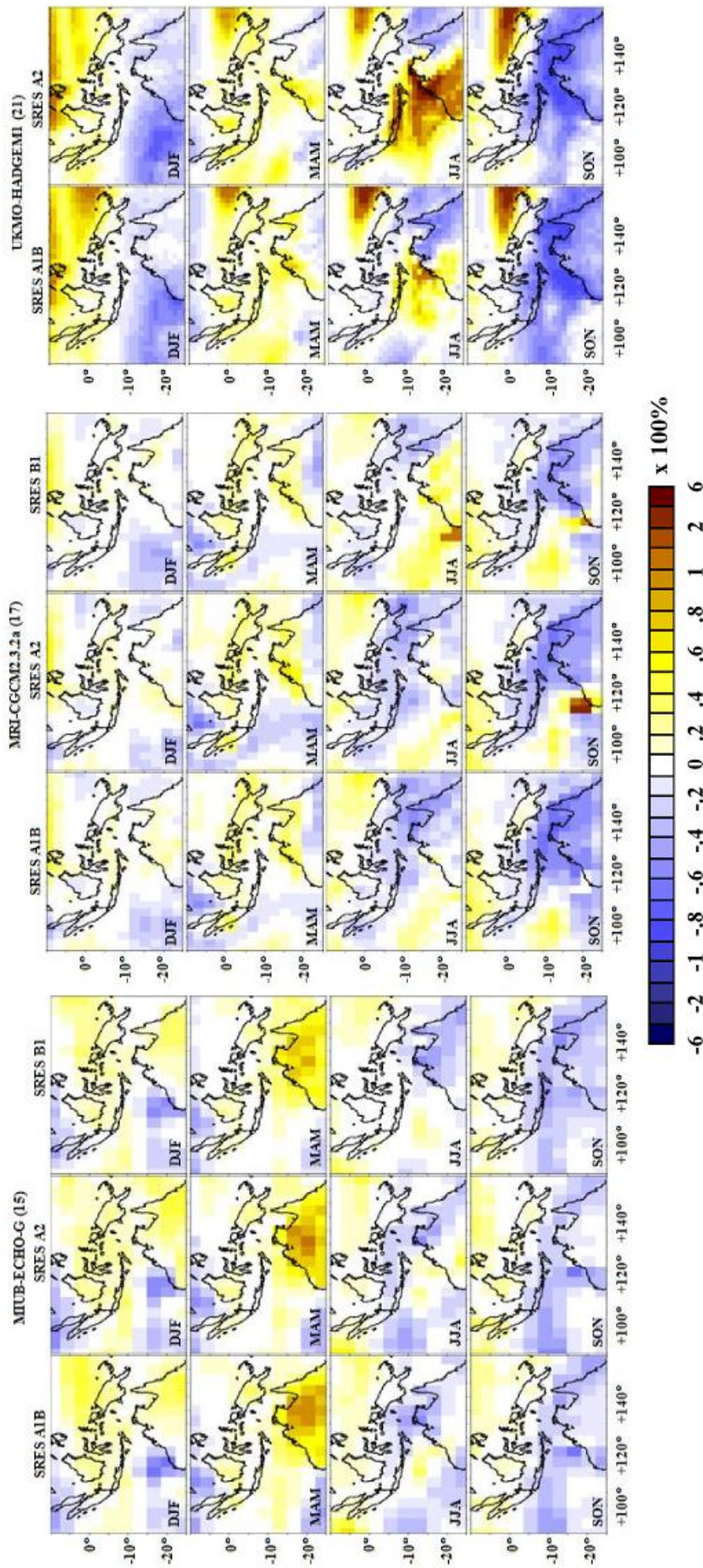


Figure 3.11: Percentage of differences between projected future rainfall and historical baseline from three selected models with three different SRES scenarios: a) ECHO-G (15) SRES A1B, A2 and BI, b) MRI-CGCM2.3.2 (17) SRES A1B, A2 and BI, and c) UKMO-HADGEM1 (21) SRES A1B and A2.

Different from the ECHO-G (15) models, the MRI-CGCM2.3.2 (17) model tends to show no changes in future rainfall over land during DJF, although there are some downward or upward changes in several parts of the region (mostly the changes do not exceed 20%; Figure 3.11b). In this model, over most parts of Indonesia and northern Australia future rainfall shows an increase in MAM and a decrease in JJA, except for the SRES B1 scenario where upward changes appear in most of northern Australia during JJA. Indication of a prolonged dry season is projected by all SRES scenarios in most part of the Austral-Indonesian region. This is related to a delayed monsoon transition during SON, particularly over southern Indonesia (this tendency is stronger in the MRI-CGCM2.3.2 (17) than in the ECHO-G (15) model).

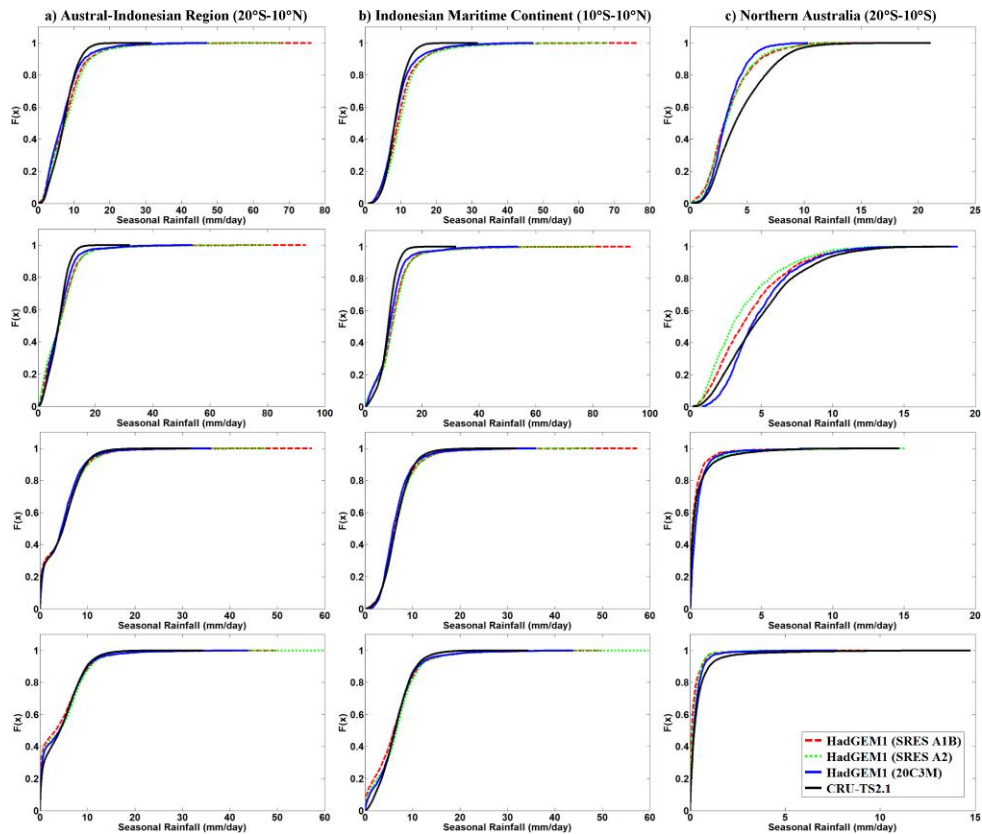


Figure 3.12: CDF of projected future rainfall of HADGEM1 (21) model on two SRES scenarios: A1B and A2 compared with its 20c3m simulation and observation: a) Austral-Indonesia, b) Indonesia, and c) northern Australia.

The UKMO-HADGEM1 (21) projects more distinct rainfall changes over the ocean area, particularly during the DJF season. At the same time, the terrestrial rainfall appears to increase over most equatorial parts of Indonesia and decreases over the western part of northern Australia. In contrast to other models, the UKMO-HADGEM1 (21) projects considerable increases during JJA particularly over the west of the northern Australian region, Java, Bali and Nusa Tenggara. Some rainfall decreases are shown over the east of northern Australia during the same season. The future rainfall seems to simulate an inverse pattern of historical rainfall over northern Australia (see Figure 3.4 on UKMO-HADGEM1 (21)). It is suspected that the increase in future rainfall is due to the shifting of false rainfall propagation into the western part of northern Australia. Therefore, the rainfall declines during the monsoon transition in SON could be a sign of prolonged dry conditions (not the shifting of dry conditions) that can cause some delays in monsoon onset.

Specific assessment of the future rainfall probability distribution using CDF for the HADGEM1 (21) model shows that the SRES A1B projections exhibit more extreme rainfall than SRES A2 scenario and historical (20C3M) simulations at all seasons, except in SON (Figure 3.12). The simulated rainfall for the whole region and for Indonesia only is consistently larger than the observed CRU data. Here, the probability of extreme rainfall is much higher for the Indonesian region than for northern Australia. This is likely to be associated with rainfall overestimation over the mountainous region in Papua. The reason is possibly due to the model sensitivity in responding to detailed topographical features in the relatively high resolution model.

### 3.6 Summary

Simulated rainfall for the Austral-Indonesian region from 21 CMIP3 GCMs (previously used for the IPCC AR4) is assessed in this study. The assessment is based on climatological consistency, interannual variability and trends during the late 20<sup>th</sup> century, and projected future rainfall scenarios. The main results of this study are summarised as follows:

- Most of the models are able to reproduce a uni-modal monsoonal pattern despite their inadequacy to correctly estimate the rainfall amount due to false rainfall as a result of the double-ITCZ problem as identified in previous studies (Dai 2006; Lin 2007).
- The rainfall mismatch in the studied region are mainly associated with (i) unrealistic locations of maximum rainfall, (ii) average position of the ITCZ which is mostly caused by a narrowing or widening of its meridional properties, (iii) the distribution of rainfall over land and ocean, and, (iv) likely problems in simulating large-scale convections associated with the monsoon circulations.
- The ECHO-G (15) is found to be the best model in simulating the rainfall amount for the whole land and ocean area during DJF and JJA, while MRI-CGCM2.3.2 (17) is best during MAM and SON. Both models are chosen based on the *CAD* criteria that indicate good model performances based on their ability to simulate the rainfall amount. Using the *KSDist* criteria, UKMO-HADGEM1 (21) is selected as the best-performing model based on its ability to consistently simulate terrestrial rainfall distributions (CDF).
- The interannual variability and trends of the simulated rainfall are found to be far from agreement with observations. Although there are several models that perform better in response to ENSO and trends more similar to the observed, their performances are inconsistent across seasons. Only two models (CSIRO Mk3.0 (4) and GFDL-CM2.1 (6)) are able to consistently simulate downward rainfall trends in all seasons similar to the observed.
- The assessment results of the future rainfall scenarios (SRES A1B, A2 and B1) from the three best-performing models (i.e. ECHO-G (15), MRI-CGCM2.3.2 (17), and UKMO-HADGEM1 (21)) vary between models, particularly in simulating DJF and JJA rainfall in the region. However, in general, the models agree in terms of their simulated rainfall changes with some increases during MAM and decreases during SON especially for southern Indonesia and northern Australia. The rainfall changes during

monsoonal transitions may lead to prolonged wet and dry seasons for those particular regions.

Based on the methods and results from this study, it is suggested that an improvement of spatial resolution in the model is beneficial particularly for the Indonesian region as it provides better representation of land-sea distribution and topography resulting in better simulation of physical processes driving rainfall in the region. It is also suggested that a combination of improved horizontal resolutions and better representation of the ocean component would possibly result in better rainfall simulations for the Austral-Indonesian region. Better physical representation of ocean, combined with good quality simulated SST patterns might generate better ocean-atmosphere coupling to reproduce more realistic rainfall. Therefore, a further study to investigate the significant role of regional/local SST in moderating the impact of large-scale climate drivers on producing the rainfall variability is essential.

## Chapter 4 The Impact of Regional SST on Rainfall Variability

Improving our understanding of the role of regional SST plays in moderating the effect of large-scale climate drivers on various timescales is important, particularly in an attempt to advance simulated SST patterns for reproducing more realistic rainfall simulations in climate models. In this Chapter, the study investigates this by identifying and analysing the patterns of seasonal rainfall and SST in the Austral-Indonesian region in order to trace their links with large-scale climate drivers such as ENSO, IOD and IPO. The analyses also separate the data into different periods based on different phases of climate regime shifts during the 20<sup>th</sup> century. The main findings of this study accentuate the importance of using regional SST data in order to improve our understanding of the rainfall variability and its driving mechanisms across different time-scales.

### 4.1 Background

It has been suggested that the study of tropical climate should include the role of ocean dynamics in the regulation of tropical sea surface temperature (SST) (Clement et al. 1996). The SST is changing the flux of the ocean sensible and latent heat (Holton 1992) and controlling the water vapour content of the atmosphere by cooling the ocean through evaporations (Clement et al. 1996). Climate model studies show that too strong a coupling between local SST and tropical convections leads to excessive convective precipitation, the simulation of unrealistic rainfall, and the formation of a double-ITCZ (Dai 2006; Lin 2007). Hence, enhancing the ocean components in climate models is essential, in particular through better representation of local SST (Chung & Ramanathan 2007; Dai 2006) that could improve ocean-atmosphere coupling for better rainfall simulations. In the Austral-Indonesian region where rainfall variability is strongly related to large-scale coupled ocean-atmospheric processes such as monsoons (e.g. Ananthakrishnan 1977; Bhaskaran & Mitchell 1998; D'Arrigo et al. 2006; Hackert & Hastenrath 1986; Hastenrath 1987), the Madden-Julian Oscillation (MJO) (Donald et al. 2006; Potemra et al. 2002; Shinoda et al. 1998; Waliser et al. 2003; Wheeler et al. 2009), the El Niño-Southern Oscillation (ENSO) (e.g. Chang et al. 2004; Haylock & McBride 2001; Hendon 2003; Kirono et al. 1999), the Indian Ocean Dipole (IOD) (Ashok et al. 2003; Boer & Faqih 2004; Cai et al. 2005a; Saji et al. 1999) and the Interdecadal Pacific Oscillation (IPO) (Folland et al. 1999, 2002; Meinke et al. 2005; Power et al. 1999a), the role of regional and local SST in moderating large scale climate processes needs to be scrutinised.

In addition, the complexity of geographical positions surrounded by vast waters and topographical features of the Indonesian Maritime Continent region (Aldrian & Susanto 2003), requires detailed analyses of the effect of ENSO (e.g. Chang et al. 2004) or any other indices of the rainfall variability in the region. The scrutiny should also apply to regional SST patterns due to complex interactions and dynamics among the local seas, and as a response to the Pacific and Indian Oceans' variability. Given that the changes on interdecadal climate drivers in the Pacific, such as IPO (Folland et al. 1999, 2002; Meinke et al. 2005) is associated with ENSO and IOD conjunctures (Saji & Yamagata 2003; Salinger et al. 2001; Wang et al. 2008), its low-frequency variability could impact on climate-related components such as

rainfall, surface temperature, stream flows and wheat crop yields (Power et al. 1999a). The analysis of the regional SST patterns could provide more understanding on the role of regional SST in moderating the effect of ENSO, IOD and IPO on rainfall variability as well as in contributing on the interaction processes among the climate drivers, particularly between ENSO and IOD where their independency remains controversial (Allan & Coauthors 2001; Dommengeset & Latif 2002; Dommengeset et al. 2006; Fischer et al. 2005; Saji et al. 1999; Saji & Yamagata 2003). Further analysis in this thesis presented in chapter 5 will contribute to the debate on the independence between ENSO and IOD using GCM simulation for the period 1800-2300.

In this Chapter, results from the empirical orthogonal function (EOF) analysis are discussed. EOF is applied in order to investigate the rainfall and SST patterns in the Austral-Indonesian region on a season-by-season basis and to investigate their relationship with interannual and interdecadal large-scale climate. Further, the patterns analysis will also be conducted on different time periods associated with well-known climate regime shifts that are already identified in many studies.

## 4.2 Data

This analysis uses the monthly SST dataset (HadISST SST Version 1.1) with a  $1^{\circ} \times 1^{\circ}$  global resolution that is constructed from quality-improved observations (Rayner et al. 2003). The dataset is used to (i) identify the dominant patterns of regional SST, (ii) to reconstruct the Niño 3.4 ENSO index ( $120^{\circ}\text{W}$ - $170^{\circ}\text{W}$ ,  $5^{\circ}\text{S}$ - $5^{\circ}\text{N}$ ) and the IOD index (dipole mode index, DMI) calculated from the difference of two SST regions in the western ( $40^{\circ}\text{E}$ - $70^{\circ}\text{E}$ ,  $10^{\circ}\text{S}$ - $10^{\circ}\text{N}$ ) and east-/south-eastern ( $90^{\circ}\text{E}$ - $110^{\circ}\text{E}$ ,  $10^{\circ}\text{S}$ - $0^{\circ}$ ) Indian Ocean. The index of SST anomaly from Niño 3.4 region is usually used to measure the strength of ENSO events that is associated with interannual rainfall variability in the Austral-Indonesian region. An increase (decrease) of SST anomaly in this region corresponds to a decrease (increase) of rainfall in the region. Similarly, the DMI is used to measure the strength of climate drivers in Indian Ocean that is also associated with rainfall variability in the Austral-Indonesian region. Positive (negative) DMI is related to an increase (decrease) of SST anomalies in the western Indian Ocean and a decrease (increase) in the east-/southeastern Indian Ocean that linked with rainfall decreases (increases) in some part of the Austral-Indonesian region.

In addition, observed sea level pressure (SLP) data (HadSLP2) is used to investigate the atmospheric conditions that relate to changes of SST and rainfall in the region. This study also uses IPO index obtained from dataset calculated by Folland et al. (2002). The index is a projected unfiltered monthly SST dataset (Rayner et al. 2003) onto the third EOF mode of global variance of low frequency filtered SST data for period 1911-1995 analysed by Folland et al. (1999).

Rainfall data is obtained from the Climatic Research Unit (CRU) dataset known as CRU TS2.1 (Mitchell & Jones 2005). The dataset is constructed from monthly weather observations and interpolated to a  $0.5^{\circ} \times 0.5^{\circ}$  grid covering the global land surfaces for the period 1901-2002. All data used in this study is normalised prior further analyses by removing the long term mean and dividing the result by the long term standard deviation. The datasets are described in more detail in Chapter 2 of this thesis.

### 4.3 The structure and connectivity of seasonal rainfall and SST

Interannual rainfall variability in the Austral-Indonesian region is associated with large-scale climate drivers such as the El Niño-Southern Oscillation (ENSO) and the Indian Ocean Dipole (IOD). The impacts of those climate drivers on rainfall variability lead to varying skills in seasonal rainfall predictability (McBride et al. 2003). Haylock & McBride (2001) find that the ENSO-rainfall relationship is particularly weak during the Australian summer monsoon period in DJF. Chang et al. (2004), however, argue that this particular finding is disputable due to the averaging procedure applied to rainfall data. By dividing the Maritime continent into three regions, Chang et al. (2004) find opposite correlations between the western and eastern part of the region. This seems to be due to geographical and topographical factors. The finding of this study emphasises the significance of scrutinising the data in order to avoid technical bias. A more advanced study that scrutinises the rainfall data for similar purposes has been conducted by Aldrian & Susanto (2003). In this study, the main Indonesian rainfall characteristics are identified before analysing their connections with ENSO and local SSTs. The inconsistent results obtained from these previous studies encourage the application of a range of methods for analysing the seasonal rainfall and regional SST relationship.

The EOF analysis is a useful method to investigate the leading empirical time-space patterns of an ocean/climate variable (Kawamura 1994; von Storch & Zwiers 1999). It is used in climate studies to analyse the empirical patterns of near-global or global SST data associated with ENSO (e.g. McBride et al. 2003; Wang & An 2005), IOD (Saji et al. 1999) and IPO (e.g. Folland et al. 1999; Meinke et al. 2005). Given that the method is quite sensitive to domain selections (Aldrian & Susanto 2003) and often overlooks local or regional variations when analysing global data, this study performs calculations on a regional level to clearly delineate time-space patterns of rainfall (e.g. Juneng & Tangang 2005) and SST for the region of interest.

#### 4.3.1 Rainfall patterns and connectivity with climate drivers

##### 4.3.1.1 Seasonal rainfall patterns, 1901-2002

This study investigates the rainfall patterns in the Austral-Indonesian region by focusing the analysis on seasonal time series data (Figure 4.1). This season-by-season rainfall analysis is performed by analysing the leading patterns of CRU TS2.1 precipitation data based on EOF analysis. The explained variance of each EOF mode is presented in Table 4.1. The approach scrutinises seasonal rainfall patterns applicable to trace the effect of regional and large-scale climate drivers and can complement the findings of previous studies (e.g. Aldrian & Susanto 2003) by providing more detail of SST-rainfall relationships.

Table 4.1: Explained variance from each EOF mode (%)

	DJF	MAM	JJA	SON
EOF1	22.0	15.4	27.5	39.1
EOF2	9.8	11.3	16.1	9.2
EOF3	8.5	7.8	7.0	5.4

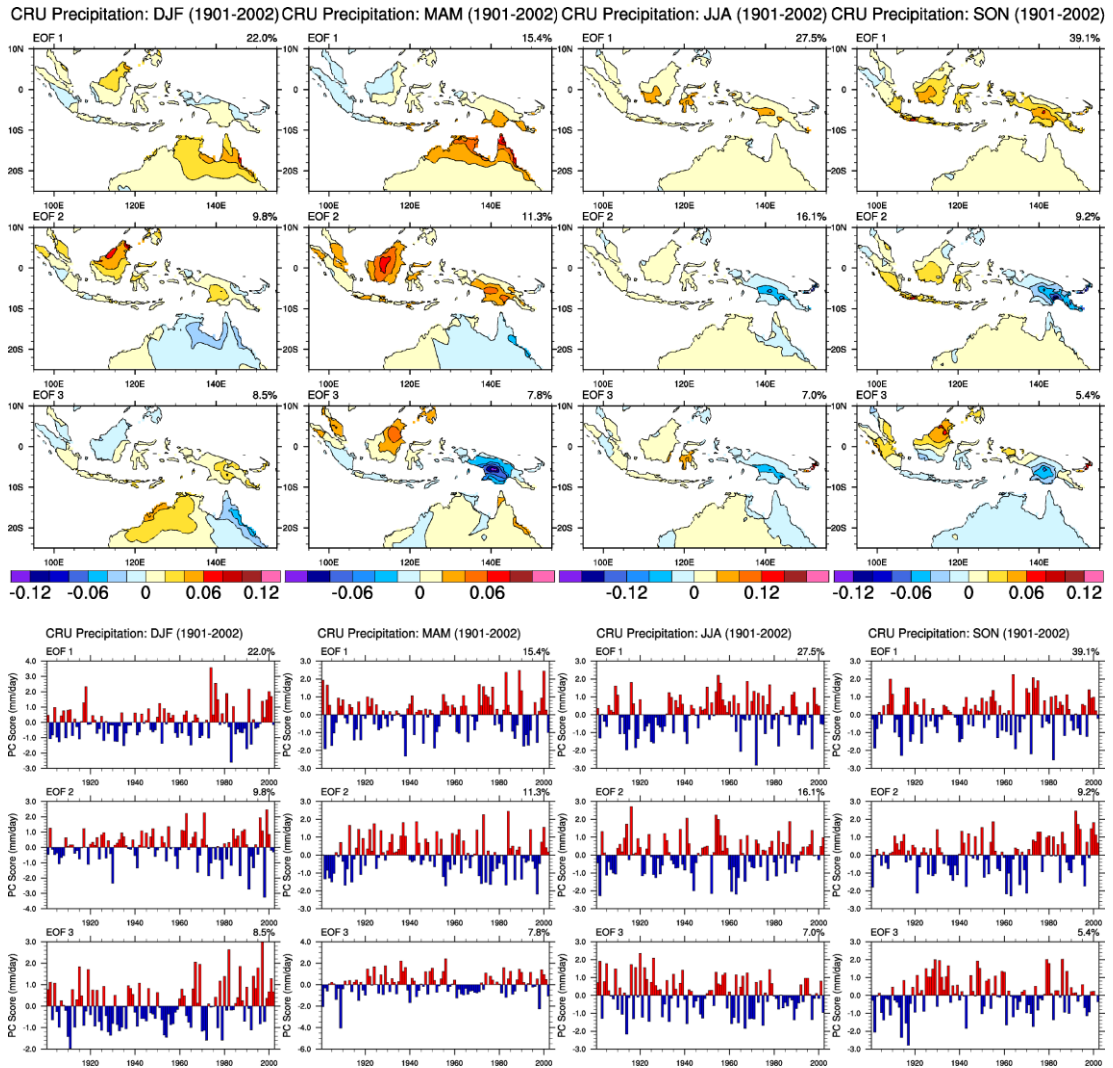


Figure 4.1: The first three EOF eigenvectors calculated to identify the leading time-space seasonal CRU TS2.1 rainfall patterns for the period 1901-2002; EOF eigenvectors (top) and principal component (PC, below). Red bars correspond to positive PC time series, while blue bars point to negative.

Figure 4.1 shows the first three leading EOFs signifying seasonal rainfall patterns in the Austral-Indonesian region. The first mode (EOF1) denotes rainfall patterns over northern Borneo and northern Australia represented by positive eigenvectors during the Austral summer monsoon peaks (DJF). A similar positive pattern over northern Australia is still visible in the same mode during monsoon transition (MAM) evidenced by a distinct positive eigenvector over northern Australia’s coastal region. These positive patterns similarly cover several areas in southern Indonesia, such as over East Java, some parts of Nusa Tenggara and southern Papua (including Papua New Guinea) (*see* Figure 1-1 for geographical information). Temporal pattern of the region with positive eigenvectors can be seen in PC time series shown in Figure 4.1, while the temporal component of the regions with negative eigenvectors can be shown by the inverse values of PC time series shown by the same figure. Here, further analysis linking the time-space patterns of seasonal rainfall in Figure 4.1 will be presented in the next subsection.

During the JJA season, the pattern shows similar eigenvector patterns in most areas of Indonesia and northern Australia, with slightly disparate values over parts of Borneo, Sulawesi, and the Papua Islands. A considerable spatial pattern appears in the next season over Indonesia. This region is correspondingly identified as the 'south monsoonal' region characterised by one annual rainfall-peak from November to March (Aldrian & Susanto 2003). The patterns are likely to be related to monsoon onset affecting the region (Moron et al. 2009).

In the second mode (EOF2), the high eigenvector pattern of DJF rainfall is mostly located over northern Borneo, northern Sumatra, eastern Java, some parts of Sulawesi and Papua, and eastern Malaysia. Near-similar rainfall over northern Australia is inversely represented through negative eigenvectors. These negative patterns also cover the area of northern Australia and small parts of Indonesia. During MAM, the EOF2 shows another distinct pattern over Borneo that is slightly shifted to the centre of the Island. The EOF2 only adds 9.8% of total variant in DJF and 11.3% in MAM (Table 4.1). During JJA and SON, the EOF2 shows positive patterns in most parts of the region with relatively strong negative eigenvectors in the eastern part, particularly around the mountainous region over Papua during JJA. In the following season (SON), some positive patterns are dominant over the southwest of Indonesia such as in southern Sumatra, most of Java, Bali and some parts of Nusa Tenggara.

The changing of rainfall signatures over northern Australia indicated by an upward trend over the western part and a downward trend in the eastern part (Shi et al. 2008) are captured by the third mode (EOF3) of DJF rainfall, which adds 8.5% of the total variance. Although the changes in trends of rainfall over both areas cannot be seen explicitly in Figure 4.1, the difference between the west and east part of the region is distinctive in the Figure. During MAM, EOF3 shows positive patterns mostly over Borneo with opposite signatures over Papua. The third mode during the JJA season indicates a negative pattern over Papua while it opposes the patterns in other regions. For SON season, the EOF3 corresponds to the rainfall patterns over the west coast of Sumatra Island, indicating strong local influences on rainfall. This pattern has similar properties with the rainfall over north-eastern Borneo.

#### ***4.3.1.2 Relationships of rainfall patterns with Indo-Pacific SST and SLP anomalies***

In this subsection, a further analysis is performed to understand the link of the rainfall patterns with possible climate drivers such as ENSO and IOD. Figure 4.2 and 4.3 demonstrate details of the correlation between the temporal components of seasonal rainfall patterns with Indo-Pacific SST and SLP anomalies. It is shown that strong correlations occur mainly with the first PC. The correlated area within SST regions is varying seasonally with the smallest area and the weakest correlations are found in MAM season (Figure 4.2). In this season, there are only a few small regions in the south-western Indian Oceans that are negatively correlated with the rainfall indicating that the variability of rainfall in the region during MAM is not much influenced by the climate variability in the Indian Ocean. Meanwhile, significant negative correlations at 5% level during this season appear over the area similar to the Niño 4 region (160°E-150°W, 5°S-5°N) accompanied by near-symmetric positive correlation regions in the northern and southern hemispheres around 30° latitude, as well as over the sea along the east coast off Papua and Australia. Further,

those SST regions will continue to develop during other seasons, i.e. JJA and SON. They will form a ‘boomerang-like’ pattern in SST anomalies as identified in a recent study (McBride et al. 2003). The boomerang-like pattern can be identified in Figure 4.2 from the formation of a region that symmetrically links the SST anomalies over the northern and eastern Pacific region with an angle forms around the Austral-Indonesian region.

In Figure 4.3, the locations where the rainfall indices are correlated significantly with SLP are not exactly comparable with the SST correlation regions. A similar instance regarding the disagreement of locations between SST and SLP are mentioned in several studies (e.g. Li et al. 2003). A little dissimilarity that we found in the correlation maps of rainfall patterns with SST and SLP is most likely due to the differences of spatial-temporal distributions of both SST and SLP datasets, including the difference in spatial grid resolutions (*see* chapter 2, subsection 2.1.1). Although it is logical that an increase (decrease) of SST will associate with a decrease (increase) of SLP, however, their spatial distributions will not be 100% similar. These are mostly related to the differences in the properties of those two variables (e.g. difference in heat capacity between ocean and atmosphere) as well as the dissimilarity of both variables on their spatial distributions where the SST only covers ocean, while SLP covers both ocean and land. All of these differences affect their time-space distributions and climatology (*see* Figure 2.2), which then influence the correlation results with the rainfall. Here, Figure 4.3 indicates that the leading rainfall index in MAM demonstrates considerable negative spatial correlation with SLP over the Austral-Indonesian region, particularly in the western part. Conversely, a spatial positive correlation is shown over an extended area in the central Pacific region with the highest correlation being found in the southern part.

The correlation areas between the rainfall index and SST anomalies increased strongly during JJA, as shown in Figure 4.2 by an area that extent over the tropical Pacific region opposite to a broader area in the Austral-Indonesian region and the eastern part of Australia within the southern Pacific region. Concurrently, there is also a significant correlation pattern over the western Indian Ocean region indicating the development of SST dipole mode (IOD) that affects rainfall, although the western area does not exactly correspond with those defined by Saji et al. (1999). The combination of correlated regions resulted in a tripole SST region affecting the rainfall variability in the Austral-Indonesian region. Given that the Austral-Indonesian region is at the centre of this tripole form, it indicates the importance of the regional SST changes in directly affecting the rainfall and as an agent to deliver the effect of Indo-Pacific climate drivers, i.e. ENSO and IOD on rainfall variability. Nevertheless, the correlation field with SLP once again signifies little differences compared to the SST correlation fields. A plausible explanation of this mismatch has been described in previous paragraph. The negative correlation with SLP located over the Austral-Indonesian region seems to widely extend into the western Indian Ocean indicating no sign of dipole mode in the region, although we can find that the positive correlation region in the SLP over the western Indian Ocean seems to shift further south between 30° and 60°S. Therefore the only distinct pattern in the SLP correlation field is a dipole between the Pacific and the Austral-Indonesian region that extends into the western Indian Ocean region.

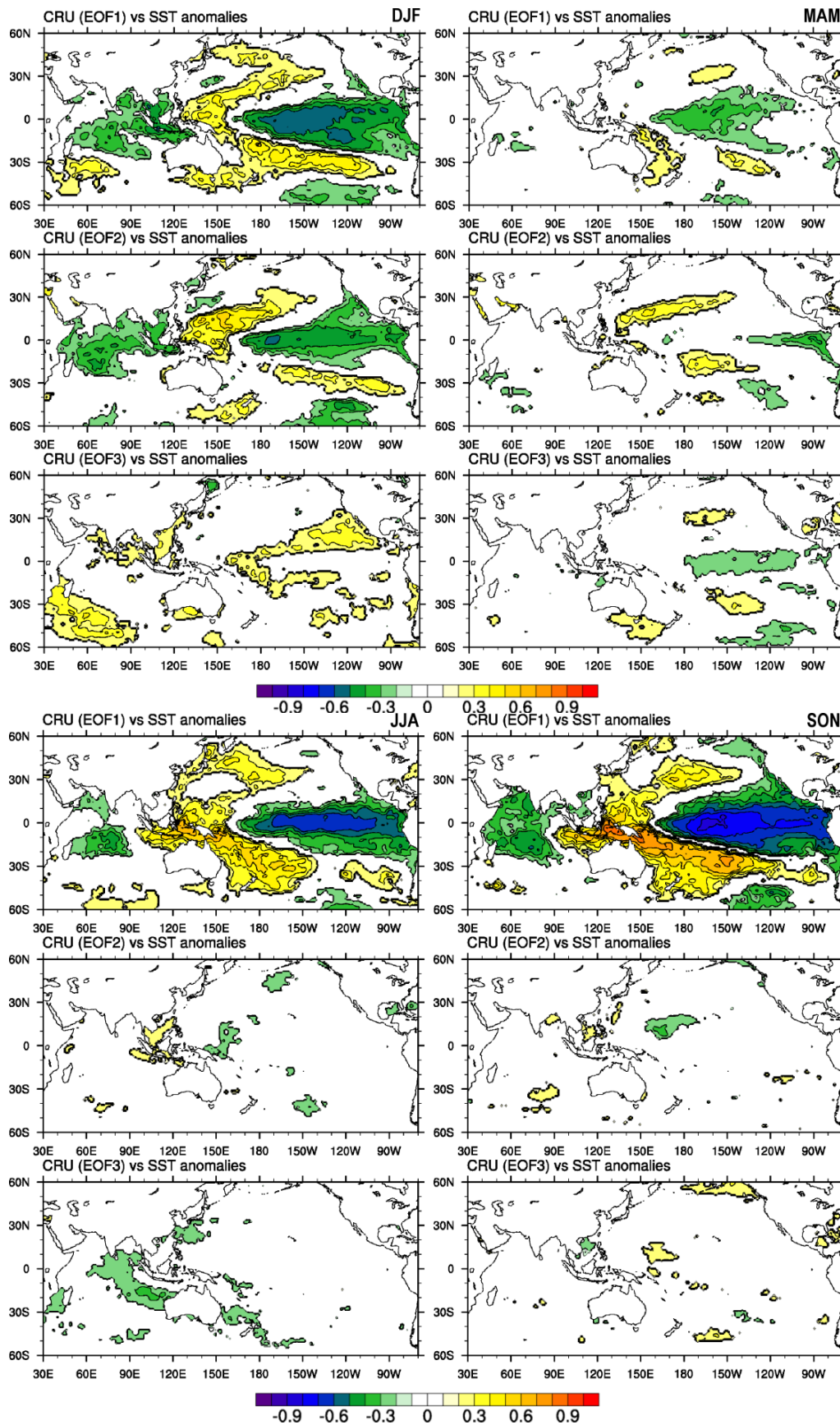


Figure 4.2: Spatial correlations between the first three EOFs of seasonal rainfall with Indo-Pacific SST anomalies (1901-2002 periods). The correlation area is significant at 5% significance level.

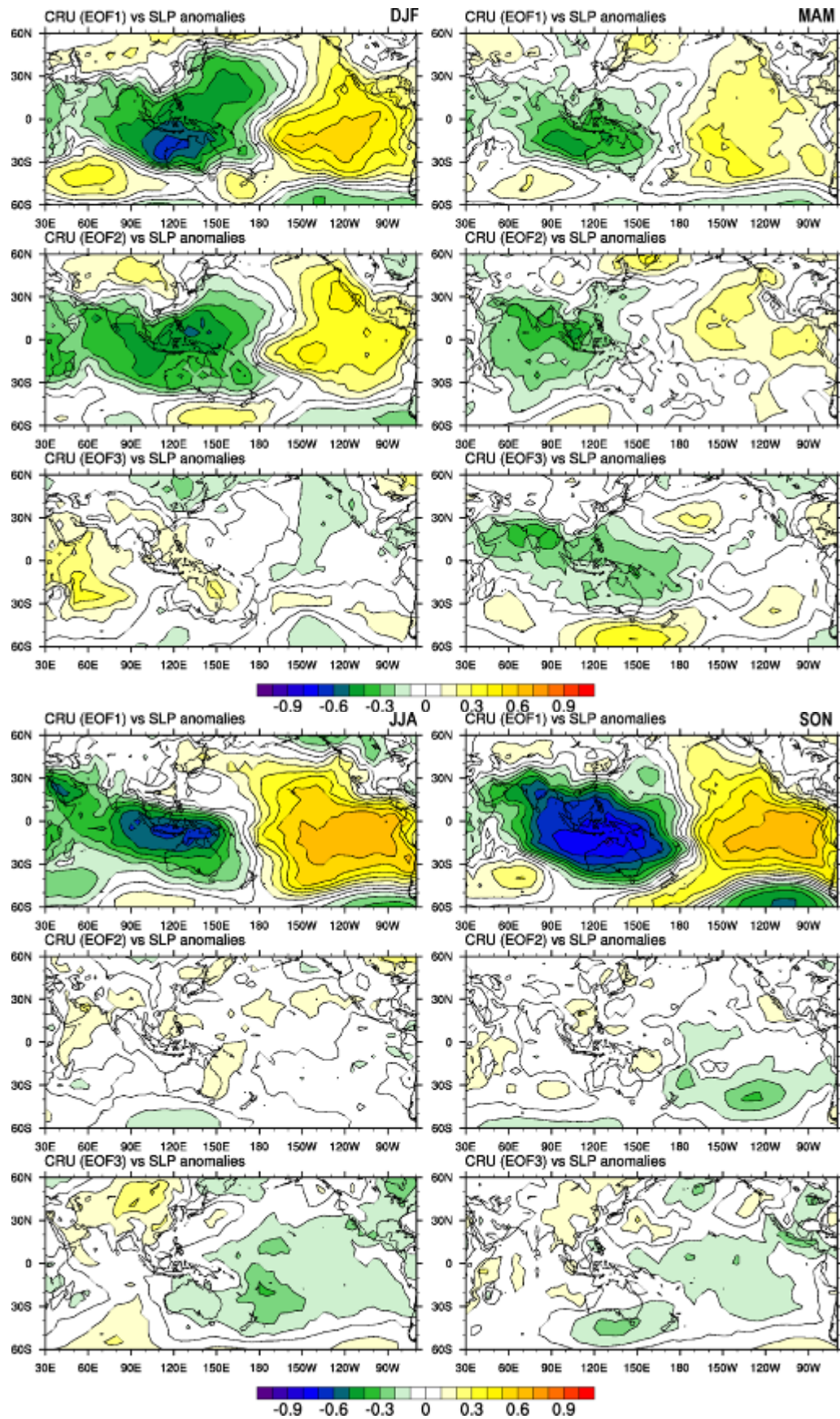


Figure 4.3: Same as Figure 4.2, but with Indo-Pacific SLP anomalies.

Similar conditions in regards to the SLP correlation fields consistently occur during Austral spring (SON), at a time of monsoonal transition. This is the season where many studies found the phase-lock between ENSO and IOD and their dominant effect on rainfall variability. Generally, the phase-locking occurs when individual behaviour shifts to a collective behaviour (Briggs & Peat 1989). In this case, ENSO and IOD occur at the same time, which usually can be optimally found during SON. The El Niño-like conditions are often prolonging the dry season and delaying wet-season onset in the region (Boer & Faqih 2004; Haylock & McBride 2001; Lo et al. 2007; Moron et al. 2009). The effects of both ENSO and IOD can be seen through the broadening of SST correlation fields over the ENSO region in the central and eastern Pacific regions as well as over the western Indian Ocean (Figure 4.4; MAM, EOF1). However, noting that the sign of IOD only appears on the correlation of rainfall index in the first mode with the SST but not with the SLP anomalies, it could possibly be an indication of ENSO domination on the rainfall variability in the region characterised by the dipole of SLP between Pacific and the Austral-Indonesian region. A further possibility is that the SST patterns that form the IOD are strongly associated with ENSO variability in the Pacific Ocean (Allan & Coauthors 2001; Dommenges & Latif 2002; Dommenges et al. 2006) and the association is irregular due to inconsistent responses of the regional SST variability in the Austral-Indonesian region. Nevertheless, further studies are needed in order to enrich the debate on such special issues.

During the Austral summer season (DJF), the spatial negative correlation field that previously appeared over the western Indian Ocean in JJA and SON seasons moves eastward into the western Austral-Indonesian region and interferes with the SST in the South China Sea region. This condition suppresses the positive correlation field eastward into the eastern part of Austral-Indonesia, over the western Pacific region. Given that the confluence between those two different correlation fields is in the centre of the Indonesian region, it indicates the importance of local ocean properties characterising the regional SST pattern and in affecting the rainfall. This could be the reason why the effect of ENSO during northern winter is found to be opposite between the western and eastern part of the Indonesian region (Chang et al. 2004). Several studies have addressed the role of the Indonesian throughflow (ITF) in transferring ENSO signal into the Indian Ocean (Annamalai et al. 2003; Song & Gordon 2004; Susanto et al. 2001; Zhao 2004). Nevertheless, during this period in DJF, the ITF is weakened by the intrusion of surface water flow from the SCS into the Java Sea and the southern Makassar Strait (Gordon et al. 2003).

While the study has discussed the distinct relationship of the first mode of rainfall indices with the Indo-Pacific SST and SLP anomalies, the correlations of these variables with the second and third modes appear much weaker. The only prevailing correlations occur in the second mode of rainfall index during DJF season. Despite others, the third mode of rainfall index in DJF has shown an opposite pattern between the western and eastern northern Australian region (Figure 4.1; DJF, EOF3). Those patterns correlate positively with SST and in the South China Sea and also with SLP over the east of northern Australia.

In general, the method used in this study by investigating the relationship between specific time-space rainfall patterns in Austral-Indonesia resulted from the EOF analysis with the SST and SLP anomalies have addressed some key understanding on season-by-season rainfall variability and its possible driving factors related to the

ocean-atmosphere interaction. Such analysis can clearly determine the dominant patterns of SST and SLP anomalies in the Indo-Pacific region that affect the rainfall variability. Here the study highlights the importance of the Austral-Indonesian region in responding to the variability by Indo-Pacific climate drivers. In the next subsection, we will focus on the leading patterns of regional SST in order to obtain a better understanding of the role of SST in modulating the impact of large-scale climate drivers on rainfall variability within the region.

### 4.3.2 Regional SST patterns and their link with rainfall anomalies

#### 4.3.2.1 Regional SST patterns, 1901-2002

Using the method outlined earlier, Figure 4.4 shows the first three leading EOF signifying regional SST patterns. The explained variance of the EOF is shown in Table 4.2. A strong pattern represented by high eigenvector values appears around the South China Sea (SCS) region during DJF and slightly reduce during MAM. It then changes into the east-/southeastern of the region particularly over Arafura Sea, the Gulf of Carpentaria and the Coral Sea regions during JJA and turns stronger in SON (Figure 4.4a). The temporal patterns of this first mode are related to SST rise (Goreau et al. 2005) (Figure 4.4b) and are possibly associated with surface warming due to climate change.

Table 4.2: Explained variance from each EOF mode (%)

	DJF	MAM	JJA	SON
EOF1	37.3	48.3	50.1	49.8
EOF2	22.3	14.9	13.6	16.1
EOF3	7.5	6.7	8.9	5.7

Despite the sign of temperature rise, the distinct pattern over the SCS during DJF and MAM possibly conforms to the ocean dynamics as indicated in the second EOF mode (EOF2). It is found that the regional SST pattern for DJF is consistent with the correlation pattern between the first mode of rainfall patterns against the SST anomalies (Figure 4.2; DJF, EOF1). Gordon et al. (2003) found a strong surface current that flows from this region through the Java Sea, causing a reduction of the ITF in the Makassar Strait during boreal winter. This condition is also weakening the role of the ITF in transmitting ENSO signals to the east/southeastern Indian Ocean and western Indonesia (Susanto & Gordon 2005). As a result, there are distinct opposite patterns between the SST in this region and the SST in the eastern part of Indonesia.

In contrast to the second mode of regional SST in DJF and MAM that demonstrate an opposite pattern between SCS and the eastern seas in Indonesia, the regional SST in JJA and SON show distinctive patterns along southern Indonesian waters. The eigenvectors are strongly concentrated in the Banda Sea, the Arafura Sea and southeast coast of Papua New Guinea (PNG) and weaker around Java, particularly during SON period. The patterns are consistent with the correlation field of the EOF1 of rainfall patterns against SST anomalies during the same seasons (Figure 4.2; JJA and SON, EOF1). One possible association regarding these conditions is the intensification of the ITF supported by the distribution of more saline Banda Sea water into the southern Makassar Strait (Gordon et al. 2003). It will possibly allow

SST dominations in controlling and optimising ENSO effects on rainfall variability during the seasons.

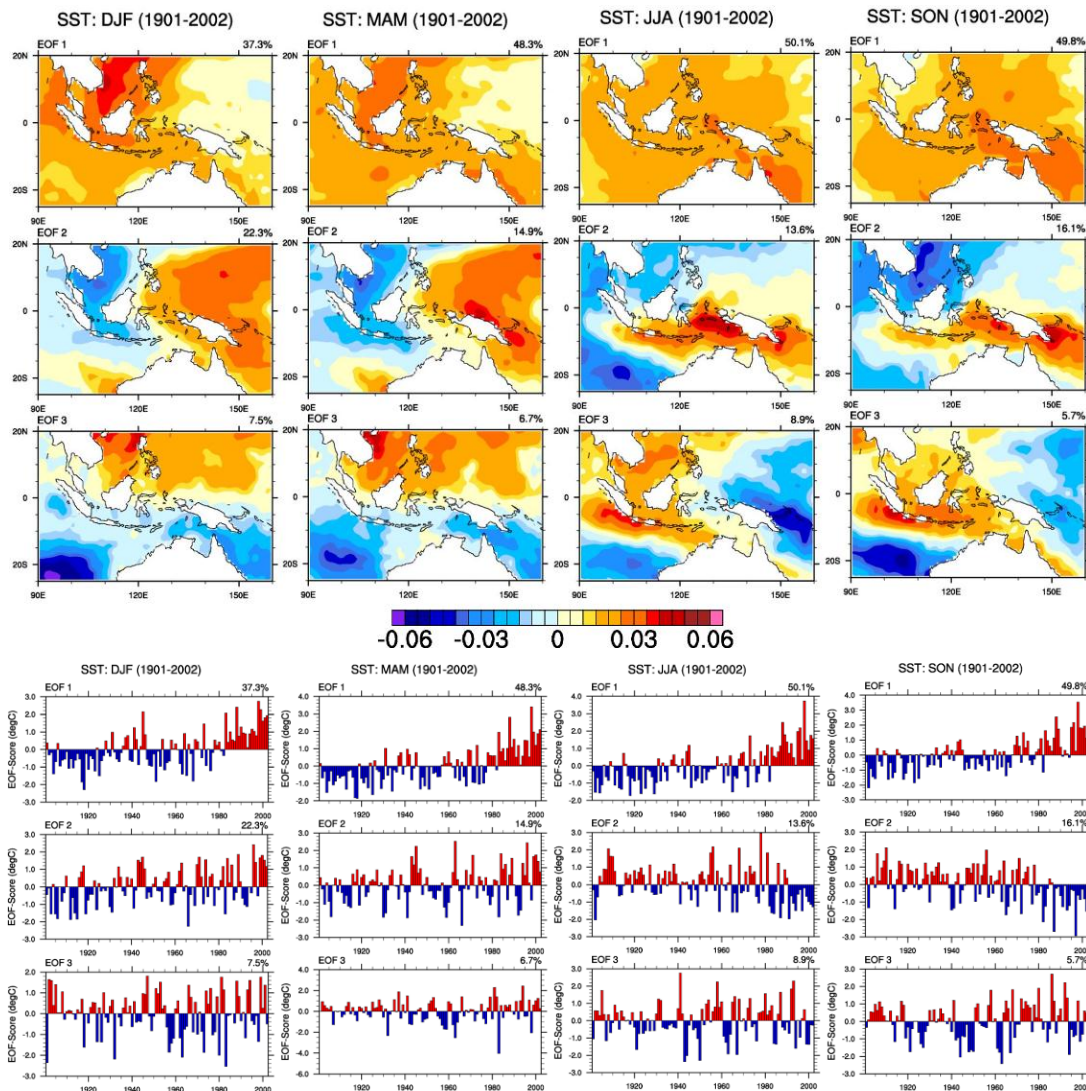


Figure 4.4: As Figure 4.1, but using SST data within the 1901-2002 period for the Austral Indonesian region; EOF eigenvectors (top) and EOF scores (below).

In addition, in the regional SST patterns represented in the third mode, there seems to be another process that characterises the SST patterns in the Austral-Indonesian region. Occasionally, patterns develop in northern Indonesia during DJF and MAM seasons and move into south-western Indonesia during JJA and SON seasons. The process seems to transport the SST signal from the SCS region into the coast off Sumatra and Java. Given that the SST pattern appears around the region linked to the IOD (Saji et al. 1999), this could be another signal that triggers the IOD variability despite its relationship with ENSO as indicated in subsection 4.3.1.2. Referring to Table 4.3 below, it is shown that the third mode of regional SST indices correlate significantly with the second mode of rainfall indices in JJA and SON seasons. Those rainfall indices are associated with the patterns in most of the studied region during JJA, except over some areas in Papua, and with the patterns in most of the south-western region in Indonesia during SON season (Figure 4.1).

Considering that those second mode of rainfall indices in JJA and SON seasons only correlate significantly with the third mode of regional SST indices, it indicates the independency of these particular SST patterns where their variability during both seasons might possibly be a cause of an irregular relationship between ENSO and IOD that obscure the dependency of IOD to ENSO events. In the case where this regional SST pattern coincides with the ENSO signal into the south-western Indonesian region, the effect on the rainfall variability could be considerable.

Table 4.3: Correlations between PC time series of regional SST and rainfall. Bold values show significant correlations at 5% significance level.

Indices		Austral-Indonesian rainfall (CRU TS2.1 dataset)											
		PC1				PC2				PC3			
		DJF	MAM	JJA	SON	DJF	MAM	JJA	SON	DJF	MAM	JJA	SON
Austral-Indonesian (regional) SST	PC1	DJF	<b>-0.23 **</b>				-0.13				<b>0.18 *</b>		
		MAM		0.02				0.12			-0.05		
		JJA			<b>0.43 ***</b>				0.06				<b>-0.17 *</b>
		SON				<b>0.57 ***</b>				0.05			0.01
	PC2	DJF	<b>0.47 ***</b>				<b>0.52 ***</b>				-0.09		
		MAM		<b>0.19 *</b>				<b>0.18 *</b>				0.12	
		JJA			<b>0.51 ***</b>				-0.03				<b>0.21 **</b>
		SON				<b>0.68 ***</b>				-0.15			0.12
	PC3	DJF	<b>0.23 **</b>				0.15				0.14		
		MAM		<b>-0.22 **</b>				0.14				0.16	
		JJA			<b>-0.17 *</b>				<b>0.42 ***</b>				0.13
		SON				0.07				<b>0.27 ***</b>			-0.06

#### 4.3.2.2 Relationship of regional SST patterns with rainfall and Indo-Pacific SLP anomalies

Figure 4.5 demonstrates that the relationships between the first mode of SST and rainfall anomalies are not well established during DJF and MAM periods, although the correlation in DJF is relatively more skilful than in MAM. In DJF, a positive relationship with the rainfall appears over some parts of Borneo, Sulawesi and in the eastern of the northern Australian region while a negative link is shown over central Sumatra. The poor SST-rainfall relationships observed during both DJF and MAM seasons are supported by positive response of regional SST in the first mode to the changing of SLP anomalies over the region (Figure 4.6). Conversely, the connection between the first modes of regional SST with rainfall is much better in JJA and SON. The SST variability is found to strongly impact the rainfall in most parts of the region. This strong relationship is in line with the significant negative correlation between SST and SLP anomalies.

In the second mode, the connectivity between the SST patterns and rainfall during DJF seems to be improved. The changing of the SST pattern in the region controls the rainfall variability over Borneo, some parts of Sumatra, Sulawesi, western and eastern Java, Bali, Nusa Tenggara, western Papua, and some parts of northern Australia. The link of the SST and SLP anomalies over Austral-Indonesia and the Pacific Ocean is found to be oppositely strong during this period. Consistent with previous findings, the relationship of the second mode of regional SST patterns against the rainfall anomalies is normally weaker during MAM period. This is signified by a small correlated region in Indonesia and northern Australia.

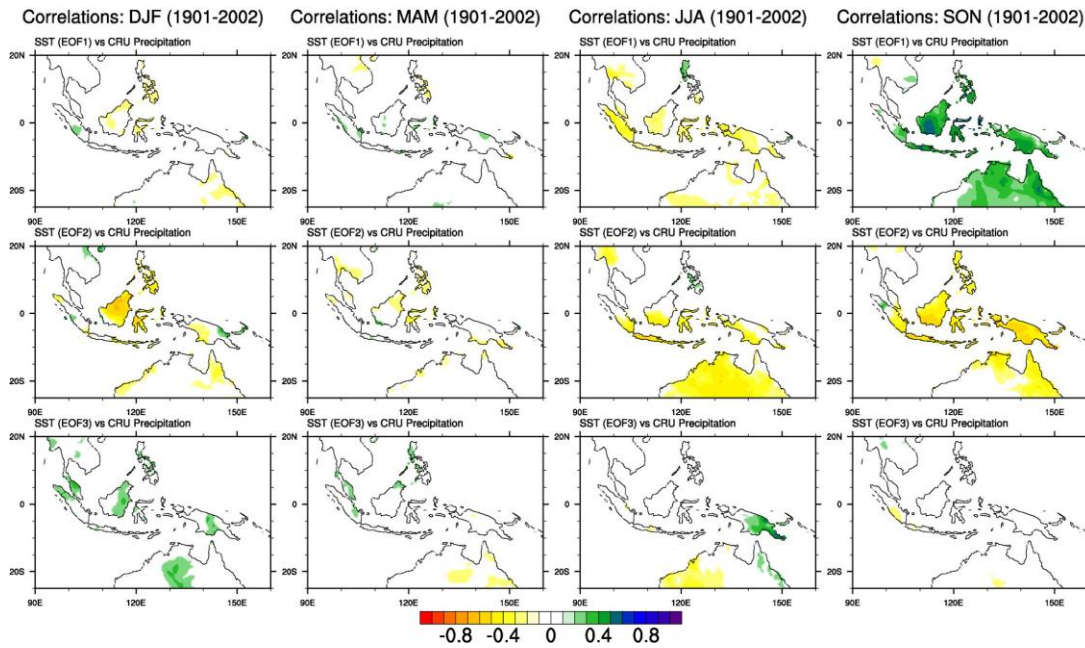


Figure 4.5: Spatial correlations between the first three EOFs of regional SST with seasonal rainfall anomalies in the Austral-Indonesian region (1901-2002 periods).

A stronger relationship is commonly established during JJA and SON. For JJA period, the correlations are positively high over most parts of northern Australia and southern Indonesia (Figure 4.5). This corresponds to a distinct SST pattern over the southern Indonesian region (Figure 4.4; JJA, EOF2) that is strongly linked with the SLP anomalies in the eastern Pacific region (Figure 4.6; JJA, EOF2) associated with ENSO variability. During warm ENSO event, increases of SST anomalies in the eastern and central Pacific regions are associated with the formation of low-pressure system in the surface atmosphere of the region. Simultaneously, negative SST anomalies establish in the regional sea within Austral-Indonesia and cause a high-pressure system associated with less rainfall over the region. Figure 4.5 shows that the variability of regional SST during SON season influences the rainfall variability over most of Indonesia except northern Sumatra. This association is weaker over the northern Australian region. Figure 4.6 demonstrates that during this SON season, the connectivity of regional SST patterns with SLP anomalies is stronger and covers broader regions.

Comparable with the finding in subsection 4.3.1.2 (Figure 4.3), the correlation of the temporal component of regional SST patterns with the SLP anomalies (Figure 4.6) also shows no dipole over the Indian Ocean. The only strong correlations appear over the Austral-Indonesian region and the Pacific Ocean. This provides further evidence of a strong link between the Pacific and the Austral-Indonesian region that determines the variability in the Indian Ocean.

In general, the overall regional SST-rainfall relationships can be summarised from the correlation results shown in Table 4.3 that measure the relationships between the PC time series of the first three leading modes of regional SST and rainfall. The result shown in this table are consistent with the correlation maps presented in Figure 4.5. For example, strong relationships between the first two PCs of regional SST and

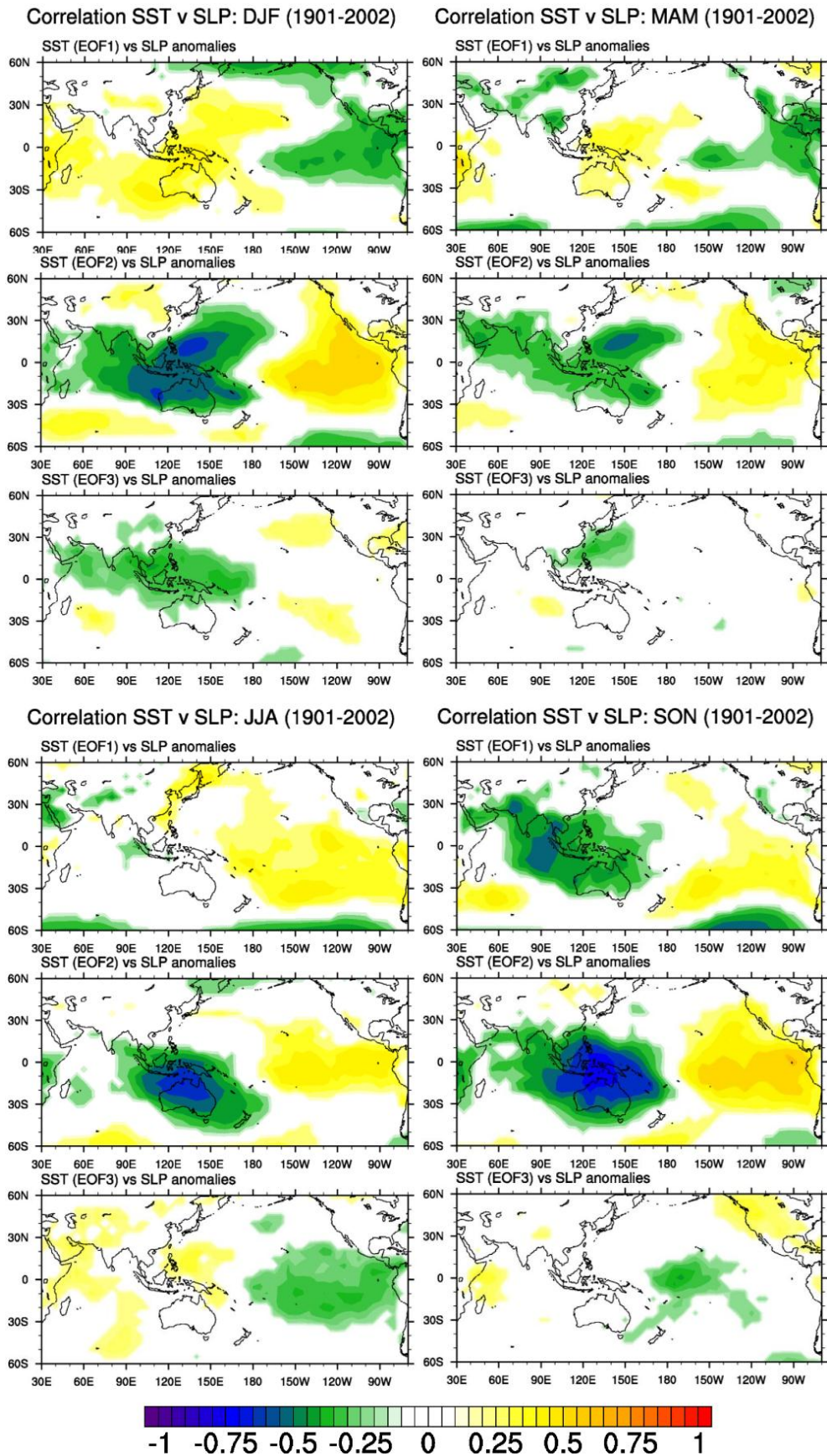


Figure 4.6: Spatial correlations between the first three EOFs of regional SST in Austral-Indonesia with seasonal Indo-Pacific SLP anomalies (1901-2002 periods).

seasonal rainfall anomalies during JJA and SON found in Figure 4.5 are coherent with the correlations between the first two PCs of regional SST and the first PC of rainfall as shown in Table 4.3. Moreover, insignificant correlations found mostly in the Austral-Indonesian region between the third mode of PC time series of regional SST and rainfall anomalies during JJA and SON (Figure 4.5) are associated with insignificant correlations with the first PC time series of regional rainfall (Table 4.3). In contrast, the correlations with the second mode of rainfall PC time series during both seasons are found to be significant, particularly during JJA. This is linked to the significantly correlated regions during JJA shown in the third mode of regional SST in Figure 4.5.

### 4.3.3 Results of power spectral analysis

In this section, the study uses Fast Fourier Transform (FFT) analysis to identify interannual to multidecadal variability in regional SST, rainfall and climate indices of Indo-Pacific climate drivers, i.e. IPO index, Nino 3.4 SST anomalies and Dipole Mode Index (DMI). The periods are defined by 2.5 to 8 year periods of ENSO-related interannual variability, 9 to 13 years of decadal variability, 14 to 18 years of interdecadal and more than 19 years of multidecadal variability (Meinke et al. 2005). This study analyses the seasonal patterns of regional SST and rainfall up to three leading EOF modes calculated in the previous section (*see* Figure 4.1 and 4.4). The FFT is only calculated for the period of 1901-2002 due to data limitations and for consistency.

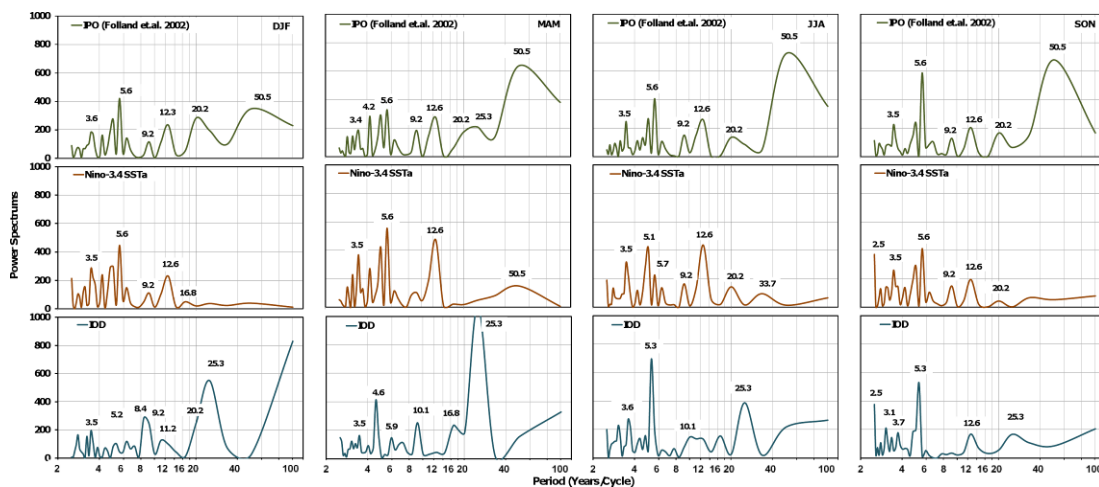


Figure 4.7: FFT Spectral analyses from IPO, ENSO (Niño 3.4 SST anomalies) and IOD (Dipole Mode Index, DMI) (1901-2002 periods). Horizontal (x) axis is transformed into logarithmic scale.

Here, the variability of three main climate drivers in Indo-Pacific, i.e. ENSO, IOD and IPO are discussed (Figure 4.7). Figure 4.7 demonstrates that the indices oscillate on different timescales, from interannual to multidecadal variability. The interannual components mostly dominate 3.5 and 5.6 year cycles characterising irregularity of ENSO cycles on the Niño 3.4 region in all seasons. The distinct power spectrums on those timescales are found to be consistent with the IPO data, indicating possible ENSO-IPO dependency. This connectivity is endorsed by their FFT results that demonstrate consistent decadal timescales around 12.6 year periods. Several studies have questioned the existence of the IPO as an ENSO-independent driver of variability. Some studies raise the possibility of the IPO simply representing the low

frequency variability component of ENSO, essentially a manifestation of an ENSO-related red noise process without any inherent predictability (Meinke et al. 2005). This might be a reasonable proposition given that the multidecadal component of both indices is not fully consistent. It should further be noted that dominant multidecadal variability in the IPO index is most likely a result of the reconstruction process obtained from the third EOF of filtered global SST data (Folland et al. 1999).

The interannual periodicity of IOD index demonstrates a strong 5.3 year cycle, particularly during JJA and SON seasons. This is somewhat similar to ENSO periodicity that has strong spectral peaks at around 5 year period (~5.6 year). The similarity of ENSO and IOD periodicities found during JJA and SON provides logical explanation that is related to the phase-locking events, causing predominant effects of ENSO and IOD (Annamalai et al. 2003; Gualdi et al. 2003; Yu & Rienecker 2000). Another dominant cycle is found on a 4.8 year cycle but only appears in MAM when the ENSO and IOD phenomena are seasonally weak. In contrast, the 25.3 years multidecadal cycle seems to determine the IOD variability in all seasons, in particularly during DJF and MAM seasons.

#### 4.3.3.1 Variability of the seasonal rainfall patterns

The power spectra of the seasonal rainfall patterns from three leading EOFs are analysed to identify their dominant variability (Figure 4.8). The interannual variability of the first mode of rainfall indices is likely to associate with ENSO. It has a cycle of between two to eight years, with strong cycles emerging around three and five years, respectively.

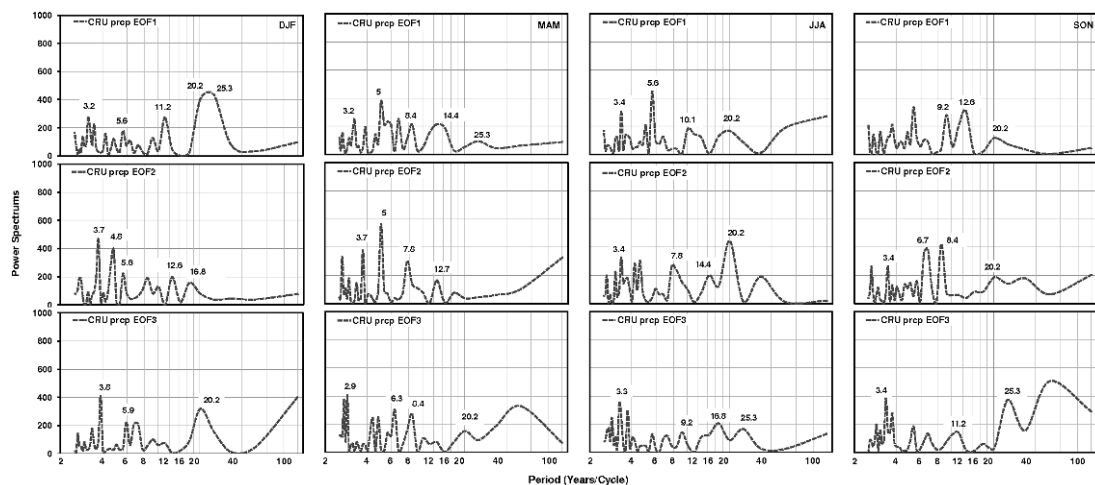


Figure 4.8: FFT Spectral analyses from the first three leading EOF of CRU TS2.1 seasonal rainfall dataset. Horizontal (x) axis is transformed into logarithmic scale.

Figure 4.8 shows inconsistent periods of decadal to interdecadal components appear between seasons with oscillatory periods around eight to almost fifteen years. This inconsistency is probably related to the links between interdecadal climate oscillations and monsoons (Krisnamurthy & Goswami 2000; Krishnan and Sugi 2003; Wang et al. 2008) that affect variations of IPO/PDO influences on seasonal rainfall as previously indicated in several studies (e.g. Brown & Comrie 2002). The figure also demonstrates that the most prevailing multidecadal component is found during DJF season with 20 to 25 year periods. There are also similar 20.2 year components in JJA and SON as well as 25.3 year in MAM. The multidecadal rainfall

variability might be associated with the IPO and could indicate considerable low-frequency climate signals impacting on rainfall variability in the region.

The second mode also has significant peaks in their power spectra at interannual and multidecadal time scales during DJF–MAM and during JJA–SON, respectively. In the third mode, the strong interannual spectrum is found at three years intervals, while the multidecadal cycle appears every twenty years but is only significant during DJF and MAM seasons. As it has been mentioned earlier, the rainfall patterns in the third mode indicate contradictory patterns between the west and east of northern Australia during DJF (subsection 4.3.1.1). This pattern is possibly related to the multidecadal variability (20 year periods) of the IPO variability (*see* Figure 4.7).

In Table 4.4 and Figure 4.9, the study analyses the relationship between the seasonal rainfall indices and the three well-known climate drivers in the Indo-Pacific, namely ENSO, IOD and IPO. Here, the climate indices are obtained from HadISST data and are analysed based on their seasonal time series data, including the IPO index. For ENSO index, the data is taken from SST anomaly of Niño 3.4 region (*See* Section 4.2 for more detail).

The first mode of rainfall indices for the Austral-Indonesian region is significantly correlated at 1% significance level with all Indo-Pacific climate indices at all seasons, except with IOD index in MAM that is found uncorrelated (Table 4.4). The scatter plots of these relationships can be seen in Figure 4.9. The correlation values are higher particularly during SON (correlation ( $r$ ) Niño 3.4 = -0.79,  $r$  IOD = -0.60 and  $r$  IPO = -0.68). This is followed by correlation values in JJA and then in DJF. The order is consistent for all climate indices. Especially for SON season, the correlation value with the Niño 3.4 region is higher than any of the other indices ( $r$  = -0.79) and is related to the changes in rainfall variability in most of the southern Indonesian region (*see* Figure 4.1 (top; EOF1, SON)).

*Table 4.4: Correlations between Indo-Pacific climate drivers SST indices with PC time series of rainfall in the Austral-Indonesian region based on 10% (\*), 5% (\*\*), and 1% (\*\*\*) significance levels.*

Indices		Austral-Indonesian rainfall (CRU TS2.1 dataset)											
		PC1				PC2				PC3			
		DJF	MAM	JJA	SON	DJF	MAM	JJA	SON	DJF	MAM	JJA	SON
Niño 3.4	DJF	-0.56 ***				-0.47 ***				0.12			
	MAM		-0.31 ***				-0.14				-0.27 ***		
	JJA			-0.70 ***				0.02				0.08	
	SON				-0.79 ***				0.03				-0.05
IOD	DJF	0.33 ***				-0.01				-0.01			
	MAM		-0.09				-0.04				-0.15		
	JJA			-0.42 ***				0.08				0.03	
	SON				-0.60 ***				-0.01				0.05
IPO	DJF	-0.50 ***				-0.28 ***				0.14			
	MAM		-0.26 ***				-0.02				-0.25 **		
	JJA			-0.51 ***				0.04				0.12	
	SON				-0.68 ***				0.04				0.10

In contrast, the relationship of the first mode of rainfall in MAM season is mostly lower than any other season. The weak relationship of rainfall in the region with ENSO index has been reported earlier in a previous study (Aldrian et al. 2003). In our analysis, this weak association is linked to the rainfall patterns in northern Australia, East Java, Bali, Nusa Tenggara and Timor, as well as southern Papua (*see*

Figure 4.1 (top; EOF1, MAM)). For other regions, there is a chance that the link with climate indices during MAM is more eminent than in other seasons. This is shown by the correlation pairs between the third mode of rainfall patterns with Niño 3.4 and with IPO index during MAM that significant at 1% and 5% significance levels with  $r=-0.27$  and  $-0.25$ , respectively. The third mode of rainfall is associated with variability mostly found on the area of north-eastern Borneo and opposite in some areas over Papua. Nevertheless, it should be noted that this rainfall signature only represents less than 10% of total variance.

For the rainfall patterns in second mode, its relationships with climate indices are considerable only during DJF with Niño 3.4 ( $r=-0.47$ ) and IPO index ( $r=-0.48$ ) while insignificant with IOD index. The similarity of their correlation values indicates a strong connectivity between ENSO and IPO.

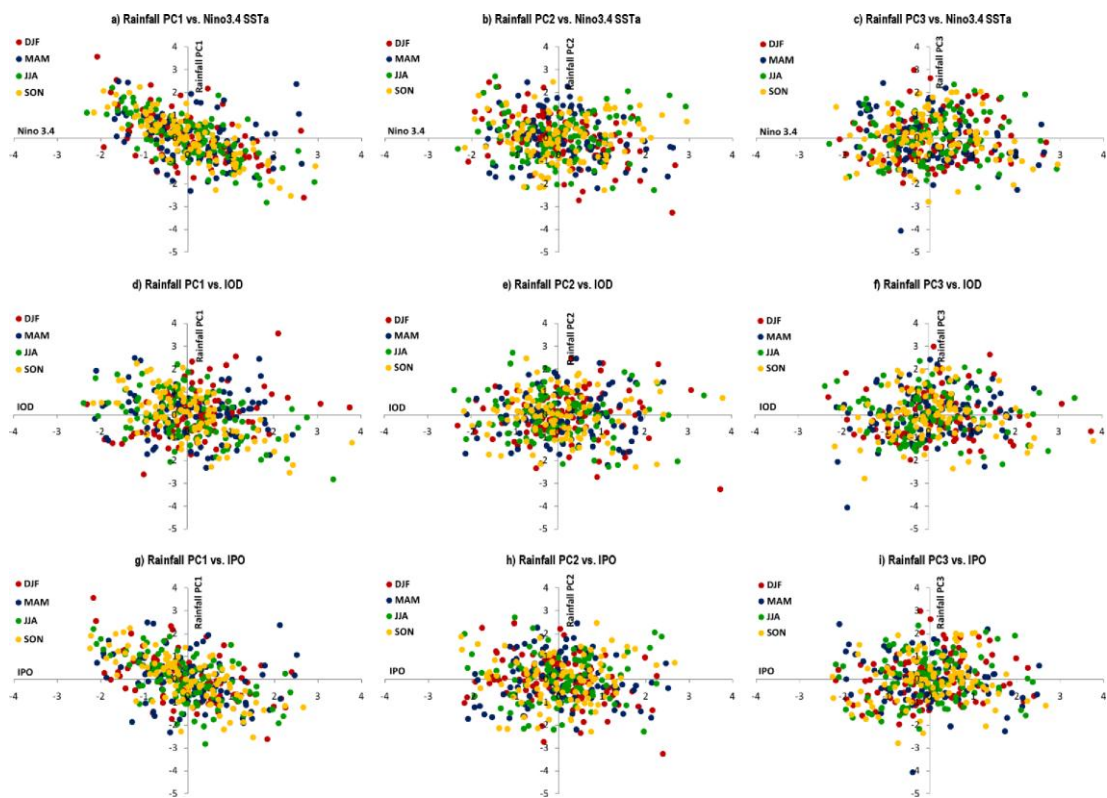


Figure 4.9: Comparison of the first three leading EOFs of rainfall with the standardised (a-c) Niño 3.4 index, (d-f) IOD index, and (g-i) IPO index. The data used is between 1901 to 2002 periods.

#### 4.3.3.2 Variability of regional SST patterns

Figure 4.10 demonstrates that the first three leading components of regional SST indices oscillate from high- to low-frequency components differently. It is suggested that the first mode corresponds to the seasonal changes of SST particularly over the South China Sea and the Coral Sea region associated with temperature rise over those particular regions (Figure 4.4). The considerable temperature rise that characterised regional SST is confirmed by dominant power spectrums on a 50.5 year cycle. This is proven by the index, which is mostly found below normal during the first half of the century and above normal on the other half (Figure 4.4).

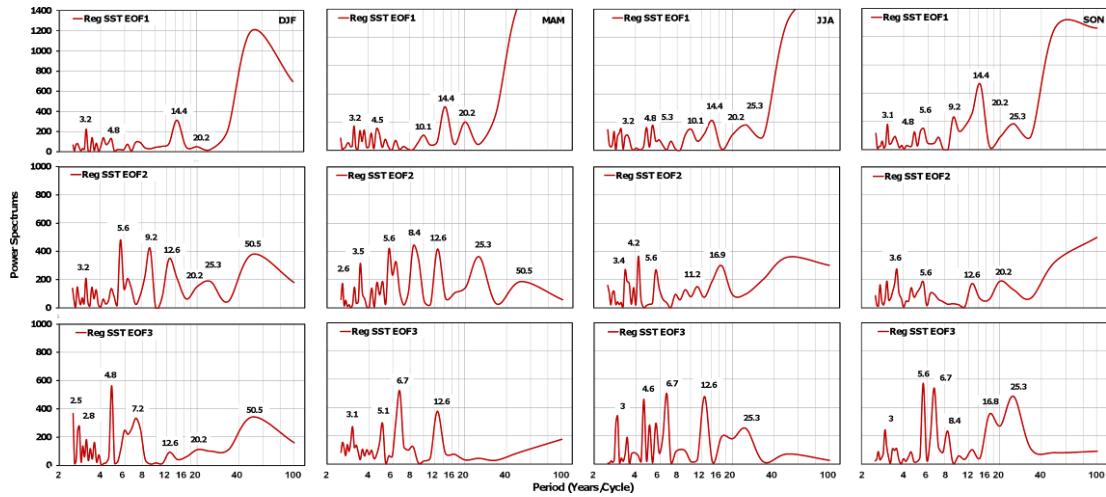


Figure 4.10: FFT Spectral analyses from the first three leading EOF of regional SST (1901-2002). Horizontal (x) axis is transformed into logarithmic scale.

In the first mode, the variability of SST is also signified by consistent 14.4 year interdecadal cycle in every season. This is different when compared to the climate indices that are dominated by decadal components around 9 to 12 years cycles. Considering the fact that the 14.4 year interdecadal variability is inconsistent with the climate indices, further investigations to assess the effect of this component on rainfall variability is needed. In the FFT of rainfall patterns (Figure 4.8), the sign of similar 14.4 year cycle can be found on the first mode in MAM and the second mode in JJA (Figure 4.8). In addition, it should also be noted that the regional SST variability in this first mode is also influenced by 20.2 year multidecadal component that is linked to the IPO variability.

Table 4.5: Correlations between Indo-Pacific climate drivers SST indices with PC time series of regional SST in the Austral-Indonesian region (1870-2006 periods) based on 10% (\*), 5% (\*\*), and 1% (\*\*\*) significance levels.

Indices	Austral-Indonesian SST (HadISST 1.1 dataset)											
	PC1				PC2				PC3			
	DJF	MAM	JJA	SON	DJF	MAM	JJA	SON	DJF	MAM	JJA	SON
Nino 3.4	DJF	0.36 ***			-0.72 ***				-0.28 ***			
	MAM		0.33 ***			-0.62 ***				-0.06		
	JJA			-0.30 ***			-0.46 ***				0.35 ***	
	SON				-0.48 ***			-0.67 ***				0.19 *
IOD	DJF	0.06			-0.33 ***				-0.04			
	MAM		-0.07			-0.37 ***				-0.23 **		
	JJA			-0.20 *			0.42 ***				0.18 *	
	SON				-0.26 **			0.68 ***				0.18 *
IPO	DJF	0.36 ***			-0.50 ***				-0.20 *			
	MAM		0.40 ***			-0.36 ***				0.04		
	JJA			0.11			-0.46 ***				0.49 **	
	SON				-0.22 **			-0.71 ***				0.24 **

Despite the decadal to multidecadal component regulating the variability in the first mode, the temporal component of regional SST also features interannual variation, although the power spectrums are not as high as in the lower-frequency timescales (Figure 4.10). The interannual variability of the first mode is associated with the ENSO index in Niño 3.4 region with significant correlations in DJF ( $r=0.36$ ), MAM ( $r=0.33$ ), JJA ( $r=-0.30$ ) and SON ( $r=-0.48$ ) (Table 4.5 and Figure 4.11). Table 4.5

shows connectivity of the regional SST index with seasonal data of the IPO index for all seasons except in JJA as well as with the IOD index particularly in JJA and SON.

In the second mode, the regional SST shows strong power spectrums particularly on interannual component (Figure 4.10). This confirms the finding in subsection 4.3.2 where the second mode of regional SST is strongly related to ENSO variability. It is shown that the prevailing interannual variability is mostly visible at around 3 and 5.6 year timescales, and the correlation with Niño 3.4, IOD and seasonal IPO index are relatively significant at all seasons. Among others, the strongest correlations are found to be consistent during SON season ( $r$  Niño 3.4=-0.67,  $r$  IOD=0.68 and  $r$  IPO=-0.71) (Table 4.5 and Figure 4.11). The FFT result also indicates decadal to multidecadal components that contribute to regional SST variability in the second mode and are possibly related to low-frequency variability in the Pacific. The power spectrums of decadal components around 8 and 12 year timescales are considerable enough to discern the low-frequency variability on this second mode, particularly during DJF and MAM seasons.

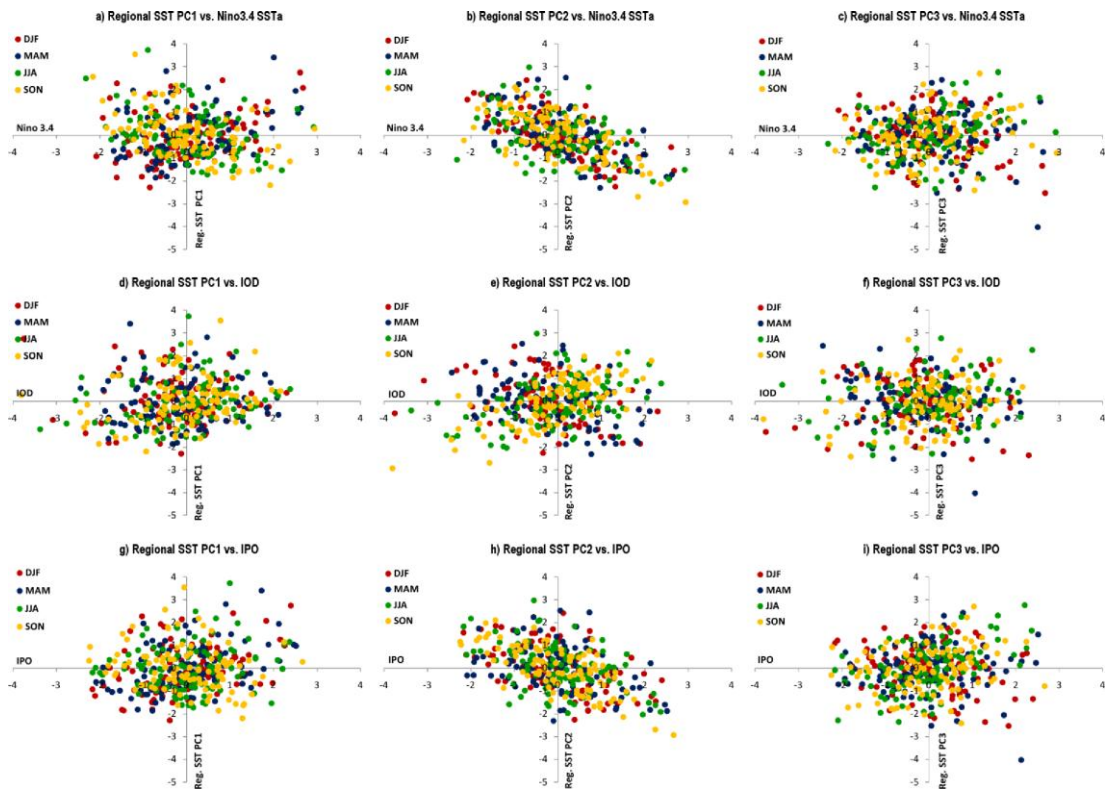


Figure 4.11: As Figure 4.9, but for three leadings EOFs of region SST.

The FFT result of regional SST index in the third mode also demonstrates variability at the range of interannual cycle but with dominant power spectrums existing in different periods, i.e., at 4.8 year period in DJF, 6.7 year in MAM and JJA, and 5.6 year in SON. Referring to the result already discussed in subsection 4.3.2, possible explanation for the inconsistency in interannual variability in the third mode is due to different seasonal responses of regional SST to ocean-atmospheric components in Indo-Pacific climate system, for example the interaction between the regional SST with the Indo-Pacific SLP anomalies (Figure 4.6; EOF3). Since the third mode of regional SST during JJA and SON are related to one of the IOD regions in the west of southern Indonesia, precisely on the coast off Java and Sumatra, the seasonal

irregularity of this particular SST mode could be a reason for the irregularity of IOD that affects its relationship with ENSO as discussed in subsection 4.3.2.1.

## **4.4 Low-frequency components of regional SST and rainfall**

### **4.4.1 Interdecadal structures**

In this subsection, the study investigates the dominant structure of regional SSTs and their relationship with rainfall variability on interdecadal timescales. The approaches by Power et al. (1999b) and McCabe and Palecki (2006) are adopted to determine the leading time-space patterns of the filtered seasonal SST data using EOF analysis. Filtering the data is aimed to remove the higher frequency spectrums such as ENSO and to isolate the leading structures of low-frequency components. The method can be calculated either by performing the low-pass band filter (e.g. Power et al. 1999b) or by simply using the moving average technique (e.g. McCabe & Palecki 2006; McCabe et al. 2004). In this section, a moving average is applied in order to isolate the low-frequency component by using ~14 year filtering window. This ~14 year window is chosen due to its dominant and consistent power spectrums on the regional SST data found in the first mode of regional SST index as described in subsection 4.3.3.2.

Here the study only analyses the first EOF mode of the filtered regional SST data. The spatial patterns obtained from the analysis show consistent results for all seasons. Obvious signs of the positive eigenvectors are mostly distributed in several local SST regions such as the sea off West Sumatra (OWS), the South China Sea (SCS), the Celebes Sea (CS), part of the Indian Ocean adjacent to West Australia (OWA), and the Coral Sea and Gulf of Carpentaria (Figure 4.12a). The approximate geographic areas of those local seas are presented in Table 4.6 and further analysis regarding their interactions with the inter-decadal climate phenomena will be discussed later in subsection 4.4.2. Those local SST zones are presumed to have an active role in regulating the low-frequency variability of regional SST associated with temperature rise. This is evident from the representation of the temporal component in the first mode and by the supremacy of positive eigenvector distributions over the region. The proportion of eigenvalues of this mode is represented in each season by 72.8% in DJF, 77.2% in MAM, 79.9% in JJA, and 80.6% in SON.

The temporal patterns represent fluctuations of the low-frequency component (Figure 4.12b) and correspond to a periodic warm (cool) phase whenever the value of SST is positive (negative). In general, four different phases appear during the late 19<sup>th</sup> and throughout the 20<sup>th</sup> centuries but are distributed inconsistently between seasons. The temporal shifting in DJF occurred in 1932, 1947, and 1972. These slightly differ with the changes during MAM that are found in 1936, 1942, 1962, 1967 and 1972. The epochs in MAM similarly happen in JJA season, while the repositioning in SON is similar to DJF although with different periods occurring in 1935, 1945, and 1965.

The correlation analysis is used to study the low-frequency SST-rainfall relationship. The leading principal component from the filtered SST data are correlated with terrestrial rainfall anomalies smoothed using the same 14-year filter. A positive correlation is related to an increase (decrease) of the regional SST index in low-frequency timescales that will relatively increase (decrease) the rainfall within the

region. An opposite situation will occur in the region that is identified with a negative correlation. The results show that the low-frequency SST-rainfall relationships vary seasonally over the regions (Figure 6).

In the Indonesian region, varying seasonal correlations are apparent over most of its main islands, such as Sumatra, Borneo (Kalimantan), Celebes (Sulawesi), Java and Papua. The rainfall correlation with the first mode of filtered SST shows a strong positive pattern over all of Sumatra during JJA period. The signs are partially changed into negatives over the northern part of the region in DJF. The Borneo (Kalimantan) Island has consecutive negative correlations during DJF to JJA and it changes into positive in SON. Positive correlations distinctly appear over Sulawesi Island during transition periods in MAM and SON, while in the other two seasons the correlations are low. The relationships over Java are mostly positive during DJF and JJA, while in MAM the signs are negative with prevailing correlation appear in central Java.

The interdecadal variability of regional SST is also found to strongly affect the low-frequency rainfall variability over the northern Australian region. Opposite correlation patterns that appear between the western and eastern part of the region during DJF season could be a rational explanation of the rainfall rise over North West Australia. Based on those correlation patterns, an increase of low-frequency regional SST index is associated with an increase of rainfall in the west of northern Australia and a decrease of rainfall in the eastern region. The opposite rainfall changes in both areas is also related to interannual changes of SST and SLP anomalies as already discussed in subsection 4.3.1.2 (*see* Figure 4.1, 4.2 and 4.3; DJF, EOF3).

In other seasons, the positive correlation pattern changes in MAM season to the centre and eastern part of the northern-Australian region with the positive sign remains in the northern part of Queensland. In JJA season, the low-frequency SST-rainfall relationship is strong over the Northern Territory. This condition changes in the next season (SON) where most of the positive correlations are spread over the centre and eastern part of the Northern Australian region.

#### **4.4.2 Rainfall climatology and low-frequency modulation of local SSTs**

In this subsection the study analyses interdecadal variability of local seas in the Austral-Indonesian region and their interactions with the low-frequency climate indices. From the analysis previously performed in subsection 4.4.1, the study identified five local SST zones based on the EOF analyses (Figure 4.12a). Those local zones (listed in Table 4.6) are presumed to have an active role in regulating the low-frequency variability within the region and play a significant role in impacting the rainfall variability. To analyse each of the selected region, the SST data extracted from these local seas are filtered using 14 years cycle as indicated in subsection 4.4.1 and the results are shown in Figure 4.13.

The IPO index (Folland et al. 1999, 2002) is used to compare the variability of each local SST to investigate their response to interdecadal climate drivers. The index is similarly filtered using 14 years moving average as the local SST data. As a note of caution, the simple filtering method used in this analysis might slightly alter the period of the well-known climate regime shifts. Nevertheless, it will not significantly

change the main low-frequency pattern found in the data. In addition, the study also uses the Pacific Decadal Oscillation (PDO) data (Mantua & Hare 2002; Mantua et al. 1997), but due to its similarity with the IPO, the study will only refer to the IPO for this analysis.

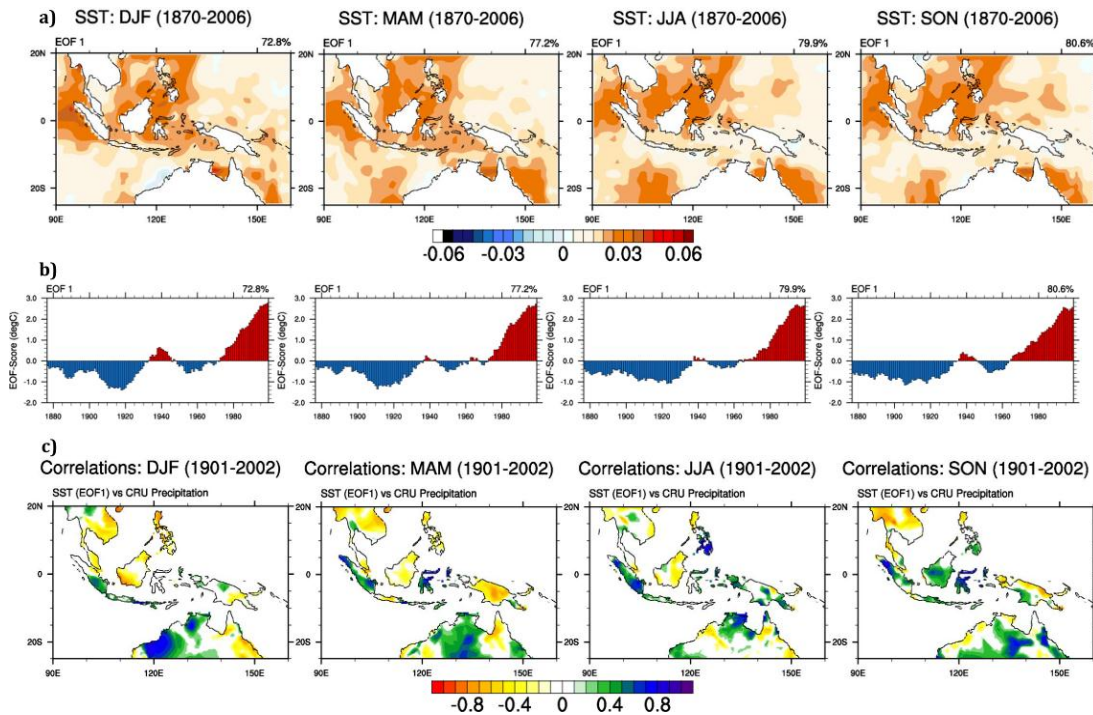


Figure 4.12: Interdecadal variability of regional SST data, a) EOF eigenvector of 14 year filtered regional SST data, b) EOF scores from the same EOF analysis, and c) correlation of EOF scores with 14 year filtered rainfall.

The sign of interdecadal variability in the local SSTs influenced by the large-scale climate index is evident. This is shown by the fluctuation of local SSTs that follow climate indices, although it is not dominant due to significant discrepancies with the SST variability associated with the strong properties of the local seas. The differences are likely caused by significant temperature rise in the local SSTs where in the first half of the century they show as cool phase (negative anomalies) and in the other half they tend to be on warm phase (positive anomalies). This is not the case for the IPO index where there is no trend of their temporal pattern. Consequently, the long-term modulations found in the IPO do not match with the epochs found in local SST anomalies. For example, between 1901-50 periods when the IPO experienced two positive phases, the local SSTs remained negative. Conversely, during the cool phase of the IPO in around 1950-80 periods, the local SSTs are less cool. In fact, for several local SST such as in the CS-GC region, the SST anomalies change into positive after 1970.

Further, the study investigates the link between the SST rises in the local seas and the rainfall anomalies on different phases of the Indo-Pacific climate regimes. Here the rainfall anomalies divided into three different phases of climate epochs are calculated based on their departure from 1901-2002 reference periods. Those three different periods are negative phases within 1947-1976 and two positive phases in the 1925-1946 and 1977-2002 periods.

Table 4.6: Identified local SST zones with strong eigenvectors obtained from interdecadal regional SST analysis

Region	Latitude	Longitude
West Coast off Sumatera and Malacca Strait	5°S – 10°N	90° – 100°E
South China Sea	Eq° – 15°N	105° – 115°E
Celebes Sea	5°S – 10°N	115° – 125°E
South Indian Ocean off West Australia	25° – 15°S	100° – 115°E
Coral Sea and Gulf of Carpentaria	25° – 10°S	135° – 158°E

In Figure 4.14, the rainfall climatology confirms negative rainfall anomalies dominating the Austral-Indonesian region during 1925-1946 periods in most of the seasons. Interestingly, it is the period when the IPO experienced positive phase and the local SSTs are mostly negative. The overriding decrease of rainfall anomalies during this episode indicates a negative relationship with the IPO index, and a positive one with the local SSTs. In the case of a consistent link between rainfall and the IPO, the distribution of rainfall anomalies during the warm phase in the late 20<sup>th</sup> century will be mostly negative. Unfortunately, this is not the case despite various responses of local rainfall to interdecadal variation of the IPO. Reversely, the rainfall relationship with the local SSTs is relatively consistent. This is indicated by the positive phase of the SSTs concurring with dominant positive rainfall across the region particularly in DJF.

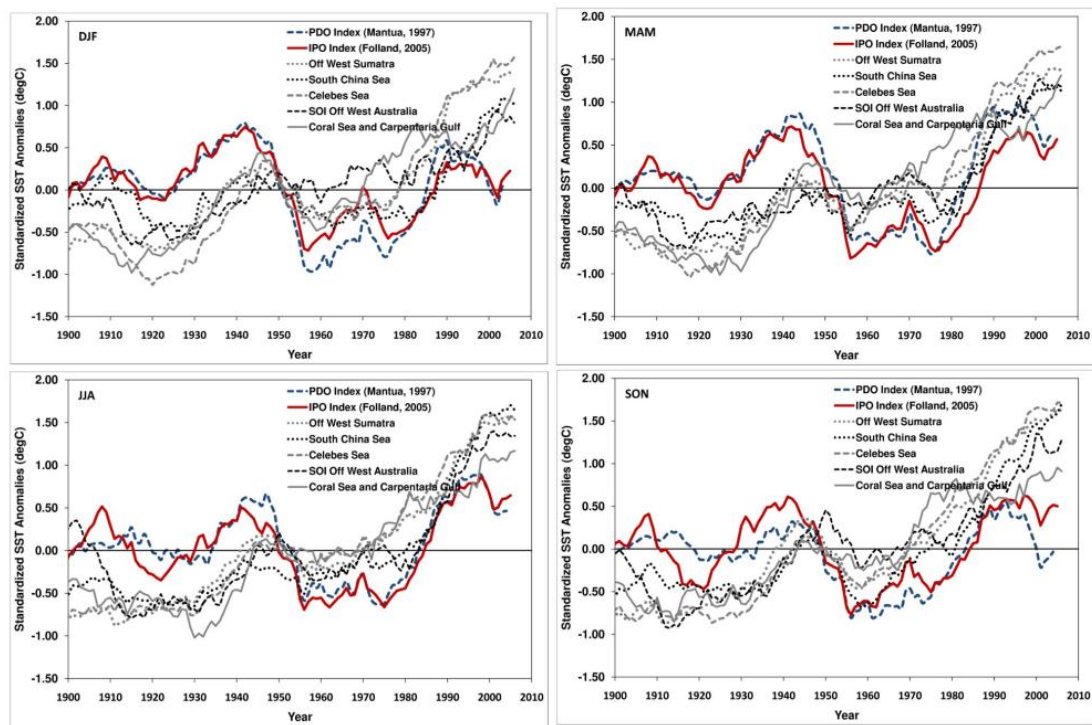


Figure 4.13: The time series of local SST filtered using 14 years moving average. The results are compared with the IPO and PDO indices performed using the same filter.

Overall, the large scale climate phenomena such as the IPO are affecting low-frequency rainfall variability by influencing the local SSTs as described previously. Nonetheless, the regional SSTs play a more important role in driving the long-term rainfall variability across the region. The regional SST-rainfall relationship also differs between seasons, and the plausible explanation of this variation is due to the differences in local responses to regional SST variability, as well as the seasonal variability of the regional SST itself.

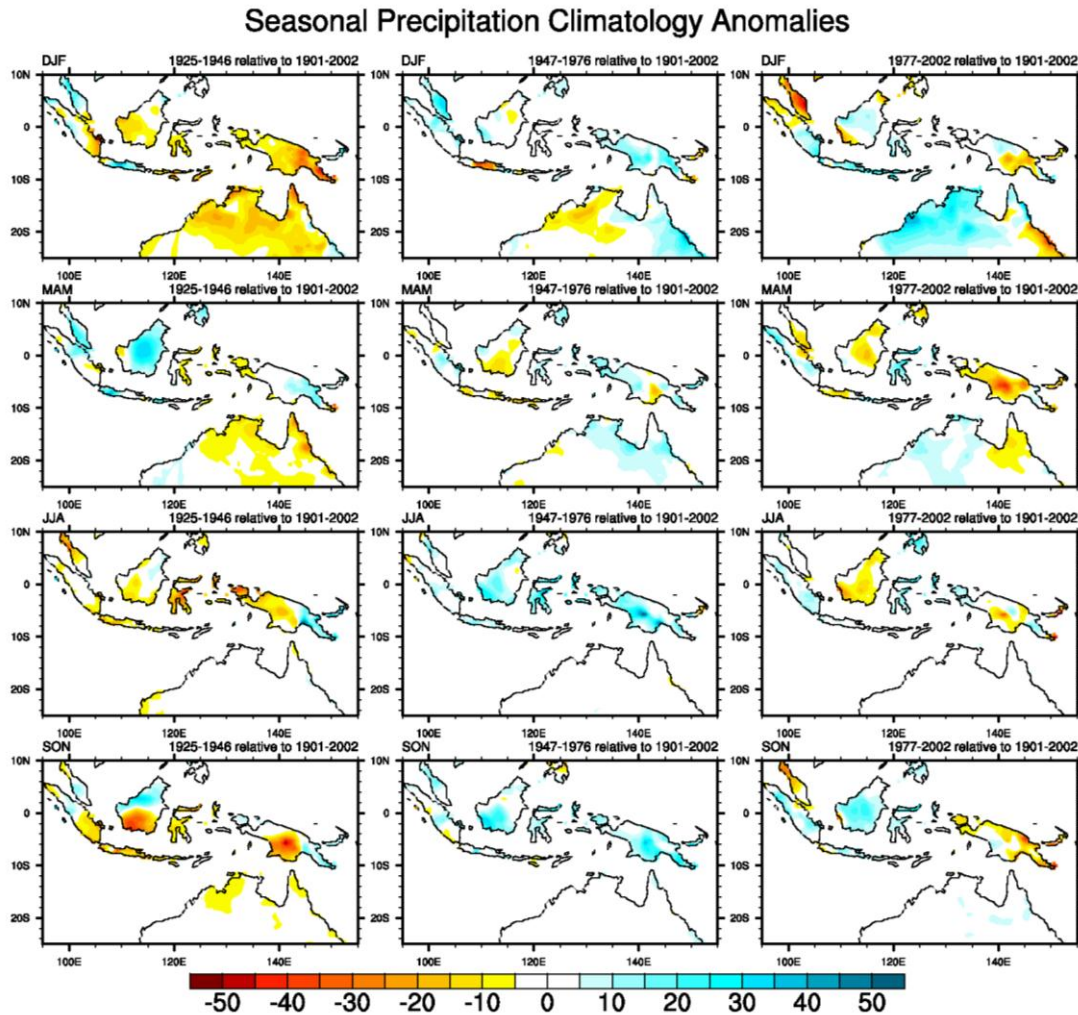


Figure 4.14: The anomalies of seasonal rainfall climatology during different phases of interdecadal variability; a) 1925-1946, b) 1947-1976, and c) 1977-2002 (units in mm/month)

The important role of regional SST in driving the regional rainfall in low-frequency variability is also supported by the correlation results between the EOF scores with the rainfall presented in Figure 4.12c. If the correlation pattern with the rainfall anomalies for the period 1977-2002 is compared, the patterns are similar for most of the regions at all seasons, except for northern Australia during JJA and SON where no differences are found in the rainfall anomalies.

### 4.4.3 Impacts of climate epochs on regional rainfall and SST patterns

In subsection 4.3.1 and 4.3.2, the study analyses the leading patterns of rainfall and regional SST in the Austral-Indonesian region. It is found that the first mode of rainfall and the second mode of regional SST patterns are closely linked to the interannual variability of Indo-pacific climate drivers. These particular regional SST patterns also show similar patterns with correlation fields of rainfall patterns in the first mode and the Indo-Pacific SST anomalies. Given that the interdecadal variability of regional/local SST variability and rainfall are impacted by the low-frequency climate drivers in the Pacific, it is important to study the changes of identified rainfall (first EOF mode) and regional SST (second EOF mode) patterns on different phases of climate regimes as in Figure 4.14.

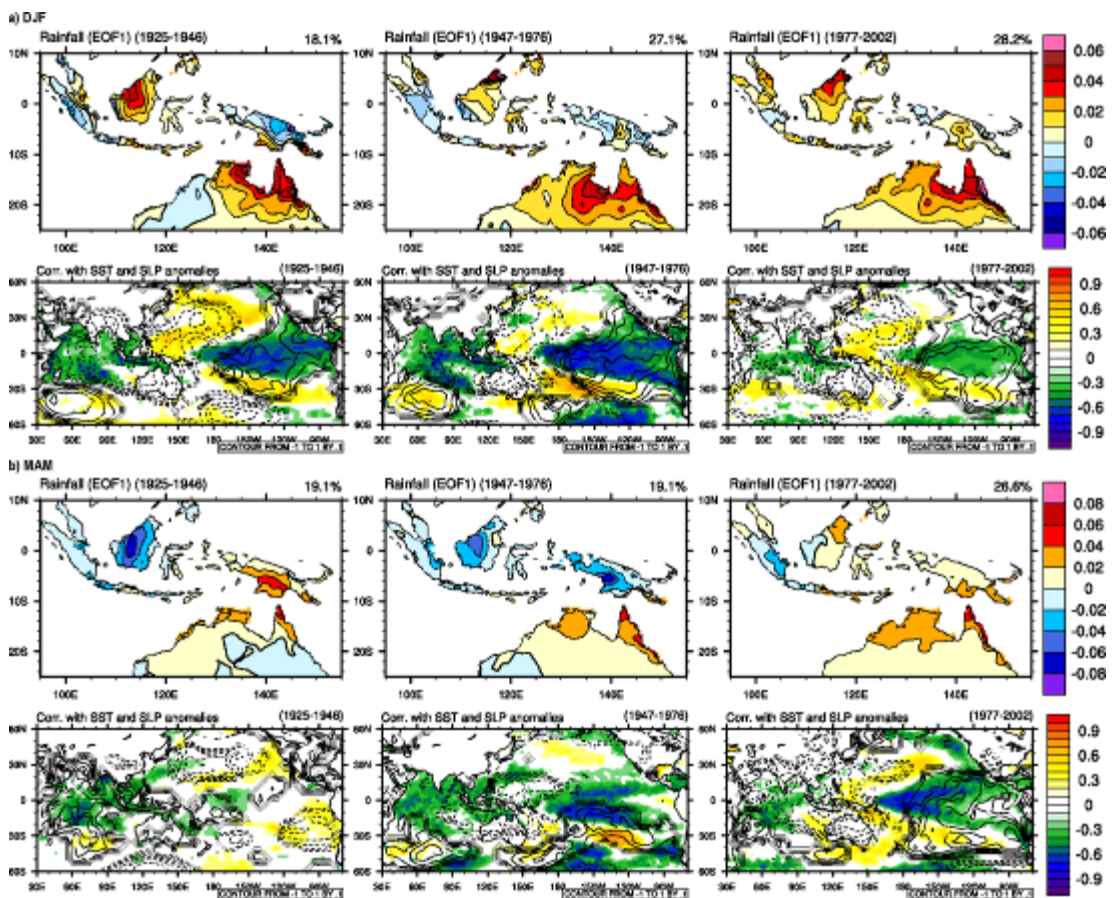


Figure 4.15(a-b): The first EOF mode of rainfall index calculated from different phases of climate regimes (1925-1946, 1947-1976 and 1977-2002) and their correlations with Indo-Pacific SST and SLP anomalies; a) DJF, and b) MAM (continue). Correlation results between the rainfall index with SST anomalies are presented by filled contour and overlaid with the correlation result of the index with SLP anomalies performed by solid (+) and dash (-) contours. The correlation patterns are significant at 5% significance level.

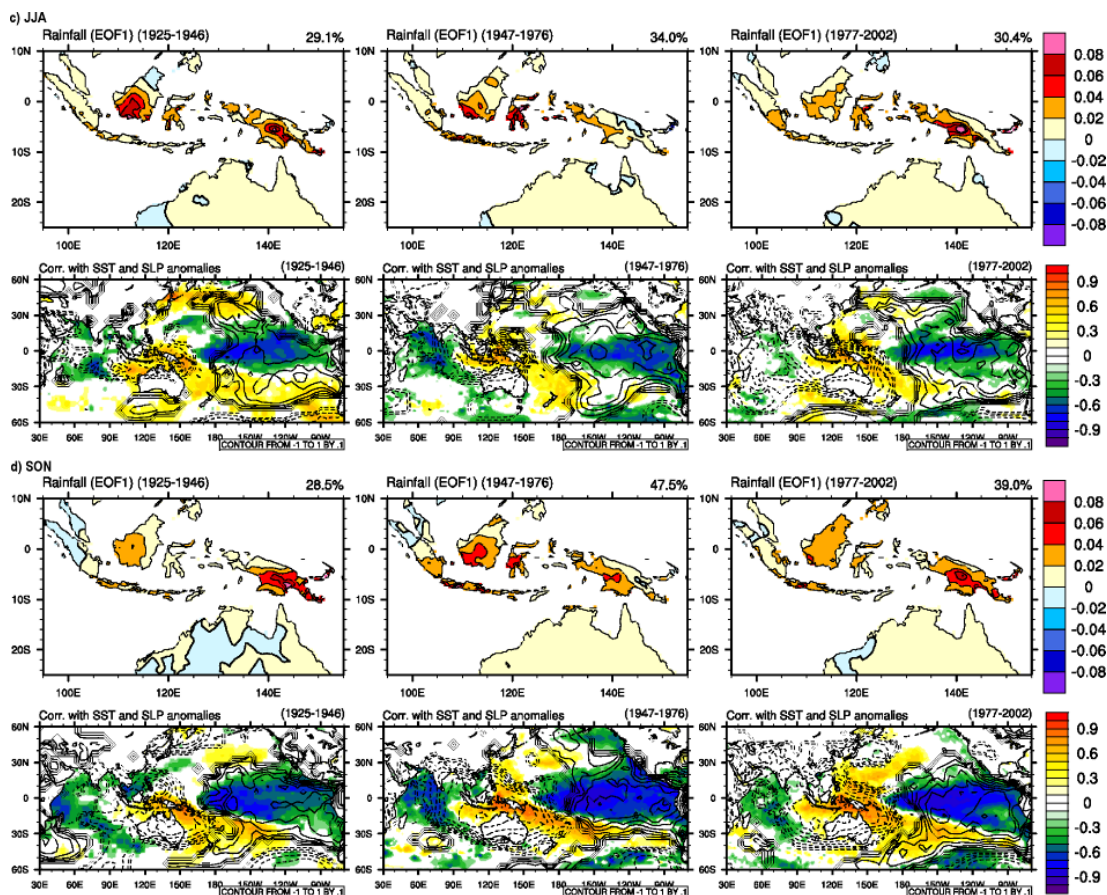


Figure 4.15(c-d): Continue from 4.15(a-b), for c) JJA and d) SON.

Here the study discusses the comparisons between the leading rainfall patterns and their correlations with SST and SLP anomalies in the Indo-Pacific region with different climate regime shifts. During the Austral summer monsoon period (DJF), predominant rainfall patterns in 1925-46 periods appear over north east Australia and some parts of Indonesia including East Java, Bali, Nusa Tenggara, Sulawesi, Borneo, Moluccas, and the coastal region of south-eastern Papua. The overriding regions are different on the negative phase (1947-1976). In this period, there is an extension of the rainfall pattern over northern Australia and some shifts in most of the Indonesian region. The pattern is reduced in Borneo, stronger over Sulawesi and shifts into the western part in Java. In periods where the strong positive phase occurs (1977-2002), the prevailing rainfall patterns appear in almost the entire Indonesian region.

In general, Figure 4.15 shows the EOF1 of seasonal rainfall patterns and their correlations with Indo-Pacific SST and SLP anomalies on three climate epochs. It is found that the first leading rainfall patterns differ between seasons and vary on different phases. The discrepancies of affected rainfall regions linked with Indo-Pacific climate drivers on different phases confirm the importance of regional SST variability in the Austral-Indonesian region. This can be clearly shown by the correlation patterns between the first modes of rainfall index with SST anomalies on different climate phases in each season. The role of regional SST in transmitting the ENSO effect is mostly governed by the SST outside the ENSO region related to the northern and southern Pacific pathways (e.g. Cai et al. 2005b). Considering the correlation between the first mode rainfall indices with SLP anomalies in the Indo-Pacific region, the study found correlation patterns over the Pacific Ocean and the

Austral-Indonesian region. The latter spreads into the western Indian Ocean resulting in no signs of dipole mode in the SLP correlation patterns. These are consistent with the results found in subsection 4.3.1.2.

The strength of the transmission from those two regions into the regional seas that usually forms a 'boomerang' pattern in the western Pacific region (McBride et al. 2003) will mostly determine the affected rainfall region (*see* Figure 4.15). The weakest effect is usually found in MAM where the western and eastern SST region conjoined and eliminated the 'boomerang' pattern. A good example of this condition can be seen during negative phase of interdecadal climate variability in 1947-1976 periods where the rainfall patterns in Indonesia were mostly negatives (Figure 4.15b). In contrast, the expansion of the 'boomerang' pattern optimises in Indonesia during SON period, allowing the formation of SST dipole in the Indian Ocean. This can be seen, for example, at the correlation patterns of rainfall patterns with the Indo-Pacific SST anomalies during 1977-2002 periods (Figure 4.15 d).

It is evident that the 'boomerang' pattern formed by the positive correlation patterns dominates the Austral-Indonesian region and suppresses the negative patterns into the western Indian Ocean. As a result, most of Indonesia will be affected by the changes in SST within the region and encounter negative feedback to SST anomalies in the central and eastern Pacific, as well as in the western Indian Ocean. The fact that the negative rainfall pattern is shown over the west of northern Australian region in 1925-46 periods (Figure 4.15a) is due to the expansion of the negative correlated region in the seas between Indonesia and northern Australia into the Coral Sea region that suppressed the influence of the positive correlation region that usually appears in the east of Australia.

More detail on the progression of the regional SST patterns in the region in different phases of climate regimes can be seen through their second EOF mode (Figure 4.16). This study finds that in different climate phases, the formations of two main contradictory patterns over the western and eastern Austral-Indonesian region, particularly during DJF and MAM seasons are incomparable between negative and positive phases. In the two positive phases, 1925-46 and 1977-2002, the eastern patterns during DJF and MAM seasons are likely to represent the 'boomerang-like' curve that interacts with opposite patterns in the western part. The distinction between those two positive periods can be seen from the pattern over the west of Australia. During the negative phases in 1947-1976 periods, the prevailing positive eigenvector appeared in the eastern part seemed to dominate the Austral-Indonesian region and isolated the opposite eastern patterns into the SCS region.

The disparity of regional SST patterns on different phases also appears during JJA and SON period. The marked differences between successive epochs are on the positioning of the patterns from the east into the southern Indonesian region as well as on the strength of the pattern in the west of Australia. In boreal summer (JJA), the SST eigenvector pattern in 1925-46 periods is located in the western part of the Austral-Indonesian region around Papua, up to the Molucas Islands. The pattern remained on the eastern part of the region and slightly weaker during 1947-76 periods. Conversely, a perfect positioning of these positive eigenvectors appears during 1977-2002 periods. Noting that the phase is related to warmer ENSO events (El Niño), the evincing pattern that forms over southern Indonesia is linked to rainfall decrease within most of the Austral-Indonesian region. Similar distributions

of the positive eigenvectors are also found during the Austral spring season (SON), except for the 1947-76 periods where the pattern seems to be failing to develop and only appears in the western coast off Papua.

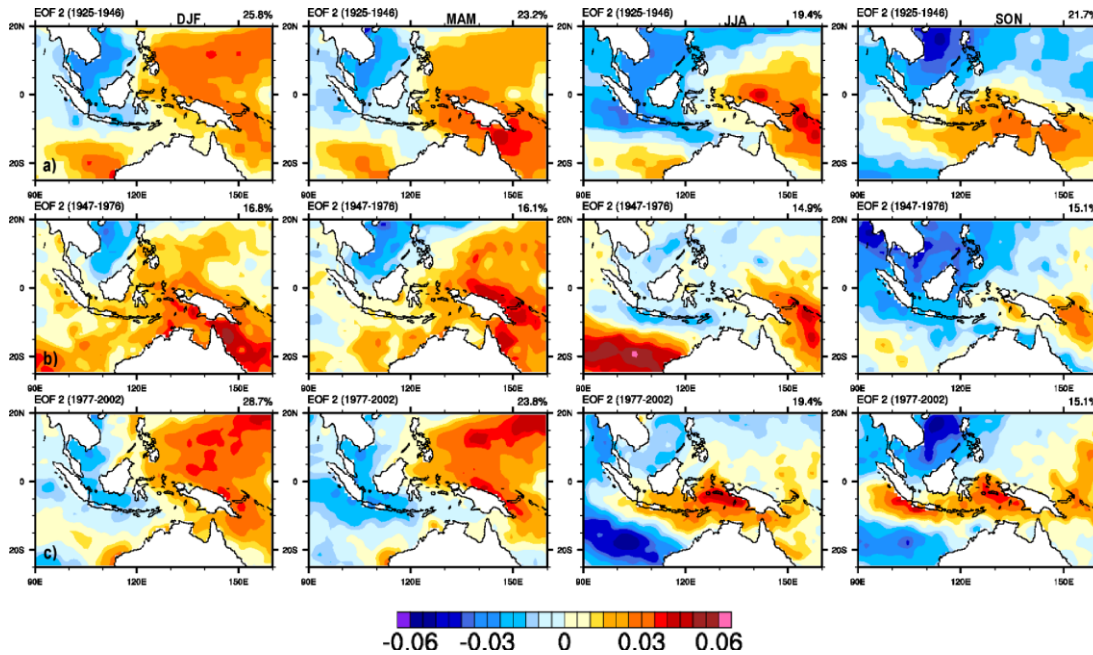


Figure 4.16: EOF2 of regional SST eigenvector distributions for three periods: a) 1925-1946, b) 1947-1976, and c) 1977-2002 (unitless).

Among the three phases, dissimilar responses are found during JJA and SON seasons over the western part of southern Indonesia, particularly over the southwest coast off Java and Sumatra. This region is related to one of IOD region that receives an inconsistent/nonlinear ENSO signal, contributing to non-linear IOD occurrence that seem to be separated from ENSO. Based on this result, it is possible that the independent IOD events are solely due to a nonlinear relationship between the SST and ENSO associated with inconsistencies in receiving ENSO signals. This is consistent with the result performed in subsection 4.3.2.1 where it shows the unique signal performed by EOF3 of regional SST that could be as a result of the deviation of the ENSO signal transmission into the west coast off Java and Sumatra.

## 4.5 Summary

In this Chapter, the study aims to improve our understanding by investigating the role of regional SST in the Austral-Indonesian region in moderating the impact of large-scale climate drivers on interannual and interdecadal rainfall variability. Several important findings are listed below:

- Analyses of seasonal SST patterns in the Austral-Indonesian region have identified the important role of regional SST in moderating the impact of large-scale climate drivers on rainfall variability. Its seasonal patterns are linked with (i) significant temperature rise, (ii) considerable ENSO and IOD interannual variability, and (iii) a unique signal that enriches the SST variability around the west coast off Java and Sumatra despite the influence of ENSO. The latest could be related to the significant role of this SST region in controlling the IOD events regardless of its dependency to ENSO.

- Despite some evidence of the link between the IPO and regional SST on interdecadal timescales, the significant temperature rise found in the regional SST during the 20<sup>th</sup> century shows more significant impact on moderating the interdecadal rainfall variability in the region. This finding accentuates the importance of using trends and low-frequency oscillations in regional SST data in order to increase rainfall predictability in the future by including those components in the long term prediction models.
- Investigation of the first mode of rainfall and the second mode of regional SST loading patterns in three different phases of climate regime shifts, i.e. a) 1925-1946, b) 1947-1976, and c) 1977-2002, suggests that the variations of interannual rainfall variability in the region in different seasons and different climate phases are determined by the strength of the transmission from the northern and southern Pacific into the regional seas.

This study emphasises the usefulness of analysing the leading seasonal rainfall and SST patterns in order to trace the link with the climate drivers affecting their variability. Furthermore, strong evidence is also found on the structure of regional SST showing the leading role of regional SST in moderating the ENSO and IOD connectivity and in controlling their dependency. Therefore, further analysis is needed and will be performed based on climate model output under a pre-industrial control simulation. This is essential in order to understand the underlying mechanisms, particularly under conditions where there is no impact of climate change.

## **Chapter 5 Rainfall Variability and ENSO-IOD Dependency in Pre-Industrial Climate**

The state-of-the-art climate model output from the CSIRO-Mk3.5 pre-industrial control simulations (Gordon et al. 2004; Smith 2007) is analysed in this Chapter. The analysis includes identification of seasonal rainfall patterns and their link with ocean-atmosphere variables. The approach used in Chapter 4 is implemented to identify the main contributing processes of the Indo-Pacific climate drivers such as ENSO and IOD in controlling the rainfall variability in the Austral-Indonesian region. An analysis of the rainfall composites during ENSO and IOD events as well as the relationship between ENSO and IOD during the simulated pre-industrial climate is discussed. Extending the results found in Chapter 4, by using the pre-industrial modelled data, this study verifies the strong relationship between rainfall variability and the large-scale mechanisms of Indo-Pacific climate drivers, i.e. ENSO and IOD. It also affirms the ENSO-IOD dependency and the role of regional/local SST in moderating the influence of ENSO upon the IOD.

### **5.1 Background**

Interannual variability of seasonal rainfall in the Austral-Indonesian region is strongly affected by Indo-Pacific climate drivers such as ENSO (e.g. Chang et al. 2004; Haylock & McBride 2001; Hendon 2003; Kirono et al. 1999) and IOD (Ashok et al. 2003; Boer & Faqih 2004; Cai et al. 2005a; Saji et al. 1999). The influence of those large scale climate drivers varies seasonally due to the monsoon (Terray et al. 2006; Terray et al. 2005a; Terray et al. 2005b) but with often discovered phase-locking events between them (Annamalai et al. 2003; Gualdi et al. 2003; Yu & Rienecker 2000), leading to a strong statistical relationship (Allan & Coauthors 2001). A recent study using GCMs suggests that the phase-locking is related to a consequence of a zonal shift in the centre of convection associated with ENSO (Fischer et al. 2005). In addition, Fischer et al. (2005) propose the role of an anomalous Hadley circulation over the eastern tropical Indian Ocean and Maritime Continent with an early northward incursion of the Southern Hemisphere southeasterly trades as the main trigger of independent IOD to ENSO events. Nevertheless, the issue regarding the dynamical process of the independent IOD to ENSO event remains controversial (Allan & Coauthors 2001; Dommengeset & Latif 2002; Dommengeset et al. 2006; Fischer et al. 2005; Saji et al. 1999; Saji & Yamagata 2003).

Previous analysis in Chapter 4 noted the importance of using the leading seasonal rainfall patterns in order to trace the mechanisms in Indo-Pacific ocean-atmosphere interactions in controlling the rainfall variability. The analysis has satisfactorily delineated the physical processes related to ENSO and IOD events as indicated in the correlation with the observed SST anomalies. It demonstrates the significant role of SST in generating the interannual variability associated with the climate drivers and in regulating the interdependency between them. In this Chapter, the method in Chapter 4 is adopted to investigate the origin of the physical processes that drive rainfall variability as simulated in the CSIRO-Mk3.5 climate model data (Gordon et al. 2004; Smith 2007) (*see* Chapter 2 for data description). In this state, there will be no impact of climate change that could possibly alter the underlying process of the ENSO-IOD relationship (e.g. Terray & Dominiak 2005). Considering the need to

analyse the role of ocean-atmosphere dynamics (Clement et al. 1996), more climate variables such as ocean surface upward sensible and latent heat flux, atmosphere water vapour content, and zonal and meridional wind stress are analysed in addition to SST and SLP data. Here the study will analyse those variables in terms of their relationship with the leading seasonal rainfall patterns. Further, the definitions of ENSO and IOD events based on the SST data will be addressed to develop rainfall composites and to investigate parallel ENSO-IOD occurrences under the modelled pre-industrial climate.

## **5.2 Simulated rainfall climatology and time series**

### **5.2.1 Rainfall climatology**

In this analysis seasonal rainfall climatology from observations and a 500 year CSIRO-Mk3.5 control run with pre-industrial climate forcing is compared for four periods: 1901-2000 (Figure 5.1b), 2001-2100 (Figure 5.1c), 2101-2200 (Figure 5.1d), and 2201-2300 (Figure 5.1e). Considering that the typical simulated control run is run under pre-industrial conditions without additional natural and anthropogenic forcing (IPCC 2005), the study finds no considerable difference in the spatial rainfall distributions between those four detached periods. Such resemblance allows this study to analyse longer data, i.e. 500 year periods (1801-2300).

The difference between the simulated and the observed climatological rainfall over land during the 1901-2000 periods is found to be small. The main difference is situated over mountainous regions such as in Papua during the MAM and JJA seasons as well as in the well-known Borneo vortex area that is associated with synoptic-scale deep convection (see Chang et al. 2005) during DJF. In the western Pacific Ocean region, rainfall is overestimated. Despite this scantness, the model is able to simulate the seasonal rainfall distribution that is linked to the monsoon propagation and the positioning of the inter-tropical convergence zone (ITCZ). This is a positive outcome that can underpin any rainfall simulations which are forced with realistic natural and anthropogenic impulses, e.g. simulating the 20<sup>th</sup> century climate (20c3m).

### **5.2.2 Terrestrial rainfall: interannual and decadal time series**

The study now examines the monthly-mean time series of averaged terrestrial rainfall (95°E-155°E, 25°S-10°N, Figure 5.2). The rainfall grid from the modelled data is delineated by conforming to the land area fraction data as outlined in Chapter 3. The long-term monthly-mean time series (Figure 5.2a) shows rainfall varies between 1 to 9 mm/day. The decadal variability seems to be repeated in every century as shown by a 13-year low-pass band filter (Figure 5.2b). The interannual variability represented by a 5-year low-pass band filter deviates more frequently during the 19<sup>th</sup> century simulation compared to the 20<sup>th</sup> century simulation. The larger variability of Mk3.5 compared to the observations can be noted by the larger amplitude in the time series of Figures 5c, 5e, 5d and 5f. Focusing the simulations only on the 20<sup>th</sup> century, the Mk3.5 control data shows more variability on its monthly-mean time series compared to the observation (Figure 5c and 5e). This is further shown in the 5-year and 13-year filtered data (Figure 5d and 5f).

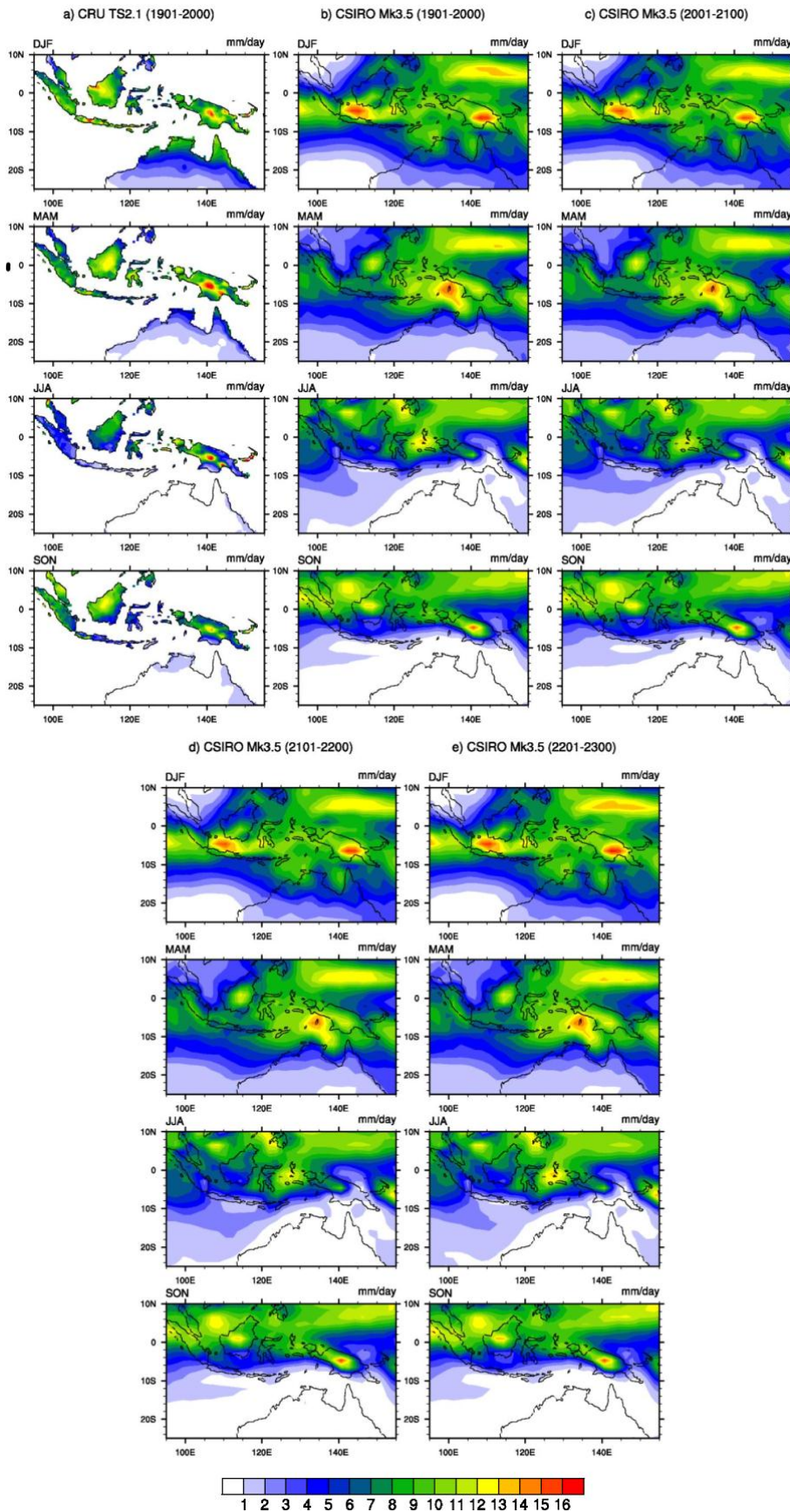


Figure 5.1: Seasonal rainfall climatology from (a) observations (100 year periods, 1901-2000), and CSIRO-Mk3.5 data: b) 1901-2000, c) 2001-2100, d) 2101-2200, and e) 2201-2300 periods (units in mm/day).

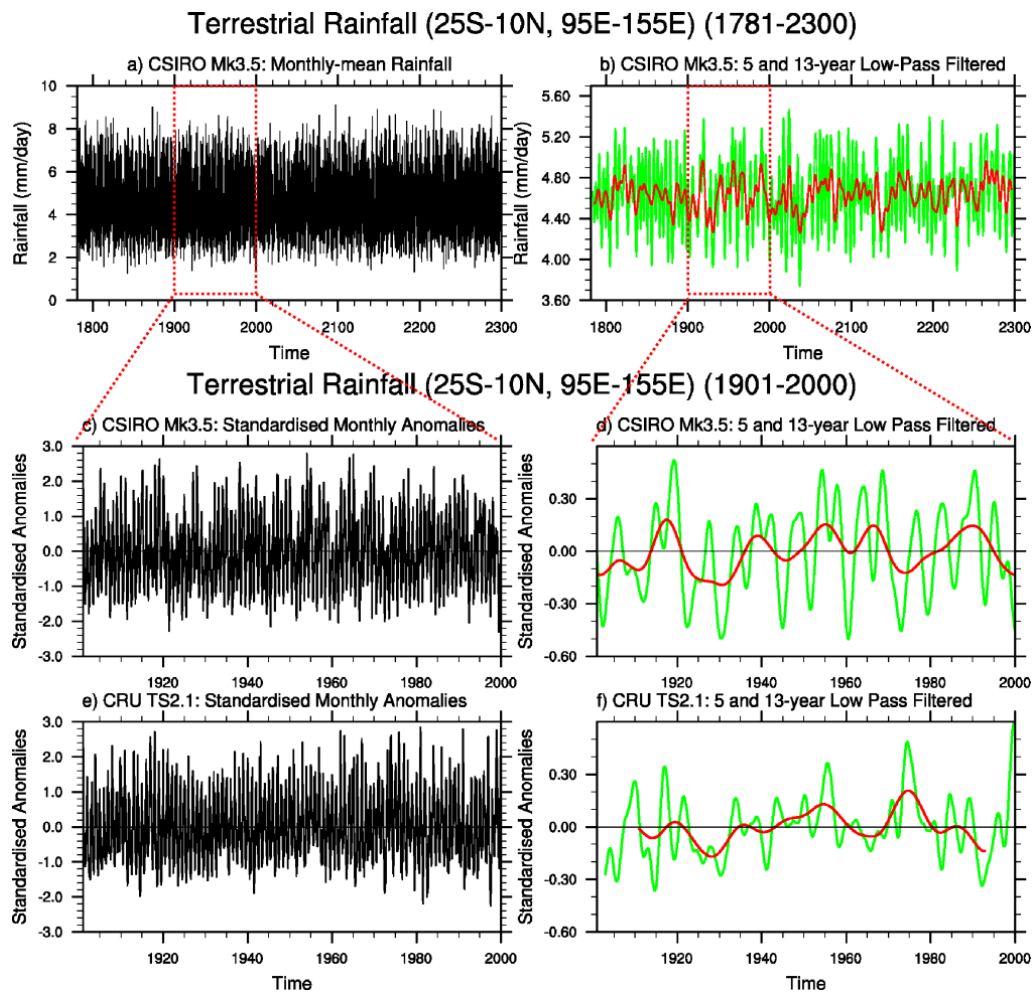


Figure 5.2: Terrestrial rainfall anomalies (mm/day) in the Austral-Indonesia region, a-d) CSIRO-Mk3.5 pre-industrial control monthly rainfall anomalies and 5-year and 13-year low-pass filtered, e-f) observed CRU TS2.1 monthly rainfall anomalies with 5-year and 13-year filtered.

### 5.3 The simulated rainfall patterns

#### 5.3.1 Terrestrial rainfall patterns based on EOF analysis

The rationale of using pre-industrial control data from the output of a climate model in this study is to investigate the physical processes of air-sea interaction involving large-scale climate drivers in controlling the rainfall variability unforced by the climate change impact. Further analysis of the model output provides substantial elucidation on the result performed in Chapter 4. Following the method used in that Chapter, Figure 5.3 demonstrates the seasonal rainfall patterns obtained from the EOF analysis of terrestrial rainfall data.

Due to the model resolution, not all parts of the terrestrial rainfall region are covered by the eigenvector maps shown in Figure 5.3. The contouring has also omitted several terrestrial rainfall grid points over the Indonesian region. The difference in the time periods of CSIRO-Mk3.5 used in Figure 5.3, which is longer than the observed data used in Figure 4.1, makes comparison between those two figures a bit difficult. However, the result shows spatial rainfall patterns that compare favourably

with the observed data as previously shown in Chapter 4 for most of EOF patterns especially for the northern Australian region. The rainfall signatures demonstrate strong positive eigenvectors over northern Australia and parts of Indonesia in the first EOF mode. The second EOF mode exhibits negative eigenvectors over most of northern Australia and eastern Indonesia, while positive patterns appear in the western section. A contrasting pattern seen in the west and east of northern Australian (EOF 3) suggests a relatively well defined rainfall pattern in the pre-industrial control run due to its similarity to the observation data as shown in Figure 4.1. The result provides the confidence to further analyse the data.

The rainfall patterns during the transition period (MAM) are associated with a positive pattern over the west of northern Australia and a negative pattern over eastern Papua. Similar signatures as in DJF are found in the second and third mode of rainfall EOFs. The shifting of the monsoon propagation during the Austral winter leaves an impression of dry conditions over northern Australia and more rainfall over some parts of northern Indonesia. These are evident from relatively low positive and stronger negative eigenvector values (Figure 5.3c). Comparable spatial rainfall patterns from the three EOF modes are consistently shown until the next transition period in SON (Figure 5.3d).

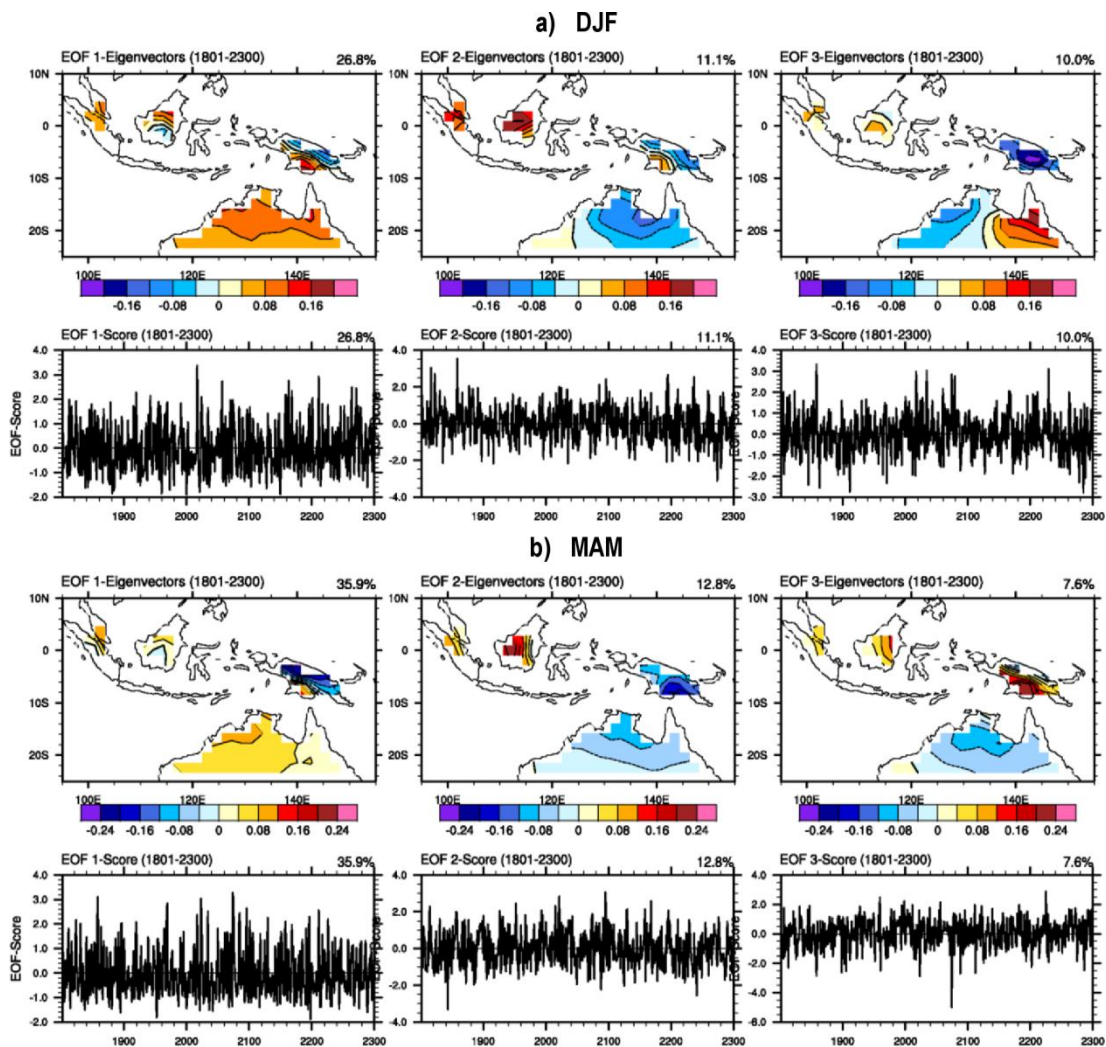


Figure 5.3: The first three modes of EOF from the standardised terrestrial rainfall anomalies (500 year periods, 1801-2300): a) DJF and b) MAM (continue).

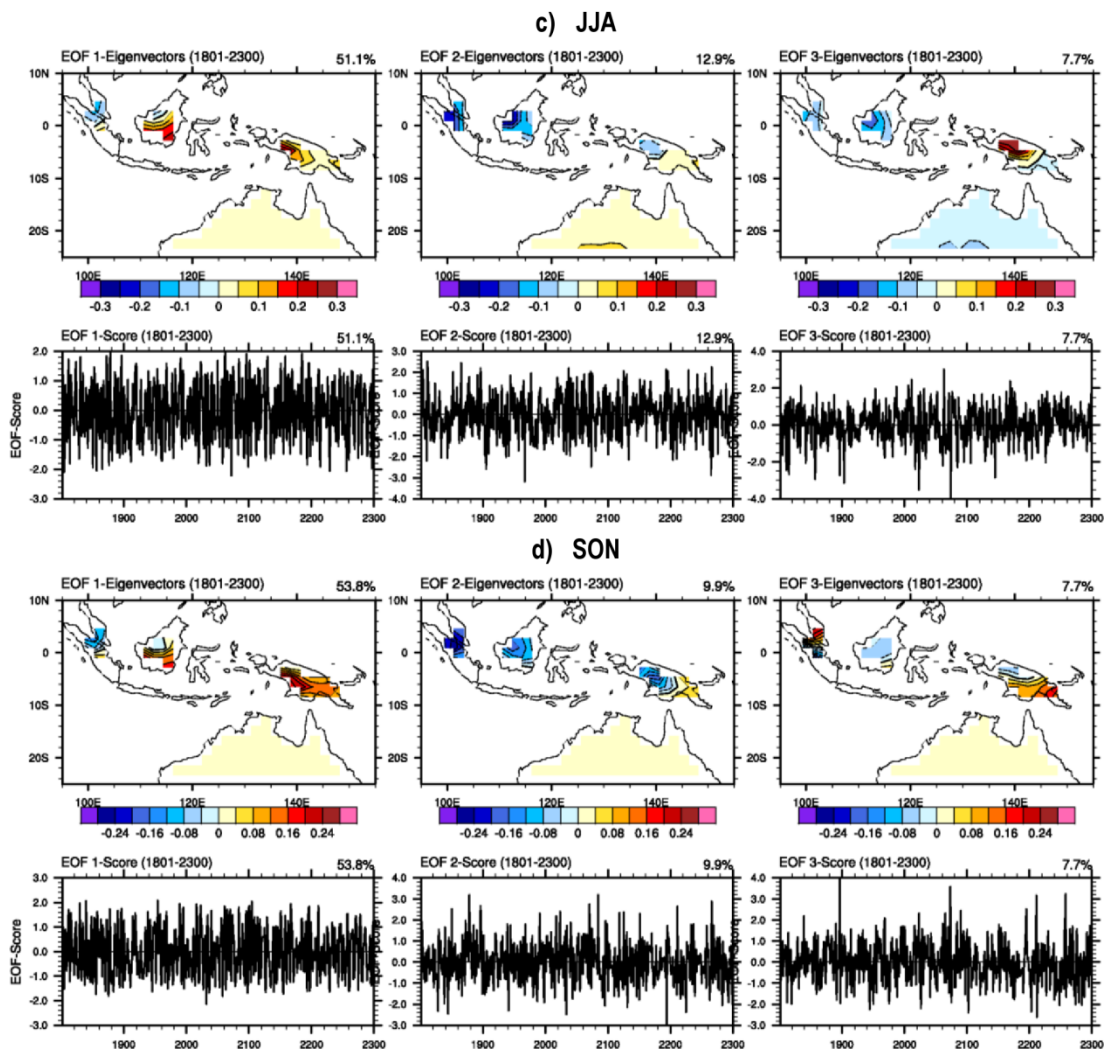


Figure 5.3: for c) JJA, and d) SON.

### 5.3.2 Links with Indo-Pacific climate variables

Given that the leading seasonal rainfall patterns are strongly related to the Indo-Pacific SST anomalies associated with ENSO and IOD (*see* Chapter 4), this study further identifies their relationship with a range of atmospheric variables simulated by the model. The atmospheric variables and their abbreviations as used in the IPCC AR4 are summarised in Table 2.2.

#### 5.3.2.1 Relationship during DJF

The rainfall variability in the Austral-Indonesian region during DJF season is mostly influenced by the Austral summer monsoon activities (Oldeman & Frere 1982). Generally, this wet season is inherently unpredictable according to previous study due to weak relationship with ENSO (e.g. Haylock & McBride 2001). The first leading mode of rainfall during this season has shown eigenvector patterns over northern Australia and most of the Indonesian region. The first impression of its time series correlated with surface temperature anomalies is that the pattern resembles the observed data as discussed in Chapter 4 (*see* Figure 4.2). The ‘boomerang’ shape of the positive SST correlation field suppressed by the negative correlations in western Indonesia is similar to the observed data, despite some disagreements of the

correlations over the west coast off Sumatra that shows a positive relationship. Nonetheless, the correlation patterns are seemingly good in the modelled pre-industrial data (Figure 5.4). This gives confidence that the leading patterns of modelled rainfall have the matching physical basis as the observed in terms of their responses to the surface temperature changes. Therefore, by analysing other atmospheric variables, the study provides a better understanding of the underlying mechanisms driving rainfall variability in the region.

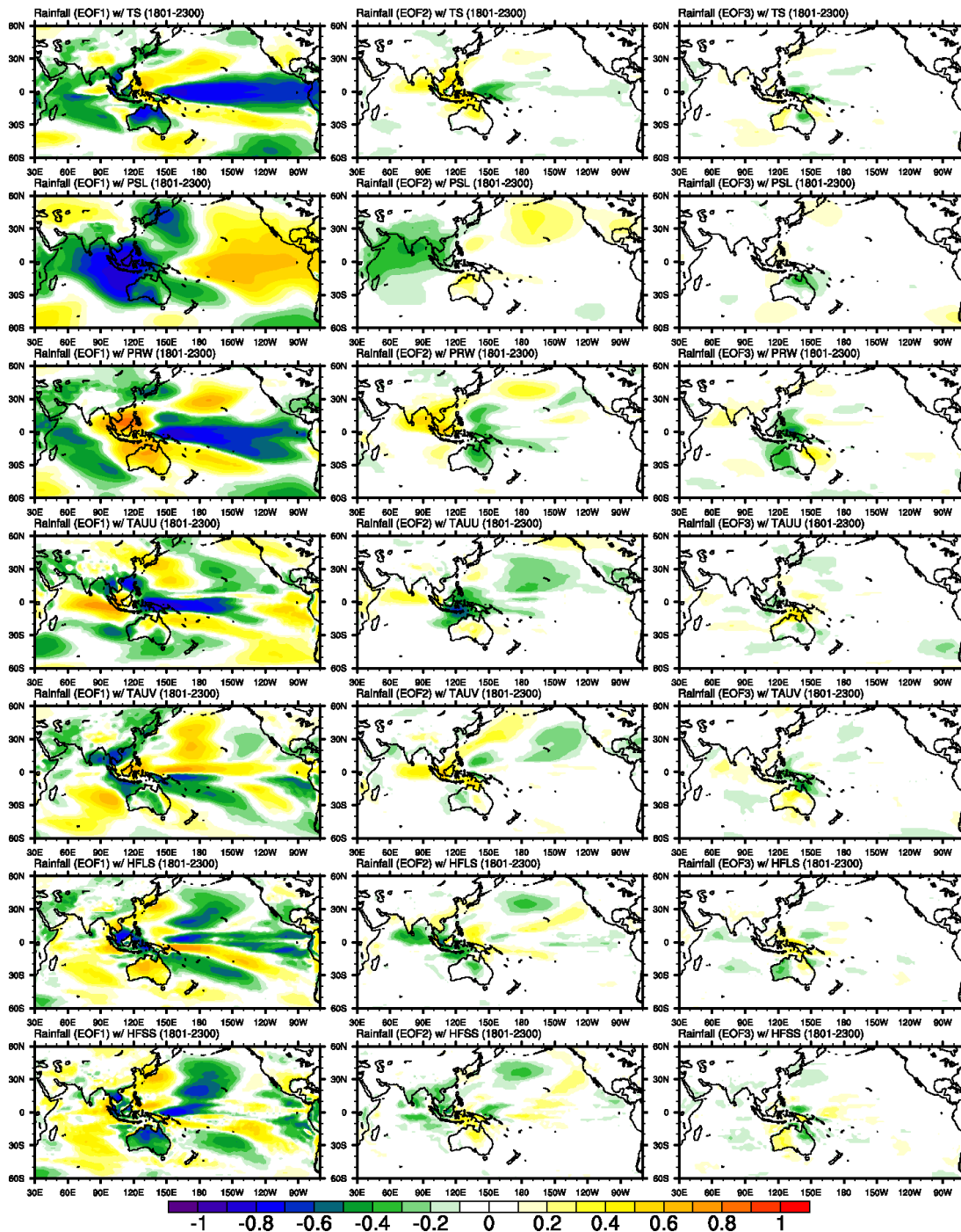


Figure 5.4: Correlations between the first three leading modes of terrestrial rainfall PC time series with several climate variables during DJF (1801-2300 periods). The coloured contour refers to significant correlations at 1% significance level.

Figure 5.4 demonstrates that the spatial patterns of the assessed climate variables (*see* Table 2.2) with the first mode of rainfall pattern are not necessarily creating similar patterns as the SST. The correlation fields formed by the sea level pressure anomalies (SLP) forms a dipole with positive correlations over the Pacific Ocean and negative correlations over Austral-Indonesia and most of the Indian Ocean. This condition is comparable with the results found in the observed data (*see* Figure 4.3).

Amongst other variables, the most nearly-comparable agreement with the surface temperature correlation patterns is found in the correlations of rainfall with atmospheric water vapour content (PRW). Its patterns demonstrate significant correlations over the Pacific and Indian Oceans that represent both ENSO and IOD conditions. Nevertheless, the correlations over Austral-Indonesia are somewhat dissimilar compared to the one that is formed by SST anomalies. This is likely related to the land-sea distributions over the region affecting the surface pattern due to significant differences between land and ocean temperature. In contrast, the PRW correlation patterns tend to be more homogeneous due to no significant obstacle(s) influencing its distribution in the atmosphere.

The study argues that significant changes of SST anomalies in the Pacific Ocean and the Indian Ocean linked to ENSO and IOD deliberately modify the PRW in the atmosphere and influence the rainfall events. During the warm (cold) ENSO episode, the relatively cold (warm) SST over the Austral-Indonesian region causes a significant decrease (increase) of precipitable water content in the atmosphere resulting in fewer (more) rainfall events.

Given that the rainfall signatures are variously distributed over the terrestrial area, the variation is likely related to the response of other atmospheric components such as surface zonal and meridional wind stresses as well as latent and sensible heat flux. During the warm ENSO event in 1997-98, a recent study found a larger wind stress and heat flux over the western Pacific Ocean warm pool than in the central Pacific Ocean (Kara et al. 2002). Here we found nearly symmetric relationships between temporal patterns of rainfall and wind stress components (zonal and meridional) over the western Pacific warm pool. This symmetric correlation patterns might give a plausible explanation of the role of tropical wind stresses over the region that reduce the ENSO influence over rainfall within the Austral-Indonesian region during wet season (DJF). Likewise, this condition is also found in the correlations of rainfall with surface latent (HFLS) and sensible heat fluxes (HFSS) (Figure 5.4).

In the second and third mode of rainfall patterns, the correlation patterns shaped by the atmospheric variables tend to show local or regional processes. Surprisingly, the SLP correlation fields in the second mode appear as a manifestation of SST differences between the Indian Ocean and the Austral-Indonesian region. This result is not in agreement with that found for the same mode from observed data (*see* Figure 4.3). Given that the third mode of rainfall patterns during DJF expresses a contrary pattern between the west and east of northern Australia, the underlying mechanisms of this signature are likely due to local influences. It mainly involves the differences of surface temperature, PRW, HFLS and HFSS only over those particular regions.

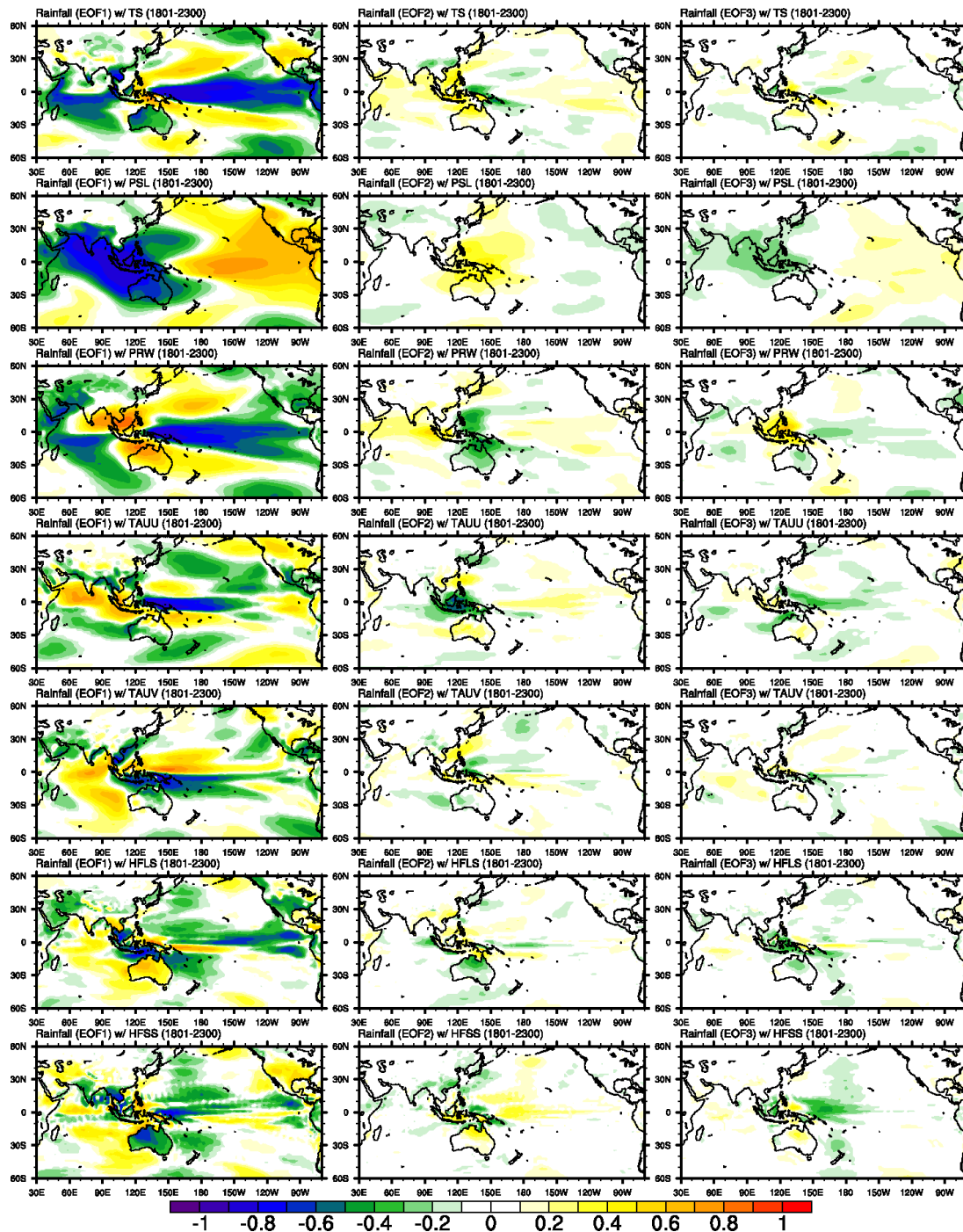


Figure 5.5: Correlations between the first three leading modes of terrestrial rainfall PC time series with several climate variables during MAM (1801-2300 periods). The coloured contour refers to significant correlations at 1% significance level.

### 5.3.2.2 Relationship during MAM

The weakest ENSO influence on rainfall variability in Indonesia is found during MAM (Aldrian et al. 2003). The analysis performed in Chapter 4 has shown a poor correlation between the SST anomalies and the first leading rainfall patterns. Significant associations only appear in the central Pacific Ocean and a small region in the western Indian Ocean. The link of the first rainfall mode with surface temperature indicates otherwise (*see* Figure 5.5). The resulting correlation pattern is

massive and is evident over the Pacific Ocean and Indian Ocean. The model possibly performs too strong ENSO events during this period. As a consequence, there is an increase in the correlation values particularly over the southern Indian Ocean. Furthermore, the use of a longer time series data (~500 years) for this correlation analysis may also contribute to this outcome to some extent.

The correlations of the first rainfall mode with pressure at sea level during MAM demonstrate a similar pattern with the previous season (DJF), but with a more developed positive correlation pattern over the Pacific region. These are slightly different with the correlations with PRW that develops positive correlations in northern Indonesia that extends to the northern Indian and Pacific Oceans. In the field of wind stress components, a few little changes in the correlation fields are evident through the reduction of negative correlations in the northern and southern Pacific Ocean. The rainfall PC time series experiences highly negative correlations with HFLS within the Austral-Indonesian region with the strongest patterns appear in southern Indonesia, between Indonesia and northern Australia. This is in contrast with the HFSS data that spreads negative and positive correlations evenly. Figure 5.5 shows that the correlation patterns with wind stress components during MAM are consistent with the result found in DJF.

In terms of the responses to the second and third mode of rainfall patterns, the atmospheric variables consistently show regional/local dominations without any significant contributions from the changes in the eastern Pacific and western Indian Ocean. In general, their correlations are more localised compared to the DJF season. The dipole on the SLP correlation in the second mode previously appeared in DJF season also seems to be vanished. This shows agreement with the fact that the development of IOD phases is relatively insignificant during the MAM transition period.

### **5.3.2.3 Relationship during JJA**

It has been well-known that the ENSO events start to develop and significantly influence the rainfall during the Austral winter season (JJA) (Aldrian et al. 2003). A recent study also shows that the IOD phase starts to develop and influence the rainfall variability in the same season (Saji et al. 1999). Referring to the analysis carried out in Chapter 4, the analysis of the modelled SST against the first mode of rainfall patterns shows an agreement by reproducing a tripole formation over the Pacific Ocean, the Indian Ocean, and the Austral-Indonesian region.

The association with surface temperature demonstrates this similarity by showing negative correlation fields over the tropical western Pacific and the western Indian Ocean (Figure 5.6). These negative correlations suppress the 'boomerang' shape-like formed by positive correlation fields into the Austral-Indonesian region. A similar pattern is also demonstrated by the rainfall correlations against PRW with some modification signed by more significant negative correlations over the Pacific ocean that penetrate into northern Indonesia connecting the western Indian Ocean. This is in contrast to an isolated positive association over southern Indonesia and most of Australia, except in the area near southwest Western Australia where the region's interannual rainfall variability is consistently linked to tropical and extra-tropical Indian Ocean SST anomalies (England et al. 2006). Here the availability of water

vapour content in the atmosphere significantly determines the rainfall variability despite other atmospheric and geographical factors.

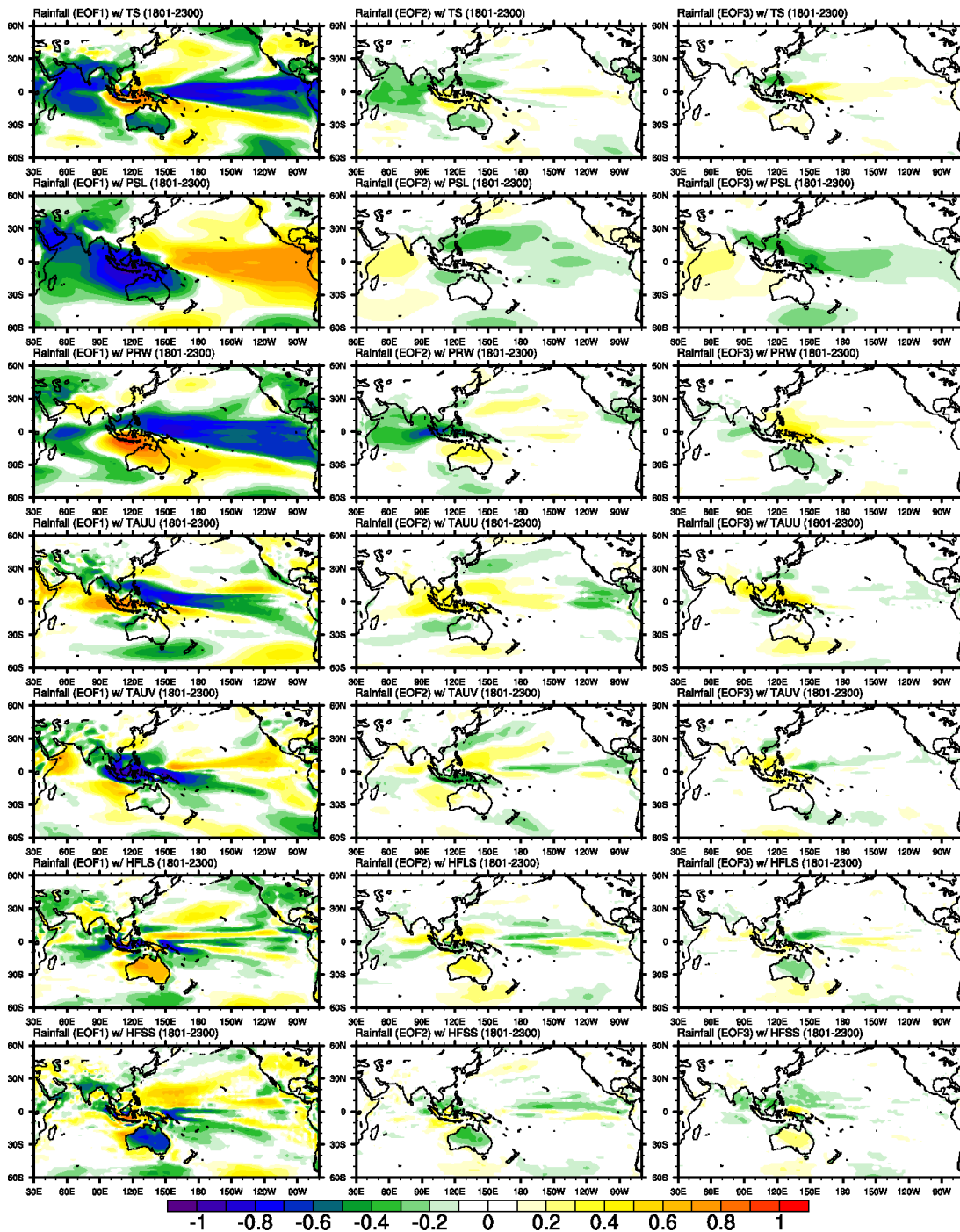


Figure 5.6: Correlations between the first three leading modes of terrestrial rainfall PC time series with several climate variables during JJA (1801-2300 periods). The coloured contour refers to significant correlations at 1% significance level.

While the transmission of ENSO signal in the ocean is through the role of SST in the Indonesian waters by transporting ocean heat mass (Cai et al. 2005b) from the Pacific into the Indian Ocean through the Indonesian throughflow (ITF) (Annamalai et al. 2005; England & Huang 2005; Gordon 1986; Gordon et al. 2003), the process in the atmosphere is found through the induction of atmospheric water vapour

content in the northern part of Indonesia into the western Indian Ocean. The penetration is influenced by zonal wind stress that also emerges at the same region and triggers the atmospheric ENSO signal into the western Indian Ocean. In this regard, the region's SST condition is also supporting the process. The role of SST in regulating the ocean surface upward sensible and latent heat flux is also important (Holton 1992) particularly through the evaporation as a cooling process of the oceans (Clement et al. 1996). This intriguing process results in a negative feedback on the atmospheric condition over the Austral-Indonesian region while at the same time adheres the IOD events.

In this study, a separate dipole process in the Indian Ocean is demonstrated by the correlations against the second mode of rainfall patterns. The differing, and relatively lower, but significant correlations over the two locations appear in the correlations of surface temperature, sea level pressure and atmospheric water vapour content. Unfortunately, the same results do not exist in the analysis of the observed SST and SLP data performed in Chapter 4. Here we found relatively strong correlations between rainfall and wind stresses components (TAUU and TAUUV) around the western Pacific and within the Austral-Indonesian region. This indicates locations where the wind stresses are strongly related with the rainfall and complements the finding of previous study that found a larger wind stress and heat flux over the western Pacific Ocean during the ENSO events (Kara et al. 2002).

#### ***5.3.2.4 Relationship during SON***

The period during monsoonal transition from the South Asian summer monsoon region to the Australian summer monsoon region in SON season has been related to the mature development of ENSO phase (Saji et al. 1999) and to considerable ENSO impact on rainfall variability particularly over Indonesia and northern Australia. In the simulated pre-industrial data analysed in this study, the correlations with several climate variables in SON season (Figure 5.7) are similar to the results in the previous season (JJA) (Figure 5.6). Nevertheless, some changes are expected due to more active ENSO and IOD intensity. The correlated SST region against the rainfall's first mode demonstrates an extension of positive correlations within the Austral-Indonesian region. This suggests that the mature phases of ENSO and IOD affect the rainfall variability more significantly (Figure 5.7).

Based on the correlation pattern of PRW, the positive correlations also develop in both the northern and southern part of the region. This is related to less water vapour content in the region's atmosphere during warm ENSO event and/or positive IOD events contributing to less rainfall occurrences that manifest into prolonged drought conditions over the region (Kirono et al. 1999; Ropelewski & Halpert 1987). The opposite condition occurs during cold ENSO episodes and/or negative IOD events. This condition has been anticipated for its effects on water supply (e.g. Power et al. 2005) and its threats on economic activities (e.g. Meinke et al. 2006; Naylor et al. 2002). Similar to what we have found in JJA, the correlations of wind stresses (TAUU and TAUUV) and heat flux (HFLS and HFSS) with the first PC mode of rainfall during SON also indicate strong correlations around the western Pacific warm pool and within the Austral-Indonesian region.

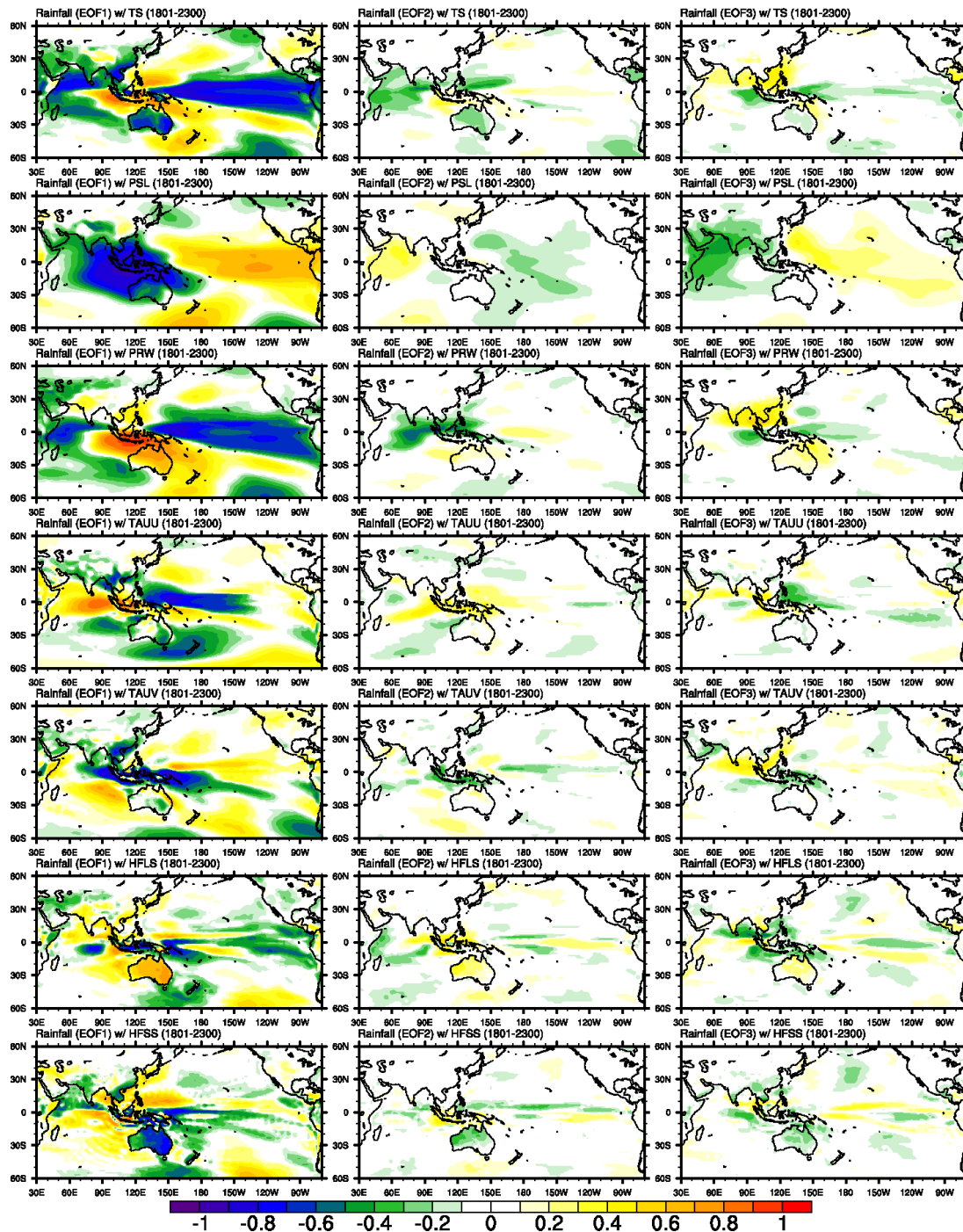


Figure 5.7: Correlations between the first three leading modes of terrestrial rainfall PC time series with several climate variables during SON (1801-2300 periods). The coloured contour refers to significant correlations at 1% significance level.

## 5.4 SST-based Indo-Pacific climate indices, and rainfall composites

### 5.4.1 Variability of ENSO indices

Figure 5.8 shows ENSO indices extracted from the SST anomalies over the well-known ENSO regions, namely Niño 1.2 (90°W-80°W, 10°S-0; Figure 5.8.a), Niño 3 (150°W-90°W, 5°S-5°N; Figure 5.8.b), Niño 4 (160°E-150°W, 5°S-5°N; Figure 5.8.c) and Niño 3.4 (170°W-120°W, 5°S-5°N; Figure 5.8.d) regions. The source of SST

data used here is obtained from the ocean component of the model with a higher horizontal resolution (namely TOS). The data is similar to the surface temperature used in the previous analysis with the only differences found in regions of sea ice (IPCC 2005).

Table 5.1: Correlations ( $r$ ) between 5-year and 13-year filtered standardised SST anomalies in various ENSO regions with terrestrial rainfall

Rainfall	Nino12	Nino3	Nino4	Nino34
5-year filter	-0.71	-0.84	-0.91	-0.87
13-year filter	-0.38	-0.60	-0.77	-0.67

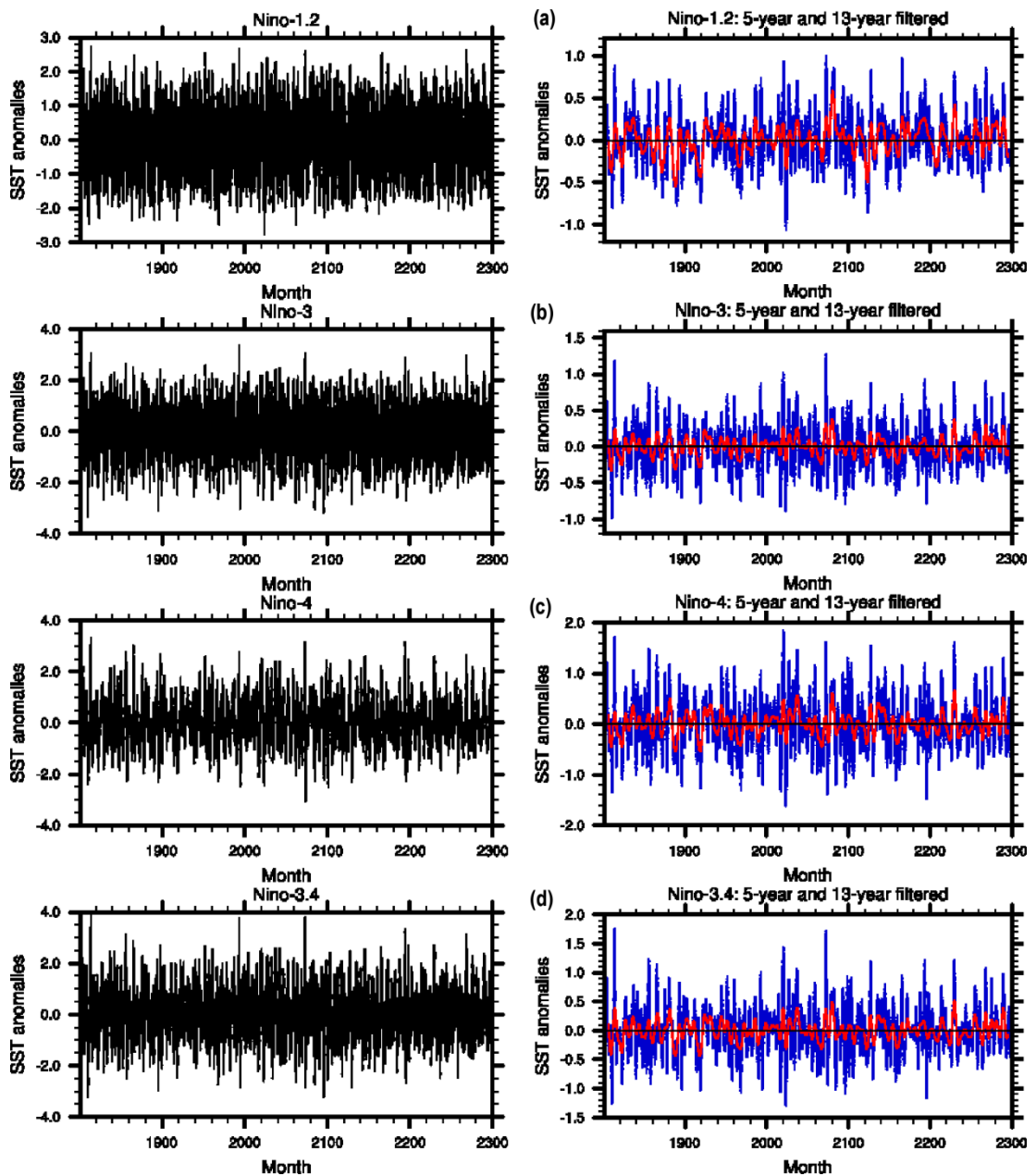


Figure 5.8: Monthly SST ENSO indices and their 5-year and 13-year filtered data from different ENSO regions: a) Nino1.2, b) Nino3, c) Nino4, and d) Nino3.4 region.

The study correlates the indices with a terrestrial rainfall time series (*see* Figure 5.2) that were filtered using 5-year and 13-year filtering windows. Both filters are used to represent interannual and interdecadal variability, respectively. The correlation results are presented in Table 5.1. Among these indices, the Niño 4 index is found to have the largest correlations against the rainfall with values of -0.91 and -0.77 in 5- and 13-year low-pass filtered data, respectively. The Niño 3.4 region is found in the second position with correlation values of -0.87 (5-year filter) and -0.67 (13-year filter). Negative signs found in the correlation values correspond to opposite relationship between Niño indices with the rainfall in the Austral-Indonesian region. It means that an increase (decrease) of SST anomaly in one of the Niño regions is associated with a decrease (increase) of rainfall within the region. Following Niño 3.4 is the Niño 3 region and Niño 1.2 with the smallest correlations. Based on these results, the terrestrial rainfall variability is strongly influenced by the nearest ENSO index. The further the ENSO region used to correlate with the rainfall, the lowest correlations are found. Therefore, using the nearest ENSO region as an indicator to study the impact on rainfall variability is important to improve the rainfall predictability which can be done by considering the time lag relationships between the SST anomalies and rainfall. This finding using the modelled pre-industrial data is consistent with the results outlined by Wang & Hendon (2007).

#### 5.4.1.1 Warm and cold ENSO episodes

Considering the results shown in Table 5.1, the study uses the Niño 4 index to define the ENSO episodes. Here, a warm ENSO episode is related to an El Niño event where the SST anomaly in the ENSO region is found above normal. In contrast, the cold ENSO episodes associated with La Niña occur when the anomaly is usually found below normal. Some studies have used the standard deviation of the SST data as a threshold to define the ENSO episodes. The warm ENSO will occur when the anomaly is above positive standard deviation and the cold ENSO when the anomaly is less than negative standard deviation. Here the 5-year low-pass filtered data is used to determine the ENSO events. It is found that the standard deviation value is  $\pm 0.5^{\circ}\text{C}$ . Therefore, any value outside this standard deviation bound will be retained as an ENSO occurrence, while any value stated otherwise will be eliminated (Figure 5.9).

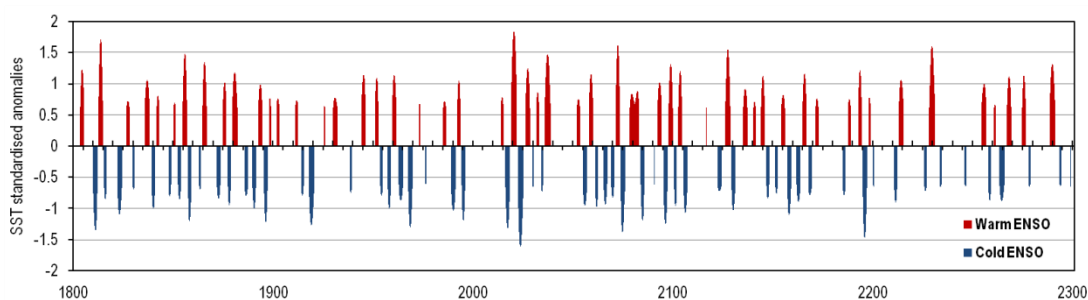


Figure 5.9: ENSO episodes defined by the 5-year filtered of standardised monthly SST anomalies in Niño 4 region. The standard deviation of the monthly-mean ENSO index averages about  $0.5^{\circ}\text{C}$ . Hence, warm and cold ENSO are considered when the value is above 0.5 and below -0.5, respectively.

Using 5-year filtered of a 500-year monthly-mean data, the Niño 4 index demonstrates 52 warm ENSO and 57 cold ENSO episodes. Therefore, on average,

together the El Niño and La Niña events are happening every 4.6 years. This indicates an agreement with the FFT result of Niño 3.4 region found in Chapter 4.

#### 5.4.1.2 ENSO composites

Relying on both warm and cold ENSO episodes defined in Figure 5.9, the rainfall composites of each El Niño and La Niña are separately performed in Figure 5.10. In the warm ENSO composite, it is found that more rainfall occurs over the western Pacific region, while less rainfall is found over Indonesia and northern Australia (Figure 5.10a). The standard deviations of this rainfall composite indicate large deviations around the Niño 4 region that is associated with considerable rainfall decreases over Indonesia (Figure 5.10b). In Figure 5.10c, the anomalies of the warm ENSO rainfall composite demonstrates three separate regions where the contrast between Niño 4 and the Austral-Indonesian region is associated with relatively small positive rainfall anomalies ( $< 0.5$  mm/day) over the western Indian Ocean and the eastern African region.

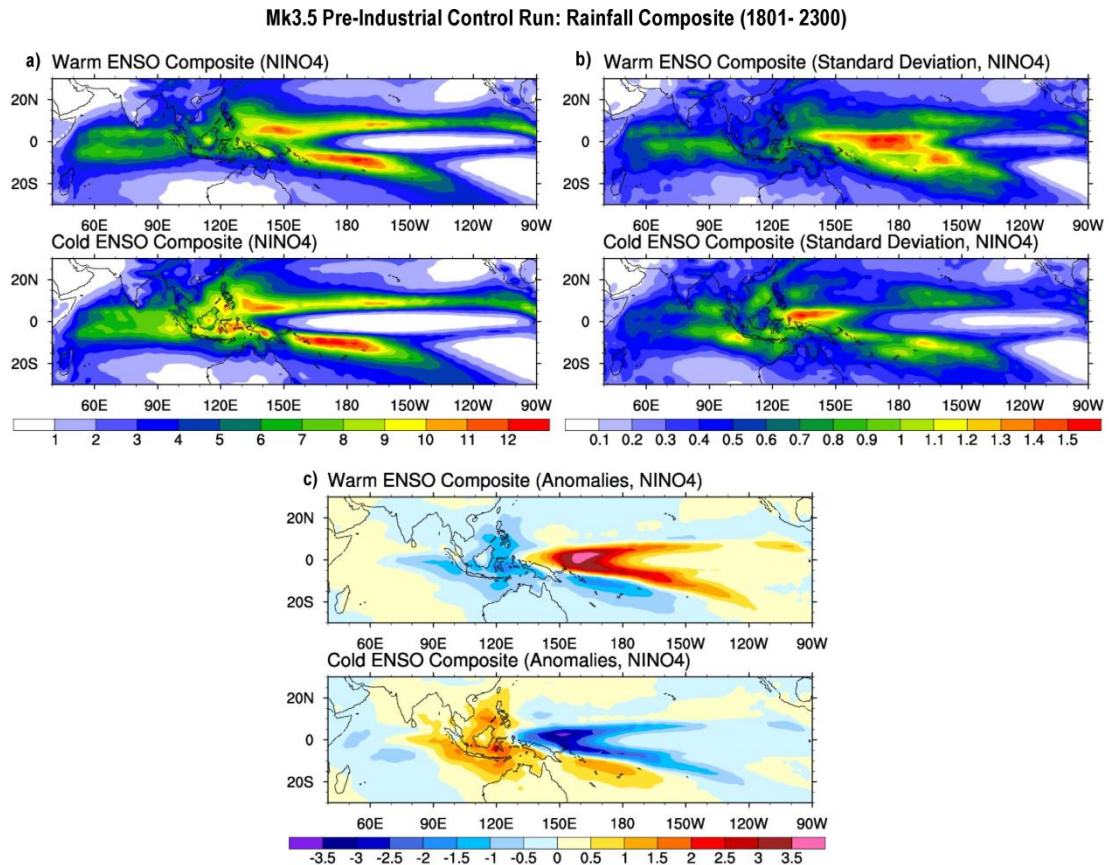


Figure 5.10: Composites of each warm and cold ENSO episodes during 1801-2300 periods simulated by CSIRO-Mk3.5 model as defined in Figure 5.9: a) monthly-mean rainfall, b) rainfall standard deviation, and c) rainfall anomalies (units in mm/day).

On the other hand, during cold ENSO episodes, the composite shows more rainfall over Austral-Indonesia (Figure 5.10a) signed with more deviations occur particularly over the eastern Indonesian region and the coast off Java and Sumatra. Significant rainfall and sea surface temperature characteristics of the Java and Sumatra west coastal region have been particularly identified in recent studies (Xie et al. 2002; Yu & Rienecker 2000; Yu et al. 2005). The rainfall anomalies in the cold ENSO composite shows an inverse condition of warm ENSO where positive anomalies are

located in the centre of the region and squeezed by negative anomalies over the western Pacific warm pool region and the western Indian Ocean region. It is shown that the range of rainfall anomalies in the western Indian Ocean during cold ENSO (0 to -1) are greater than during warm ENSO (0 to 0.5). This leads to a possibility that the region is suffering more from the impact of La Niña (cold ENSO) than El Niño (warm ENSO) in the pre-industrial simulations. The characteristics of rainfall in the western Indian Ocean and in the west coast off Java and Sumatra are somewhat related to the impact of IOD events. In the next section, the variability of IOD index and rainfall composite during the events are discussed.

#### 5.4.2 Variability of IOD index (DMI)

Saji et al. (1999) defines an index to measure the strength of IOD events based on the gradient of SST in the western (40°E-70°E, 10°S-10°N) and east-/southeastern (90°E-110°E, 10°S-0°) Indian Ocean. The index is usually called as the Dipole Mode Index (DMI) (Saji et al. 1999). In Figure 5.11, the DMI components are extracted from the two corresponding regions in order to calculate the index. Figure 5.11a shows the monthly-mean of standardised SST anomalies in the western Indian Ocean along with its 5- and 13-year filtered data. Its standardised monthly data indicates the range of anomalies between -3 and 3°C with more frequent anomalies around -2 and -1°C as well as around 1 and 2°C.

Figure 5.11b shows standardised SST anomalies over the east/southeast Indian Ocean. Here the positive (negative) anomaly is often associated with cold (warm) ENSO events causing above normal SST anomalies in the Austral-Indonesian region including in the west coast off Java and Sumatra. Nevertheless, the influences of the ENSO itself to the SST variability in the region are not consistently significant at all seasons. This can be seen from the previous results discussed in Chapter 4 where the penetration of ENSO effects mostly occurs during JJA and SON seasons. This condition could be a considerable factor why most of the IOD events maturely transpire only during those seasons.

*Table 5.2: Correlations ( $r$ ) between 5-year and 13-year filtered standardised SST anomalies in a single IOD domain (western or eastern Indian Ocean) and IOD index with rainfall terrestrial rainfall in the Austral-Indonesian region.*

Rainfall	IODw	IODe	IOD
<b>5-year filter</b>	-0.65	0.50	-0.70
<b>13-year filter</b>	-0.51	0.33	-0.56

In Figure 5.11c, the DMI is performed based on the gradient of the dipole. It is demonstrated that in monthly-mean time series, the variability of the index is relatively flatter around the negative values, between -1° and -2°. In contrast, the variation of the positive index is larger, i.e. between 0° to almost 4°. The likely cause of this condition is the fact that the SST anomalies in the east/southeastern region are also less varied on their positive values (Figure 5.11b (left)). It can be interpreted that the warm ENSO events will contribute to more variation on the SST anomalies compared to the cold ENSO episodes.

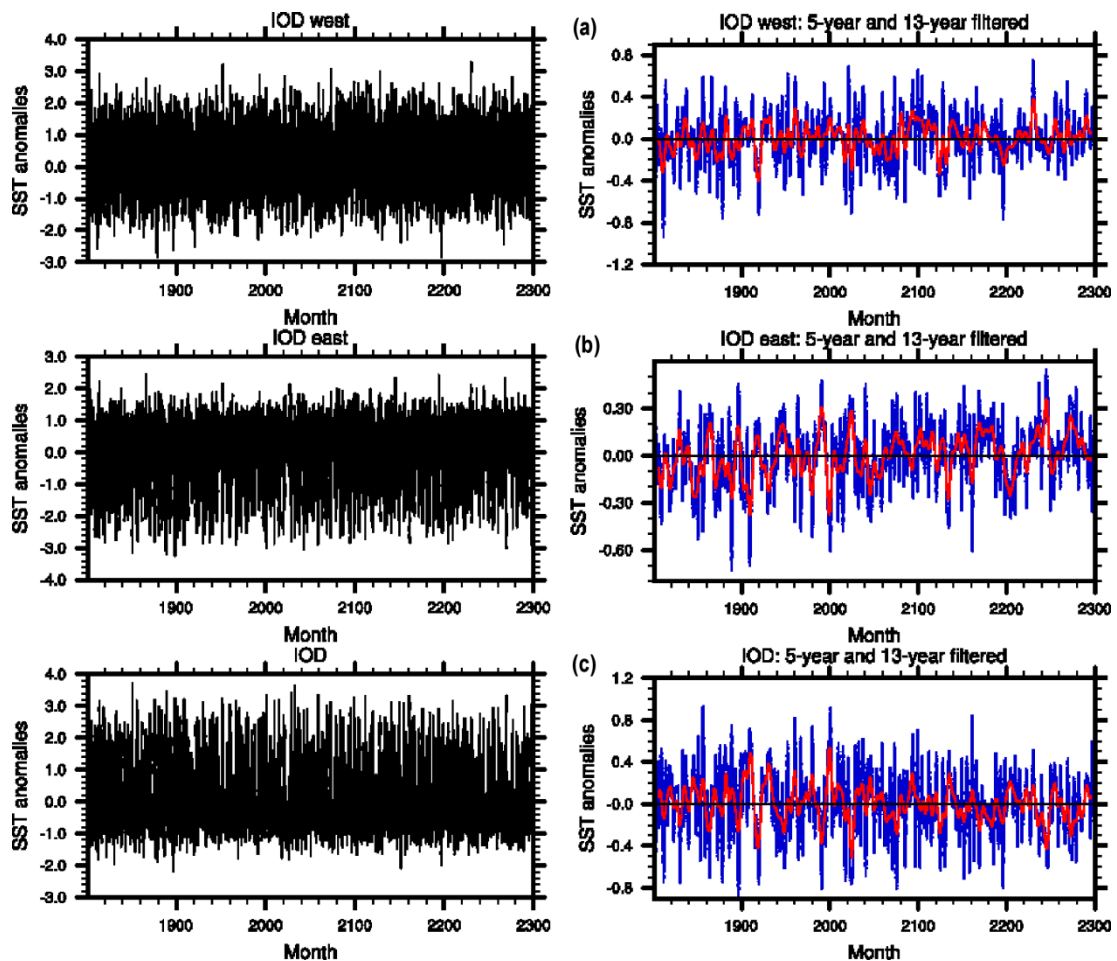


Figure 5.11: Monthly Indian Ocean SST indices and their 5-year and 13-year filtered data: a) western IO, b) south-eastern IO, and c) IOD index.

In Table 5.2, the study correlates the DMI index and each of its dipole components with the terrestrial rainfall in the Austral-Indonesian region. The results show that the rainfall variability is strongly correlated with DMI with correlation values of  $-0.70$  and  $-0.56$  respectively using 5- and 13-year low-pass filtered data. Negative correlation signs correspond to contradictory relationship between DMI and rainfall. Since the DMI is calculated from the difference between the SST in the western and the eastern part of Indian Ocean, an increase of SST anomaly in the western part that is simultaneously followed by the decrease of SST anomaly in the eastern part will reproduce a positively high DMI value. This positive index is strongly linked with the rainfall decrease over some of the Austral-Indonesian region. From the correlation results presented in Table 5.2, the lowest positive correlations are found in the east/southeastern Indian Ocean.

#### 5.4.2.1 Positive and negative IOD events

Similar to the method that was used for defining the ENSO index in Niño 4 region, here the study uses the standard deviation of DMI in order to determine the positive and negative IOD events. It is found that the standard deviation of the DMI from the pre-industrial data is about  $0.35^{\circ}\text{C}$ . This is slightly different with the standard deviation currently used as a threshold for IOD forecast in the POAMA forecast system used by the Bureau of Meteorology, Australia, which is around  $0.4^{\circ}\text{C}$  ([see http://www.bom.gov.au/climate/coupled\\_model/about-POAMA-outlooks.shtml](http://www.bom.gov.au/climate/coupled_model/about-POAMA-outlooks.shtml)).

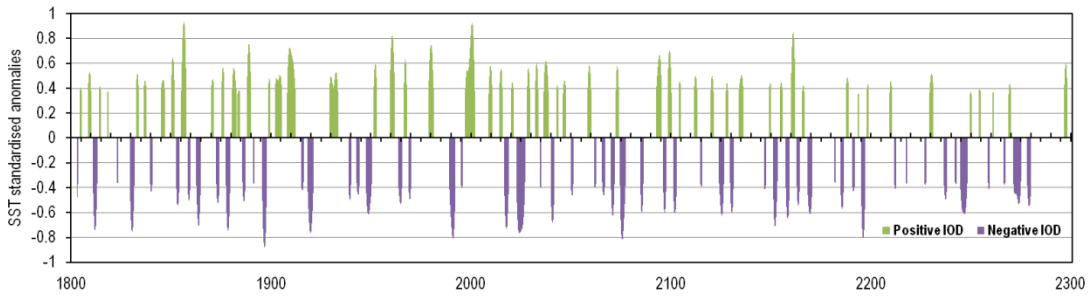


Figure 5.12: IOD events defined by the 5-year filtered of standardised monthly SST differences between the western and south-eastern Indian Ocean as defined by Saji et al. (1999). The standard deviation of the monthly-mean DMI is about  $0.35^{\circ}\text{C}$ . Hence, positive and negative IOD are considered when the values are larger than  $0.35^{\circ}$  and lower than  $-0.35^{\circ}$ , respectively.

Based on the 5-year filter of a 500-year monthly-mean data, it is found that the positive IOD events occur 54 times while the negative IOD events happen 56 times. The total number of the IOD events (=110) is almost comparable with the total of ENSO episodes (=109). This gives a strong sense that there is some dependency between those Indo-Pacific climate drivers under the simulated pre-industrial climate.

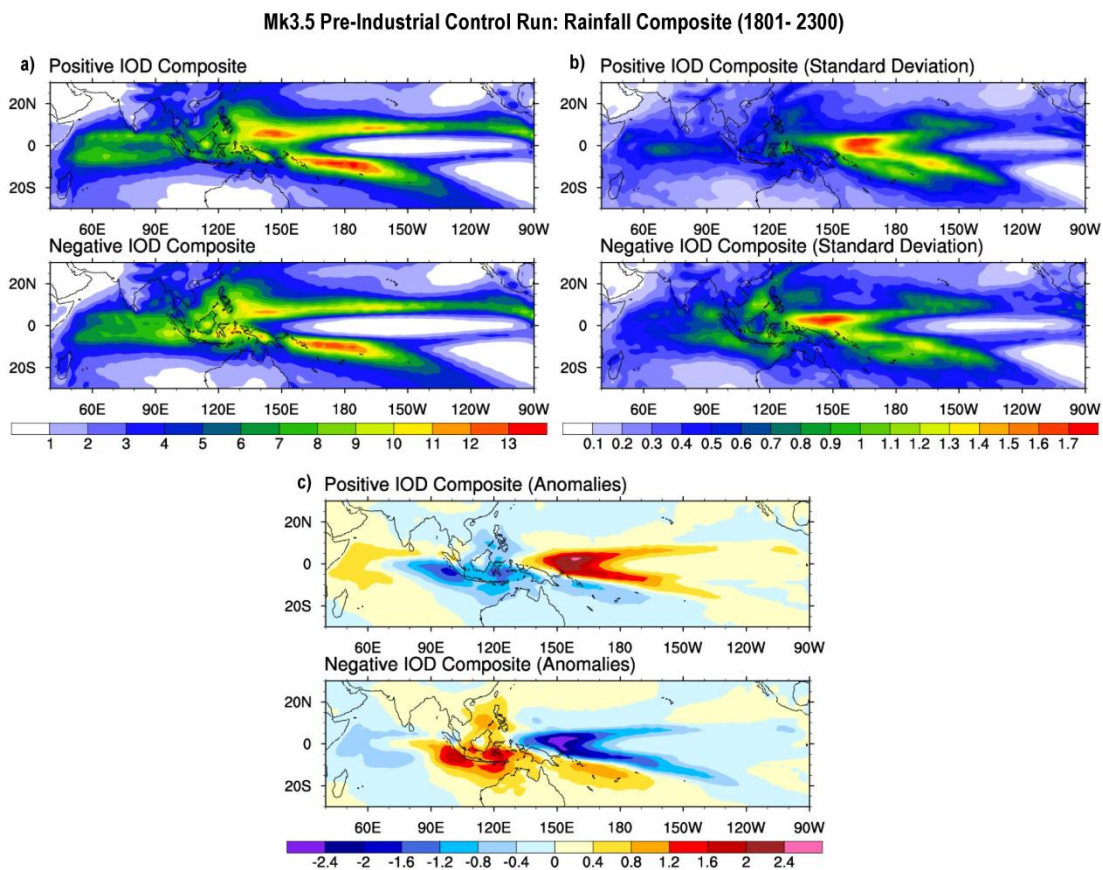


Figure 5.13: Composites of each positive and negative IOD events during 1801-2300 periods simulated by CSIRO-Mk3.5 model as defined in Figure 5.12: a) monthly-mean rainfall, b) rainfall standard deviation, and c) rainfall anomalies (units in mm/day).

### 5.4.2.2 IOD composites

In order to create rainfall composites during the positive and negative IOD events, the study refers to the IOD events determined in Figure 5.12. It is shown in Figure 5.13 that the rainfall composite resulting during the positive and negative IOD shows comparable results with the warm and cold ENSO composites, respectively. The main dispute is related to the strength of the rainfall anomalies both over the Austral-Indonesian region and the western Indian Ocean. It is found that the rainfall anomalies over the central and western Austral-Indonesian region are considerably higher (lower) than the one resulting in cold (warm) ENSO composites. The condition is vice versa for the western Indian Ocean.

### 5.4.3 Dependency of IOD and ENSO in pre-Industrial climate

In this subsection, the study discusses the association between IOD and ENSO under the simulated pre-industrial climate. Based on the definition of ENSO and IOD events using SST data as performed in Figure 5.9 and 5.12, the parallel occurrences between those two indices are investigated in order to measure their dependency (Figure 5.14). It is noted that in the 500-year simulated climate, there are 109 ENSO episodes and 110 IOD events. Among these traces, there is a 71.2% parallel occurrence where the IOD events arise at the same time as ENSO. This is made up of 31.1% side-by-side episodes between warm ENSO and positive IOD, and a 40.2% of cold ENSO and negative IOD happening concurrently. The rest of the fraction consists of 14.2% sovereign ENSO episodes and 14.6% independent IOD events. These statistics have given a clear indication that there is a strong connectivity between the IOD and ENSO.

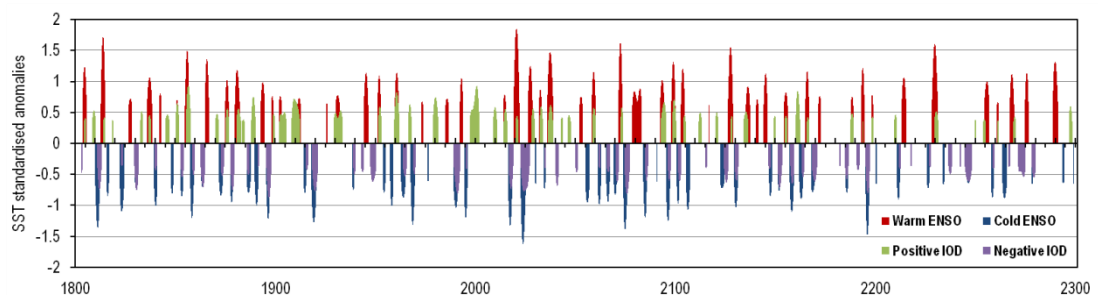


Figure 5.14: Combined ENSO-IOD occurrences as defined in Figure 5.9 and 5.12.

Further, the relationship between ENSO and IOD and its contributing components are shown in Table 5.3. The result shows that the ENSO indices from different Niño regions have a fairly strong relationship with the SST anomalies from one of the dipoles in the Indian Ocean, i.e. in the western part of the region (IODw). Here the strongest link is demonstrated by the Niño 4 region either in the 5- ( $r=0.71$ ) or 13-years low-pass filtered data ( $r=0.67$ ). Such a strong relationship is associated to the condition where the active ENSO events will deliberately relate to the changes of SST anomalies in IODw. In contrast, the correlations of ENSO indices with the other side of the dipole, i.e. the east/southeastern Indian Ocean (IODe) are consistently much weaker. This gives a sound agreement that the independency of IOD for a certain level is more regulated by the regional SST condition in the Austral-Indonesian region, particularly around the west coast off Java and Sumatra (e.g. Du et al. 2008). Following the findings in Chapter 4, the role of regional SST in the

Austral-Indonesian region in providing alternative signal to the IOD events is significant despite its seasonal phase-lock association with ENSO in JJA and SON seasons. Further, given that the changing of SST in the region is more impacted by climate change (*see* Chapter 4) than the SST in the Pacific Ocean, the chance for an increasing independent signal that trigger the IOD is probable.

*Table 5.3: Correlations ( $r$ ) between 5-year and 13-year filtered standardised ENSO indices and DMI*

<b>5-year filter</b>	Nino12	Nino3	Nino4	Nino34
<b>IODw</b>	0.76	0.58	0.71	0.62
<b>IODe</b>	-0.17	-0.28	-0.35	-0.30
<b>IOD</b>	0.54	0.51	0.63	0.55
<b>13-year filter</b>	Nino12	Nino3	Nino4	Nino34
<b>IODw</b>	0.61	0.58	0.67	0.62
<b>IODe</b>	0.27	0.10	0.00	0.07
<b>IOD</b>	0.10	0.23	0.36	0.27

## 5.5 Summary

In this Chapter the climate model output from the CSIRO-Mk3.5 pre-industrial control run was used to investigate the leading seasonal rainfall patterns and their associations with the ocean-atmosphere variables. The approach used in this study is proficient in identifying the climate drivers causing rainfall variability and the relationship between ENSO and IOD. Below are the main results obtained from this study:

- The seasonal rainfall patterns resulting from the model are nearly-comparable with the observed data presented in Chapter 4. As a result, the correlation fields of their first leading mode with sea surface temperature are similar to the observed data by showing significant ENSO-IOD structures.
- The correlation patterns of the leading seasonal rainfall patterns against the atmospheric water vapour content (PRW) indicate an atmospheric ENSO signal transmission that triggers the IOD events. It is detected from the induction of PRW in the north of the Indonesian region into the western Indian Ocean during the boreal summer monsoon season (JJA). This penetration is suppressed by zonal wind stress that also emerges from the western Pacific into the north of the Indonesian region.
- The analyses of rainfall composites during ENSO and IOD episodes show comparable results, indicating a strong connection between the two processes found in the simulated pre-industrial data.
- The study gives a sound finding that the independent IOD to ENSO event is more regulated by the regional SST condition in the Austral-Indonesian region instead of in the western Indian Ocean, particularly around the west coast off Java and Sumatra.

## Chapter 6 Conclusions

This study aimed to improve our understanding of rainfall variability in the tropical Austral-Indonesian region and to identify key climate phenomena driving rainfall variability. In particular, the roles of regional SST in moderating the effect of large-scale climate drivers such as ENSO, IOD and PDO on rainfall variability were investigated. Several research questions arose after a careful review of the literature:

- 1) How well do climate models perform in simulating rainfall over the Austral-Indonesian region and what is the future of the rainfall in the region?
- 2) What role does regional SST play in controlling rainfall variability and what is the impact of climate regime shifts?
- 3) How is regional SST influencing rainfall variability in a pre-industrial climate simulation?

### 6.1 Simulated Rainfall Assessment for Austral-Indonesia

Several studies identified some issues in climate models that were largely responsible for a failure to adequately simulate rainfall particularly, over the Tropical region. Those issues were related to an incorrect positioning of the Inter Tropical Convergence Zone (ITCZ) (Barsugli et al. 2004; Dai 2006; Hack et al. 2006; Lau et al. 1996), difficulties representing the land-sea distributions that were mostly found in coarse resolution models (Lau et al. 1996), and failure in simulating monsoon circulations (Gadgil & Sajani 1998; Zhang et al. 1997).

By using the latest sets of data from climate models, namely the WCRP CMIP3 multi-model dataset, the study evaluated the simulated rainfall from 21 GCMs for the Austral-Indonesian region based on climatological consistency, interannual variability and trends during the late 20<sup>th</sup> century, and future rainfall projections. In general, the result showed that most of the models were able to follow uni-modal monsoonal pattern. It was despite their inadequacy to correctly estimate the rainfall amount due to false rainfall as a result of double-ITCZ problem as identified in previous studies (Dai 2006; Lin 2007). Most of the rainfall mismatches found in current models were mainly associated with (i) unrealistic locations of maximum rainfall, (ii) average position of the ITCZ which was mostly caused by a narrowing or widening of its meridional properties, (iii) the distribution of rainfall over land and ocean, and (iv) problems in simulating large-scale convections associated with the Monsoon circulations. In addition, the study suggested that most of the models suffer from the failures in simulating comparable trends and interannual variability related to ENSO events. This was related to an incorrect representation of ENSO dynamics (Dai 2006) and excessive tropical rainfall that was linked to low precipitation in the equatorial Pacific (Lin 2007).

Here the study found the ECHO-G (15) and MRI-CGCM2.3.2 (17) as the best-performing models in terms of their ability in simulating the rainfall amount for the whole land and ocean area respectively, during the monsoons activities (DJF and JJA) and during transition periods (MAM and SON). Both models were chosen based on the CAD criteria. Through independent assessment of terrestrial rainfall using the *KSDist* criteria, UKMO-HADGEM1 (21) was selected as the best-performing model based on its ability to consistently simulate terrestrial rainfall distributions (CDF). The assessment results of the future rainfall scenarios (SRES

A1B, A2 and B1) from those three best-performing models indicated different results, particularly in simulating DJF and JJA rainfall in the region. In general, the models simulated rainfall changes with some increases during MAM and decreases during SON, especially for southern Indonesia and northern Australia. The rainfall changes during monsoonal transitions may lead to prolonged wet and dry seasons for those particular regions.

The study suggested that an improvement of spatial resolution in models will be beneficial particularly for the Indonesian region as it provides better representation on land-sea distribution and topography resulting in better physical processes driving rainfall in the region. In addition, a combination of improved horizontal resolutions and better representation of the ocean component would possibly reproduce better rainfall simulations for the Austral-Indonesian region. A proper ocean component, in particular with good quality simulated SST patterns, might generate better ocean-atmosphere coupling to reproduce more realistic rainfall. Therefore, a further study to investigate the significant role of regional/local SST in moderating the impact of large-scale climate drivers on driving the rainfall variability will be essential.

## **6.2 The Impact of Regional SST on Rainfall Variability**

Studies suggested that enhancing the ocean components in climate models were essential, in particular through better representation of local SST (Dai 2006, Chung & Ramanathan 2007) that could possibly improve ocean-atmosphere coupling for better rainfall simulations. In particular for the Austral-Indonesian region investigated in this study, analysing the role of regional SST plays in moderating the impact of large-scale climate drivers on interannual and interdecadal rainfall variability were important for performing better SST representation in climate models.

The identifications of seasonal SST patterns performed in this study showed the important role of regional SST in moderating the impact of large-scale climate drivers on rainfall variability. First, the SST patterns represented by the first EOF mode were related to significant temperature rise where the spatial eigenvector patterns confirm the hotspot areas indicating temperature rise on sea surface over the region found in previous studies (Goreau et al. 2005). Second, the SST patterns of the second EOF mode were associated with considerable ENSO and IOD interannual variability shown by the SST patterns that were linked with the seasonal ocean properties in transmitting interannual variability signals from the Pacific into the Indian Ocean, including the ITF mechanisms and the surface water flow from the South China Sea region that inhibits the southward movement of the ITF particularly during the boreal winter period (DJF) (Gordon et al. 2003; Susanto & Gordon 2005). Third, the SST patterns a unique signal that enriches the SST variability around the west coast off Java and Sumatra, despite the influence of ENSO. This was represented by the third mode where the patterns represent SST distributions from the northern Austral-Indonesian region (DJF and MAM) into south-western Indonesia (JJA and SON) through the SCS region and around the coast off Sumatra and Java associated with the IOD index (Saji et al. 1999).

Despite some evidence found on the link between the IPO and regional SST on interdecadal timescales, the significant temperature rise found in the regional SST during the 20<sup>th</sup> century shows a more significant impact on moderating the

interdecadal rainfall variability in the region. This finding accentuated the importance of using regional SST data in order to increase the rainfall predictability on longer timescales. In addition, based on the investigation of the first mode of rainfall and the second mode of regional SST loading patterns in three different phases of climate regime shifts, i.e. a) 1925-1946, b) 1947-1976, and c) 1977-2002, it was suggested that the variations of interannual rainfall variability in the region in different seasons and different climate phases were determined by the strength of the transmission of interannual signals from the northern and the southern Pacific into the regional seas.

This study emphasised the usefulness of analysing the seasonal rainfall and SST patterns in order to trace the link with the climate drivers affecting their variability. Strong evidence was found on the structures of regional SST showing their important role in moderating the ENSO and IOD connectivity and dependency. Further analysis based on climate model output under pre-industrial control simulation was conducted. This would be essential in order to understand the underlying mechanisms particularly in conditions where there is no impact of climate change.

### **6.3 Rainfall Variability and ENSO-IOD Dependency in Pre-Industrial Climate**

The debate over the mechanisms in the ENSO-IOD relationship is ongoing (Allan & Coauthors 2001; Dommenges & Latif 2002; Dommenges et al. 2006; Fischer et al. 2005; Saji et al. 1999; Saji & Yamagata 2003) with current analyses focused on the use of climate model simulation in order to understand the underlying mechanism(s) (e.g. Ashok et al. 2004; Fischer et al. 2005). In this Chapter, the climate model output from the CSIRO-Mk3.5 pre-industrial control run was used to investigate the leading seasonal rainfall patterns and their associations with the ocean-atmosphere variables. Applying the methods used in Chapter 4, the study investigated the link of seasonal rainfall patterns with Indo-Pacific climate drivers in an unforced climate change-related condition (pre-industrial climate). The investigations were based upon different ocean-atmospheric variables mostly on surface level. These datasets include surface temperature, sea level pressure, atmospheric water vapour content, zonal and meridional wind stress, as well as ocean surface upward sensible and latent heat fluxes.

The study found that the seasonal rainfall patterns resulting from the model were almost-comparable with the result of observed data presented in Chapter 4. Here, the correlation patterns of the first leading mode of rainfall patterns with sea surface temperature were similar to the observed data by showing significant ENSO-IOD structures. The correlation patterns were similarly found in the correlation with the PRW dataset. This indicated an atmospheric ENSO signal transmission that was associated with the IOD dependency upon ENSO. The correlation patterns during the Asian summer monsoon season (JJA) demonstrated the induction of PRW in the north of the Indonesian region into the western Indian Ocean. This penetration was suppressed by zonal wind stress that also emerges from the western Pacific into the north of the Indonesian region and coupling with the SST in the region. As a result, the study finds a strong correlation between the Niño 4 index with the SST anomalies in the western Indian Ocean. Such atmospheric processes that occur in the northern Indonesian region might be slightly inconsistent from the ones that happen in the ocean. For the regional SST in the Austral-Indonesian region, the ENSO signal

transmission process was influenced by the complex land-sea distribution within the region, involving the role of oceanic properties such as the Indonesian throughflow (ITF). This process caused a poor statistical relationship between the Niño 4 region with the SST in the west coast off Java and Sumatra.

Here, the study suggested a sound finding that the independency of IOD is more regulated by the regional SST condition in the Austral-Indonesian region, particularly around the west coast off Java and Sumatra, rather than in the western Indian Ocean. Given that there was an evidence of considerable SST warming within the regional seas as shown in Chapter 4, the changing SST condition in the regional seas might alter the IOD variability and its connectivity with ENSO in the future. In addition, the analysis of rainfall composites during ENSO and IOD episodes supported this result by showing comparable results between the two processes.

## **6.4 Future Directions**

This study has shown the important role of regional SST in moderating the impact of large-scale climate drivers on rainfall variability in different time scales, as well as in determining the connectivity between climate drivers, i.e. ENSO and IOD. It has also shown that better coupling between the regional/local SST with the atmospheric component leads to better improvement of global climate models despite the need to improve the model resolution for better terrestrial rainfall simulation in the region. Based on these results, further studies need to be conducted in order to gain more understanding on the role of the regional SST particularly in a changing climate, on how it behaves in moderating the rainfall and determining the ENSO-IOD connectivity. A deployment of dynamical downscaling techniques, e.g. using regional climate model (RCM), would be another option to advance the predictive skill and climate projections. This can be done by simulating the model based on either different SST set ups or GCM projection outputs.

## References

- AchutaRao, K & Sperber, K 2006, 'ENSO simulation in coupled ocean-atmosphere models: are the current models better?' *Climate Dynamics*, vol. 27, no. 1, pp. 1-15, doi: 0.1007/s00382-006-0119-7.
- Aldrian, E & Susanto, RD 2003, 'Identification of three dominant rainfall regions within Indonesia and their relationship to sea surface temperature', *International Journal of Climatology*, vol. 23, pp. 1435-52, doi: 10.1002/joc.950.
- Aldrian, E, Gates, LD & Widodo, FH 2003, 'Variability of Indonesian rainfall and the influence of ENSO and resolution in ECHAM4 simulations and in the reanalysis', 346, Max-Planck-Institut für Meteorologie, Hamburg, Germany.
- Allan, R, Chambers, D, Drosowsky, W, Hendon, H, Latif, M, Nicholls, N, Smith, I, Stone, R & Tourre, Y 2001, 'Is there an Indian Ocean dipole, and is it independent of the El Niño - Southern Oscillation?', *CLIVAR Exchanges*, vol. 6, pp. 18-22.
- Allan, RJ & Ansell, TJ 2006, 'A new globally-complete monthly historical gridded mean sea level pressure data set (HadSLP2): 1850-2004', *Journal of Climate*, vol. 19, no. 22, pp. 5816-42, doi: 10.1175/JCLI3937.1.
- Ananthakrishnan, R 1977, 'Some aspects of the monsoon circulation and monsoon rainfall', *Pure and Applied Geophysics*, vol. 115, no. 5 - 6, pp. 1209-49, doi: 10.1007/BF00874407.
- Annamalai, H, Potemra, J, Murtugudde, R & McCreary, JP 2005, 'Effect of Preconditioning on the Extreme Climate Events in the Tropical Indian Ocean', *Journal of Climate*, vol. 18, pp. 3450-69, doi: 10.1175/JCLI3494.1.
- Annamalai, H, Murtugudde, R, Potemra, J, Xie, SP, Liu, P & Wang, B 2003, 'Coupled dynamics over the Indian Ocean: spring initiation of the Zonal Mode', *Deep-Sea Research Part II, Topical Studies in Oceanography*, vol. 50, no. 12/13, p. 2305, doi: 10.1016/S0967-0645(03)00058-4.
- Arblaster, JM, Meehl, GA & Moore, AM 2002, 'Interdecadal modulation of Australian rainfall', *Climate Dynamics*, vol. 18, pp. 519-31, doi: 10.1007/s00382-001-0191-y.
- Ashok, K, Guan, Z & Yamagata, T 2003, 'Influence of the Indian Ocean Dipole on the Australian winter rainfall', *Geophysical Research Letters*, vol. 30, doi: 10.1029/2003GL017926.
- Ashok, K, Guan, Z, Saji, NH & Yamagata, T 2004, 'Individual and combined influences of ENSO and the Indian Ocean Dipole on the Indian Summer Monsoon', *Journal of Climate*, vol. 17, pp. 3141-55.
- Barnett, TP, Pierce, DW, Latif, M, Dommenges, D & Saravanan, R 1999, 'Interdecadal interactions between the tropics and midlatitudes in the Pacific basin', *Geophysical Research Letters*, vol. 26, pp. 615-8.

Barsugli, J, Shin, S-i & Sardeshmukh, PD 2004, 'Tropical climate regimes and global climate sensitivity in a simple setting', *Journal of the Atmospheric Sciences*, vol. 62, pp. 1226-40, doi: 10.1175/JAS3404.1.

Belinda, M, Simmonds, I & Smith, IN 2007, 'Association between Australian rainfall and the Southern Annular Mode', *International Journal of Climatology*, vol. 27, pp. 109–121, doi: 10.1002/joc.1370.

Benestad, RE 2005, 'Climate change scenarios for northern Europe from multi-model IPCC AR4 climate simulations', *Geophysical Research Letters*, vol. 32, p. 17704, doi: 10.1029/2005GL023401.

Bhaskaran, B & Mitchell, JFB 1998, 'Simulated changes in Southeast Asian monsoon precipitation resulting from anthropogenic emissions', *International Journal of Climatology*, vol. 18, pp. 1455-62, doi: 10.1002/(SICI)1097-0088(19981115)18:13<1455::AID-JOC331>3.0.CO;2-D.

Bleck, R 2002, 'An oceanic general circulation model framed in hybrid isopycnic-Cartesian coordinates', *Ocean Modelling*, vol. 4, pp. 55-88, doi: 10.1016/S1463-5003(01)00012-9.

Boer, R & Subbiah, AR 2005, 'Agriculture drought in Indonesia', *In Monitoring and Predicting Agriculture Drought*, pp. 330-344 (V.K. Boken, A.P. Cracknell and R.L. Heathcote. eds), Oxford University Press, Oxford.

Boer, R & Faqih, A 2004, 'Global climate forcing factors and rainfall variability in West Java: case study in Bandung district', *Indonesian Journal of Agricultural Meteorology*, vol. 18, no. 2, pp. 1-12.

Brown, DP & Comrie, AC 2002, 'Sub-regional seasonal precipitation linkages to SOI and PDO in the Southwest United States', *Atmospheric Science Letters*, vol. 3, no. 2-4, pp. 94-102.

Cai, W, Whetton, PH & Pittock, AB 2001, 'Fluctuations of the relationship between ENSO and northeast Australian rainfall', *Climate Dynamics*, vol. 17, pp. 421-32, doi: 10.1007/PL00013738.

Cai, W, Hendon, HH & Meyers, G 2005a, 'Indian Ocean Dipolelike Variability in the CSIRO Mark 3 Coupled Climate Model', *Journal of Climate*, vol. 18, pp. 1449-68, doi: 10.1175/JCLI3332.1.

Cai, W, Meyers, G & Shi, G 2005b, 'Transmission of ENSO signal to the Indian Ocean', *Geophysical Research Letters*, vol. 32, p. 05616, doi:10.1029/2004GL021736.

Cai, W, Sullivan, A & Cowan, T 2009, 'Rainfall teleconnections with Indo-Pacific variability in the WCRP CMIP3 models', *Journal of Climate*, vol. preprint, no. 2009, doi: 10.1175/2009JCLI2694.1.

Cai, W, Whetton, P & Karoly, DJ 2003, 'The response of the Antarctic Oscillation to increasing and stabilized atmospheric CO<sub>2</sub>', *Journal of Climate*, vol. 16, pp. 1525–1538, doi: 10.1175/1520-0442(2003)016<1525:TROTAO>2.0.CO;2.

Chang, CP, Harr, PA & Chen, HJ 2005, 'Synoptic Disturbances over the Equatorial South China Sea and Western Maritime Continent during Boreal Winter', *Monthly Weather Review*, vol. 133, no. 3, pp. 489-503, doi: 10.1175/MWR-2868.1.

Chang, CP, Wang, Z, Ju, JH & Li, T 2004, 'On the relationship between western maritime continent monsoon rainfall and ENSO during northern winter', *Journal of Climate*, vol. 17, no. 3, pp. 665-72, doi: 10.1175/1520-0442(2004)017<0665:OTRBWM>2.0.CO;2.

Chen, T-C, Wang, S-Y, Huang, W-R & Yen, M-C 2004, 'Variation of the East Asian summer monsoon rainfall', *Journal of Climate*, vol. 17, no. 4, pp. 744-62, doi: 10.1175/1520-0442(2004)017<0744:VOTEAS>2.0.CO;2.

Chung, CE & Ramanathan, V 2007, 'Relationship between trends in land precipitation and tropical SST gradient', *Geophysical Research Letters*, vol. 34, no. L16809, doi: 10.1029/2007GL030491.

Clement, AC, Seager, R, Cane, MA & Zebiak, SE 1996, 'An ocean dynamical thermostat', *Journal of Climate*, vol. 9, no. 9, pp. 2190 - 6, doi: 10.1175/1520-0442(1996)009<2190:AODT>2.0.CO;2.

Collier, MA, Dix, MR & Hirst, AC 2007, 'CSIRO Mk3 climate system model and meeting the strict IPCC AR4 data requirements', paper presented to MODSIM07 International Congress on Modelling and Simulation : Land, water & environmental management : integrated systems for sustainability, Christchurch, New Zealand, 10-13 December 2007.

Collier, MA, Dix, MR, Hirst, AC, Davies, HL, Elliott, TI, Gordon, HB, Morgan, P, O'Farrell, SP, Rotstayn, LD & Watterson, IG 2008, *IPCC standard output from the CSIRO Mk3.0 climate system model*, Melbourne, Victoria.

Collins, WD, Bitz, CM, Blackmon, ML, Bonan, GB, Bretherton, CS, Carton, JA, Chang, P, Doney, SC, Hack, JJ, Henderson, TB, Kiehl, JT, Large, WG, McKenna, DS, Santer, BD & Smith, RD 2006, 'The Community Climate System Model Version 3 (CCSM3)', *Journal of Climate*, vol. 19, no. 11, pp. 2122-43, doi: 10.1175/JCLI3761.1.

Cook, GD & Heerdegen, RG 2001, 'Spatial variation in the duration of the rainy season in monsoonal Australia', *International Journal of Climatology*, vol. 21, pp. 1723-32, doi: 10.1002/joc.704.

Covey, C, AchutaRao, KM, Cubasch, U, Jones, P, Lambert, SJ, Mann, ME, Phillips, TJ & Taylor, KE 2003, 'An overview of results from the Coupled Model Intercomparison Project', *Global and Planetary Change*, vol. 37, no. 1-2, pp. 103-33, doi: 10.1016/S0921-8181(02)00193-5.

CSIRO & BOM 2007, *Climate change in Australia: technical report 2007*, CSIRO.

D'Arrigo, R, Wilson, R, Palmer, J, Krusic, P, Curtis, A, Sakulich, J, Bijaksana, S, Zulaikah, S & Ngkoimani, LO 2006, 'Monsoon drought over Java, Indonesia, during the past two centuries', *Geophysical Research Letters*, vol. 33, no. L04709, doi: 10.1029/2005GL025465.

- Dai, A 2006, 'Precipitation characteristics in eighteen coupled climate models', *Journal of Climate*, vol. 19, no. 18, pp. 4605-30, doi: 10.1175/JCLI3884.1.
- Dare, RA & Davidson, NE 2004, 'Characteristics of Tropical Cyclones in the Australian Region', *Monthly Weather Review*, vol. 132, no. 12, pp. 3049-65, doi: 10.1175/MWR2834.1.
- Delworth, TL, Broccoli, AJ, Rosati, A, Stouffer, RJ, Balaji, V, Beesley, JA, Cooke, WF, Dixon, KW, Dunne, J, Dunne, KA, Durachta, JW, Findell, KL, Ginoux, P, Gnanadesikan, A, Gordon, CT, Griffies, SM, Rich Gudgel, Harrison, MJ, Held, IM, Hemler, RS, Horowitz, LW, Klein, SA, Knutson, TR, Kushner, PJ, Langenhorst, AR, Lee, H-C, Lin, S-J, Lu, J, Malyshev, SL, Milly, PCD, Ramaswamy, V, Russell, J, M. Daniel Schwarzkopf, Shevliakova, E, Sirutis, JJ, Spelman, MJ, Stern, WF, Winton, M, Wittenberg, AT, Wyman, B, Zeng, F & Zhang, R 2006, 'GFDL's CM2 Global Coupled Climate Models. Part I: Formulation and Simulation Characteristics', *Journal of Climate*, vol. 19, no. 5, pp. 643-74., doi: 10.1175/JCLI3629.1.
- Dommenget, D & Latif, M 2002, 'A cautionary note on the interpretation of EOFs', *Journal of Climate*, vol. 15, pp. 216-25.
- Dommenget, D, Semenov, V & Latif, M 2006, 'Impacts of the tropical Indian and Atlantic Oceans on ENSO', *Geophysical Research Letters*, vol. 33, no. L11701, doi: 10.1029/2006GL025871.
- Donald, A, Meinke, H, Power, B, Maia, AdHN, Wheeler, MC, White, N, Stone, RC & Ribbe, J 2006, 'Near-global impact of the Madden-Julian Oscillation on rainfall', *Geophysical Research Letters*, vol. 33, no. L09704, doi: 10.1029/2005GL025155.
- Du, Y, Qu, T & Meyers, G 2008, 'Interannual Variability of Sea Surface Temperature off Java and Sumatra in a Global GCM', *Journal of Climate*, vol. 21, no. 11, pp. 2451-65, doi: 10.1175/2007JCLI1753.1.
- England, MH & Huang, F 2005, 'On the Interannual Variability of the Indonesian Throughflow and Its Linkage with ENSO', *Journal of Climate*, vol. 18, no. 9, pp. 1435-44, doi: 10.1175/JCLI3322.1.
- England, MH, Ummenhofer, CC & Santoso, A 2006, 'Interannual Rainfall Extremes over Southwest Western Australia Linked to Indian Ocean Climate Variability', *Journal of Climate*, vol. 19, no. 10, pp. 1948-69, doi: 10.1175/JCLI3700.1.
- Faqih, A 2004, 'Analisis korelasi debit air masuk musim kemarau pada waduk seri DAS Citarum dengan perubahan suhu permukaan laut global (Correlation Analysis of Citarum Dams Inflows with Global Sea Surface Temperatures in Dry Season)', *Indonesian Journal of Agricultural Meteorology*, vol. 18, no. 1, pp. 1-13.
- Ferranti, L, Slingo, JM, Palmer, T & Hoskins, B 1997, 'Relations between interannual and intraseasonal monsoon variability as diagnosed from AMIP integrations', *The Quarterly Journal of the Royal Meteorological Society*, vol. 123, no. 541, pp. 1323-57, doi: 10.1002/qj.49712354110.

- Fischer, AS, Terray, P, Guilyardi, E, Gualdi, S & Delecluse, P 2005, 'Two Independent Triggers for the Indian Ocean Dipole/Zonal Mode in a Coupled GCM', *Journal of Climate*, vol. 18, no. 17, pp. 3428-49, doi: 10.1175/JCLI3478.1.
- Folland, CK, Parker, DE, Colman, A & Washington, R 1999, 'Large scale modes of ocean surface temperature since the late nineteenth century', in A Navarra (ed.), *Beyond El Nino: Decadal and Interdecadal Climate Variability*, Springer-Verlag, Berlin, pp. 73- 102.
- Folland, CK, Renwick, JA, Salinger, MJ & Mullan, AB 2002, 'Relative influences of the Interdecadal Pacific Oscillation and ENSO on the South Pacific Convergence Zone', *Geophysical Research Letters*, vol. 29, no. 13, doi: 10.1029/2001GL014201.
- Gadgil, S & Sajani, S 1998, 'Monsoon precipitation in the AMIP runs', *Climate Dynamics*, vol. 14, no. 9, pp. 659-89, doi: 10.1007/s003820050248
- Goosse, H, Barriat, PY, Lefebvre, W, Loutre, MF & Zunz, V 2009, 'Introduction to climate dynamics and climate modeling', Chapter 5: Brief history of climate: causes and mechanisms, pp. 109-144, Online textbook available at <http://www.climate.be/textbook>.
- Gordon, AL 1986, 'Interocean exchange of thermocline water', *Journal of Geophysical Research*, vol. 91, pp. 5037-46.
- Gordon, AL, Susanto, RD & Vranes, K 2003, 'Cool Indonesian throughflow as a consequence of restricted surface layer flow', *Nature*, vol. 425, p. 824, doi: 10.1038/nature02038.
- Gordon, C, Cooper, C, Senior, CA, Banks, H, Gregory, JM, Johns, TC, Mitchell, JFB & Wood, RA 2000, 'The Simulation of SST, sea ice extents and ocean heat transport in a version of the Hadley Centre coupled model without flux adjustments', *Climate Dynamics*, vol. 16, pp. 147-68.
- Gordon, HB, Rotstayn, LD, McGregor, JL, Dix, MR, Kowalczyk, EA, O'Farrell, SP, Waterman, LJ, Hirst, AC, Wilson, MA, Collier, SG, Watterson, IG & Elliott, TI 2002, *The CSIRO Mk3 climate system model*, 60, CSIRO Australia.
- Gordon, HB, Rotstayn, LD, McGregor, JL, Dix, MR, Kowalczyk, EA, O'Farrell, SP, Waterman, LJ, Hirst, AC, Wilson, SG, Collier, MA, Watterson, IG & Elliott, TI 2004, *The CSIRO Mk3 climate system model*, CSIRO Marine and Atmospheric Research, Melbourne.
- Goreau, TJ, Hayes, RL & McAllister, D 2005, 'Regional patterns of sea surface temperature rise: implications for global ocean circulation change and the future of coral reefs and fisheries', *World Resource Review*, vol. 17 no. 3, pp. 350-74.
- Grant, AP & Walsh, KJE 2001, 'Interdecadal variability in north-east Australian tropical cyclone formation', *Atmospheric Science Letters*, vol. 2, no. 1-4, pp. 9-17, doi: 10.1006/asle.2001.0038.
- Gualdi, SE, Guilyardi, A, Navarra, S, Masina & Delecluse, P 2003, 'The interannual variability in the tropical Indian Ocean as simulated by a CGCM', *Climate Dynamics*, vol. 20, pp. 567-82, doi: 10.1007/s00382-002-0295-z.

Guilyardi, E 2006, 'El Niño mean state seasonal cycle interactions in a multi-model ensemble', *Climate Dynamics*, vol. 26, pp. 329-48, doi: 10.1007/s00382-005-0084-6.

Hack, JJ, Caron, JM, Danabasoglu, G, Oleson, KW, Bitz, C & Truesdale, JE 2006, 'CCSM-CAM3 Climate Simulation Sensitivity to Changes in Horizontal Resolution', *Journal of Climate*, vol. 19, no. 11, pp. 2267-89, doi: 10.1175/JCLI3764.1.

Hackert, EC & Hastenrath, S 1986, 'Mechanisms of Java Rainfall Anomalies', *Monthly Weather Review*, vol. 114, no. 4, pp. 745-57, doi: 10.1175/1520-0493(1986)114<0745:MOJRA>2.0.CO;2.

Hall, JD, Matthews, AJ & Karoly, DJ 2001, 'The Modulation of Tropical Cyclone Activity in the Australian Region by the Madden-Julian Oscillation', *Monthly Weather Review*, vol. 129, no. 12, p. 2970, doi: 10.1175/1520-0493(2001)129<2970:TMOTCA>2.0.CO;2.

Halldor, B & Venegas, SA 1997, *A manual for EOF and SVD analyses of climate data*, McGill University, CCGCR Report No. 97-1, Montréal, Québec.

Hannachi, A 2004, *A primer for EOF analysis of climate data*, Department of Meteorology, University of Reading, Reading RG6 6BB, U.K., March 24, 2004.

Hastenrath, S 1987, 'Predictability of Java Monsoon Rainfall Anomalies: A Case Study', *Journal of Applied Meteorology*, vol. 26, no. 1, pp. 133-41.

Haylock, M & McBride, J 2001, 'Spatial coherence and predictability of Indonesian wet season rainfall', *Journal of Climate*, vol. 14, no. 18, pp. 3882-7, doi: 10.1175/1520-0442(2001)014<3882:SCAPOI>2.0.CO;2.

Hendon, HH 2003, 'Indonesian rainfall variability: Impacts of ENSO and local air-sea interaction', *Journal of Climate*, vol. 16, no. 11, pp. 1775-90, doi: 10.1175/1520-0442(2003)016<1775:IRVIOE>2.0.CO;2.

Hobbs, JE 1998, 'Present Climates of Australia and New Zealand', in JE Hobbs, JA Lindesay & HA Bridgman (eds), *Climate of the southern continents: present, past and future*, Wiley, Chichester, pp. 63-105.

Hollander, M & Wolfe, DA 1999, *Nonparametric statistical methods*, Second edn, Wiley series in probability and statistics, John Wiley & Sons, Inc., New York, USA.

Holton, J 1992, *An introduction to dynamic meteorology*, 3rd edn, Academic Press, San Diego, pp. 117-140.

IPCC 2005, *Requirements for IPCC Standard Output Contributed to the PCMDI Archive*, <[http://www-pcmdi.llnl.gov/ipcc/IPCC\\_output\\_requirements.htm](http://www-pcmdi.llnl.gov/ipcc/IPCC_output_requirements.htm)>.

---- 2007, *Climate Change 2007: The physical science basis. Contribution of Working Group I to the Fourth Assessment Report of the Intergovernmental Panel on Climate Change*, Cambridge University Press, Cambridge, United Kingdom and New York, NY, USA.

Johns, T, Durman, C, Banks, H, Roberts, M, McLaren, A, Ridley, J, Senior, C, Williams, K, Jones, A, Keen, A, Rickard, G, Cusack, S, Joshi, M, Ringer, M, Dong,

B, Spencer, H, Pardaens, RHJGA, Lowe, J, Bodas-Salcedo, A, Stark, S & Searl, Y 2004, *HadGEM1 – Model description and analysis of preliminary experiments for the IPCC Fourth Assessment Report*, UK Met Office, Exeter, UK.

Jolliffe, IT 2002, *Principal Component Analysis*, 2nd edn, Springer-Verlag New York, Incorporated New York.

Juneng, L & Tangang, FT 2005, 'Evolution of ENSO-related rainfall anomalies in Southeast Asia region and its relationship with atmosphere ocean variations in Indo-Pacific sector', *Climate Dynamics*, vol. 25, no. 4, pp. 337-50, doi: 10.1007/s00382-005-0031-6.

Jungclaus, JH, Keenlyside, N, Botzet, M, Haak, H, Luo, J-J, Latif, M, Marotzke, J, Mikolajewicz, U & Roeckner, E 2005, 'Ocean Circulation and Tropical Variability in the Coupled Model ECHAM5/MPI-OM', *Journal of Climate*, vol. 19, no. 16, pp. 3952–72, doi: 10.1175/JCLI3827.1.

K-1 model developers 2004, *K-1 coupled model (MIROC) description*, Center for Climate System Research, University of Tokyo, Tokyo.

K.-M. Lau, HTW 2007, 'Detecting trends in tropical rainfall characteristics, 1979-2003', *International Journal of Climatology*, vol. 27, no. 8, pp. 979-88.

Kajikawa, Y, Wang, B & Yang, J 2009, 'A multi-time scale Australian monsoon index', *International Journal of Climatology*, doi: 10.1002/joc.1955.

Kara, AB, Rochford, PA & Hurlburt, HE 2002, 'Air-sea flux estimates and the 1997-1998 ENSO event', *Boundary-Layer Meteorology*, vol. 103, pp. 439-58.

Kawamura, R 1994, 'A rotated EOF analysis of global sea surface temperature variability with interannual and interdecadal scales', *J. Phys. Oceanogr.*, vol. 24, pp. 707–15.

Kim, S-J, Flato, GM, de Boer, GJ & McFarlane, NA 2002, 'A coupled climate model simulation of the Last Glacial Maximum, Part 1: transient multi-decadal response', *Climate Dyn.*, vol. 19, pp. 515–37.

Kirono, DGC, Tapper, NJ & McBride, JL 1999, 'Documenting Indonesian rainfall in the 1997/1998 El Nino event', *Physical Geography*, vol. 20, no. 5, pp. 422-35.

Krishnamurthy, V & Goswami, BN 2000), 'Indian Monsoon-ENSO Relationship on Interdecadal Timescale', *Journal of Climate*, vol. 13, pp. 579-595.

Krishnan, R & Sugi M 2003, 'Pacific decadal oscillation and variability of the Indian summer monsoon rainfall', *Climate Dynamics*, vol. 21, pp 233-242.

Kumar, MRR & Sreejith, OP 2005, 'On some aspects of precipitation over the tropical Indian Ocean using satellite data', *International Journal of Remote Sensing*, vol. 26, no. 8, pp. 1717-28.

Lau, KM, Sud, Y & Kim, JH 1996, 'Intercomparison of hydrologic processes in AMIP GCMs', *Bulletin of the American Meteorological Society*, vol. 77, Issue 10, pp.2209-2228.

Legutke, S & Voss, R 1999, *The Hamburg Atmosphere-Ocean Coupled Circulation Model ECHO-G*, German Climate Computer Centre (DKRZ), Hamburg.

Li, T, Wang, B, Chang, CP & Zhang, Y 2003, 'A Theory for the Indian Ocean Dipole-Zonal Mode', *Journal of Atmospheric Sciences*, vol. 60, pp. 2119-35.

Lin, J-L 2007, 'The double-ITCZ problem in IPCC AR4 coupled GCMs : Ocean-atmosphere feedback analysis', *Journal of Climate*, vol. 20, no. 18, pp. 4497-525.

Lin, J-L, Kiladis, GN, Mapes, BE, Weickmann, KM, Sperber, KR, Lin, W, Wheeler, MC, Schubert, SD, Del Genio, A, Donner, LJ, Emori, S, Gueremy, J-F, Hourdin, F, Rasch, PJ, Roeckner, E & Scinocca, JF 2006, 'Tropical Intraseasonal Variability in 14 IPCC AR4 Climate Models. Part I: Convective Signals', *Journal of Climate*, vol. 19, no. 12, pp. 2665-90.

Lo, F, Wheeler, MC, Meinke, H & Donald, A 2007, 'Probabilistic forecasts of the onset of the North Australian wet season', *Monthly Weather Review*, vol. 135, pp. 3506-20.

Lorenz, EN 1956, *Empirical orthogonal functions and statistical weather prediction*, Dept. of Meteor., MIT.

Lucarini, L & Russell, GL 2002, 'Comparison of mean climate trends in the northern hemisphere between National Centers for Environmental Prediction and two atmosphere-ocean model forced runs', *J. Geophys. Res.*, vol. D15.

Madden, RA & Julian, PR 1994, 'Observations of the 40-50-Day Tropical Oscillation-A Review', *Monthly Weather Review*, vol. 122, no. 5, pp. 814-37.

Maia, AHN, Meinke, H, Lennox, S & Stone, RC 2007, 'Inferential, non-parametric statistics to assess quality of probabilistic forecast systems', *Monthly Weather Review*, vol. 135, pp. 351-62, doi: 10.1175/MWR3291.1.

Mantua, NJ & Hare, SR 2002, 'The pacific decadal oscillation', *Journal of Oceanography*, vol. 58, pp. 35-44.

Mantua, NJ, Hare, SR, Zhang, Y, Wallace, JM & Francis, RC 1997, 'A pacific interdecadal climate oscillation with impacts on salmon production', *Bull. Amer. Meteor. Soc.*, vol. 78, pp. 1069-79.

Marti, O, et al. 2005, *The new IPSL climate system model: IPSLCM4*, Institut Pierre Simon Laplace des Sciences de l'Environnement Global, , IPSL, Case 101, 4 place Jussieu, Paris, France.

Maxino, CC, McAvaney, BJ, Pitman, AJ & Perkins, SE 2007, 'Ranking the AR4 climate models over the Murray-Darling Basin using simulated maximum temperature, minimum temperature and precipitation', *International Journal of Climatology*, doi: 10.1002/joc.1612.

McBride, J & Winarso, PA 2002, 'The Climate', in IJ Partridge & M Ma'shum (eds), *Will it rain?: The effect of the Southern Oscillation and El Nino in Indonesia*, Publishing Service, DPI, Brisbane, Australia, vol. Information Series QI01016.

- McBride, JL & Nicholls, N 1983, 'Seasonal Relationships between Australian Rainfall and the Southern Oscillation', *Monthly Weather Review*, vol. 111, no. 10, pp. 1998-2004.
- McBride, JL, Haylock, MR & Nicholls, N 2003, 'Relationships between the Maritime Continent Heat Source and the El Niño-Southern Oscillation Phenomenon', *Journal of Climate*, vol. 16, pp. 2905-14.
- McCabe, GJ & Palecki, MA 2006, 'Multidecadal climate variability of global lands and oceans', *International Journal of Climatology*, vol. 26, no. 7, pp. 849-65.
- McCabe, GJ, Palecki, MA & Betancourt, JL 2004, 'Pacific and Atlantic ocean influences on multidecadal drought frequency in the United States.' *PNAS*, vol. 101, no. 12, pp. 4137-41.
- McPhaden, MJ 2004, 'Evolution of the 2002/03 El Niño', *Bulletin of the American Meteorological Society*, vol. 85, no. 5, pp. 677-95, doi: 10.1175/BAMS-85-5-677.
- Meehl, GA, Covey, C, McAvaney, B, Latif, M & Stouffer, RJ 2005, 'Overview of the Coupled Model Intercomparison Project', *Bulletin of the American Meteorological Society*, vol. 86, Issue 1, pp.89-93, vol. 86, pp. 89-93.
- Meinke, H, Nelson, R, Kokic, P, Stone, R, Selvaraju, R & Baethgen, W 2006, 'Actionable climate knowledge: from analysis to synthesis', *Climate Research*, vol. 33, pp. 101–10.
- Meinke, H, deVoil, P, Hammer, GL, Power, S, Allan, R, Stone, RC, Folland, C & Potgieter, A 2005, 'Rainfall Variability at Decadal and Longer Time Scales: Signal or Noise?' *Journal of Climate*, vol. 18, no. 1, pp. 89-96.
- Mitchell, TD & Jones, PD 2005, 'An improved method of constructing a database of monthly climate observations and associated high-resolution grids', *International Journal of Climatology*, vol. 25, no. 6, pp. 693-712.
- Mitra, AK, Gupta, MD, Singh, SV & Krishnamurti, TN 2003, 'Daily Rainfall for the Indian Monsoon Region from Merged Satellite and Rain Gauge Values: Large-Scale Analysis from Real-Time Data', *Journal of Hydrometeorology*, vol. 4, no. 5, pp. 769-81.
- Moise, AF, Colman, RA & Zhang, H 2005, *Coupled model simulations of Australian surface precipitation and temperature and their response to global warming in 18 CMIP2 models*, 106, BMRC.
- Moron, V, Robertson, AW & Boer, R 2009, 'Spatial Coherence and Seasonal Predictability of Monsoon Onset over Indonesia', *J. Climate*, vol. 22, pp. 840-50, doi: 10.1175/2008JCLI2435.1.
- Mpelasoka, FS, Collier, MA, Suppiah, R & Arancibia, JP 2007, 'Application of Palmer Drought Severity Index to observed and enhanced greenhouse conditions using CSIRO Mk3 GCM simulations. ' paper presented to MODSIM07 conference, Christchurch, New Zealand.

- Murphy, BF & Ribbe, J 2004, 'Variability of southeastern Queensland rainfall and climate indices', *International Journal of Climatology*, vol. 24, no. 6, pp. 703-21.
- Naylor, RL, Falcon, W, Wada, N & Rochberg, D 2002, 'Using El Nino-Southern Oscillation Climate Data to Improve Food Policy Planning in Indonesia', *Bulletin of Indonesian Economic Studies*, vol. 38, no. 1, pp. 75-91.
- Naylor, RL, Battisti, DS, Vimont, DJ, Falcon, WP & Burke, MB 2007, 'Assessing risks of climate variability and climate change for Indonesian rice agriculture', *PNAS*, vol. 104, no. 19, pp. 7752-7.
- Nicholls, N 1981, 'Air-sea interaction and the possibility of long-range weather prediction in the Indonesian Archipelago', *Mon. Wea. Rev.*, vol. 109, pp. 2435-43.
- 1995, 'All-India Summer Monsoon Rainfall and Sea Surface Temperatures around Northern Australia and Indonesia', *Journal of Climate*, vol. 8, no. 5, pp. 1463-7.
- 2001, 'The insignificance of significance testing', *Bull. Amer. Meteor. Soc.*, vol. 82, pp. 981-6.
- Nicholls, N & Kariko, A 1993, 'East Australian Rainfall Events: Interannual Variations, Trends, and Relationships with the Southern Oscillation', *Journal of Climate*, vol. 6, no. 6, pp. 1141-52.
- Nott, J 2006, 'Tropical Cyclones and the Evolution of the Sedimentary Coast of Northern Australia', *Journal of Coastal Research*, vol. 22, no. 1, pp. 49-62.
- Oldeman, LR & Frere, M 1982, *Technical report on a study of the agroclimatology of the humid tropics of southeast Asia*, FAO/UNESCO/WMO, Rome.
- Perkins, SE, Pitman, AJ, Holbrook, NJ & McAneney, J 2007, 'Evaluation of the AR4 climate models' simulated daily maximum temperature, minimum temperature and precipitation over Australia using probability density functions', *Journal of Climate*, vol. 20, pp. 4356-76, doi: 10.1175/JCLI4253.1.
- Pezza, AB & Ambrizzi, T 2003, 'Variability of Southern Hemisphere Cyclone and Anticyclone Behavior: Further Analysis', *Journal of Climate*, vol. 16, pp. 1075-83.
- Philander, S 1983, 'El Nino southern oscillation phenomena', *Nature*, vol. 302, pp. 295-301, doi: 10.1038/302295a0.
- Philander, SG 1990, *El Niño, La Niña, and the southern oscillation*, International geophysics series, v. 46, Academic Press, San Diego, pp. 293.
- Pope, VD, Gallani, ML, Rowntree, PR & Stratton, RA 2000, 'The impact of new physical parametrizations in the Hadley Centre climate model: HadAM3', *Climate Dynamics*, vol. 16, pp. 123-46.
- Potemra, JT, Hautala, SL, Sprintall, J & Pandoe, W 2002, 'Interaction between the Indonesian Seas and the Indian Ocean in Observations and Numerical Models', *Journal of Physical Oceanography*, vol. 32, no. 6, p. 1838.

Potgieter, AB, Hammer, GL, Meinke, H, Stone, RC & Goddard, L 2005, 'Three Putative Types of El Niño Revealed by Spatial Variability in Impact on Australian Wheat Yield', *Journal of Climate*, vol. 18, no. 10, pp. 1566-74, doi: 10.1175/JCLI3349.1.

Power, S, Sadler, B & Nicholls, N 2005, 'The Influence of Climate Science on Water Management in Western Australia: Lessons for Climate Scientists', *Bulletin of the American Meteorological Society*, vol. 86, no. 6, pp. 839-44, doi: 10.1175/BAMS-86-6-839

Power, S, Casey, T, Folland, C, Colman, A & Mehta, V 1999a, 'Inter-decadal modulation of the impact of ENSO on Australia', *Climate Dynamics*, vol. 15, no. 5, pp. 319-24, doi: 10.1007/s003820050284

Power, S, Tseitkin, F, Mehta, V, Lavery, B, Torok, S & Holbrook, N 1999b, 'Decadal climate variability in Australia during the twentieth century', *International Journal of Climatology*, vol. 19, no. 2, pp. 169-84, doi: 10.1002/(SICI)1097-0088(199902)19:2<169::AID-JOC356>3.0.CO;2-Y.

Rayner, NA, Parker, DE, Horton, EB, Folland, CK, Alexander, LV, Rowell, DP, Kent, EC & Kaplan, A 2003, 'Global analyses of sea surface temperature, sea ice, and night marine air temperature since the late nineteenth century', *J. Geophys. Res.*, vol. 108, no. D14, doi: 4407 10.1029/2002JD002670.

Reichler, T & Kim, J 2008, 'How well do coupled models simulate today's climate?' *Bulletin of the American Meteorological Society*, vol. 89, no. 3, pp. 303-11.

Ropelewski, CF & Halpert, MS 1987, 'Global and regional scale precipitation patterns associated with the El Niño/Southern Oscillation', *Monthly Weather Review*, vol. 115, pp. 1606-26.

Russell, GL, Miller, JR & Rind, D 1995, 'A coupled atmosphere-ocean model for transient climate change studies.' *Atmos.-Ocean*, vol. 33, pp. 683-730.

Russell, GL, Miller, JR, Rind, D, Ruedy, RA, Schmidt, GA & Sheth, S 2000, 'Comparison of model and observed regional temperature changes during the past 40 years', *J. Geophys. Res.*, vol. 105, pp. 14891-8.

Saji, NH & Yamagata, T 2003, 'Structure of SST and surface wind variability during Indian Ocean Dipole Mode events: COADS observations', *Journal of Climate*, vol. 16, no. 16, pp. 2735-51.

Saji, NH, Goswami, BN, Vinayachandran, PN & Yamagata, T 1999, 'A dipole mode in the tropical Indian Ocean', *Nature*, vol. 401, pp. 360-3.

Salas-Méllia, D 2002, 'A global coupled sea ice-ocean model', *Ocean Modelling*, vol. 4.

Salinger, MJ, Renwick, JA & Mullan, AB 2001, 'Interdecadal Pacific Oscillation and South Pacific climate', *International Journal of Climatology*, vol. 21, no. 14, pp. 1705-21.

Schmidt, GA, Aleinov, I, Bell, N, Bauer, M, Bauer, S, Cairns, B, Faluvegi, G, Hu, Y, Kiang, NY, Koch, D, Lerner, J, Nazarenko, L, Perlwitz, J, Thresher, D, Ruedy, R, Cheng, Y, Lo, KK, Oinas, V, Sato, M, Tausnev, N, Yao, MS, Hansen, JE, Canuto, V, Genio, AD, Hall, TM, Lacis, AA, Miller, RL, Rind, D, Russell, GL, Shindell, DT, Friend, AD, Kelley, M, Romanou, A, Perlwitz, J, Stone, PH, Sun, S 2005, 'Present-Day Atmospheric Simulations Using GISS ModelE: Comparison to In Situ, Satellite, and Reanalysis Data', *Journal of Climate*, vol. 19, no. 2, pp. 153–192, DOI: 10.1175/JCLI3612.1.

Shi, G 2008, 'Variability and change of the Indo-Pacific climate system and their Impacts upon Australia rainfall', University of Southern Queensland.

Shi, G, Cai, W, Cowan, T, Ribbe, J, Rotstayn, L & Dix, M 2008, 'Variability and trend of north west Australia rainfall: Observations and coupled climate modeling', *Journal of Climate*, vol. 21, no. 12, doi: DOI: 10.1175/2007JCLI1908.1.

Shinoda, T, Hendon, HH & Glick, J 1998, 'Intraseasonal Variability of Surface Fluxes and Sea Surface Temperature in the Tropical Western Pacific and Indian Oceans', *Journal of Climate*, vol. 11, no. 7, p. 1685.

Smith, IN 2007, 'Global climate modelling within CSIRO: 1981 to 2006', *Australian Meteorological Magazine*, vol. 56, pp. 153-166.

Song, Q & Gordon, AL 2004, 'Significance of the vertical profile of the Indonesian Throughflow transport to the Indian Ocean', *Geophysical Research Letters*, vol. 31, p. 16307.

Srinivasan, G, Hulme, M & Jones, C 1995, 'An evaluation of the spatial and interannual variability of tropical precipitation as simulated by GCMs', *Geophysical Research Letters*, vol. 22, pp. 1697-700.

Sun, Y, Solomon, S, Dai, A & Portmann, RW 2007, 'How often will it rain?' *Journal of Climate*, vol. 20, pp. 4801-18, doi: DOI: 10.1175/JCLI4263.1.

Suppiah, R 2004, 'Trends in the southern oscillation phenomenon and Australian rainfall and changes in their relationship', *International Journal of Climatology*, vol. 24, pp. 269-90.

Suppiah et al. 2007, Australian climate change projections derived from simulations performed for the IPCC 4<sup>th</sup> assessment report, *Australian Meteorological Magazine*, 56, 131-152.

Susanto, RD & Gordon, AL 2005, 'Velocity and transport of the Makassar Strait throughflow', *Journal of Geophysical Research (Oceans)*, vol. 110, p. 01005.

Susanto, RD, Gordon, AL & Zheng, Q 2001, 'Upwelling along the coasts of Java and Sumatra and its relation to ENSO', *Geophysical Research Letters*, vol. 28, pp. 1599-602.

Szoeke, SPd & Xie, S-P 2007, 'The tropical Eastern Pacific seasonal cycle: Assessment of errors and mechanisms in IPCC AR4 coupled Ocean–Atmosphere General Circulation Models', *Journal of Climate*, vol. 21, no. 11, pp. 2573–90, doi: DOI: 10.1175/2007JCLI1975.1.

- Takahashi, HG & Yasunari, T 2006, 'A Climatological Monsoon Break in Rainfall over Indochina-A Singularity in the Seasonal March of the Asian Summer Monsoon', *Journal of Climate*, vol. 19, no. 8, pp. 1545-56.
- Terray, P & Dominiak, S 2005, 'Indian Ocean sea surface temperature and El Niño-Southern Oscillation: A new perspective', *Journal of Climate*, vol. 18, pp. 1351-68.
- Terray, P, Dominiak, S & Delecluse, P 2005a, 'Role of the southern Indian Ocean in the transitions of the monsoon-ENSO system during recent decades', *Climate Dynamics*, vol. 24, pp. 169-95.
- Terray, P, Chauvin, F & Douville, H 2006, 'Impact of southeast Indian Ocean sea surface temperature anomalies on monsoon-ENSO-dipole variability in a coupled ocean-atmosphere model', *Climate Dynamic*, doi: DOI 10.1007/s00382-006-0192-y.
- Terray, P, Guilyardi, E, Fischer, AS & Delecluse, P 2005b, 'Dynamics of the Indian monsoon and ENSO relationships in the SINTEX global coupled model', *Climate Dynamics*, vol. 24, pp. 145-68.
- Thompson, DWJ & Wallace, JM 2000 'Annular Modes in the Extratropical Circulation. Part I: Month-to-month variability', *Journal of Climate*, vol. 13, pp. 1000-1016.
- UNDP 1998, *Kebakaran hutan dan lahan di Indonesia: dampak, faktor dan evaluasi*, Kantor Menteri Negara Lingkungan Hidup, United Nation Development Program, Jakarta.
- Vera, C, Silvestri, G, Liebmann, B & Gonza'lez, P 2006, 'Climate change scenarios for seasonal precipitation in South America from IPCC-AR4 models', *Geophysical Research Letters*, vol. 33, no. L13707, doi: doi:10.1029/2006GL025759.
- Volodin, EM & Diansky, NA 2004, 'El-Nino reproduction in coupled general circulation model of atmosphere and ocean', *Russian meteorology and hydrology*, vol. 12, pp. 5-14.
- von Storch, H & Zwiers, F 1999, *Statistical analysis in climate research*, Cambridge University Press, Cambridge, United Kingdom, pp. 293-312.
- Waliser, DE, Murtugudde, R & Lucas, LE 2003, 'Indo-Pacific Ocean response to atmospheric intraseasonal variability: 1. Austral summer and the Madden-Julian Oscillation', *Journal of Geophysical Research (Oceans)*, vol. 108e, pp. 29-1.
- Wall, ME, Rechtsteiner, A & Rocha, LM 2003, 'Singular value decomposition and principal component analysis', in DP Berrar, W Dubitzky & M Granzow (eds), *A practical approach to microarray data analysis*, Kluwer: Norwell, MA pp. 91-109.
- Walpole, RE, Myers, RH, Myers, SL & Ye, K 2002, *Probability & statistics for engineers & scientists*, 7th edn, Prentice-Hall, Inc., Upper Saddle River, New Jersey, USA.
- Wang, B & An, S-I 2005, A method for detecting season-dependent modes of climate variability: S-EOF analysis, *Geophysical Research Letters*, vol. 32, 15710.

Wang, B, Yang, J, Zhou, T & Wang, B 2008, 'Interdecadal Changes in the Major Modes of Asian-Australian Monsoon Variability: Strengthening Relationship with ENSO since the Late 1970s', *Journal of Climate*, vol. 21, no. 8, pp. 1771-89.

Wang, G & Hendon, HH 2007, 'Sensitivity of Australian rainfall to inter-El Niño variations', *Journal of Climate*, vol. 20, no. 16, pp. 4211-26, doi: DOI: 10.1175/JCLI4228.1.

Washington, WM, Weatherly, J. W., Meehl, G. A., Semtner Jr., A. J., B, T. W., Craig, A. P., Strand Jr., W. G., Arblaster, & J., W, V. B., James, R., and Zhang, Y. 2000, 'Parallel climate model (PCM) control and transient simulations', *Climate Dynamics*, vol. 16, pp. 755-74.

Watterson, IG 2008, Calculation of probability density functions for temperature and precipitation change under global warming, *Journal of Geophysical Research*, 113, D12106, doi: 10.1029/2007/JD009254.

Webster, PJ, Moore, AM, Loschnigg, JP & Leben, RR 1999, 'Coupled ocean-atmosphere dynamics in the Indian Ocean during 1997-98', *Nature*, vol. 401, pp. 356-60.

Wheeler, MC, Hendon, HH, Cleland, S, Meinke, H & Donald, A 2009, 'Impacts of the Madden-Julian oscillation on Australian rainfall and circulation', *Journal of Climate*, vol. 22, pp. 1482-98. DOI: 10.175/2008JCLI595.1.

Whetton, P, Macadam, I, Bathols, J & O'Grady, J 2007, 'Assessment of the use of current climate patterns to evaluate regional enhanced greenhouse response pattern of climate models', *Geophysical Research Letters*, vol. 34, no. L14701, doi: 10.1029/2007GL030025, 2007.

White, WB & Cayan, DR 2000, 'A global El Niño-Southern Oscillation wave in surface temperature and pressure and its interdecadal modulation from 1900 to 1997', *Journal of Geophysical Research*, vol. 105, pp. 11223-42.

Xie, P & Arkin, PA 1996, 'Analyses of global monthly precipitation using gauge observations, satellite estimates, and numerical model predictions', *J. Climate*, vol. 9, pp. 840-58.

---- 1997, 'Global precipitation: a 17-year monthly analysis based on gauge observations, satellite estimates, and numerical model outputs', *Bulletin of the American Meteorological Society*, vol. 78, no. 11, pp. 2549-58.

Xie, S-P, Annamalai, H, Schott, FA & McCreary, JP, Jr. 2002, 'Structure and mechanisms of South Indian Ocean climate variability', *Journal of Climate*, vol. 15, pp. 864-78.

Yu, L & Rienecker, MM 2000, 'Indian Ocean warming of 1997-1998', *Journal of Geophysical Research*, vol. 105, pp. 16923-40.

Yu, W, Xiang, B, Liu, L & Liu, N 2005, 'Understanding the origins of interannual thermocline variations in the tropical Indian Ocean', *Geophysical Research Letters*, vol. 32, p. 24706.

Yu, Y, Zhang, X & Guo, Y 2004, 'Global coupled ocean- atmosphere general circulation models in LASG/IAP', *Adv. Atmos. Sci.*, vol. 21, pp. 444–55.

Yukimoto, S & Noda, A 2002, *Improvements of the Meteorological Research Institute Global Ocean-atmosphere Coupled GCM (MRI-CGCM2) and its climate sensitivity*, NIES, Japan.

Zhang, Y, Sperber, KR, Boyle, JS, Dix, M, Ferranti, L, Kitoh, A, Lau, KM, Miyakoda, K, Randall, D, Takacs, L & Wetherald, R 1997, 'East Asian winter monsoon: results from eight AMIP models', *Climate Dynamics*, vol. 13, no. 11, pp. 797-820.

Zhao, Q 2004, 'Role of sea surface wind stress forcing on transport between Tropical Pacific and Indian Ocean', paper presented to 35th COSPAR Scientific Assembly, January 1, 2004.

Zhou, J & Lau, KM 2001, 'Principal modes of interannual and decadal variability of summer rainfall over South America', *International Journal of Climatology*, vol. 21, pp. 1623-44.

Zveryaev, II & Allan, RP 2005, 'Water vapor variability in the tropics and its links to dynamics and precipitation', *Journal of Geophysical Research (Atmospheres)*, vol. 110, p. 21112.

## Glossary and Acronyms

**AMIP:** the Atmospheric Model Intercomparison Project

**Austral-Indonesia:** an area used in this study covering most of Maritime Continent region particularly Indonesia combined with the northern Australian region

**CAD:** Cumulative Absolute Difference

**CDF:** Cumulative Distribution Function

**CMAP:** CPC (Climate Prediction Centre) Merge Analysis of Precipitation

**CPC:** Climate Prediction Centre

**CRU:** Climatic Research Unit

**CS-GC:** Coral Sea and Gulf of Carpentaria

**CSIRO:** Australian Commonwealth Scientific and Research Organisation

**DJF:** December, January, February

**DMI:** Dipole Mode Index

**ENSO:** El Niño-Southern Oscillation

**EOF:** Empirical Orthogonal Function

**ESG:** Earth System Grid

**FFT:** Fast Fourier Transform

**GCM:** Global Circulation Model

**GISST:** the Global Sea Ice and Sea Surface Temperature

**HadISST:** is a recent SST data provided by the Hadley Centre, Met Office that substitutes for the global sea ice and sea surface temperature (GISST) dataset. It covers global SST and sea ice concentration with a  $1^\circ \times 1^\circ$  horizontal grid resolution available from 1871 to the present.

**HadSLP2:** is a combination of quality controlled terrestrial and marine pressure series. It was set in a  $5^\circ \times 5^\circ$  horizontal grid resolution from 1850 to 2004.

**HFLS:** CF standard name for surface upward latent heat flux (unit  $\text{W}\cdot\text{m}^{-2}$ )

**HFSS:** CF standard name for surface upward sensible heat flux (unit  $\text{W}\cdot\text{m}^{-2}$ )

**IO:** Indian Ocean

**IOD:** Indian Ocean Dipole

**IPCC AR4:** Intergovernmental Panel on Climate Change Fourth Assessment Report

**IPO:** Interdecadal Pacific Variability

**ITCZ:** Inter-tropical Convergence Zone

**ITF:** Indonesian Throughflow

**JJA:** June, July, August

**KS test:** Kolmogorov-Smirnov test

**KSDist:** the Kolmogorov-Smirnov Distance; is a parameter used by the two-sample Kolmogorov-Smirnov test that quantifies the maximal vertical distance between CDFs. In this study, it compares the absolute differences between CDFs from the modelled and the observed data.

**La Niña:** below normal temperature anomaly in the central and eastern Pacific region (an opposite of El Niño condition)

**LF:** Low-Frequency

**MAM:** March, April, May

**Maritime Continent:** a term normally used to describe a specifically defined area in Southeast Asia with unique features such as islands of variable size featuring significant mountain ranges of volcanic origin and surrounded by vast waters. This area mostly covers the Indonesian region and the surrounding Southeast Asian countries.

**MJO:** Madden-Julian Oscillation

**Monsoon:** a seasonal prevailing wind that lasts for several months and associated with extensive rainfall due to more active convergence zone. The Austral summer monsoon normally lasts from December to February or March bringing more rainfall over most of Indonesia and northern Australia

**Niño index:** SST region used to measure ENSO

**NOAA:** US National Oceanic and Atmospheric Administration

**OPeNDAP:** a software framework that enabled simple access to remote data by simplifying all aspects of scientific data networking. OPeNDAP servers are used to provide access to local data from different remote locations regardless of local storage format.

**PCMDI:** Program for Climate Model Diagnosis and Intercomparison

**PDF:** Probability Density Function

**PDO:** Pacific Decadal Oscillation

**PNG:** Papua New Guinea

**POAMA:** the Predictive Ocean Atmosphere Model for Australia

**PR:** CF standard name for precipitation flux (unit in  $\text{kg}\cdot\text{m}^{-2}\cdot\text{s}^{-1}$ )

**PSL:** CF standard name for air pressure at sea level (unit in Pa)

**RCM:** Regional Climate Model

**SAM:** Southern Annular Mode

**SCS:** South China Sea

**SLP:** Sea Level Pressure

**SOI:** Southern Oscillation Index

**SON:** September, October, November

**SRES:** Special Report on Emissions Scenarios

**SST:** Sea Surface Temperature

**TAUU:** CF standard name for surface downward eastward stress (unit in Pa)

**TAUV:** CF standard name for surface downward northward stress (unit in Pa)

**TOS:** CF standard name for sea surface temperature from the ocean component (unit in K)

**TS:** CF standard name for surface temperature (unit in K)

**WCRP CMIP3:** the World Climate Research Programme, phase 3 of the Coupled Model Intercomparison Project